AWPP
J697e
1987.

EQUILIBRIUM ADSORPTION AND DIFFUSE REFLECTANCE SPECTROSCOPIC STUDIES OF ADSORPTIOCHROMIC SPIROPYRANS

by

MICHAEL J. JOZWIAKOWSKI

A thesis submitted in partial fulfillment of the requirements for the degree of

DOCTOR OF PHILOSOPHY

(Pharmacy - Pharmaceutics)

at the

University of Wisconsin-Madison

1987

May

"The real benefits come not from what you knew would happen but from the discoveries and capabilities you run into when you open the new horizon."

David Black, 1987
NASA scientist in charge of
implementing the space station
Newsweek, January 19, 1987.

Table of Contents

	Page
ACKNOWLEDGEMENTS	ii
ABSTRACT	vii
I. BACKGROUND	1
A. Solution Chemistry of Spiropyrans	1
1. Structure and Synthesis of the Colorless Form	1
2. Photochromism and the Colored Species	8
3. Kinetics of Thermal Recombination Reactions	15
4. Solvatochromism	23
B. Spiropyrans Adsorbed to Solid Surfaces	25
1. Qualitative Adsorptiochromism	26
2. Quantitative Adsorption Data	28
3. Behavior of Related Cyanine Dyes on Solid Substrates	33
C. The Spectra of Adsorbed Species	36
1. Suspension Transmission Spectroscopy	37
2. Diffuse Reflectance Spectroscopy	40
D. The Adsorbent Surface	47
1. Silicas	48
2. Alumina	52
3. Other Adsorbents	54
E. Langmuirian Adsorption	57

Page

II. INTRODUCTION TO THE PROJECT 62

III. EXPERIMENTAL METHODS 66

A. Materials 66

B. Apparatus 78

C. Experimental Procedures 80

1. Synthesis of Spiropyrans and Characterization of Materials 80

2. Solvatochromic Studies 82

3. Adsorption Isotherms 83

4. Spectral Measurements of Adsorbed Spiropyrans . . . 85

D. Data Treatment 88

IV. RESULTS 99

A. Spiropyran Synthesis and Characterization of Materials 99

B. Solvatochromic Studies 115

C. Adsorption Isotherms 129

D. Suspension Transmission Spectra 191

E. Diffuse Reflectance Spectra 199

V. DISCUSSION 231

A. Spiropyran Synthesis and Characterization of Materials 231

B. Solvatochromic Studies 232

Page

C. Adsorption Isotherms 235

D. Suspension Transmission Spectra 249

E. Diffuse Reflectance Spectra 253

F. Future Work 289

G. Conclusions 291

VI. REFERENCES 293

APPENDIX A. Sample Calculations for the BET Method 303

APPENDIX B. Calculations for the Binding Isotherms 306

APPENDIX C. Sample Printout of the Duggleby Program 308

APPENDIX D. Derivation of the Equilibrium Model 310

ABSTRACT

EQUILIBRIUM ADSORPTION AND DIFFUSE REFLECTANCE SPECTROSCOPIC STUDIES OF ADSORPTIOCHROMIC SPIROPYRANS

Michael J. Jozwiakowski

Under the supervision of Professor Kenneth A. Connors

Spiropyrans exist in solution in equilibrium between a closed, colorless form and an open, planar colored species resembling a merocyanine dye. We have studied the stabilization of the chromophore upon adsorption to hydrophilic surfaces from nonpolar solvents. Four solvatochromic indolinobenzopyrans were synthesized and their solution spectral properties were examined. These experiments indicated that the ratio of colored/colorless spiropyran, and hence the apparent absorptivity, was dependent on the polarity of the medium. 6-nitro-1,3,3-trimethyl-spiro[2H-benzopyran-2,2'-indoline] showed hypsochromic solvatochromic shifts with an increase in solvent polarity; indolino-naphtho-spiropyran showed bathochromic shifts, along with a stationary visible peak. A correlation of the frequency of maximum absorption with Kosower's Z values of solvent polarity yielded an estimate of silica surface polarity equivalent to that of 70% ethanol in water.

Spiropyrans showed Langmuirian adsorption behavior onto hydrophilic adsorbents. The isotherms were determined on silica

gel, silicic acid, alumina, titanium dioxide, talc, and microcrystalline cellulose at 25.0°C. The binding constants for spiropyrans ranged from 5×10^2 M^{-1} to 1.5×10^4 M^{-1}; malachite green on silica gel had a binding constant of 3.2×10^5 M^{-1}. The capacities for the spiropyrans ranged from 0.2-0.6 mg/m^2; malachite green on silica gel had a capacity of only 0.014 mg/m^2. Secondary effects grouped the data into subsets determined by the spiropyran adsorbate. An equilibrium model was developed which predicted a dependence of the observed binding constant on both pre- and post-adsorptive equilibria between colorless and colored spiropyran.

A diffuse reflectance spectroscopic method was used to study the spectra of the adsorbed species. The adsorption colors of spiropyrans were found to be a function of the spiropyran identity, the adsorbent identity, the extent of surface coverage, and the relative absorptivities at a short wavelength peak (436-472 nm) and a longer wavelength visible peak (550 nm). The Kubelka-Munk function plotted versus the surface coverage of adsorbate in nanomoles/m^2 was linear at low coverages. The slopes are interpreted as giving insight into the polarity of the interfacial environment. Spiropyrans (and other cyanine dyes) had a reduced ability to color a silica surface when compared to permanent cationic dyes, based on a comparison of their solution

absorptivities. This difference becomes greater at higher coverages. A two-state model assuming spiropyrans have a surface colored/colorless equilibrium, in which the fraction of colored species decreases with surface coverage, adequately accounts for the observed effects.

Kenneth A. Connors

Major professor's approval

I. BACKGROUND

A. Solution Chemistry of Spiropyrans

The spiropyrans are heterocyclic organic molecules which can exhibit a vast array of colored or colorless modifications. Generally, the relative amounts of a colored and colorless species are governed by an equilibrium constant. Light, temperature, and the properties of the molecule's immediate environment profoundly affect this equilibrium constant. It is the difference in polarity of the two species that accounts for the environmental effect; usually the colored form is zwitterionic, and hence present to a greater degree in polar media. A number of reviews of the chemistry of the spiropyran class are available, often emphasizing a certain aspect of their behavior (1-7).

1. Structure and Synthesis of the Colorless Form

Many families of spiropyrans are known, each containing a different parent ring system and populated by specific examples with different substituents (1). The necessary features are the "spiro" carbon (shared by two rings) and a connected "pyran" oxygen (part of a six-membered pyran ring). The most commonly studied spiropyrans

to date have been of the indolinobenzopyran or BIPS family, illustrated by the examples in Figure 1. The asterisk indicates the spiro carbon, adjacent to the pyran oxygen. Because of the tetrahedral bonding nature of the spiro carbon, the two halves of the molecule are perpendicular in orientation; a CPK model of 6-NO_2-BIPS clearly illustrates this point (Fig. 2). This same carbon serves to isolate the two halves electronically; spiropyrans in this form absorb only ultraviolet light (8). The indolinonaphthospiropyrans (INS), illustrated by the third compound of Figure 1, contain an additional aromatic ring. This ring is in conjugation with the benzopyran portion of the molecule, essentially causing it to behave as a 5,6-benzene-BIPS. Substituent effects carry through to the pyran ring, though to a weaker extent than in the BIPS compounds (3, 5). The colored forms arise when the spiro carbon-pyran oxygen bond cleaves heterolytically, resulting in a planar molecule with zwitterionic character and extensive conjugation along the length of the molecule (1, 3, 5, 9). The colored form can consist of a large number of isomeric forms in equilibrium with each other (1, 5). The net result is a significant increase in molecule polarity, which is the basis for many of the further properties of spiropyrans discussed later.

The ease of preparation of BIPS molecules is one reason they have been the most extensively studied spiropyran family. The synthetic procedure consists of condensing a methyleneindoline (e.g. Fischer's base) and a substituted salicylaldehyde. Equimolar

SPIROPYRAN STRUCTURES

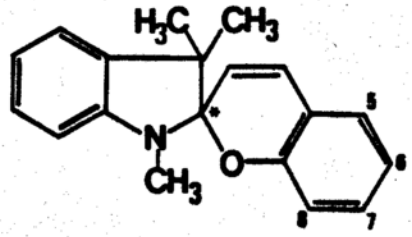

(6-H)BIPS

(benzo-indolino-pyran)

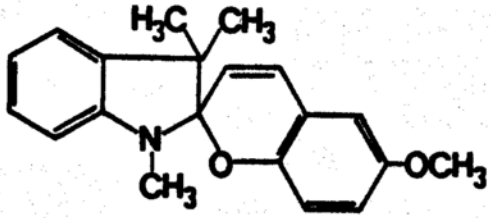

6-OCH_3-BIPS

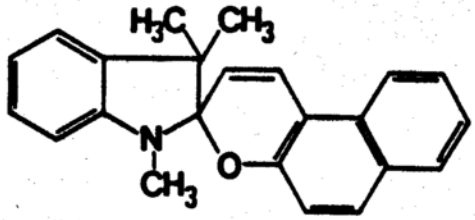

INS

(indolino-naphtho-spiropyran)

Figure 1. Structures

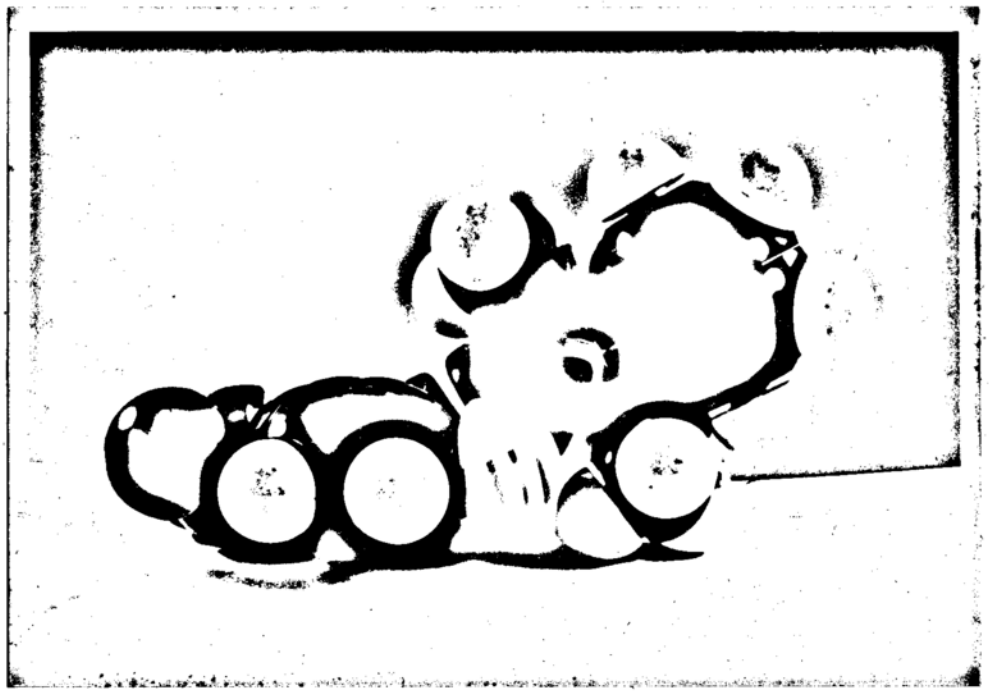

Figure 2. CPK Model of 6-NO_2-BIPS

amounts of each reagent are continuously refluxed in boiling alcohol to obtain a crystalline solid. It is then purified through recrystallization to a sharp melting point. Figure 3 shows the appropriate reagents and product in the synthesis of 6-NO_2-BIPS. Yields are generally in excess of 70% (1, 10), and the variety of substituted salicylaldehydes commercially available gives the possibility of synthesizing BIPS with different substituents. The aldol condensation reaction proceeds via dehydration and subsequent ring closure, forming the pyran ring as the reaction proceeds. The carbonyl oxygen from the salicylaldehyde is lost in the dehydration; the phenolic oxygen remains as the pyran oxygen (1).

The color formation in the reaction flask begins almost immediately, and is a positive test for the presence of salicylaldehydes in a methyleneindoline alcoholic solution (1). A significant portion of the product exists in the open, colored, planar form in the polar environment of the alcohol. Upon recrystallization and drying, the solid crystalline spiropyran is usually pale in color (2, 10). The melting points are often sharp and yield highly colored liquids (1, 2, 9, 10, 11). This phenomenon is known as thermochromism; the molecules being less constrained in the melt than in the crystal, they quickly reflect the increased equilibrium constant from the heating process. Apart from its aesthetic appeal, this thermochromism can be useful in positive identification of the synthetic product (or analysis for the reagent identity). Table 1 shows how the melt color, in combination with

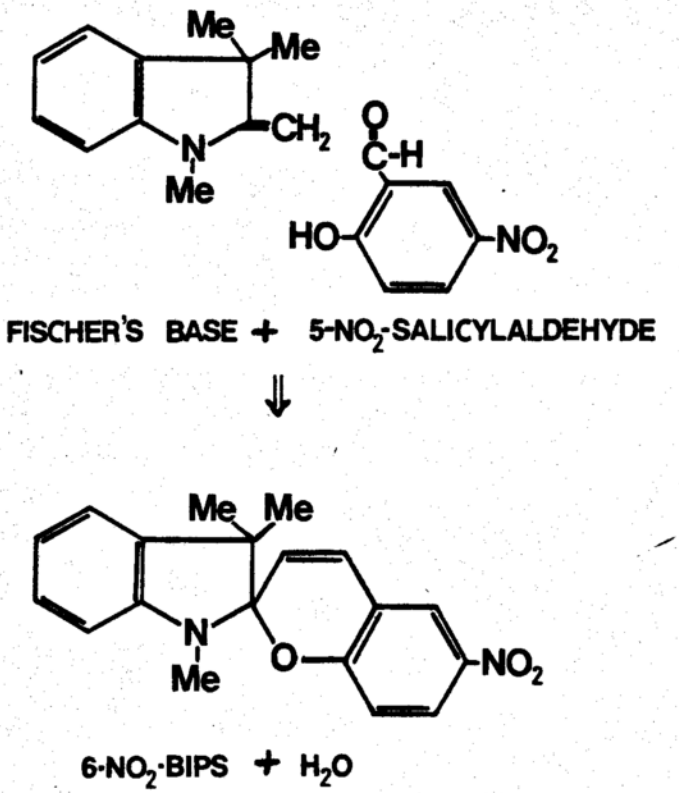

Figure 3. Synthesis of 6-NO_2-BIPS

Table I. Thermochromism of BIPS Compounds.

Substituent	Melting point/°C	Color
6-NO_2	177-178	dark blue
7-NO_2	107-108	orange
6-NO_2-8-Br	255-256	purple
6-NO_2-8-F	302-304	purple
6-OCH_3-8-NO_2	116-117	green
6-8-dibromo	115-116	light blue

(Ref. 11)

the melting temperature, positively identifies members of a BIPS family.

If dissolved in nonpolar solvents, the BIPS compounds are generally colorless or faintly colored (1, 2, 5). The equilibrium constant K, defined as:

$$K = \frac{[\text{colored}]}{[\text{colorless}]}$$

is therefore quite low in nonpolar media, but increases with medium polarity. This constant, K, is dependent upon the temperature, and increases as temperature increases. There is a temperature above which enough colored form is present to see it visually, and this temperature depends on substituent effects of the different BIPS compounds, as well as the solvent polarity. High temperatures, polar solvents, and certain substituents favor the colored species. Some spiropyrans are colorless even in acetone at room temperature (12), while others are colored only in polar solvents at room temperature (2). The majority of BIPS and INS compounds will darken upon heating colorless nonpolar solutions; this phenomenon also goes by the name thermochromism (5, 6, 10).

2. Photochromism and the Colored Species

Photochromism is a reversible phenomenon in which a chemical changes its absorption spectrum transiently upon exposure to electromagnetic radiation of the appropriate excitation wavelength.

Photochromism is not an exclusive property of spiropyrans, rather triarylmethane dyes (13), leucocyanides, keto-enol pairs, tautomers, and even inorganics can undergo photochromism (1). Spiropyrans usually are colored by uv light and decolorized by visible light, with thermal components in either direction. The thermochromic and photochromic products are identical (1, 6), and the two processes are often difficult to separate. Figure 4 illustrates the process for 6-NO_2-BIPS. The closed form predominates in nonpolar solvents at room temperature. When ultraviolet light (approx. 366 nm) strikes the molecule, the carbon-oxygen bond ruptures heterolytically. The resultant open species is highly colored, and can be represented as a resonant hybrid structure with zwitterionic and quinoidal character (1). Placing the colored irradiated solution in the dark results in rapid thermal fading to the colorless, favored form in nonpolar solvents in the absence of ultraviolet light. Some spiropyrans fade so rapidly and have such weak photochromism that it is only apparent under extreme conditions (1). INS turns red-violet under ultraviolet light only at temperatures less than -90°C (6). Absorptivities for the visible species have been estimated by assuming 100% conversion at low temperatures. Apparent absorptivities from thermochromic experiments indicate that even at 120°C, only a small degree of conversion is required to produce visible color, since the absorptivity of the colored species is 10^4 - 10^5 in methylcyclohexane (5). Even the intensely blue photochromic

Figure 4. Photochromism of 6-NO_2-BIPS

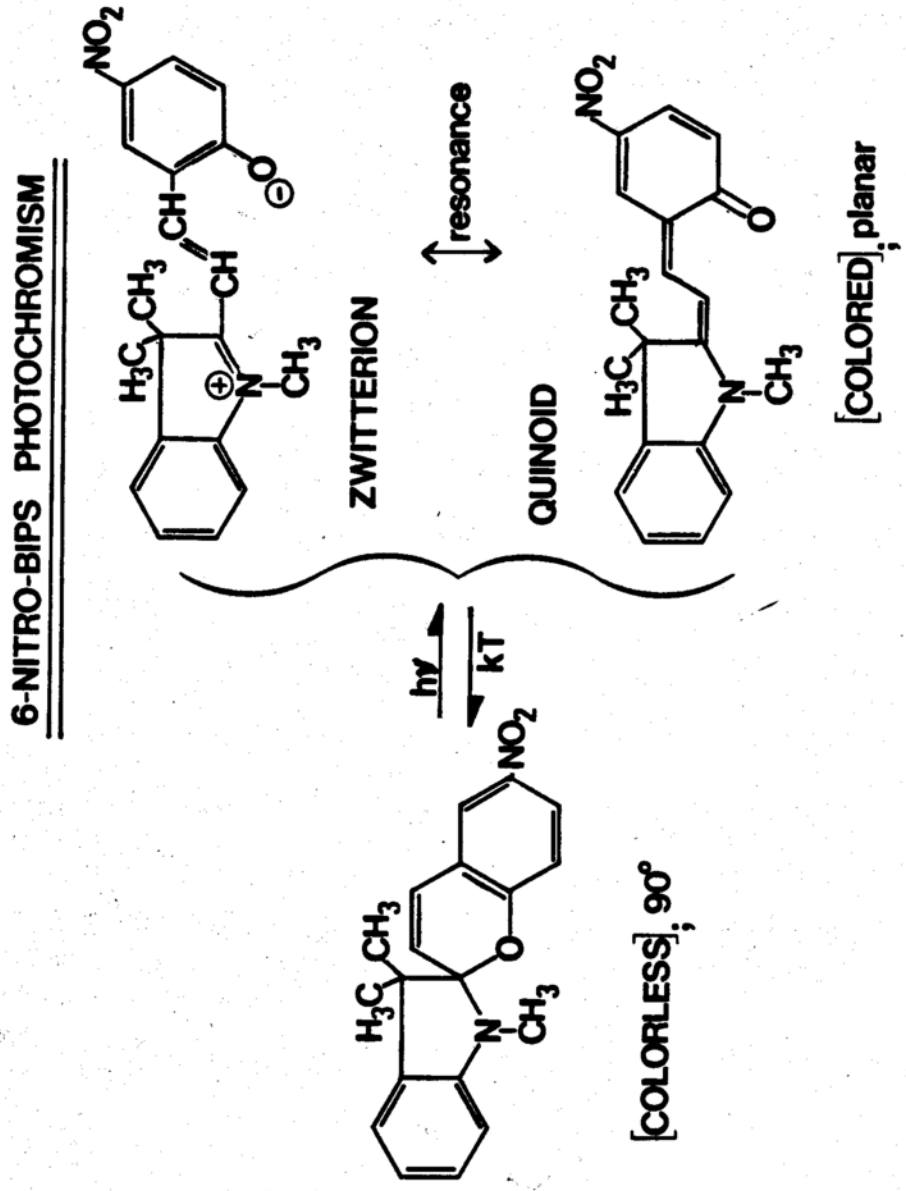

solutions from uv irradiation of 6-NO_2-BIPS in cyclohexane probably represent less than 1% colored form (1, 8). The quantum yield for 6-NO_2-BIPS photochromism was found to be 0.12-0.15 with 313-366 nm excitation (4). To obtain this figure, the absorptivity had to be estimated by the decreasing intensity of the uv peak at 265 nm. It was estimated at 2.4-4.8 x 10^4 liters/mole·cm. Flannery (8) estimated the same number to be between 3.5 and 5.2 x 10^4 ℓ/mole·cm. The absorptivity for INS, determined in a similar manner, was 6.5-8.5 x 10^4 ℓ/mole·cm (6). Thus it appears that the open forms of spiropyrans have absorptivities near those of indicators and dyes, and very little conversion is required to see the visual effect.

Experiments with NMR clearly show that the spiro structure exists in the colorless form only (1). There is chemical, spectroscopic, and kinetic evidence (1) that the colored form is zwitterionic, not a free radical. The photochemical reaction proceeds through both singlet and triplet excited states, lying 53-57 kcal/mole above the ground state (14). The reaction is clearly reversible, sometimes requiring only seconds between cycles (15). The rates of reversal can vary with temperature, giving rise to heats of interconversion of 3-7 kcal/mole (16).

The spectrum of the closed, colorless form in the ultraviolet region has been recorded by many researchers (1). The small amounts of colored form present have little effect on the spectrum. In nonpolar solvents, uv assays for spiropyrans follow Beer's Law (8). Each spiropyran has characteristic broad, smooth peaks between

250-350 nm, generally with absorptivities of 1-10 x 10^3 ℓ/mole·cm (1). This spectrum changes very little with changes in solvent; on the contrary irradiation to the colored form produces very different spectra in the visible region for different solvents.

The colored species presents many problems in obtaining its true absorption spectrum. Since the colorless form is more stable (8), by 1-3 kcal/mole in polar solvents and 5-8 kcal/mole in nonpolar solvents, one cannot obtain colored form in the pure state. Most spiropyrans fade thermally at a rate significant with respect to the time required to record the spectrum. Flash spectroscopy or rapid scanning spectrophotometers must be used, or the spectrum will need to be corrected for fading. The true λ_{max} will be shorter than the observed λ_{max} when recording via decreasing wavelength (1). Side illumination with constant uv light can also be used to record a photostationary state.

All spectral data to this date support the notion that the open, colored form of a spiropyran behaves like a merocyanine dye (17). Absorptivities in alcohols are reported to be 3-4 x 10^4 ℓ/mole·cm (18); efficiently absorbing spiropyrans such as 6-NO_2-BIPS exhibit absorptivities of 5.4-7.4 x 10^4 ℓ/mole·cm in toluene (19). An NMR spectrum of the irradiated solution reveals a downfield shift ($\sim$4 ppm) of the N-methyl group, reflecting the partial positive character of the indoline nitrogen in the zwitterionic form. If the colored solution is allowed to revert to its colorless modification, the N-methyl peak moves to approximate

that of Fischer's base (20, 21). Planar, heterocyclic dyes with cationic character and high absorptivities are also representative of the cyanine dyes (22). Cyanine dyes are generally symmetrical (23), with nitrogen atoms on either end of a conjugated chain system connecting two rings (24). The absorption of light promotes a non-bonding orbital electron to the lowest unoccupied molecular orbital, with little change in electron density in the excited state. Consequently, the cyanines have narrow absorption bands of high absorptivity, giving brilliant colors. Dyes such as Orange G (of the polymethine class) have chromophores strongly resembling those of open form spiropyrans (25). [Figure 9 illustrates this structural resemblance for BIPS and two cyanine dyes.]

More specifically, spiropyran chromophores mimic those of merocyanines, a subset of the cyanines in which one nitrogen is replaced by an oxygen atom (26). Brooker has written extensively on the properties of merocyanine dyes (26-29), whose coloration properties are important in photographic processes. In measuring the spectra of merocyanines at extremely low temperatures, it was discovered that they may exist in closed spiropyran-like colorless forms (30), though the conditions required can be extreme.

The pyran oxygen plays the role of the other electronegative atom in the spiropyran system (1). Merocyanines are generally neutral (24), as opposed to cationic cyanines. The zwitterionic nature of photochromically-induced merocyanines gives them the positively-charged nitrogen characteristic of the cyanine class, yet

maintains the overall neutrality of the merocyanine sub-class with the partially negative oxygen atom (31). Merocyanines are notorious for aggregating into stacks (28, 29, 31), and spectroscopic evidence indicates that these are J-aggregate stacks which can form quasicrystals (32, 33). J-aggregates, named for their initial observation by Jelley (34), exhibit red-shifted absorption and are arranged with parallel molecular dipoles in the stack (31). Merocyanine/spiropyran pairs can also exhibit H-aggregates, blue-shifted and with anti-parallel arrangement. In photographic emulsions, aggregated cyanines exist on silver halide surfaces after their adsorption from solution (35).

The addition of acid to an organic solution of spiropyrans has a profound influence on the absorption spectrum (1, 6, 7, 12, 36). The usual intense uv band decreases in intensity and shifts from 245 nm to 230 nm, and the visible peak broadens, weakens, and shifts 125 nm hypsochromically (1, 6, 7). 6-NO_2-BIPS forms a solid yellow salt when ethanolic solutions are treated with HCl (1). Infrared spectra identified two distinct products, both hydrogen addition cations. One form is the acidified analog of the closed species, with a quaternary nitrogen group resulting from protonation at the indoline nitrogen. The second form (produced by irradiating the first) is the analog of the open form, with the phenolate becoming a hydroxy group and the extra bond to nitrogen coming from the ring (1). The salt spectra from acidified spiropyran solutions are identical to those of acidified merocyanine dye solutions (6), stressing again

the structural and chemical similarities of the two groups. BIPS and INS spiropyran skeletons show acid λ_{max} of 480-490 nm, some being eradicated by strong visible light (36). These new structures with new spectra can be thought of as spiropyran-acid complexes (12).

Complexation is one method of "fixing" the photochromic reaction, or freezing it on the side of the colored form. Polymer films and viscous solutions also show the thermal fading recombination reaction (1), as does adsorption to a solid/solution interface (37). The complexation is a selective chemical reaction upon the reactive phenolate anion, present only in the colored form. 7-Cl-BIPS chelates divalent cations of copper, nickel, cobalt, and zinc to turn intensely red, the exact λ_{max} dependent upon the pH of the aqueous ethanol (15). Orange-red complexes of the same metal ions with 8-piperidyl-6-NO_2-BIPS demonstrated enhanced chelation ability under heat and light conditions expected to favor the merocyanine form (38). With other spiropyrans, red-purple complexes demonstrated a temperature dependence on their rates of formation (39). There seems to be little doubt that many of the spectral properties of dyes are also seen in solutions of spiropyrans.

3. Kinetics of Thermal Recombination Reactions

The reverse reaction to photochromic coloration, known as photobleaching or thermal recombination, can be spontaneous in the dark or induced by visible light. Regardless of the conditions, the mechanism is identical; the double bond in the conjugated chain

becomes cis, and the pyran ring reforms (1, 8). The long term kinetics of this reaction follows first-order kinetics, and can be studied in solution in ordinary spectrophotometers. Flash spectroscopy in viscous media at low temperatures show completely different behavior at short times.

A short flash of light is followed by the formation of several different colored species, which then approach a thermal equilibrium containing predominantly the single most stable isomer (1). Thereafter, the mixture approximates a single colored species fading to the colorless species, under first-order kinetics. In toluene at -30°C, 4 milliseconds after an ultraviolet light flash, 6-NO_2-BIPS shows a peak at 590 nm and shoulders at 560 and 630 nm (40). One of the colored species was shown to be the result of consecutive photoreactions (41), another was found to be the sole route back to colorless spiropyran (1). Other workers (7) noted the disappearance of the peaks depended on the temperature, some forms being stable at high temperatures only. On the basis of these data, a scheme was developed for the short-term kinetics of 6-NO_2-BIPS.

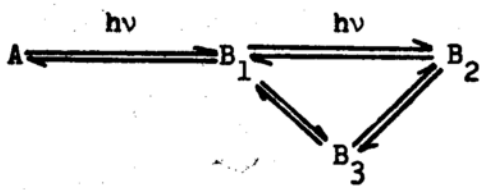

A symbolizes uncolored 6-NO_2-BIPS (1) and B stands for the three colored species. B_1 is the thermodynamically stable species

responsible for long-term first-order photobleaching, B_2 is a short-lived species produced by two photoreactions, and B_3 lives long enough to contribute to the fading in some solvents. The λ_{max} values for each isomer vary with solvent and temperature.

The long-term kinetics are governed by the disappearance of a single colored species unimolecularly (42). Often the semi-logarithmic plot is curved at early reaction times, especially at low temperatures (1). This is due in part to increased errors at early time points and in part to the kinetics discussed previously at short times. For the most part, the time frames of the two phenomena are such that one can be ignored when studying the other. Hirschberg studied the effect of visible light on the color eradication process. He found half-lives of 5-50 seconds for 5-OCH_3-BIPS colored form, with a dependence on the visible wavelength employed. Unsubstituted BIPS gave half lives of 10-1000 seconds in ethanol and toluene with wavelength and the presence of acids/bases as important variables (36).

Simpler studies discounting the effect of light show the good agreement obtained on assuming first-order recombination. Flannery (8) studied the decoloration of 6-NO_2-BIPS in ethanol at 28.8°C by following the disappearance of the visible peak at 535 nm. Studies in the absence of light readily reveal the role of the solvent in the kinetics of thermal decay. Table II lists the rate constants for first-order decay back to the colorless form along with the activation energy of decoloration as a function of solvent.

Table II. Kinetics of Thermal Decay of 6-NO_2-BIPS.

Solvent	$10^4 k_1/sec^{-1}$	$E_a/kcal \cdot mole^{-1}$
Ethanol	3.76	24.7
Acetone	47.3	23.9
Chloroform	133	23.3
Carbon Tetrachloride	211	16.2
Benzene	1120	16.5

(Ref. 8)

Obviously this rate is quite dependent on the nature of the solvent. It is normally found that the colored species fades about 10^2 times as rapidly in toluene as in ethanol (1). This is consistent with the view of the colored species as a zwitterion, the lifetime of which is related to solvent dielectric constant. Hydrogen-bonding alcohols stabilize the polar colored transient (8) so that it has a greater chance of being in the appropriate conformation to generate a pyran ring when the two point ions come close enough to react. Flannery has found three separate correlations for the observed rate constant with dielectric constant; one for hydroxylic solvents, one for polar aprotic solvents, and one for nonpolar aprotic solvents (8). Bertelson (1) has correlated observed fading rate constants for 6-NO_2-BIPS with Brownstein's S (43) and Kosower's Z (44) values of solvent polarity.

Spiropyrans with different structures fade at different rates. Generally, parent ring systems of BIPS and INS type spiropyrans fade faster than those of other skeletal structures (1). Within each group, the effect of substituents on the thermal stability of the colored transient can be significant (3). Berman, Fox, and Thomson (11) found rate constants from 6.33×10^{-6} sec^{-1} for 6-NO_2-8-F-BIPS to 1.32×10^{-2} sec^{-1} for 6-OCH_3-8-NO_2-BIPS in ethanol at 6°C. Bertelson (1) correlated the thermal fade rates with Hammett substituent constants for BIPS compounds in ethanol and toluene at 20°C. These linear free energy relationships show that electron withdrawing substituents (NO_2) accelerate the thermal fading

reaction, whereas electron donating substituents (NH_2, OCH_3) decelerate the reaction. It is concluded that a decrease in electron density of the reaction site favors recombination of the ring system.

In the dark, a spiropyran/solvent system reaches a thermal equilibrium. Equilibrium constants, defined as the ratio of colored to colorless form present, can be estimated by assumption of an absorptivity of the colored form through structural analogies. Bowman lists the equilibrium constants for 5,7-dichloro-6-NO_2-BIPS in toluene as a function of temperature (1). As expected from the discussion on thermochromism, a greater fraction of colored form exists at higher temperatures. Similar experiments in ethanolic solutions show that at any given temperature, the more polar solvent has a greater fraction of colored species. Bercovici et al. (7) list the percent conversion to colored form for five BIPS molecules at 0°C, 50°C, and 80°C. In a 1-propanol/2-propanol solvent mixture, 6-NO_2-BIPS was 0.0053, 0.0086, and 0.0126% converted at the three temperatures studied, respectively. They report that, in hydrocarbon solvents, the colorless form is favored by approximately 10^6:1. Flannery (8) estimated the equilibrium constants for 6-NO_2-BIPS at 25°C by comparing apparent Beer's Law slopes with estimated absorptivity. He also determined the dependence of the equilibrium constants on temperature, and calculated thermodynamic parameters. Table III gives the equilibrium constant and enthalpy change in four solvents, along with associated estimated

Table III. Equilibrium Data for 6-NO_2-BIPS at 25°C.

Solvent	$10^5 K$	ΔH°/kcal·mole^{-1}
Ethanol	843 ± 271	2.1 ± 0.4
Acetone	134 ± 43	1.8 ± 0.3
Chloroform	9.76 ± 3.15	0.52 ± 0.22
Benzene	4.10 ± 1.31	4.4 ± 0.4

(Ref. 8)

uncertainties after multiple determinations. Their estimate of 8.5 x 10^{-3} for K at 25°C is larger than the result of Bercovici et al., and corresponds to just under 1% conversion. This could be a reporting error by either author, since on a percent basis, the one result equals the other. Alternatively, the difference could be ascribed to different estimates of the extinction coefficient of the colored form. Lastly, the difference could be real, since Flannery's experimental procedures show no protection from light. A photochromic increase in colored form from room light could account for the higher constants he reports.

Theoretically, an infinite number of cycles between colored and colorless forms are possible. Practically, continuous exposure to ultraviolet light results in lessened capacity for conversion. Fatigue is defined as the decrease in difference between the absorbance of a photoexcited solution and a photobleached solution. Usually an increase in "background" absorbance is noted, with a consequential lessened increase in absorbance under ultraviolet light. Structure and fatigue are related; most spiropyrans can undergo 100-10,000 cycles before showing fatigue (1).

Total fatigue of a 6-NO_2-BIPS solution in benzene resulted in recovery of 96% of the starting material. Various salicylaldehyde, salicylic acid, and 1,3,3-trimethyl-2-(hydroxymethylene)-indoline decomposition products were isolated as nonvolatile substances (1). Later studies showed a release of carbon monoxide, carbon dioxide, formaldehyde, and phenol (45). Each of these isolated decomposition

products inhibits photocoloration of fresh 6-NO_2-BIPS, and were demonstrated to be formed by photooxidation. The presence of phenol and benzaldehyde (in toluene) is evidence that peroxide intermediates are involved. Aerated spiropyran solutions also showed electron spin resonance signals attributed to peroxy radicals (1). Electron withdrawing substituents, which show increased fatigue, stabilize the homolytic cleavage product (open biradical) (46). These radicals go on to react with oxygen to form peroxy radicals, well-established among merocyanine dyes. Thus, a constant bombardment with ultraviolet light ties up increasing amounts of the starting material in low probability, but irreversible, side reactions associated with decomposition, and ultimately, fatigue.

4. Solvatochromism

A number of species are known that change their spectra with an accompanying change in solvent. The aforementioned Z values of Kosower (44) are based on the change in frequency of a charge transfer absorption band of alkylpyridinium iodides with solvent polarity. Tetramethyl pyridine oxide compounds (TEMPO) also have visible absorption bands affected monotonically with solvent polarity (47). The phenomenon of solvatochromism is especially prominent among dyes (48), including the merocyanine dyes that are known to structurally resemble open spiropyrans (27, 28). Brooker (29) studied the effect of solvents on the spectra of merocyanine dyes, and concluded that there are significant differences between

specific merocyanine structures. Blue-shifting dyes, which show hypsochromic changes in λ_{max} with increased solvent polarity, correlate with the solvent polarity data of Kosower and others. Red-shifting dyes, which tended to be the more polar merocyanines, gave a different rank solvent polarity order. Transition energies plotted versus mole fraction in binary solvent mixtures usually result in sigmoidal curves. One composition usually elicits the highest apparent absorptivity.

Spiropyrans behave as expected, most of them showing gradual blue (hypsochromic) shifts with increased solvent polarity (1). The absorptivity usually decreases in the most polar solvents; exceptions to all of these observations are seen with some substituents. It must further be noted that solvent polarity changes will affect the fraction of colored species in solution (8), therefore apparent changes in absorptivity may not be real.

A number of researchers have tabulated transition energies for spiropyrans in different solvents, but few of these studies have been carefully done (1). 6-NO_2-BIPS was reported to give λ_{max} values of 523 nm in methanol and 616 nm in methylcyclohexane, with transition energies of 48-58 kcal/mole. 5,7-dichloro-6-NO_2-BIPS also gave hypsochromic shifts with increased solvent polarity, complicated by the appearance of additional peaks in solvents of low polarity (1). Namba and Suzuki (49) tabulated hypsochromic shifts exhibited by 1-(β-carboxyethyl)-3,3-dimethyl-6-NO_2-spiro [indoline2,2'-H-benzopyran] in water-dioxane mixtures. This

spiropyran had an absorption maximum at 600 nm in pure dioxane and at 528 nm in a solution of mole fraction water 0.88 (49). The absorption maxima of some of the BIPS compounds when expressed in cm^{-1} give reasonably linear correlations with Kosower's Z values or Brownstein's S values. Wavenumbers are directly proportional to transition energies via Planck's constant, but wavelengths are not, they are indirectly proportional via the speed of light.

It is evident from the amount and quality of the available literature that the spiropyrans have been characterized fairly well in solution. Their study was motivated by the search for transient imaging methods (National Cash Register) and flash blindness goggles for the battlefield (U.S. Defense Dept.). Eyeglasses which darken in sunlight contain similar photochromic compounds. It has also been observed that spiropyrans are surface-active (50), lowering the interfacial tension between benzene and water. They also tend to adsorb to solid-liquid interfaces, especially in nonpolar solvents onto hydrophilic absorbents which favor the open, polar species. Much less is presently known about the physical chemistry of this adsorption process, and the factors that govern the spectrum of the colored species once adsorbed (1).

B. Spiropyrans Adsorbed to Solid Surfaces

Preliminary investigations account for the bulk of the literature involving adsorbed spiropyrans. Generally, a system of spiropyran/solvent/adsorbent is prepared, and the resultant

adsorbate color is noted. If the adsorbent/solvent suspension is allowed to settle, it is seen that the solution phase has not changed, rather it is the adsorbate at the solid/liquid interface that has become colored. This adsorption-stimulated production of visible color has been referred to as "adsorptiochromism."

1. Qualitative Adsorptiochromism

Dibenzospiropyrans was observed to take on a deep violet color when adsorbed from benzene onto activated alumina or dried silica gel (51). β-Dinaphthaspiropyran adsorbed from xylene onto activated alumina yields an immediate bluish-green color (52). The addition of silica gel to a colorless solution of 6-NO_2-BIPS in cyclohexane produces a bright red adsorbate (53). Blue and violet colors result when silica and alumina are added to benzene solutions of substituted bis-spiro-2-pyrans (54). A more comprehensive study involving BIPS compounds was done by Bertelson; some of his results showing the profound effect of substituents on adsorption color are summarized in Table IV (1). Aside from the substituent effect, an effect is observed when changing the solvent. "Ground" on his table refers to the adsorption color produced in the absence of solvent, by grinding the BIPS with the adsorbent in a ball mill.

The adsorption colors have been shown to be due to the same chromophore responsible for the photochromic or thermochromic product (1, 55, 56), although not necessarily the same mixture of isomers. Bertelson found that if the suspensions were filtered

Table IV. Adsorption Colors of BIPS Compounds on Silica.

BIPS	Solvent	Adsorption Color
8-allyl	benzene	orange
	ethanol	yellow
5-Cl-8-OCH_3-6-NO_2	ground	green
	benzene	yellow-orange
6-OCH_3-8-NO_2	benzene	deep red
	ethanol	green
8-OCH_3-6-NO_2	benzene	deep red
	ethanol	red
	ground	purple
6-NO_2	benzene	red
	cyclohexane	bright red
	ground	red
	ethanol	(none)

(Ref. 1)

quickly and dried, the colored adsorbent (by virtue of adsorbed spiropyran) was very stable (1). He also found that the degree of hydration of the adsorbent was important; intensely dried adsorbents gave paler colors. Kortum and Bayer (57) also noted differences in the appearance of INS/adsorbent systems depending on the degree of drying the adsorbents (Al_2O_3, MgO, and NaCl) were subjected to.

Desorption can be achieved by washing the colored adsorbent with polar solvents such as methanol (52-54). The reversibility of the reaction is also demonstrated by the phenomenon of photobleaching (1, 53, 55). 6-NO_2-BIPS on silica gel gives a stable red color in the dark. Intense irradiation with wavelengths greater than 350 nm will cause the adsorbed spiropyran to revert to its colorless modification (55). Reversible photobleaching has also been reported for BIPS, 6-NO_2-8-OCH_3-BIPS, 5'-Cl-6-NO_2-BIPS, and 8'-NO_2-INS (1). Evans et al. (53) noted that the bright red color of 6-NO_2-BIPS (on silica from 5×10^{-4} M cyclohexane solution) developed full intensity in a few hours. The half life of coloration was 43 ± 5 minutes. Methanol could desorb the BIPS, and visible light (>350 nm) could completely photobleach the powder in 10 seconds. Subsequent recoloration in the dark began almost immediately; the color was restored with a half life of 41 ± 5 minutes, essentially at the same rate.

2. Quantitative Adsorption Data

Few quantitative studies on the sorption properties of

spiropyrans have been performed. Technical reports restricted from publication probably exist at Eastman Kodak, National Cash Register, and the U.S. Defense Dept. (1), though they may also be largely qualitative. The sole exception is some work done by Bertelson, who studied the adsorption of BIPS compounds onto silica gel and Attapulgus clay from benzene at 25°C (1). He found poor agreement with the Freundlich equation, but good agreement with the Langmuir adsorption model. Brown shows the linearized version of one of Bertelson's isotherms in his book (1), that of 6-NO_2-BIPS/benzene/silica gel. The concentration scale is unitless; if it is expressed in molar units it yields a binding constant of 74 M^{-1}. No indication of the grade, particle size, pretreatment, or source of the silica gel was given. Table V lists the estimated monolayer capacities found for various BIPS on the two adsorbents employed. Since the surface area and extent of drying of the silica gel is unknown, the usefulness of these figures is comparative only.

Bertelson also examined the rate of approach to equilibrium for the 6-NO_2-BIPS/Silica gel system. Figure 5 reproduces the experimental results. Note that it takes approximately 25 hours to reach one-half the value of the system capacity. This sharply contrasts with the observations of Evans et al. (53) with regards to half-lives of coloration for the same system. Apparently the system reaches maximum color intensity well before adsorption of spiropyran is complete, in fact it has barely begun. The rates of adsorption do not differ for experiments performed under uv light

Table V. Quantitative Adsorption of Spiropyrans[a]

Adsorbate	Adsorbent	Capacity[b]/(mg/g)
BIPS	Silica Gel	62
8-OCH_3-BIPS	Silica Gel	87
8-OCH_3-6-NO_2-BIPS	Silica Gel	53
6-NO_2-BIPS	Silica Gel	135
	Attapulgus Clay	23

[a]All determined from benzene at 25°C.

[b]Reference (1).

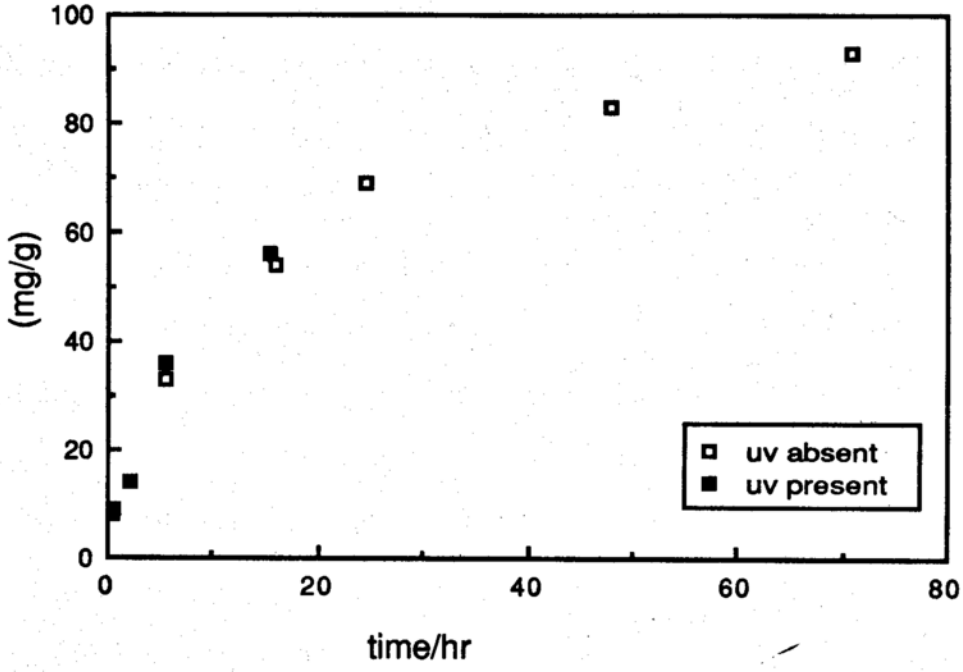

Figure 5. Adsorption rate of 6-NO_2-BIPS by silica gel from benzene, 25°C. Experiment performed both in absence and presence of ultraviolet light. Reference (1).

and in the dark. Additionally, the equilibrium isotherms coincide; a value of 128 mg/g was obtained for an isotherm obtained in the dark instead of in normal room light (1). Combined with previous estimates of the fraction of colored species in an irradiated solution, this supports the notion that the colorless species adsorbs to the interface, subsequently becoming colored. Irradiation reduces the amount of colorless spiropyran by only a few percent, but increases the amount of colored species in the nonpolar solvent by many orders of magnitude. Thus, if the colored species was primarily responsible for adsorption to the interface, a concomitant increase in the adsorption rate would be expected; this is not seen. Spiropyrans adsorb most strongly to hydrophilic adsorbents from nonpolar solvents. This suggests a "partitioning" or selective adsorption of the more polar colored species. It is now generally accepted that the first explanation, that the colorless species first adsorbs to the interface, is the more likely (1). Colorless spiropyran is adsorbed, and the surface acts as a strongly polarizing medium, shifting the equilibrium in favor of the colored form. Besides the adsorption rate evidence, the numerical superiority of colorless form in nonpolar solvents provides the greater driving force out of solution. Colored adsorbates are generated easily with adsorption in a ball mill, where primarily colorless solid spiropyran is ground together with adsorbent. Even in the absence of the reservoir of colored species available through equilibrium in the solution, color is generated rapidly and

completely (1). 3'-methylbenzo-β-naphthospiropyran and dibenzospiropyran are completely colorless in all solvents tested at all temperatures, yet still give adsorption colors immediately on silica gel and alumina (1, 51). The adsorbent is thought to act as an extremely polar solvent (1, 54), shifting the position of the equilibrium on the surface by stabilizing the colored form. In the same manner, colorless bases of malachite green and crystal violet become colored (as the dye salts) upon adsorption to silica gel and alumina (58). The adsorbates in this case are polarized by the strong dielectric present at the interface.

The adsorption process shows reversible character, as previously discussed, but is not experimentally quantitatively reversible. The fact that the desorption curves do not completely coincide with the adsorption curves may be attributed to degradation of the spiropyran on the silica surface (1). 6-NO_2-7-OCH_3-BIPS gave up its corresponding salicylaldehyde when chromatographed over silica without irradiation (46).

3. Behavior of Related Cyanine Dyes on Solid Substrates

Comprehensive studies of a number of spiropyrans adsorbed to well-characterized adsorbents are lacking, but as in solution, comparison to their cyanine dye analogs may be instructive. The adsorption of cyanine dyes has been widely studied, because of their use as sensitizers of photographic emulsions (59). Comparison of the data generated with the known solution chemistry of these dyes

leads to the conclusion that both molecular and aggregated adsorbed states exist (59, 60, 61).

Cyanines adsorbed to AgBr show absorption maxima in good agreement with those of the aggregated dyes in solution (59). Emerson et al. (60) examined a cyanine dye with particularly sharp, distinct absorption peaks using electron microscopy, x-ray diffraction, and absorption spectroscopy. This dye sensitizes silver halide microcrystals in photographic films so that the transparent crystals respond to light absorbed only by the dye. They were able to resolve separate peaks of the monomer, dimer, trimer and tetramer. They also observed fine structure due to the H-aggregate, a conveniently located methyl group inhibiting J-aggregation in this particular cyanine. Along with the x-ray crystallographic results, they assigned a deck-of-cards structure to the aggregate, with the long axis of the molecule perpendicular to the aggregate axis. Davey (61), working for Kodak, studied adsorption of cyanine dyes to AgBr/AgI mixtures. He found that the dye molecules are first adsorbed singularly, probably lying flat to maximize interaction with the surface. At higher coverages, as the surface becomes crowded, there is subsequent rearrangement to edge-on, close-packed arrangement suggestive of the solution aggregates. The light absorption characteristics of the packed layer are those of the aggregate, with a great deal of intermolecular interaction, and the nitrogen edge of the stack oriented towards the surface.

Herz et al. (35) found similar concentration-dependent spectral properties for 1-1'-diethyl-2-2'-cyanine (Pseudocyanine). It exhibits a monomeric band (523 nm), a dimeric band (480 nm), and a long wavelength J-band (570 nm) in aqueous solution. Adsorption to mica, silver, and silver halide surfaces resulted in changing ratios of the corresponding adsorbed species peaks with concentration. Maximum capacities suggested that the dye was adsorbed edge-on, with intermolecular spacings close to that of the J-band aggregate in solution (4 Å). Coverages exceeding 5% of the available surface area were necessary before the J-band appeared, the formation of the aggregates later suggested that dye-dye interactions outcompete dye-solid interactions. Cationic cyanines adsorbed to silver halide surfaces with the free energies of adsorption of 6-11 kcal/mole, following the Langmuir equation (62).

West et al. (63) also noted the Langmuirian adsorption of cyanines to photographic emulsions. They estimated heats of adsorption of 10-12 kcal/mole from isotherms at 40-60°C. Planar cyanines showed steep initial isotherms (high binding constants); oxacarbocyanines were less tightly adsorbed and showed cooperativity. They interpreted this to be the case for planar cyanines with first additions to the surface; for oxacarbocyanines the cooperativity became evident later once a critical concentration was reached. They envisioned the early molecules to be adsorbed flat, because of van der Waals forces contributing from the ring to the surface. With increasing coverage, the lateral interactions

strengthen and ultimately pull the molecules on edge.

The same research group also adsorbed some merocyanine dyes to photographic emulsions. One of the compounds studied, in particular, (3-ethyl-5- (3-methyl-2-thiazolinylidene) -ethylidene-rhodanine), had a chromophore much like an open BIPS molecule. It extends from a methyl-nitrogen in one ring, through a two-carbon chain of alternating double and single bonds, and terminates with an oxygen atom attached to a carbon in a ring system. They also showed simple Langmuir curves, with saturation values consistent with edge-on orientation. The absorption spectrum, however, showed no evidence of J-bands, which are not a prerequisite for edge-on parallel stacking. A single-reciprocal plot can be made by reading points from the plot in this paper; the resulting linearized Langmuir plot showed a correlation coefficient of 0.9998, and a saturation capacity of 3.8×10^{-6} moles/gram. The binding constant thus extracted was 8.05×10^{5} M^{-1} (quite strong), and from the surface area given, each merocyanine molecule occupied 58.5 A^2 of surface.

From the studies of cyanines and merocyanines, it seems reasonable to expect Langmuirian behavior for spiropyran adsorption. They may also yield concentration-dependent spectra, which could be interpreted as indicative of intermolecular interaction.

C. <u>The Spectra of Adsorbed Species</u>

Interaction with the adsorbent can alter the light absorption

spectrum of an adsorbate. More significant changes are seen with systems exhibiting chemisorption than with simple physisorption (64). Semi-solid systems will usually scatter some light, in addition to transmission and absorption seen also with solutions. To obtain the spectrum of the adsorbed species, the reference cell usually contains adsorbent to cancel out its contribution. One then need only attempt to minimize the scattering in transmission measurements or account for it mathematically in reflectance measurements. The difference in adsorbate spectrum before and after adsorption depends on the chemistry of the solid surface, and therefore can yield information about the properties of that surface (65-69).

1. Suspension Transmission Spectroscopy

Spectra of turbid slurries of adsorbate/adsorbent/solvent can often be taken in the ordinary transmission mode, and may be similar to the spectra of solutions of the adsorbate (1). Robin and Trueblood (70) have measured the ultraviolet spectra of organic molecules adsorbed on silicic acid. The close similarity of the refractive indices of silicic acid (1.420) and cyclohexane (1.426) render the solid essentially transparent in this medium. Spectrophotometric measurements down to 235 nm were possible before light scattering and refraction from slurry inhomogeneities increased the opacity of the system. Herz et al. (35) obtained transmission spectra of cyanines adsorbed to silver halides in

gelatin dispersions by utilizing adsorbates with high absorptivities and small amounts of adsorbent. Investigators in recent years have turned to microporous silica gels immersed in organic solvents of comparable refractive indices for transparency. The large surface areas (hundreds of m^2/g) are necessary to place sufficient absorbing material in the light path to rise clearly above the scattering baseline (71). Blue shifts were seen for substituted pyridinium iodides when compared to chloroform solution absorbances. Weis and Leermakers (53, 55, 71) have employed silica gel/cyclohexane slurries to study spectral shifts of adsorbates. Most of the compounds in which the silanol protons interacted with electronegative nitrogen atoms produced blue shifts upon adsorption (55). Removal of air bubbles, agitation to extend suspension time, and lack of significant desorption were cited as variables commensurate with successful reproducibility.

The adsorbed species spectra of spiropyrans on silica gel have been measured by this technique (53, 72). 5-Br-6-NO_2-8-OCH_3-BIPS spectra on silicas with different silanol contents were measured in thin cuvettes for a benzene slurry (72). Evans et al. (53) employed the technique of Weis and Leermakers (55) while studying photobleaching of 6-NO_2-BIPS adsorbed onto silica gel. Figure 6 reproduces their spectral tracings comparing the colored spectrum in methanol, the colorless spectrum in cyclohexane, and the transmission spectrum of the adsorbate on silica gel in a cyclohexane slurry. The smoothness and resolution of the peaks is

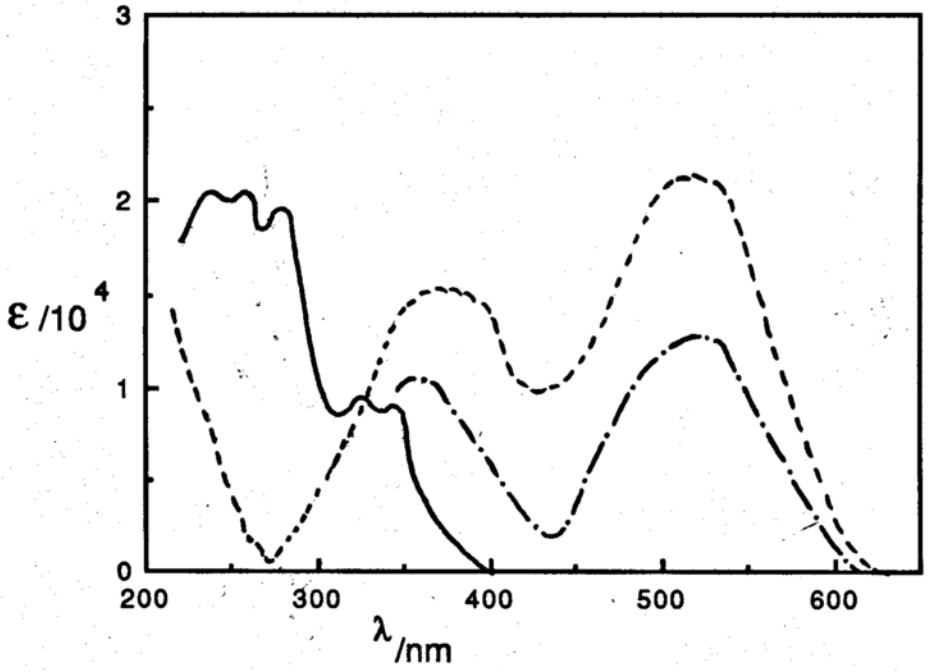

Figure 6. Ultraviolet/visible spectra of 6-NO_2-BIPS in methanol (—·—·), in cyclohexane (——), and in a slurry of silica/cylohexane (----). Reference (53).

as good in the slurry as in solution. Note the minima at 400-450 nm which seem to be characteristic of all BIPS spectra. The drawback to the method is that it is specific to a few adsorbents; it has received only limited use for silica type solids with the appropriate refractive indices.

2. Diffuse Reflectance Spectroscopy

A newer and more general technique for obtaining adsorbed substance spectra is that of diffuse reflectance spectroscopy; reviews by Wendlandt (73) and Kortüm (74) are available. The experimental equipment and actual procedures for measurement are set forth in less comprehensive summaries (64, 75).

Incident light striking a packed powder can be absorbed, transmitted, or scattered as reflection. Particles larger than the wavelength of light employed show much specular or mirror-like reflection. Smaller particles show predominately diffuse reflectance, or scattering at angularly independent intensities (74). Consequently a blue cupric sulfate pentahydrate crystal will become paler as its particle size is decreased via trituration; the absorption color lessens in proportion to the increased whiteness from scattering (76). It is this diffuse component, assumed isotropic, that is measured in diffuse reflectance spectroscopy after experimentally limiting specular reflectance. In closely packed layers, Mie's theories of single scattering fail. Interference patterns arise from multiple scattering. With

sufficiently thick layers, isotropic scattering is expected. Smooth, glossy surfaces have high amounts of specular reflectance, but rough, matte surfaces show primarily diffuse reflectance.

For a sufficiently thick layer with a large number of scattering particles, phenomenological theories are available that describe the scattering of closely packed layers. A random distribution of powders and diffuse incident radiation yields an isotropic distribution. Discontinuum theories model the scattering elements as spheres or layers (74), while continuum theories treat the layer as a homogeneous system (77). The theory of Kubelka and Munk is the most widely accepted description of the process and is easy to employ experimentally (64, 73, 76, 77). The optical properties of the medium are described by an absorption coefficient (k) and a scattering coefficient (s), constant throughout (73). Penetrating light must either be absorbed, or scattered back, and the flux in either direction can be reduced by either process. The derivation is simplified by assuming an infinitely thick layer, defined as that which eliminates the phenomenon of transmittance (76), easily satisfied in practice. Other assumptions include:

(1) Random particle distribution in the layer

(2) Particle size small compared to layer thickness

(3) Diffuse irradiation of the layer

(4) Isotropic scattering, allowing spectral components to be ignored

Reflectance can range from $R = 0$ (ideal black background, $k = \infty$) to

$R = \infty$ (ideal white background, $k = 0$). Experimental design provides the conditions of the assumptions, and all real systems fall between the two ideal conditions (74). Solution of the two differential equations of light flux at infinite layer thickness yields a solution in terms of measured R_∞ values. $F(R_\infty)$ is obtained through the Kubelka-Munk function, and depends only on the ratio k/s, not their absolute values (74). The Kubelka-Munk equation

$$F(R_\infty) = \frac{k}{s} = \frac{(1 - R_\infty)^2}{2R_\infty} \qquad (1)$$

effectively converts R_∞ readings into the analog of absorbance, discounting for the scattering. The values obtained experimentally are relative to the standard used (R_∞'), not absolute. They can be corrected to absolute measurements through multiplication by known MgO reflectances (78) from freshly burned magnesium ribbon. This is the most ideal white substance known, though since it must be prepared fresh, $BaSO_4$ is often used in the experimental equipment as a highly reflective coating (74). Reproducibility of 1-2% is easy to achieve, consequently a variety of white standards can usually be regarded as totally reflective, and correction with MgO is rare (64).

Infinite layer thicknesses can generally be obtained with 1-2 mm path lengths, though finer-grained Aerosils can require up to 1.0 cm (64). If regular reflection (specular) can be minimized to $\leq$ 2%,

plots of $F(R_\infty)$ for theory versus $F(R_\infty)$ by experiment are linear, with slope 1.0, up to $F(R_\infty) \approx 10\text{-}20$ (74). At higher "absorbances" deviations arise due to irregular packing density, nonisotropic scattering, loss by internal scattering, and increased proportions of specular reflection. In regions where $F(R_\infty)$ is proportional to k, the so-called "typical color curve" for the substance can be obtained. This refers to a spectrum with the same general shape and λ_{max} as in solution for molecules unperturbed on the solid. In order to satisfy this, all of the assumptions of the Kubelka-Munk theory must be valid, and s must be independent of wavelength. Coarse powders meet the second condition, whereas finer powders often show an increased scattering coefficient in the ultraviolet, distorting this portion of the spectrum (64). The Kubelka-Munk function has been confirmed by using colored glass beads (79). The typical color curve of the beads was obtained through transmittance measurements and converted to absorbance units. Reflectance measurements of the triturated glass powder versus colorless glass reference powder were converted to $F(R_\infty)$ vs. wave number in cm^{-1}. Parallel shifts in the ordinate axis were able to bring the two spectra into superposition.

The practical method for eliminating regular reflection and satisfying the requirements of the Kubelka-Munk function is called the dilution method (64). The sample under investigation is diluted by grinding/mixing with the non-absorbing white standard and measured versus the white standard as a reference. At sufficient

dilution (1:100-1:100,000) both cells have the same surface geometry and particle size, and regular reflection cancels. Kortüm and Schreyer (80) studied the spectrum of anthraquinone in alcoholic solution and adsorbed on NaCl. The reflectance spectrum of the pure anthraquinone solid bears little resemblance to that in solution, particle size effects and specular reflection distorting it. Adsorption onto NaCl and mixing were accomplished in a ball mill, the reflectance spectrum being measured versus pure NaCl. With increasing dilution, the peaks become sharper and more akin to the solution spectrum until below 3×10^{-4} mole fraction, when the spectrum becomes independent of dilution. The advantages of the dilution method are that R_∞ can be shifted to the lower-error mid-range values, s is given by that of the diluent, regular reflection cancels, and the particle size dependence of k is eliminated.

In a series of powders with increasing amounts of adsorbate, a plot of log $F(R_\infty)$ vs. λ shows parallel curves corresponding to shifts along the ordinate at low concentrations. Kortüm shows this for flavazin adsorbed on starch (74), and cautions that at higher coverages interactions between adsorbates introduce spectral changes. With a high standard surface area and low coverage, $F(R_\infty)$ is proportional to concentration:

$$F(R_\infty) = \frac{k}{s} \quad \alpha \quad \frac{\varepsilon c}{s} \qquad (2)$$

At higher coverages, this linearity fails, as does the Beer-Lambert law in high solution concentrations. The linearity is valid at any wavelength, but different slopes are obtained. This is analogous to the wavelength dependence of absorptivity in Beer's Law. The deviation limit is usually around 10^{-3} mole fraction adsorbate, and is thought to be part of the approach to saturation of the surface (64), when adsorbates are forced into proximity. Kortüm and Dalkrug (81) have used the point of curvature to estimate surface areas of NaCl, claiming accuracy approximately the same as the BET method. Diffuse reflectance spectroscopy is quite sensitive for low coverages of adsorbate and can be used for quantitative analysis. The standard deviation of the method can be as low as 1-2% in sample analysis at constant particle size, moisture levels, temperature and wavelength (74).

Most commercially available spectrophotometers have optional attachments for applying this method. These integrating spheres are coated internally with $BaSO_4$ and focus light scattered from all directions to a photomultiplier. Reading error for the R_∞ value is generally 0.2%, leading to 1-2% error in the function $F(R_\infty)$. The error increases for R_∞ approaching 0 or 1, so mid-range measurements are optimal. The sample preparation should be standardized, using either a constant ball mill grinding time or isothermal solution adsorption in excess of the equilibration time. The sample must have physical homogeneity, it should be well mixed, and the packing density should be standard. Condensation on powders decreases the

refractive index and hence the scattering coefficient, therefore $F(R_\infty)$ increases. Moist samples appear darker than they are, so samples should be thoroughly dried and protected if hygroscopic. Water insoluble white standards such as silica gel minimize the moisture effect.

Diffuse reflectance spectroscopy finds a wide variety of applications in situations where absorption by standard techniques fails. The paint/pigment industry uses it extensively, since the color an eye sees is a function of both spectrum and scattering coefficient. Ferric oxides can be brown, red, black, yellow or orange depending on the oxidation extent and the crystal size and structure (74). When the Kubelka-Munk expression is valid and the dilution method is used, spectra of multi-component pigments are additive and contain isosbestic points. In the study of adsorbed molecules, low coverage yields the spectrum of the isolated adsorbed molecule. Chemisorption reactions limited to monomolecular adsorption are especially instructive to study via this technique. Kortüm, Vogel, and Braun (82) studied the acid-base reaction of DMAB (dimethylaminoazobenzene), which changes from yellow to red as it adsorbs to silica gel. Water is a stronger base and in humid air gradually displaces DMAB and leaves the surface yellow. Kortüm et al. (83) studied the photochemical fading of a substituted pyridine adsorbed on silica or MgO. The photo-induced blue color fades too rapidly in solution but its kinetics are slow enough to study conventionally in the adsorbed state. Other uses include the study

of cleavage at the surface of malachite green lactone (84), analysis of dyes adsorbed to thin-layer chromatography plates (85), fermentation process control (86), and study of cyanine adsorption in photographic emulsions (35).

The use of this technique in the pharmaceutical industry has not been as widespread, though some accounts exist. It has been used to study first-order fading of a red dye in lactose tablets as a function of light, concentration and time (87). Italian researchers have used diffuse reflectance to analyze for cimetidine in the presence of excipients (88). It can be an aid in tristimulus color determination of solid dosage forms and color matching of table or ointment dyes (89).

Kortüm and Bayer (57) have published the only reflectance spectra of spiropyrans in the adsorbed state. They published the spectra of INS on Al_2O_3, MgO, and NaCl. They report the heterolytic cleavage at the surface (chemisorption) to an extent not seen in solution. Moisture had a significant effect on the spectra, and the adsorbents had to be desiccated thoroughly. They assigned a new band seen at 20,800 cm^{-1} to a salt-like compound, in which the lattice cations protonate the phenolate portion of the zwitterion. They postulated side-by-side adsorption of the "free" INS and the "cation" INS, both of which reached saturation $F(R_\infty)$ values.

D. The Adsorbent Surface

The nature of the solid surface determines whether or not a

given molecule will adsorb to it. High specific surface area, polarity, and insolubility in cyclohexane are prerequisites for finding an adsorbent suitable for studying the adsorptiochromism of spiropyrans. A summary of some of the chemical properties of adsorbents fulfilling these requirements follows.

1. Silicas

The classic treatise on silica chemistry is that of Iler (90), which summarizes most of what is known about its surface structure. Crystalline silica can be quartz (stable below 870°C), tridymite (stable up to 1470°C), or cristobalite (stable above 1470°C). Crystalline silicas are water insoluble below 150°C; amorphous silicas are minimally water soluble. Soluble silicates can be orthosilicates (no silica bound to each other), metasilicates (each Si linked to two others through oxygen) or complex polysilicates. Silica generally refers to silicic anhydride (or silicon dioxide, SiO_2). Silicic acid is essentially hydrated silica (55), and is formed by equilibrating SiO_2 with H_2O (90). Mono-silicic acid, $Si(OH)_4$, is formed in the process, though commercially available silicic acids usually contain some metasilicates as well. Particle sizes are generally less than 100 microns, and surface areas can exceed 500 m^2/g (55).

Mono-silicic acid ages in aqueous solution to form polymeric silicic acids as silanol (SiOH) groups condense to form siloxane (Si-O-Si) groups. The silanols are acidic, the Si-O attraction

being stronger than the O-H attraction. The silanol groups dissociate in aqueous solution to produce a pH of 4.6 (91). In acidic solution, the silica polymerizes to silica gel, as primary particles stick together to form porous networks. In alkaline solution, when the silanols dissociate and charged particles result, the primary particles remain discrete and colloidal silica is formed (90). Fumed silicas are colloidal silicas of millimicron particle size formed by burning $SiCl_4$ with H_2 and O_2. Fumes are collected on a cool plate after reaction at 1800°C. The cooling is too rapid for crystalline positions to be assumed, hence the product is amorphous. Aerosil (Degussa) and Cab-O-Sil (Cabot Corp.) are the commonest fumed silica brand names used in industry. Alkali sols of colloidal silica are stabilized by the negatively charged particle repulsion. Gel formation in acid solution can be followed by viscosity increases over time. First, spherical primary particles form as siloxane linkages are made. In acid solution, collision results in condensation bridges between particles, resulting in a tangled network of branched chains throughout the medium. Drying the gel leaves pore space and shrinks the network. The enormous surface areas of silica gels implies very thin walls separating the pore spaces (92). Using a specific gravity of 1.9 for silica and a surface area of 300-400 m^2/g, it has been calculated that the walls are, on the average, two silicon atoms thick. The open skeleton structure probably has thick bases near the center of the primary particles and walls only one atom thick near the outer surface (92).

Closest neighbors in the silica particle are approximately crystalline, distant neighbors are random (90). Approximately 8 Si atoms exist per square millimicron; fully hydrated surface has one -OH for each Si atom. The interior atoms satisfy their valences with neighboring O and Si atoms, but those at the surface are unsaturated. Water adds to the reactive surface as tetrahedral silicon strives for complete coordination. The proton of water adds to the exposed oxygen atoms. the hydroxy group adds to the Si, resulting in a completely hydroxylated surface. A continuum of hydration degrees between fully hydrated and fully dehydrated is possible.

Dehydration of silica gels begins with the removal of physically adsorbed water by drying at 110°C. Water remaining beyond this temperature is present as a monolayer of "bound" hydroxyls, and the amount is proportional to gel surface area (90). From 110°-600°C, water evolves from the dehydration of surface Si-OH groups. Above 600°C, the last 5.4% of water weight is removed with sintering and loss of surface area (93). Infrared spectroscopy has identified three types of silanol groups (94, 95). There are the free, isolated -OH groups absorbing at 3750 cm^{-1}, and hydrogen bonded groups downfield and broadened at 3650 and 3550 cm^{-1} (94). This is interpreted as a hydrogen bonding effect. In addition to the free -OH groups, adjacent -OH groups can interact. Thirdly, there are the siloxane linkages, which can hydrate to form silanols reversibly.

The free hydroxyl groups are thought to be responsible for specific adsorption (94). The remaining hydroxyl groups account for less specific, general adsorption. The most strongly adsorbed compounds are those which are capable of acting as proton acceptors (70) in hydrogen bonds. Adsorption of organic compounds usually depends on the attraction of O and N containing polar groups to the silanol surface (90). A large number of such groups in one molecule strengthens the bond. Nonpolar solvents should be used if competition for adsorbate sites by water exceeds the binding strength of the adsorbate under study (55). There is an approximate Gaussian distribution of energy sites on the surface. Low energy sites contribute little to analytical separations, and the high energy sites are usually associated with water. The "middle activity" sites are the most numerous and important analytically (93). Methyl red has been used to measure the "specific hydroxylated surface area" of silica gel in aqueous solution (96). This gives a more realistic measure of surface area than the BET method, which is done on the dry solid. The competition of water with methyl red for adsorption sites is readily seen on comparing the capacities of silica gels stored at different relative humidities.

Hydrophobic silicas are commercially available, these are formed by reacting the surface silanols to form esterils. Not all of the silicon atoms can be reacted because of steric hindrance (90), but Si-O-R groups profoundly affect the adsorption properties

of silicas. Heating the silicas with alcohols (R-OH) results in chemical bonding of the alkyl (R) group, which will not desorb in vacuum as will adsorbed H_2O. The lack of ability to adsorb methyl red indicates a high degree of alkylation, since it adsorbs only to hydroxylated regions (90, 96). Aerosil-R972 is a commercially available example of this class of silicas which is completely methylated due to the small-sized R group.

2. Alumina

The chemistry of alumina and its various hydroxides has been reviewed recently by Misra (97). Alumina (or aluminum oxide, Al_2O_3) is the only stable oxide of aluminum; it is a hexagonal crystal system referred to as corundum. Rubies and sapphires are colored varieties of corundum. Corundum is the final dehydration/thermal decomposition product of all aluminum hydroxides. The lattice is best described as composed of hexagonal closely-packed oxygen atoms with aluminum ions in two-thirds of the interstitial spaces, or as an assignment of alternating oxygen and aluminum layers (97).

Bauxite ore is the chief source of alumina raw materials. It is refined to remove impurities and precipitated to form aluminum trihydroxide (gibbsite). Dehydration in the temperature range of 250-800°C results in alumina. The water driven out leaves a highly porous, high surface area "activated" alumina. Dehydration above 1100°C would form alpha-corundum, the truly anhydrous version with

delta x-ray diffraction patterns (97). Transition aluminas are formed by dehydration at lower temperatures, and are given the gamma designation though the diffraction patterns are less defined. The transition aluminas generally have a low degree of crystallinity but are useful adsorbents and catalysts.

Nitrogen adsorption has been used to study the development of the pore-like structure of alumina upon dehydration of aluminum hydroxides. $Al(OH)_3$ of 2 m^2/g lost H_2O weight of 8% in heating to 400°C, when the surface area peaked at 350 m^2/g (97). As with silicas, further heating reduces the surface area, which gradually decreases over the temperature range 400-1200°C. The highest surface area corresponds to 0.5 moles of H_2O per mole of Al_2O_3. The specific hydroxide starting material and drying characteristics determine the final pore size distribution of the alumina obtained.

Peri and Hannan (98) studied the hydroxyl groups on gamma alumina, finding water evolution even beyond 1000°C. Infrared peaks for adsorbed free water disappear after heating to 400°C. The infrared absorption peaks decreased in intensity but became more defined with further heating. After evacuation at 650-700°C, three well-defined maxima existed at 3698, 3737 and 3795 cm^{-1}. All three peaks correspond to hydrogen atoms which are exchangeable for deuterium. The resultant frequencies all change to 2700-2800 cm^{-1}. The peak at 3698 cm^{-1} was found to be the most "acidic" in hydrogen exchange. Burwell (99) studied gamma alumina of 120-140 mesh cut and a surface area of 160 m^2/g from American Cyanamid Company. It

was a loose-packed bed of 10 nm primary particles with fully hydroxylated surfaces. The hydroxyl groups disappeared and partial conversion to delta alumina was seen in heating to 950°C.

The pH of the hydroxide solution can be adjusted before dehydration to the aluminum oxide, resulting in different surface character. Neutral activated alumina is produced from pH 7.0 slurries, and its adsorbent uses are primarily for neutral organic compounds. Basic alumina can be made from a pH 9.5 slurry; its cation-exchanging properties make it useful for adsorbing basic substances. Similarly an acid-washed alumina (pH 4.5) is used to separate acids, and has good anion-exchanging properties. Alumina is inert to most gases, and has been used to dry them commercially (97). Other uses include drying of solvents, water purification, color and odor removal, and chromatography. Activated aluminas contain both Lewis acid (Al^{+3}) and Lewis base (O^{-2}) sites, and can adsorb most organic compounds. The activity of chromatographic alumina is usually reported by grades, the number referring to an empirical test of water adsorption. The highest activity, Brockman grade I, is seen with aluminas having a high level of dehydroxylation (100).

3. Other Adsorbents

The surface of titanium dioxide has been well studied, and the current status of research has been reviewed by Parfitt (101). Both common forms, rutile and anatase, have six oxygen atoms surrounding

each titanium at the corners of the octahedron and three titanium atoms around each oxygen somewhat like an equilateral triangle. Anion impurities from the production process may still be present, and these can alter the surface chemistry. Infrared data show the existence of hydroxyl surface functions, 12-14/nm^2 on anatase at theoretical saturation. Heating removes hydroxyls, and rehydroxylation is often incomplete, suggesting partial stabilization of the oxide surface. Cycling hydroxylation/dehydroxylation processes show an ever-decreasing temperature for hydroxyl removal; eventually no specific -OH sites form and the surface becomes an electron acceptor with incompletely coordinated titanium present.

The TiO_2 surface is amphoteric; terminal hydroxyls bound to one titanium are basic, bridged hydroxyls bound to two sites are acids (101). The Langmuirian adsorption of NaOH showed that half the hydroxyl had a pK of about 2.9, the rest had a pK of 12.7. The bridged hydroxyls showed an infrared peak at 3700 cm^{-1}, the hydrogen-bonding terminal hydroxyls absorbed at 3670 cm^{-1}. CO_2 adsorbed preferentially to the more basic bridged hydroxyls, but both exchanged with deuterium equally. The two different hydroxyls result in two different titanium atoms, only one acidic enough to interact with pyridine vapor. Anatase showed a point of zero charge of 6.2 and an isoelectric point of 6.1.

Esters can form with the reactive hydroxyl groups as on silica. H_2O vapor also reacts with the surface; after complete hydroxylation

via dissociative adsorption, molecular water may adsorb on the surface. The extent of H_2O adsorbed and the presence of impurities both strongly affect the physical adsorption of adsorbates to the surface. Adsorption heats are higher on anatase than on rutile TiO_2. The anatase surface has been shown to be 12% covered with high energy sites, which may be a certain crystal face and can be removed with x-rays. Titanium dioxide is used extensively for its opacity effect in pigments, though anatase forms which are of small particle size and do not agglomerate are available (102) for other uses.

Talc is a native, hydrous magnesium silicate or soapstone often mixed with some aluminum silicate (103). USP Talc is a finely powdered mica silicate (90) treated with boiling dilute HCl, washed, and dried. It appears as a fine white or grayish crystalline powder free of grit that adheres to the skin and other surfaces. Coarser talc is used as a filtering medium and is reputed to pose little danger of adsorption and retention of active ingredients (103). It is certainly less adsorptive than silica gel or alumina, in part due to its lower specific surface area. The milled product can have particles less than 0.5 microns in diameter (90), but the solid is not as porous.

Microcrystalline cellulose is prepared by hydrolyzing wood pulp (containing fibrils of β-1,4-glycosidic linkages) to its constituent microcrystals, then allowing them to aggregate (104). The product is insoluble in water and most organic solvents, and slightly

soluble in NaOH solution. It produces a pH of 5.5-7.0 when dispersed in water. It is purer and retains less moisture than other forms of cellulose. The reaggregation of suspended microcrystals (hundreds of times longer than they are wide) has been likened to a pile of randomly associated matchsticks. The internal pores can be on the order of 10-100 Å. A degree of polymerization of 200-300 with a fairly narrow distribution is achieved. The surface of the microcrystals is covered with free hydroxyl groups, though not as densely as silica since the unit glucose residues are much larger than atomic size. Commercial products such as Avicel form viscous colloidal dispersions in water, where the viscosity is highly pH-dependent, maximizing at pH 10.0. The particle sizes in such preparations average 10-100 microns. They have been used to control rheology, add fiber to food, stabilize emulsions, lubricate tablets, and increase powder flow (104).

E. Langmuirian Adsorption

Adsorption from solution to the solid/liquid interface can follow a number of functional forms when its extent is examined as a function of concentration. Langmuir adsorption is characterized by a monotonic increase in amount adsorbed going toward saturation, following a hyperbolic curve. The theory was first developed for adsorption of gases onto dry solids (105), but is often applicable in solution for chemisorption or ion-exchange processes where saturation of sites is expected. It assumes that no

lateral interactions take place between adsorbed molecules, the adsorbed layer is an ideal monolayer, covered sites have no more influence on the process, the surface is largely homogeneous, and adsorbed solvent takes up the same area as adsorbate if competition exists (106). Derivations based on equilibria or statistical thermodynamics have been published elsewhere (105); all give a two-parameter model of hyperbolic shape. Plots of the amount adsorbed per unit weight of adsorbent versus pressure or concentration of adsorbate are shaped by the two parameters defining the system. The affinity or binding constant (K) reflects the tendency to adsorb relative to pure solvent wetting the surface, whereas the capacity (in units of maximum amount of adsorbate per weight adsorbent) is a measure of saturation coverage. If x represents the amount of solute adsorbed by a weight m of adsorbent, and the amount bound is determined by the difference in solution concentration before and after equilibration, the Langmuir adsorption isotherm can be expressed by:

$$\left(\frac{x}{m}\right) = \frac{K(x/m)_{max}\, C_{eq}}{1 + K\, C_{eq}} \qquad (3)$$

where C_{eq} represents the concentration of adsorbate at equilibrium (107). K is expressed in reciprocal concentration units (the choice of units for C_{eq} lies with the experimenter), and the capacity, $(x/m)_{max}$, will be in the same units used to express (x/m). If

the adsorbent surface area is known, (x/m) can be expressed per m^2 of surface area, and molar amounts can also be substituted for gravimetric units.

In practice, the two constant parameters are extracted from the data through the use of linear plotting forms of equation (3). There are a number of different manipulations that can transform the Langmuir expression (or any rectangular hyperbola) into a linearized form (108). Equation (4) is the double reciprocal or Lineweaver-Burk plot, popular in enzyme binding studies.

$$\frac{1}{(x/m)} = \frac{1}{K(x/m)_{max} C_{eq}} + \frac{1}{(x/m)_{max}} \qquad (4)$$

Plotting $1/(x/m)$ versus $1/C_{eq}$ yields capacity as the reciprocal of the y intercept and K as the ratio intercept/slope. The single reciprocal or Scott plot of equation (5) is the usual form in adsorption studies.

$$\frac{C_{eq}}{(x/m)} = \frac{C_{eq}}{(x/m)_{max}} + \frac{1}{K(x/m)_{max}} \qquad (5)$$

Plotting the left hand side versus C_{eq} gives a good estimate of capacity (1/slope), which then permits K to be extracted from slope/y intercept. In the double reciprocal plot, the capacity was obtained from the less exact estimate of the y intercept, or confounded with K in the reciprocal of the slope. The Scott plot

allows a fairly accurate assessment of the saturation coverage of adsorbate. The Scatchard plot, equation (6), is a non-inverted linear form in y.

$$(x/m)/C_{eq} = -K(x/m) + K(x/m)_{max} \qquad (6)$$

It is the most sensitive to curvature since -K is equal to the slope. Any heterogeneities in the surface will be reflected by a changing value of K, high energy sites showing steeper slopes than lower energy sites. A perfectly linear Scatchard plot would indicate sites of equal binding energy, and is seen mostly in simple stoichiometric complex binding. A perfect hyperbola shows slight deviation near low values of (x/m) due to rounding errors, and even data which appear to be excellent via the Scott plot often show considerable curvature in the Scatchard plot, as a consequence of experimental error.

Most researchers will vary either the amount of adsorbate or the amount of adsorbent and measure binding differences by the change in surface concentration. Phase separation can be achieved either through centrifugation or filtration, after which C_{eq} is measured for the filtrate or supernatant. Recommendations for measurement techniques and data treatment were recently passed by the International Union of Pure and Applied Chemistry (109). Adsorbent swelling, filter and vessel wall effects, solvent evaporation, and surface heterogeneity are cautioned against.

Langmuirian adsorption on silicas has been commonly reported (110, 111), for both organic liquids and more polar solids. Many cases of cationic dyes adsorbed onto silicas, or cyanine dyes adsorbed onto silver halides, also show Langmuirian behavior (112, 113, 35, 62, 63). A photochromic azo dye showed adsorption characteristic of this model in both the light and the dark (114). It is certainly not surprising that the lone isotherm determined for a spiropyran on silica gel also fits the Langmuir model (1).

II. INTRODUCTION TO THE PROJECT

The spiropyran literature is quite extensive in certain areas, such as the photochromic effect, the solvatochromic effect, or the general solution chemistry of the family. This is the logical place to begin when new compounds are developed; many of the applications for spiropyrans depend on their chemistry in solution. The physical chemistry and behavior of spiropyrans at the solid/liquid interface has only been explored qualitatively. Observations regarding the general adsorptiochromic effect from nonpolar solvents onto hydrophilic solids have been recorded. A few rough isotherms on poorly characterized solids exist in the literature (1), the author of these admitting their preliminary nature and addressing the need for more comprehensive studies in this area. The present project is intended to provide some of this information.

The unique chemistry of the spiropyrans promises phenomena to observe beyond quantitative isotherms. The qualitative observations generated by a few researchers have shown that the choice of adsorbate, adsorbent, and solvent can produce almost the entire spectrum of visible colors. Possibly the properties of the solid surface promote heterolytic cleavage of the adsorbed spiropyran to

produce the colored form. Chemisorption may then be a stabilization method for the chromophore, favoring the open species and altering the equilibrium from that of the solution.

The reason for the appearance of a wide array of colors from a few simple substituted BIPS compounds is unknown. It is obvious that changing the substituents on the aromatic ring influences the spectrum of the adsorbed species. The small number of studies and differing pretreatments thus far leave the question of adsorbent effect on color open. The solvent in competition with the adsorbate may also have an effect on the resultant spectrum. It remains to be investigated whether the color differences are specific interactions between spiropyran and surface or a continuum of spectral shifts analogous to the solvatochromism exhibited in polar solutions. Quantitative spectra, rather than qualitative color observations, are needed to answer that question.

Cyanines and other dyes show Langmuirian adsorption behavior. Preliminary studies indicate that this is also true for spiropyrans adsorbing to polar solids. Comprehensive studies performed in the same laboratory, with the same batch, are needed to verify this on well-characterized solids. Constant pretreatment conditions, solvent, and technique applied to adsorbents of known surface area should clarify this matter. The effect of the solution equilibrium on the binding constant may be observed, especially in temperature-dependent binding studies.

The spectral properties of spiropyrans are very much a function

of their environment. Solution spectroscopy has demonstrated their dependence on polarity and acidity. Adsorbed spiropyrans may be excellent probes of the solid/liquid interface for this reason. The differences in spectra may be traced ultimately to different properties of the interface. The stabilizing effect of the solid substrate on the colored form in the equilibrium suggests the possible use of the adsorbed form as an analytical tool. The specific interactions responsible for binding could form the basis for colorimetric detection of species with the appropriate functionalities. Analyses for metal ions already exist based on these principles using spiropyrans (15, 38, 39); other means of "fixing" the visibly absorbing form might be found.

The approach to this project's objectives will be achieved through two basic types of studies. A number of BIPS compounds will be synthesized and purified in order to compile a data base for adsorption to different interfaces. Adsorption to solids of known surface area will be accomplished by using the difference in solution concentration method, employing filtration for phase separation. Quantitative isotherms will be produced to verify the type of adsorption and produce inferences about surface orientation. Both the effect of changing the adsorbent and the substituents on the spiropyran will be examined. The minimum surface area or structural requirements of the adsorbent will be determined which are necessary for measurement of quantitative adsorption. Spectral studies will account for most of the remaining experiments. The

methods of suspension transmission spectroscopy and diffuse reflectance spectroscopy will be explored. Once a number of spectra have been produced, it may become clearer whether the colors reflect specific interactions (such as hydrogen bonding) or a solid phase "solvatochromism." Normal dyes as well as spiropyrans will be studied on some surfaces, in order to gauge the influence of the pre-adsorptive equilibrium and to test the existence of a post-adsorptive equilibrium. The concentration effect on these spectra may exhibit characteristics of aggregating adsorbates, as with the cyanine dyes. Relationships between the adsorption parameters and the spectra may emerge. The technique of diffuse reflectance spectroscopy, little used in the pharmaceutical industry, will be extended by these studies.

III. EXPERIMENTAL METHODS

A. Materials

The commercially acquired chemicals were those used for spiropyran synthesis, comparative dyes, solid adsorbents, and solvents. Table VI lists the chemicals, sources, lot numbers, and molecular weights of the compounds used in the synthetic procedures. Table VII reports the same details for the indicator/dyes used in the study. Figures 7 and 8 illustrate the structures of the cationic indicator/dyes. Figure 9 compares the structures of the two cyanine dyes used with that of the open form of BIPS. Table VIII lists the suppliers and grades of the solvents employed in the study. Aqueous work was performed using doubly-distilled water deionized by a Barnstead PCS System.

The solid adsorbents were fairly well-characterized in most cases. Most were of known particle size and surface area; those whose surface areas were unknown were studied by the BET method. Table IX lists the suppliers and lot numbers for the major adsorbents used for this project. More detailed information from the adsorbent manufacturers follows, along with a physical description.

Table VI. Chemicals Used in Spiropyran Synthesis.

Chemical	Source	Lot no.	Mol. wt.
1,3,3-Trimethyl-2-methyleneindoline	Eastman Kodak Co. Rochester, NY	A8B B9A	173.76
5-nitro-salicylaldehyde	Eastman Kodak Co. Rochester, NY	A10H	167.12
5-methoxy-salicylaldehyde	Aldrich Chem. Co. Milwaukee, WI	None	152.15
Salicylaldehyde	Aldrich Chem. Co. Milwaukee, WI	1217EL	122.12
5-chloro-salicylaldehyde	Aldrich Chem. Co. Milwaukee, WI	5717LL	156.57
2-hydroxy-1-naphthaldehyde	Aldrich Chem. Co. Milwaukee, WI	3912DK	172.18

Table VII. Indicator/dyes Used in the Study.

Chemical (Abbreviation)	Source	Lot no.	Mol. wt.
Malachite Green Hydrochloride (MG)	Aldrich Chem. Co. Milwaukee, WI	0906CL	382.94
Methylene Blue (MB)	Manufacturing Chemists Norwood, OH	A57	319.84
Methyl Red (MR)	National Aniline Division New York, NY	193P	269.29
Janus Green B (JGB)	Aldrich Chem. Co. Milwaukee, WI	2524JE	511.07
Gentian Violet (GV)	Hartman-Leddon Co. Philadelphia, PA	8092P	408.00
Quinaldine Red (QR)	Eastman Organic Chem. Rochester, NY	156A	430.34
1,1'-Diethyl-2,2'-Cyanine Iodide (Pseudocyanine, PsCy)	Sigma Chem. Co. St. Louis, MO	124F-0121	454.40
Merocyanine 540 (M_{540})	Sigma Chem. Co. St. Louis, MO	84F-0512	569.70

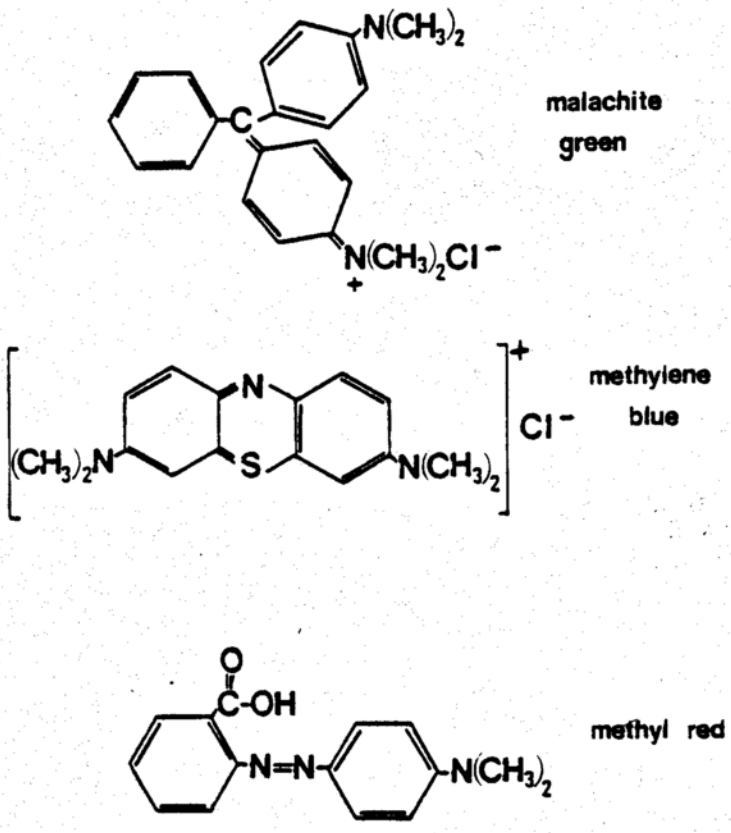

Figure 7. Indicator/dyes used in the study for comparative purposes.

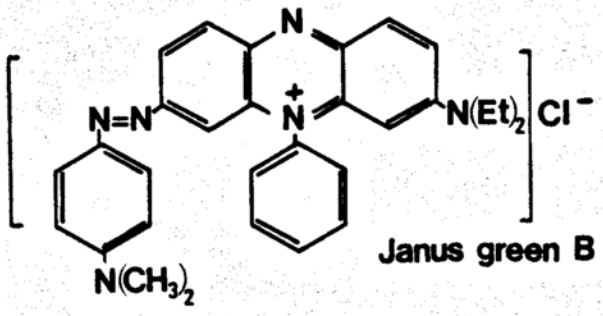

Janus green B

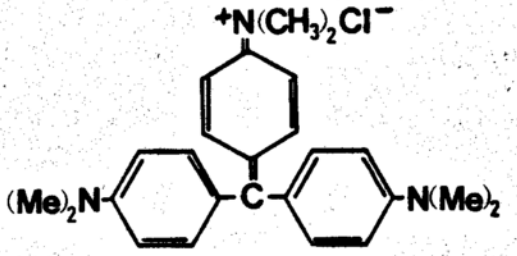

gentian violet

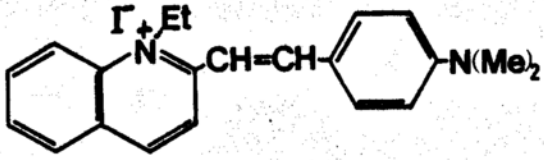

quinaldine red

Figure 8. Indicator/dyes used in the study for comparative purposes.

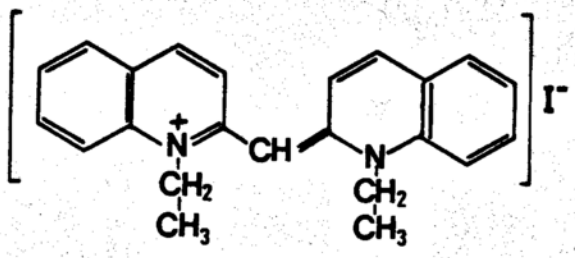

pseudocyanine

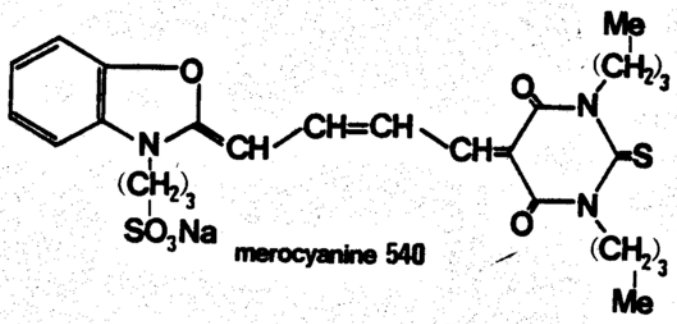

merocyanine 540

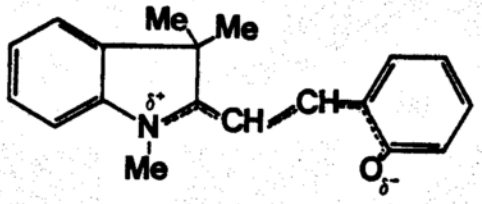

BIPS open form

Figure 9. Cyanine dyes and their structural resemblance to the open form of a spiropyran.

Table VIII. Source and Grade of Solvents Used.

Solvent	Supplier	Grade
Cyclohexane	Aldrich Chem. Co.	ACS reagent
Cyclohexane	Aldrich Chem. Co.	spectrophotometric
Glycerin	J.T. Baker Chem. Co.	anhydrous ACS reagent
Isopropanol	Aldrich Chem. Co.	spectrophotometric
Isopropanol	Mallinckrodt, Inc.	analytical reagent
Acetone	Aldrich Chem. Co.	spectrophotometric
Methylene Chloride	Aldrich Chem. Co.	ACS reagent
Methanol	Fisher Scientific Co.	certified ACS
Ethanol	Fisher Scientific Co.	certified ACS
DMSO	Fisher Scientific Co.	certified spectranalyzed
Acetonitrile	American Burdick and Jackson	high purity uv
DMF	J.T. Baker Chem. Co.	"Baker Analyzed" reagent
Chloroform	Burdick & Jackson Labs	chromatographic
n-Amyl Alcohol	Fisher Scientific Co.	certified
1-octanol	Aldrich Chem. Co.	HPLC grade
Benzyl Alcohol	Fisher Scientific Co.	not specified
Toluene	Mallinckrodt, Inc.	analytical reagent
Pyridine	Columbus Chem. Industries	ACS

Table VIII (continued)

Solvent	Supplier	Grade
Glacial Acetic Acid	DuPont Industrial Chem.	ACS
Xylene	Aldrich Chem. Co.	analytical reagent
p-Dioxane	Fisher Scientific Co.	certified

Table IX. Adsorbent Sources and Lot Numbers.

Adsorbent	Source	Lot Number
Silica Gel, 300 m^2/g	Analtech, Inc. Newark, DE	None (catalog #14050)
Silica Gel, 500 m^2/g	Analtech, Inc. Newark, DE	None (catalog #10050)
Silicic Acid	Mallinckrodt, Inc. St. Louis, MO	ATZ
Alumina	Aldrich Chem. Co. Milwaukee, WI	2305 CM
Titanium Dioxide	Colorcon, Inc. West Point, PA	85-H-238
Talc	Mallinckrodt, Inc. Paris, KY	8476 KACY
Avicel microcrystalline cellulose	FMC Corporation Philadelphia, PA	1605
Aerosil R-972	Degussa, Inc. West Germany	None
Cab-O-Sil M-5	Cabot Corporation Boston, MA	1F-087

1. Silica Gel, 500 m^2/g

This is sold as a bulk adsorbent for TLC and HPLC by Analtech, and is also available with $CaSO_4$ binder or a fluorescent indicator. It is a very fine, bright white powder with a BET surface area of 500 m^2/g. The particles are 10 $\pm$ 4 microns in diameter, and have pore diameters up to 60 Å (115).

2. Silica Gel, 300 m^2/g

This is similar to the previous adsorbent, but is of larger particle size (35-75 micron diameter) and pore size (150 Å), and of greater flowability. It is coarser in appearance but still white, and has a BET surface area of 300 m^2/g (115).

3. Silicic Acid

The silicic acid used (Mallinckrodt) was analytical reagent grade hydrated silica, with an approximate formula of H_2SiO_3 (Form. wt. 78). It was a fine white powder (100 mesh) intended for chromatographic use.

4. Alumina

Activated aluminum oxide (Aldrich) had a density of 3.970 g/cc and a formula weight of 101.96. It was standard grade neutral alumina, of Brockman activity I. The powder was medium-grained (150 mesh) and bright white, with a mean particle diameter measuring 58 Å. Surface area measured by BET analysis was 155 m^2/g.

5. Titanium Dioxide

USP grade TiO_2 was used (Colorcon), its primary use being as an opacifier for pigmentation. It was a bulk reagent of primarily the anatase crystalline form, hence required pretreatment, which will be described shortly.

6. Talc

The talc utilized was also USP grade; it consisted of extremely fine off-white particles of hydrous magnesium silicate that adhered readily to most surfaces and floated into the air easily upon perturbation.

7. Microcrystalline cellulose

Avicel brand microcrystalline cellulose (FMC Corp.) type PH-101, with an average particle size of 50 microns, was used. It is a lumpy off-white powder with low flowability. Less than 0.1% was over 60 mesh particle size; 22% was greater than 200 mesh. It contains approximately 3.9% water that is lost on drying, and produces a pH in water of 6.4. It is insoluble in organic solvents and is used as a binder, disintegrant, granulator, anti-caker, and lubricant.

8. Aerosil R-972

Aerosil R-972 is a brand of hydrophobic esteril produced by Degussa. It is a fumed silica of average particle diameter 0.016 microns, later reacted to methylate most of the surface hydroxyl groups. It has a BET surface area of 120 $\pm$ 30 m^2/g, and a very low density of packing of 50 g/ℓ (116).

The tapped volume is 2000 ml/100 grams, and the off-white powder (slight bluish tinge) is fluffy and soapy to the touch. After two hours at 110°C, less than 0.5% by weight of moisture remains. Its hydrophobicity suits this grade for use in flow improvement and addition of water resistance to formulations.

9. Cab-O-Sil M-5

This grade of Cab-O-Sil (Cabot Corp.) is a fumed silica of primary particle diameter 0.014 microns. It has a bulk density of two pounds per cubic foot. The appearance is similar to Aerosil R-972, but it loses 1.5% by weight on heating to 105°C (95). The BET surface area is 200 ± 25 m^2/g.

The filtration system consisted of Gelman 25 mm filter holders equipped with GA-8 Metricel membrane (cellulose triacetate) filters with pore size 0.2 microns. Disposable plastic syringes (Monoject, St. Louis, MO) holding 12 ml were connected to provide filtration pressure. The Luer-Lock syringes (lot 713566) are made of polypropylene and have rubber tips. Disposable culture tubes of borosilicate glass (VWR Scientific, San Francisco, CA) and dimensions 18 x 150 mm were used to capture the filtrate. Parafilm "M" laboratory film (American Can Company, Greenwich, CT) protected the samples from leakage in the water temperature bath. Whatman #2 filter paper (9 cm circles), lot 5065, captured the adsorbent when the phases were separated. Quartz cells suitable for ultraviolet

use were employed for analyses below 400 nm. Optical glass cells (McCarthy Scientific Co., Fullerton, CA) were used for visible studies and to hold powders in reflectance measurements.

B. Apparatus

The synthesis set-up consisted of a heating mantle, a 1000 ml roundbottom flask, a Pyrex Y-tube, and a 65 cm condensing tube connected to the cold tap water faucet. Reflux condensation could be carried out indefinitely with the heating Variac set at 40. Melting point determinations of the products were performed on a Thomas Capillary Melting Point Apparatus (Philadelphia, PA). It was necessary to use a Bransonic 12 sonicator (Shelton, CT) to dissolve spiropyrans in cyclohexane in a reasonable length of time. Photochromism of 6-NO_2-BIPS was visualized by irradiating the solution with a Chromato-Vue light cabinet (Ultra-Violet Products, San Gabriel, CA) set at long wave uv. Product identification was checked with a Finnigan 4000 mass spectrometer (Sunnyvale, CA).

Equilibrations took place in a CH/P Model 2564 Shaker Bath (Forma Scientific, Marietta, OH) set at a speed of 5½. It was calibrated thermostatically with an NBS certified thermometer (Ertco #C-76058, New York) at 25.00°C, and held its temperature to within ±0.05°C of the set temperature. Adsorbents were dried in a Blue Line drying oven (Blue M Electric Co., Chicgo, IL) until a constant weight was achieved. The surface area measurements required for adsorbents of unknown surface area were done on a Quantasorb system

(Quanta-Chrome Corp., Syosset, NY) with a Quantachrome flow regulator mixing H_2 and N_2 gases.

Ultraviolet spectrophotometric assays were performed on either a Varian 2200 spectrophotometer with a Haake 851 temperature control circulator or a Perkin-Elmer 559A uv/vis spectrophotometer. The latter was used for most determinations of visible spectra of dyes, and also for reading the spectra of glycerin suspensions of silica powders. The Perkin-Elmer 559A could be fitted with an integrating sphere attachment (094-012) that was capable of holding samples up to 6 mm thick on the solid sample holder (103-303) with pressure plates. Samples needed to be at least 6 x 8 mm but no greater than 40 x 40 mm. The sphere was 76 mm in diameter and was coated with highly reflective $BaSO_4$. The signal was intensified by a photomultiplier. The diffuse reflectance spectrum could be recorded from 250-800 nm. Standard white plates (103-750) were provided for reference, and 2 mm path-length optical glass cells were used to hold powders for spectral analysis. Slit widths of 4.0 nm, scan rates of 120 nm/min, and the % transmittance mode were used; either the reflectance data or its first or second derivative were obtained.

A Nikon FE-2 single lens reflex camera (35 mm) was used to take the color photographs in this manuscript. Slide film (ASA 25) was used, and a Tamron 28-80 macro-zoom lens; exposures were determined by thru-the-lens metering. Those figures not reproduced by pen and ink were produced on an Apple MacIntosh computer, using Cricket

Graph software, and a Laser Writer printer.

C. Experimental Procedures

1. Synthesis of Spiropyrans and Characterization of Materials

The spiropyrans were synthesized following the method of Przystal et al. (15). Equimolar amounts of Fischer's base and a substituted salicylaldehyde were refluxed for 4 hours in isopropyl alcohol. Sixty ml of solvent was used for every 0.03 moles of salicylaldehyde. Salicylaldehyde itself is a clear liquid, whereas most of the substituted salicylaldehydes are pale solids. Fischer's base is an intensely dark red liquid. Within minutes, the mixture becomes bright purple as spiropyran is formed. INS and 6-NO_2-BIPS solutions develop precipitates as the reaction mixture cools. 6-OCH_3-BIPS and 6-H-BIPS solutions remain clear, and must be scratched and placed in the freezer overnight to induce crystal formation.

Recrystallization from petroleum ether, accomplished in the literature, was rejected owing to the low solubility of spiropyrans, even in heated solvent. Methanol recrystallization of 6-NO_2-BIPS was successful, though large volumes of methanol were required to dissolve the solid. The other spiropyrans (and subsequent batches of 6-NO_2-BIPS) were recrystallized from a 90:10 ethanol/water mixture. In some cases (6-OCH_3-BIPS, 6-H-BIPS), the addition of water is required to obtain a reasonable yield. This additional

water should be added slowly to allow time for crystal growth. Rapid addition results in the formation of a large number of microcrystals, which filter poorly. The products were dried at 70°C to a constant weight to drive off solvent. Normally three to four hours was sufficient; at this time the isopropyl alcohol odor is no longer apparent.

An ultraviolet spectroscopic assay was developed for each spiropyran in cyclohexane. The spectrum was recorded from 200 nm to 400 nm versus a reference blank. Several broad peaks from 275-350 nm were evident that were unique for each spiropyran. Beer's law plots were made at a wavelength at which the spectrum was in a plateau region. All spiropyrans used gave linear plots up to an absorbance of 1.5; dilution of solutions with higher absorbances gave more consistent results. Saturated solutions of spiropyrans in cyclohexane were rotated end-over-end in 14 ml vials in a 25°C water bath. The samples were filtered after three days and diluted for ultraviolet analysis. The solubilities thus determined represented a concentration limit for adsorption studies from cyclohexane.

Most of the adsorbents were commercially available in well-characterized states. Talc, TiO_2, silicic acid, and microcrystalline cellulose samples were of unknown surface area. The Quantasorb system described earlier was employed in determining these surface areas by nitrogen adsorption. The method of Brunauer, Emmett, and Teller (BET) was used (117). Samples were evacuated for at least 5 hours at 110°C under a nitrogen atmosphere. The area

under the curve of 3-4 desorption cycles was averaged at N_2/H_2 contents of 0.1, 0.2, and 0.3. Flow rates were adjusted to a total pressure of 20 psi. Appendix A contains a sample calculation of surface area using the BET method.

2. Solvatochromic Studies

Each of the spiropyrans was subjected to qualitative solvatochromic studies. An amount sufficient to cause detectable coloration of the solvent was dissolved in 50 ml of solvent. Ten to fifty mg of spiropyran was generally required; though in less polar solvents sonication was often required to generate enough colored species. INS and 6-NO_2-BIPS were used for quantitative solvatochromic experiments. The frequencies of maximum absorption (in cm^{-1}) were tabulated for each solvent or solvent mixture. Since the spiropyrans are water insoluble, the polar end of the scale is not exploited fully in solvatochromic work. Binary solvent mixtures and an extraction procedure extended this end of the graph. The binary solvent system used was acetone/water; spiropyrans are highly soluble in acetone, and water increases the polarity of the medium without precipitating the spiropyran from solution. The aforementioned extraction method enabled the measurement of the visible spectrum of the open form of 6-NO_2-BIPS in pure water. A 10^{-3}M solution of 6-NO_2-BIPS in cyclohexane was placed over an equal volume of water in a separatory funnel. The funnel was then irradiated in the ultraviolet light cabinet for one minute,

producing the photochromic blue form of 6-NO_2-BIPS in the cyclohexane phase. Since this form is highly polar (with zwitterionic character), shaking of the funnel results in transfer of some of the 6-NO_2-BIPS across the interface. This can be visualized by the appearance of an orange color in the previously colorless water phase. Rapid decantation and scanning of the water phase gives the spectrum. In 5-10 minutes, the orange color fades, and the 6-NO_2-BIPS returns to the more favorable cyclohexane phase. If that phase has been removed, the solute precipitates or adsorbs to the container walls.

3. Adsorption Isotherms

Adsorption isotherms at 25°C were determined for four different spiropyrans, each on 3 to 9 adsorbents. INS and 6-NO_2-BIPS received the most intensive study, after spectroscopic work revealed that these two spiropyrans showed the greatest differences in behavior. Preliminary results were obtained for INS and 6-NO_2-BIPS on silica gel at elevated temperatures. Equilibration times were experimentally determined by preparing replicate samples and following the decrease in solution absorbance due to spiropyran. Except for drying them, most adsorbents were used as received. The exception to this was titanium dioxide, which was of a lower grade and required cleanup. The cleanup procedure used was that of Busca et al. (118), purported to remove chloride and to fully oxidize unreacted Ti. Oxygen (5 psi) was bubbled through distilled water

and into a beaker of TiO_2 at 400-425°C in a column oven. (The gas is vented to a hood, since it may contain HCl.) Overnight treatment of the solid was found to be equivalent to 20 washings with water. The TiO_2 was sieved prior to this treatment, the fraction passing through 100 mesh screen and caught on 170 mesh screen (90 mm opening) being used.

Adsorption isotherms were measured in cyclohexane. Literature reports had used benzene, which is now considered carcinogenic. Infrared studies have demonstrated that cyclohexane does not interact significantly with the silica surface (119). The hydrophilic adsorbents employed are insoluble in cyclohexane, but the adsorbates (spiropyrans) are readily soluble. Furthermore, ultraviolet assays for spiropyrans in cyclohexane proved feasible. A stock solution of spiropyran in cyclohexane was prepared: 8×10^{-3}M for 6-NO_2-BIPS studies (close to the solubility limit) and 12×10^{-3}M for the other spiropyrans. Solutions of higher concentration than 1×10^{-3}M usually had to be sonicated to obtain dissolution within 15 minutes. The solutions then were cooled before being brought to volume. Dilutions of the stock solution were made to define the entire adsorption curve; adsorbent weight was usually held constant. Fifty ml of spiropyran solutions covering the concentration range of 2×10^{-4}M - 8×10^{-3}M were prepared for the case of 6-NO_2-BIPS on silica gel adsorbent.

In order to obtain a known weight of dried adsorbent, the approximate amount required for a significant decrease in solution

concentration was first placed into preweighed 250 ml flasks having ground glass stoppers. These samples were dried to constant weight at 110°C, the exact time of drying being pre-determined for each adsorbent. The stoppered flasks were cooled and re-weighed; the adsorbent weight was calculated by difference. 0.20-3.00 grams of adsorbent was used, the lesser amounts corresponding to higher surface area adsorbents and vice versa. The diluted stock solutions were quantitatively transferred to the flasks, which served as vessels for the duration of the adsorption process. The flasks were wrapped in water-repellent Parafilm and placed in the shaker bath until equilibrated.

At the expiration of the equilibration time, the flasks were removed from the bath. The supernatant was filtered by the Gelman system previously described, and the filtrate was analyzed by ultraviolet spectroscopy for remaining spiropyran. The solid phase was filtered, allowed to dry, and saved for spectral analysis.

4. Spectral Measurements of Adsorbed Spiropyrans

The spectral measurements consisted of suspension transmission spectroscopy and diffuse reflectance spectroscopy. Evans et al. (53) and Robin and Trueblood (70) used cyclohexane/silica mixtures because the two components had closely matching refractive indices. They could obtain transmission spectra by packing enough silica in the cell to produce slurries with sedimentation volumes of 100%, or used mini-stirrers to continuously mix the cell. We used

glycerin/silica mixtures, which had the added advantage of a high viscosity, and hence long suspension times without mixing. The refractive index of glycerin is 1.475 (120), close enough to that of silica (1.420) to prevent significant scattering. Above 260 nm, these suspensions were nearly transparent (70); the net result is that a colored adsorbate on the silica surface is held in the path of the spectrophotometer light beam by the matrix. (Mineral oil proved to be inferior to glycerin by virtue of increased turbidity, dissolution and desorption of spiropyran, and the nonavailability of superior spectrophotometric grades.) 25-150 mg of spiropyran/silica adsorbate-adsorbent solid was levigated with a small amount of glycerin, and diluted with 20 ml total glycerin to form a colored suspension. Its spectrum was read versus a reference cell containing 100 mg of pure adsorbent suspended in glycerin. With practice, mixing the components homogeneously, and reducing bubbles to a minimum, smooth spectra resulted. Residual turbidity, evidenced by nonzero baselines, is always present but is minor for small particle size adsorbents. After verification of the method using Orange G dye, spectra of spiropyrans on silicas could be obtained. Other adsorbents had inappropriate refractive indices for this technique.

Diffuse reflectance spectroscopy, using the Perkin-Elmer 559A spectrophotometer equipped with an integrating sphere, was applicable to all adsorbents studied. Spectra were measured only after running a baseline with pure adsorbent in both cells, and

verifying that it was flat and gave 100% R_∞' values in the range of interest. As in solution spectroscopy, one need only replace the sample cell with the sample to be measured and run the spectrum. The cells were filled with solid, cleaned on the outside with tissue, and tapped to the packing density. Homogeneity of the sample was important, and more difficult to achieve than with solutions. Particle aggregates should be broken up so that the particle size and geometry resembles that of pure adsorbent, a requirement for the dilution method to work correctly. It is best to begin recording the spectrum at 850 nm, where little absorption takes place, in order to observe the initial value of the digital readout. If this deviates significantly from 100%, repositioning, re-clearing, or re-zeroing often corrects this discrepancy. Photochromic adsorbates (such as spiropyrans) should be protected from light prior to measurement. The instrument was also capable of recording the first derivative spectrum of reflectance versus wavelength. Such spectra showed differences in early times after adsorption began, but were similar thereafter.

The reflectance spectra of permanent dyes on silica gel were also recorded for comparative purposes. Preparation of samples with known adsorbed dye content followed the procedure for isotherm measurement, except that temperature control was not necessary. As with the spiropyran/silica samples, these showed new peaks and maximal absorption at major peaks at high coverages. These have been interpreted by others as indicative of approaching saturation

of the surface, with consequent intermolecular interaction (35, 74, 84).

D. Data Treatment

Isotherm calculations yielded the amount of solute adsorbed (in mg/g) from the change in solution concentration of adsorbate. A graph of $(mg/g)_{adsorbed}$ versus C_{eq} (equilibrium concentration of adsorbate in molar units) constituted the adsorption isotherm. A stepwise sample calculation from C_{eq} to $(mg/g)_{ads}$ appears in Appendix B. To obtain the two parameters necessary to describe the Langmuirian adsorption isotherm, namely capacity and binding constant, a nonlinear regression program by Duggleby (121) was used. An Apple IIe computer using flexible disks was utilized to run the program. The Duggleby program is written in BASIC, and can use weighted or non-weighted regression to fit a number of different functional forms to a data set. It easily adapts to fit the two-parameter rectangular hyperbola, and has been used in enzyme binding studies. The program output consists of the best-fit parameters, comparison of the input data with the fitted data, and standard errors of the parameters. The standard errors are approximate error estimates from nonlinear regression that are for comparative purposes; they do not correspond precisely to any of the common statistical error measurements. The program requires initial estimates of the two parameters that are reasonably close to the final "correct" values. The program is written such that the

independent variable in the denominator has no coefficient, hence equation (3) must be rewritten as:

$$(x/m) = \frac{(x/m)_{max} C_{eq}}{1/K + C_{eq}} \qquad (7)$$

Parameter B(1) in the program then refers to the capacity, $(x/m)_{max}$, and parameter B(2) is 1/K, the reciprocal of the binding constant. A sample printout of experimental results from the Duggleby program appears in Appendix C.

The initial estimates required for the program were obtained from linearized plotting forms of the Langmuir equation. The least-squares linear regression was done on a Casio FX-702P computer. The Scatchard plot was used as a tool to determine which points were most representative of the data set. Relative errors were large at low concentrations, and including these points in the analysis significantly affected the estimates of the capacity, so these points were selectively rejected. The points at high concentrations have lower relative errors. Figure 10 shows a Scatchard plot of INS adsorbed on alumina at 25°C. Note the deviation of low-concentration points on the Scatchard plot; the rejected points are marked with an "x." Points which fell more than two standard deviations from the line (roughly defined by the high-concentration points) were rejected. The remaining points were then subjected to Scott plot analysis, the slope and y intercept

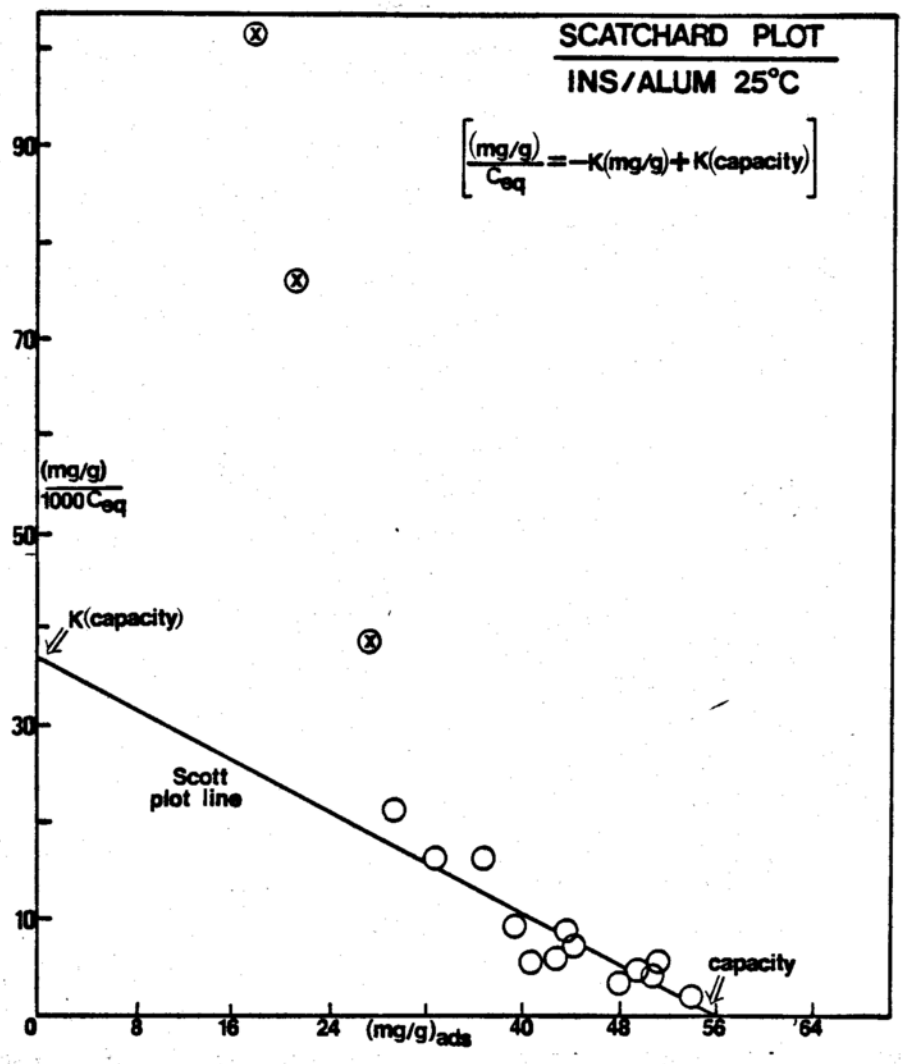

Figure 10. Scatchard plot for INS adsorbed on alumina at 25°C. Low coverage points marked by "x" were rejected by virtue of their deviation from the line.

yielding the initial parameter estimates. The Scott plot for these data is shown in Figure 11. The rejected points, if included, would alter the apparent intercept and binding constant estimate from the Scott plot. The line defined by the Scott plot parameters is drawn on the Scatchard plot; note that it fits the remaining (accepted) data reasonably well. Figure 12, showing the binding curve for this data set, illustrates that even the points rejected for initial parameter estimates fall close to the rectangular hyperbola defined by the Duggleby parameters. If the deviant points were retained in the initial analysis, the calculated curve gave a poorer fit for the high coverage data. In the determination of amount adsorbed from the difference in concentration, assay errors are magnified, so that ordinate errors exceed abscissa errors. Ten replicates in a study of 6-NO_2-BIPS adsorbing to Aerosil R-972 in cyclohexane yielded an assay standard deviation of 0.67%. Transformation to $(mg/g)_{ads}$ resulted in a 3% standard deviation, or 4.5X error magnification. The absolute error, originating from the assay, is invariant along the abscissa scale. Thus, points in the plateau region of the isotherm (where the slope is small) show greater deviations from the fitted curve. Points in the steeply rising portion of the isotherm show only small deviations from the curve, owing to its large slope and the smaller error in the x direction. Therefore, the best-fit hyperbola is obtained by emphasizing the mid to high range points at the expense of the low range points, which have the highest relative errors. Some researchers simply do not use low concentration

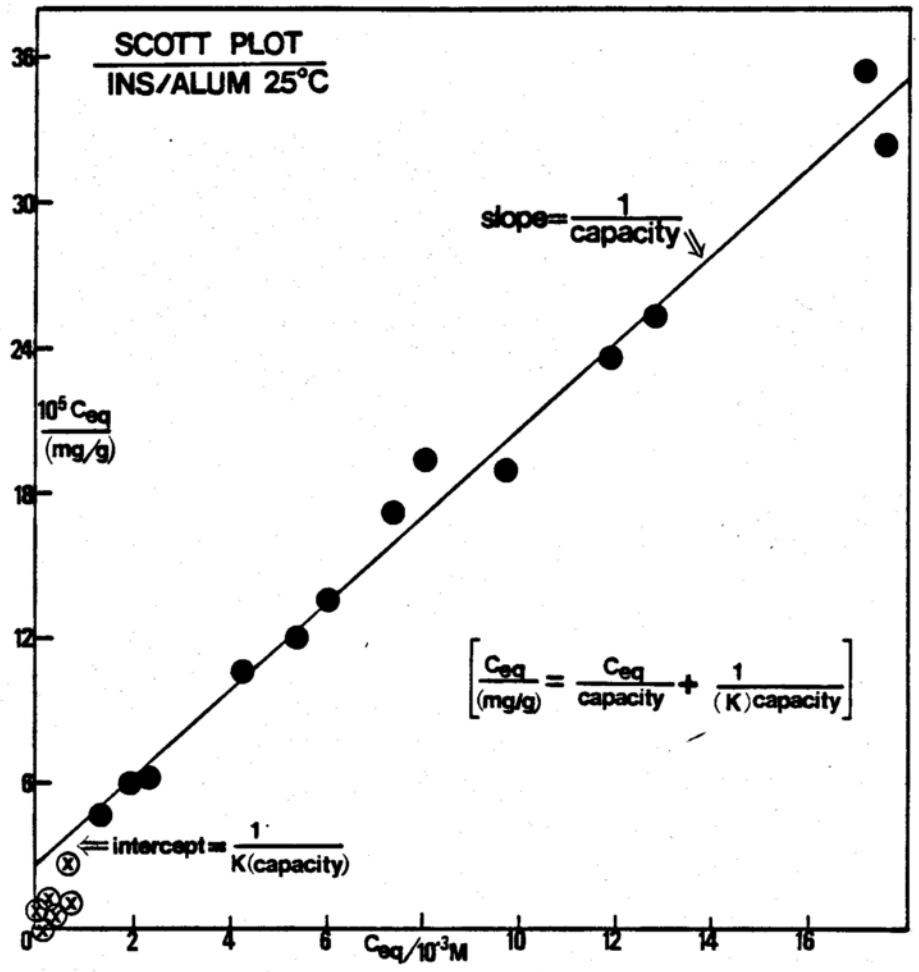

Figure 11. Scott plot for INS adsorbed on alumina at 25°C. Low concentration points marked by "x" were not included in the least-squares linear regression.

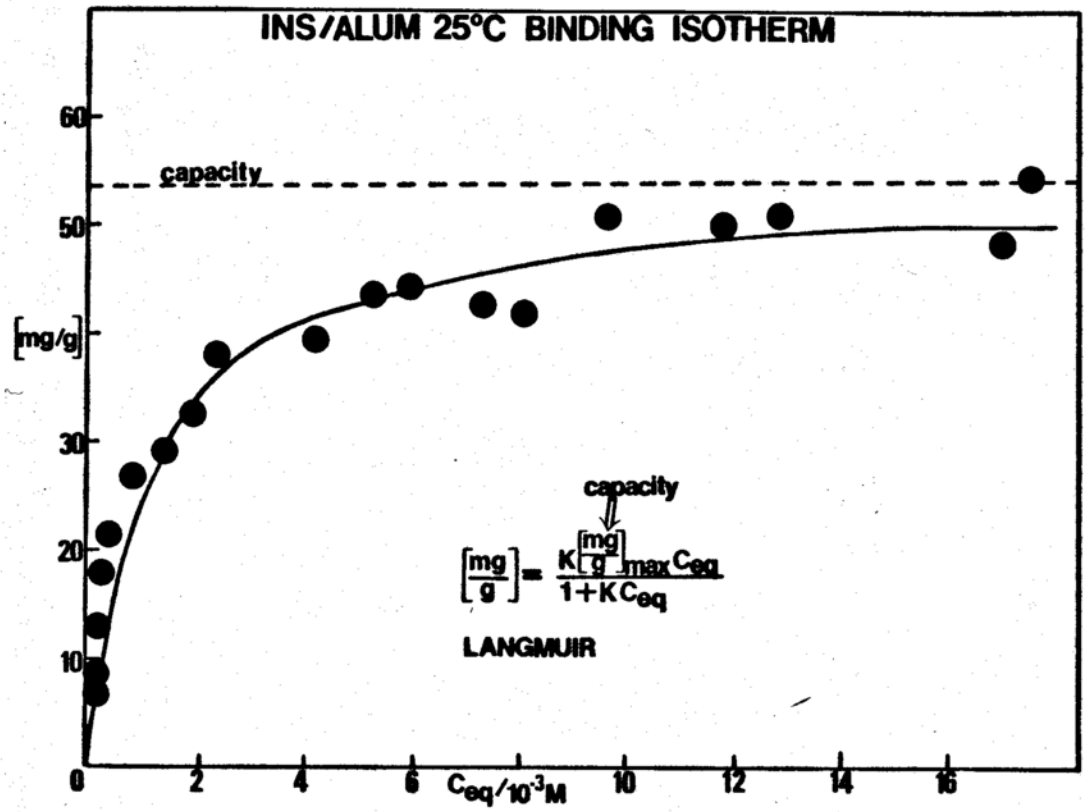

Figure 12. Binding isotherm for the adsorption of INS to alumina at 25°C. The fitted curve was determined by nonlinear regression. All original data points are shown.

points, but for strongly-bound adsorbates this results in no data points on the rising portion of the curve.

A propagation of errors treatment was also used to estimate errors in the two parameters defining the isotherm. The error in a function can be determined from the input variances of its component variables (122). Least-squares linear regression treatment yields variances of the slope (σ_m^2) and y intercept (σ_b^2), from which capacity and the binding constant are derived in the Scott plot. The following equations were derived which yield the variance in the capacity (σ_{cap}^2) and the variance in the binding constant (σ_K^2) from error propagation theory:

$$\sigma_{cap}^2 = \frac{\sigma_m^2}{(\text{slope})^4} \qquad (8)$$

$$\sigma_K^2 = \frac{\sigma_m^2}{(\text{y intercept})^2} + \frac{\sigma_b^2 (\text{slope})^2}{(\text{y intercept})^4} \qquad (9)$$

Applied to a malachite green/silica gel isotherm, which had a Scott plot correlation coefficient of 0.9993, the capacity exhibited a relative standard deviation of 3.7%, and the binding constant had a relative standard deviation of 67.7%. This arises from the fact that the y intercept is imprecise; and σ_b^2 appears only in the expression for σ_K^2, where it is the dominant term. The malachite green/silica gel system was chosen because it was an exceptionally

smooth curve; the relative standard deviation for K in other cases exceeded 100%. It was concluded that this treatment gave reasonable errors only for the capacity. Thereafter, the standard errors via the Duggleby program were used when expressing parameter error estimates.

Reflectance data consist of tracings of R'_∞ versus λ(nm); see Figure 13 for an example for INS adsorbed on silicic acid at different coverages. These raw data must be converted (via the Kubelka-Munk function, equation (1)) to $F(R'_\infty)$ values and then replotted versus wavelength. This results in spectra with the appropriate peak positions and shapes, the "typical color curves" for the system. Figure 14 shows the result for the INS/silicic acid data, transformed at several different coverages. Calculation at every 10 nm is usually sufficient to sketch out the spectrum. The coverages are expressed in units of $(\text{nanomoles/m}^2)_{ads}$, termed "g." After calculating coverage in (mg/g) via isotherm methods, division by 1000 x (molecular weight of adsorbate) yields coverage in (moles/g). Further division by the surface area of the adsorbent (in m^2/g) yields (moles/m^2); the nanomole unit then gives conveniently small numbers. Expression of the surface coverage of adsorbate in terms of "g" places it in dimensions of moles/(length)^2, a surface concentration measurement. Analogously, the molar absorptivity (ε), is expressed (in solution) in units determined by the product bc, since A is dimensionless in Beer's law. Thus, cm.moles/liter becomes (length)(moles)/(length)3 =

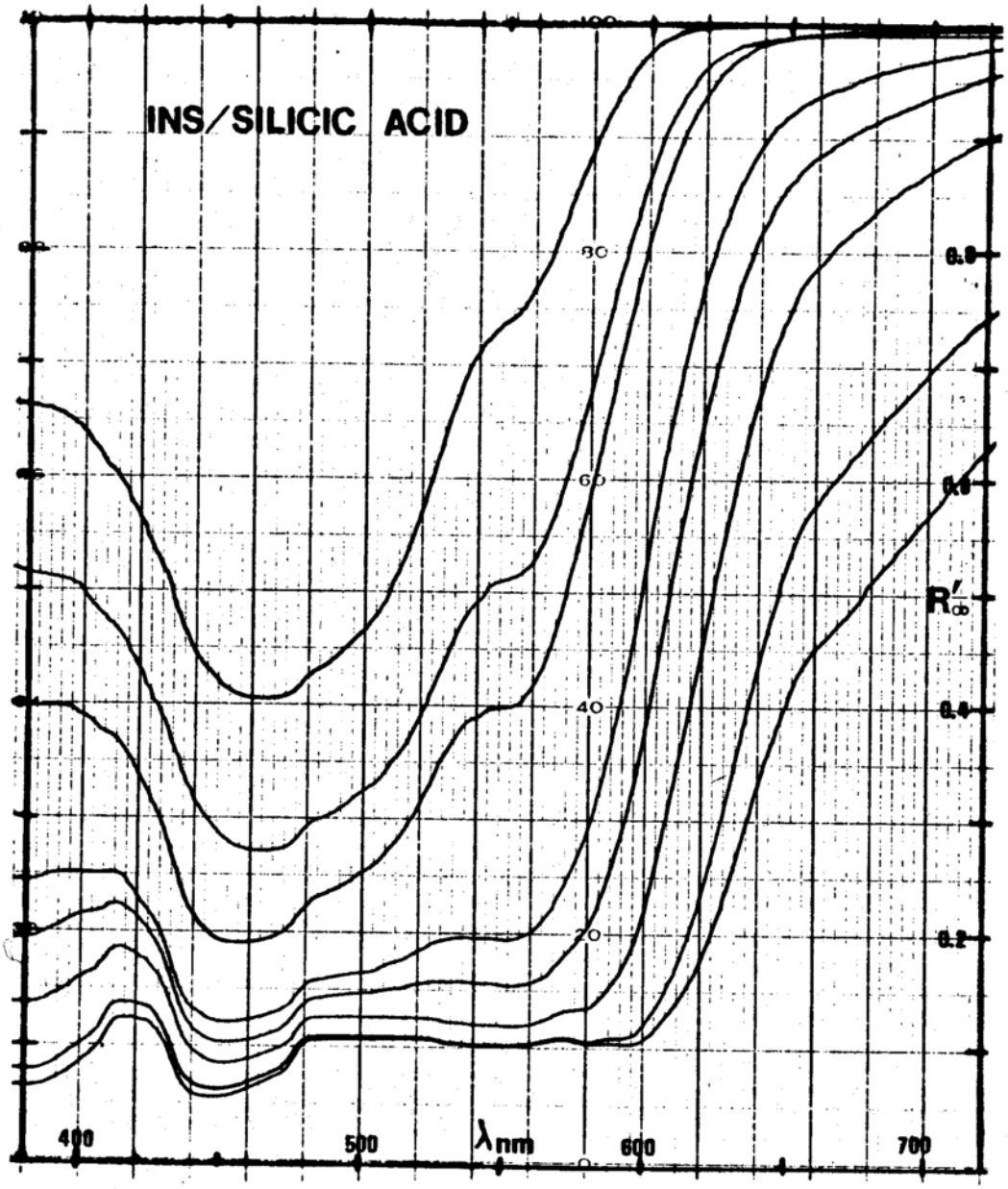

Figure 13. Reflectance data for the adsorption of of INS to silicic acid at different surface coverages.

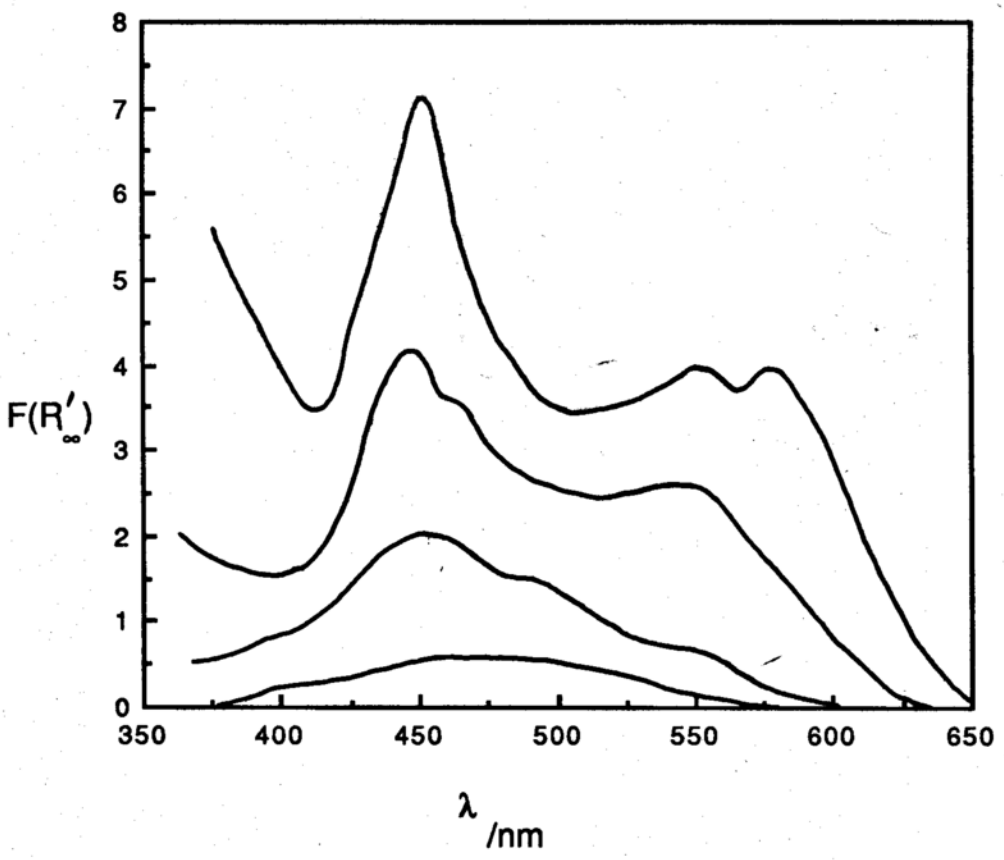

Figure 14. Reflectance spectra for INS on silicic acid with variable surface coverage. g = 1.1 nanomoles/m² (faint orange), g = 5.3 (light orange), g = 27.7 (red-orange), and g = 161.2 (red-violet).

moles/(length)^2. Expressing "g" in nanomoles/m^2 gives "f" units of m^2/nanomoles in equation (10), which is written by analogy with Beer's law, equation (11), so that "f" and "ε" are dimensionally

$$F(R'_\infty) = fg \qquad (10)$$

$$A = \varepsilon bc \qquad (11)$$

equivalent. Equation (10) is the surface analog of Beer's law. Both "f" and "ε" are constant only at a specified wavelength. The spectra that result from this treatment (see Figures 13 and 14) will roughly invert the raw R'_∞ data and sharpen the peaks. The first, second, fourth, and sixth curves from the top in Figure 13 are transformed to make Figure 14.

IV. RESULTS

A. Spiropyran Synthesis and Characterization of Materials

The reflux condensation reaction produced spiropyrans from a salicylaldehyde and Fischer's base in good yields. Table X lists the reaction yields, melting points, and melt colors for the four spiropyrans synthesized. The product crystals exhibited a number of different colors, depending on the recrystallization solvent. 6-OCH_3-BIPS was light pink, 6-H-BIPS was pale orange, INS was red-brown, and 6-NO_2-BIPS varied from a light green to a dark brown. Regardless of its color in the solid state, each dissolved spiropyran exhibited a characteristic spectrum in solution. The product identities were verified using mass spectrometry. Figure 15 shows the mass spectrum for 6-H-BIPS beyond 130 Daltons. The most prominent features are the molecular peak (277) and peaks corresponding to the loss of one, two, or three methyl groups (262, 247, and 232, respectively). The large peak at 159 appeared in all mass spectra; this corresponds to a decomposition product resembling Fischer's base with the loss of the terminal methylene group ($=CH_2$). A peak at 144 is the demethylated version of this product.

Table X. Reaction Products in Spiropyran Syntheses.

Spiropyran	Reaction Yield[a]	Melting Pt./°C	Melt Color
6-NO_2-BIPS	87.4%	177.5-178.0[b]	dark blue
6-H-BIPS	59.8%	91.5-92.0	light orange
6-OCH_3-BIPS	75.0%	75.5-77.0	colorless
INS	62.5%	175.0-177.0[b]	red-purple

[a]Final yields, some lost during recrystallization.

[b]Two batches were made, both gave the same value.

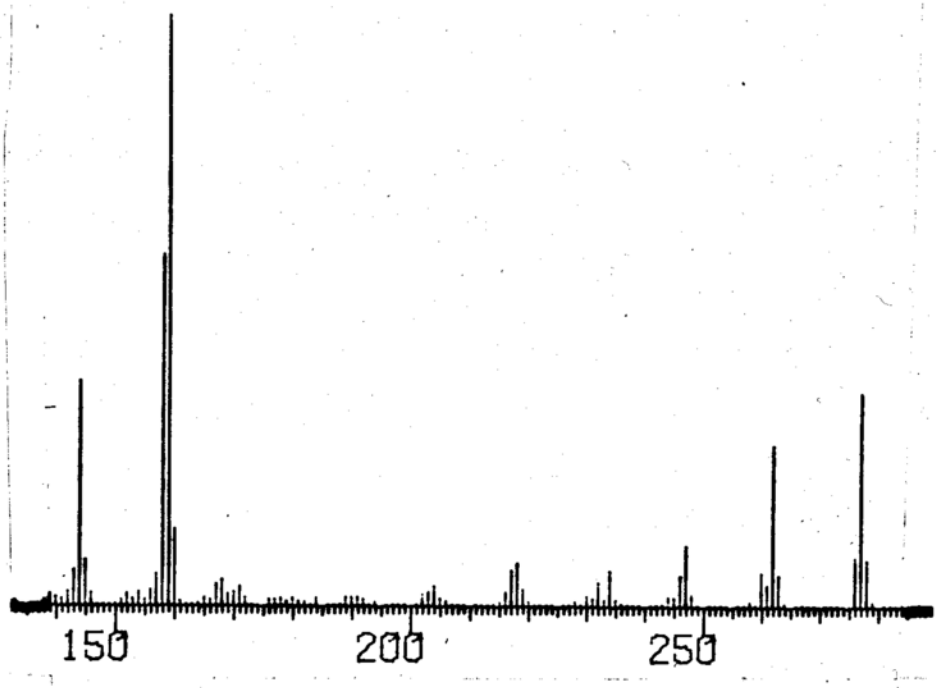

Figure 15. Mass spectrum of 6-H-BIPS.

Mass spectra for 6-NO_2-BIPS, 6-OCH_3-BIPS, and INS showed essentially the same features. A solvent peak (isopranol = 60) is evident in the latter three cases. None of the reactant salicylaldehyde was detected in any of the spectra.

The ultraviolet absorption spectra for INS and 6-NO_2-BIPS in cyclohexane are shown in Figure 16; those for 6-OCH_3-BIPS and 6-H-BIPS in cyclohexane appear in Figure 17. The wavelengths chosen for analysis of each spiropyran in cyclohexane via Beer's law are indicated by an arrow. Table XI summarizes the parameters associated with each linear Beer's law plot. Absorptivities were redetermined for the second batches of 6-NO_2-BIPS and INS that it became necessary to produce. The ultraviolet spectrum for 6-NO_2-BIPS in methanol was also recorded. It was essentially the same as that in cyclohexane, except for a broadening of the analytical peak (beyond 330 nm) and a reduction in ε (to 9.4 x 10^3 ℓ/mole·cm).

The solubilities of the spiropyrans in cyclohexane were vastly different. Table XII gives the results of the solubility determinations at 25°C. Attempts to measure an aqueous solubility for any of these spiropyrans failed. It took nearly fifteen minutes of constant stirring to wet the powder; two days of stirring resulted in insufficient dissolution to produce a measurable absorbance at any wavelength. Solubilities in alcohols or acetone were fairly high; these solvents proved convenient for cleaning the glassware.

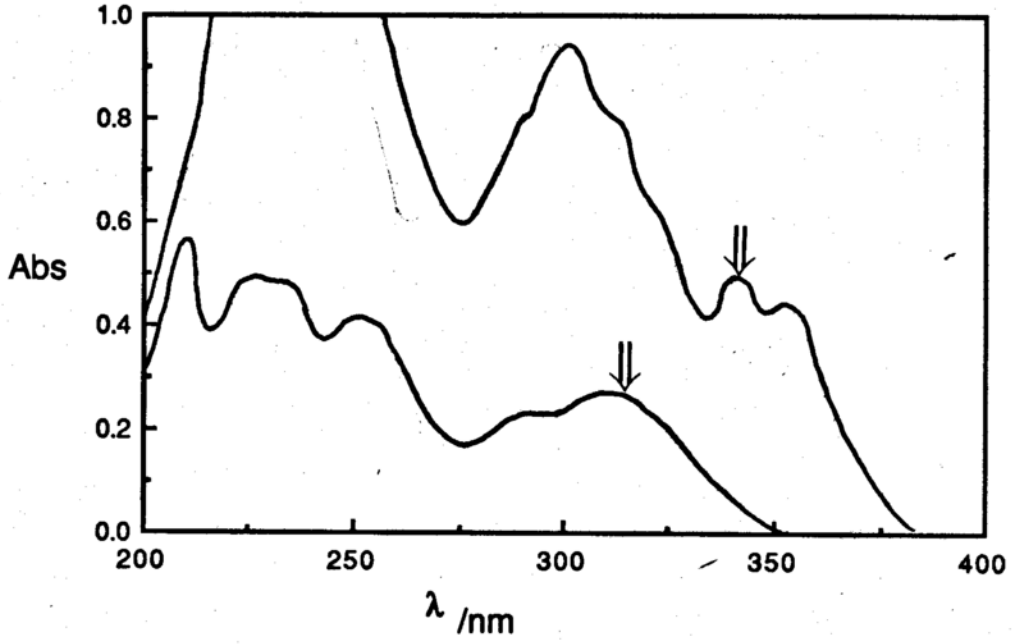

Figure 16. Ultraviolet spectra for 6-NO_2-BIPS ($2x10^{-5}$M, lower curve) and INS ($9.2x10^{-5}$M, upper curve) in cyclohexane. Arrows indicate analytical wavelengths.

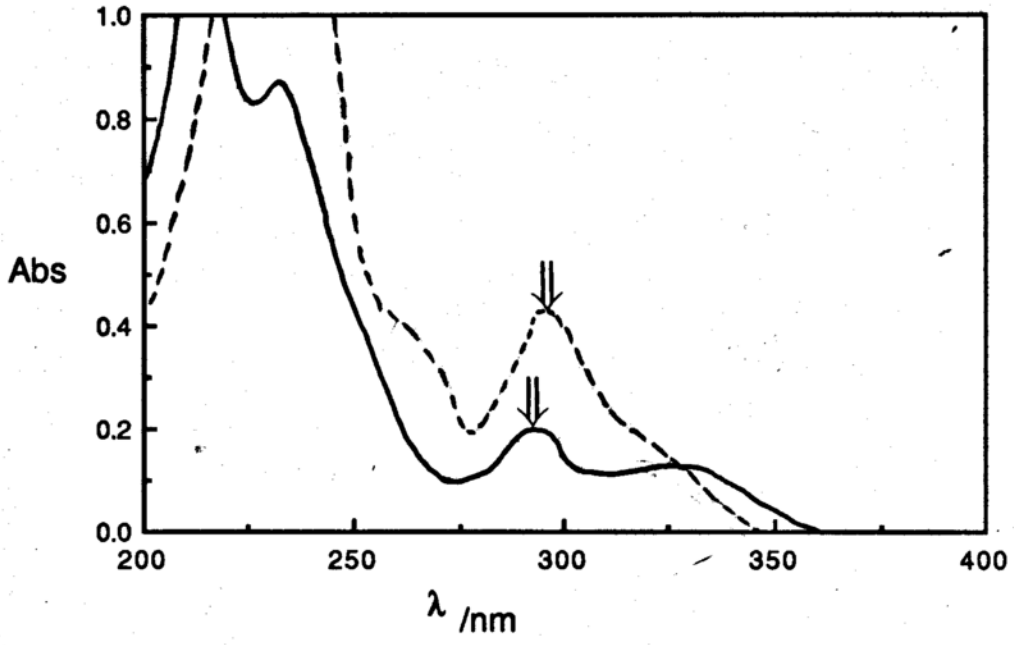

Figure 17. Ultraviolet spectra for 6-H-BIPS (- - - - - 5.6×10^{-5}M) and 6-OCH_3-BIPS (——5.3×10^{-5}M) in cyclohexane. Arrows indicate analytical wavelengths.

Table XI. Beer's Law Plots of Spiropyrans in Cyclohexane.

Spiropyran	Wave-length/ nm	Correlation coefficient	y intercept	$\varepsilon/\ell \cdot mole^{-1} \cdot cm^{-1}$
6-NO_2-BIPS	320	0.99974	+0.001	10.09×10^3
(2nd batch)		0.99991	+0.011	9.96×10^3
INS	345	0.99999	+0.002	4.67×10^3
(2nd batch)		0.99995	+0.004	4.54×10^3
6-H-BIPS	295	0.99984	+0.004	6.56×10^3
6-OCH_3-BIPS	292	0.99998	-0.006	5.77×10^3

Table XII. Solubility of Spiropyrans in Cyclohexane, 25°C.

Spiropyran	Solubility/M ± std. deviation	RSD/%[a]
6-NO_2-BIPS	$1.012 \times 10^{-2} \pm 0.011 \times 10^{-2}$	1.09
INS	$3.26 \times 10^{-2} \pm 0.11 \times 10^{-2}$	3.37
6-H-BIPS	3.89 ± 0.23	5.91
6-OCH_3-BIPS	$3.80 \times 10^{-1} \pm 1.07 \times 10^{-1}$	35.5[b]

[a]relative standard deviation, in percent

[b]n = 3, due to small sample size available

Some variability in the absorptivities of the spiropyrans was observed. The dilution and pipetting process introduced very little error; six samples of 6-OCH_3-BIPS were diluted to 5×10^{-5}M and the resulting absorbance readings were 0.449 ± 0.004. It was determined that much of the variation was eliminated by doing a separate Beer's law plot for each batch. Adequate protection from light also increased the assay reliability. Variation in the absorptivity with time, presumably due to solution degradation, was followed at three concentrations for 6-OCH_3-BIPS and 6-NO_2-BIPS. Figure 18 shows the results, presented as log ε versus time (hours). From the approximately linear plots, it was concluded that less than 5-10% degradation occurs in the first two weeks after preparation of a fresh solution. In the 3-7 days used for isotherm equilibrations, this source of loss of spiropyrans will have negligible effect on the assay result.

Cyclohexane solutions of 6-H-BIPS and INS showed no coloration in the presence or absence of uv light, excepting for a slight yellow tinge in highly concentrated INS solutions. 6-OCH_3-BIPS/cyclohexane solutions were faintly pink; sonication, uv light, and increased concentrations darkened these solutions. 6-NO_2-BIPS/cyclohexane solutions are faintly pink at high concentrations, but show sharp spectral changes dependent on the lighting conditions. Only the 6-NO_2-BIPS solutions showed obvious photochromic changes upon irradiation at 366 nm in a light cabinet. Intensely blue solutions result after 5-10 seconds; these fade to clear or faint

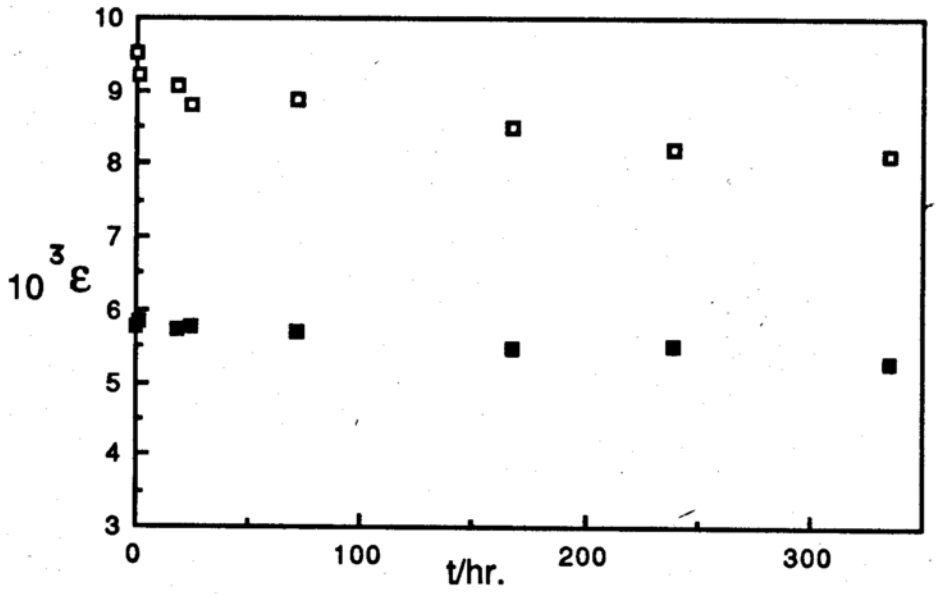

Figure 18. Variation of absorptivity with time.

□ 6-NO_2-BIPS, 320nm.

■ 6-OCH_3-BIPS, 292nm.

pink solutions at roughly the same rate when placed in the dark. Figure 19 shows the spectra in cyclohexane of the colored forms of 6-OCH_3-BIPS and 6-NO_2-BIPS. Figure 20 shows flasks of 6-NO_2-BIPS in cyclohexane, and their increasing amounts of coloration from the dark, from room light, and after irradiation with ultraviolet light. Solutions of the spiropyrans in dilute HCl were bright yellow. The compounds exhibited high absorptivities and required much dilution in order to record their spectra. The yellow 6-NO_2-BIPS solution showed a broad peak centered at 315 nm, spilling into the visible. The yellow-orange INS solution had a broad peak centered at 445 nm, consistent with literature reports of the effect of acid on spiropyran spectra (36).

Aqueous spectra of the dyes used were recorded, and Beer's law plots were made at the absorption maxima. Table XIII summarizes the λ_{max}, absorptivities, and correlation coefficients for these dyes. Linearity was found in all cases for absorbances up to A = 1.5.

BET surface areas, measured for those adsorbents not having reported surface areas, are shown in Table XIV. Listed are the correlation coefficient for the plot of the constant y versus nitrogen content, the surface area found, weight of adsorbent used, and specific surface area (in m^2/g). The silica-type adsorbents contained 5-10% water by weight, and were dried to constant weight in 2 hours at 110°C. Alumina lost very little water weight; one hour was sufficient to dry it completely. Talc and TiO_2 lost 2-5% water weight and required two hours to dry. Microcrystalline

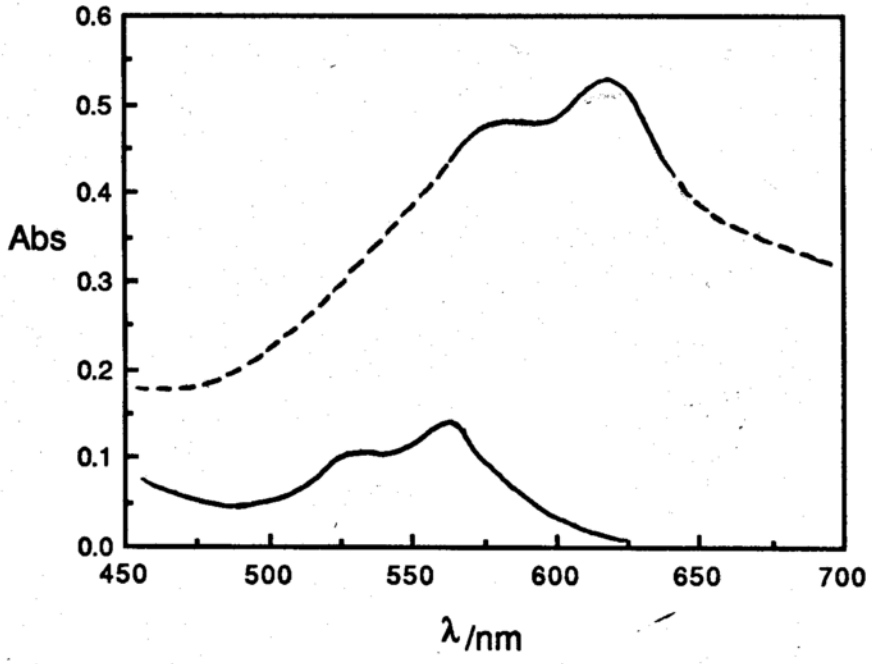

Figure 19. Visible spectra of 6-OCH_3-BIPS (——— $2x10^{-2}$M) and 6-NO_2-BIPS (- - —— - $1x10^{-3}$M, irradiated under uv light for five min.) in cyclohexane.

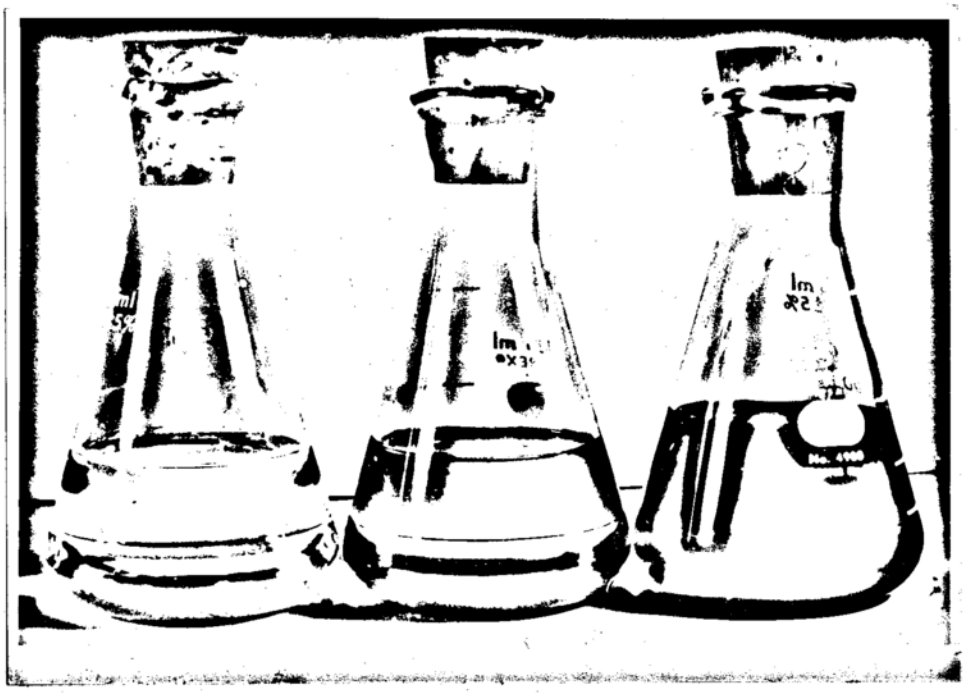

Figure 20. 6-NO_2-BIPS in cyclohexane ($1x10^{-3}$M) in varying degrees of light. Left to right: stored in the dark, under room light, and after 30 sec irradiation at 366nm.

Table XIII. Beer's Law Parameters for Aqueous Dye Solutions.

Indicator/dye	λ_{max}	$\varepsilon/\ell \cdot mole^{-1} \cdot cm^{-1}$	Correlation coefficient
Methyl Red	520	2.78×10^4	0.99991
Methylene Blue	663	12.6×10^4	0.99899
Malachite Green	615	7.12×10^4	0.99952
Janus Green B	608	3.50×10^4	0.99945
Merocyanine 540	501	6.75×10^4	0.99877
Pseudocyanine	522	7.07×10^4	0.99916
Quinaldine Red	498	3.69×10^4	0.99949
Gentian Violet	590	8.87×10^4	0.99919

Table XIV. BET Surface Area Results.

Adsorbent	Plot correlation	Surface area/m^2	weight/g	Specific area/(m^2/g)
Talc	0.999979	4.565	0.5833	7.8
Silicic Acid	0.997257	14.212	0.0396	358.9
Avicel MCC	0.999485	0.6597	0.5503	1.2
TiO_2	0.999999	10.554	12.176	8.7

cellulose lost 6-8% weight in two hours at 110°C. Aerosil R-972 did not lose any weight from adsorbed water upon drying, but was dried at 110°C for one hour for the sake of consistency.

B. Solvatochromic Studies

Qualitative observations were made of the visible colors exhibited when BIPS compounds were dissolved in various solvents. 6-NO_2-BIPS solutions often required ultraviolet irradiation in order to produce the color; 6-H-BIPS and 6-OCH_3-BIPS solutions showed little or no photochromism at room temperature. Table XV lists the observed colors for these three BIPS compounds in a number of solvents. The asterisk indicates solutions that are essentially colorless until irradiated or that darken considerably upon irradiation. 6-NO_2-BIPS solutions were generally more apt to exhibit coloration in all solvents; other BIPS generally gave faint colors or remained colorless even after irradiation. Approximately 50-100 mg of solid BIPS were dissolved in 50 ml of solvent with sonication to make these observations.

Quantitative visible spectra of spiropyrans dissolved in polar solvents were highly dependent on the degree of exposure to uv light that the solutions received. The magnitude of the absorbance response varied from experiment to experiment; and was deemed an unreliable analytical tool. Apparent Beer's law plots could be made in the manner of Flannery (8); these could yield estimates of the colored fraction in solution upon assuming an absorptivity value. A single experiment could yield data with a high correlation coefficient, though the slope could differ by $\pm$50% in replicate trials. Figure 21 shows the results of an apparent Beer's law plot

Table XV. Solvatochromism of Three BIPS Compounds.

Solution Color[a]			
6-NO_2-BIPS	6-H-BIPS	6-OCH_3-BIPS	Solvent
blue*	colorless	lt. red-purple*	Cyclohexane
red*	red-orange	lt. blue	Methanol
dk. pink*	purple	lt. pink*	Isopropanol
purple	yellow*	lt. orange	Acetone
blue*	lt. yellow	lt. orange	Toluene
dk. purple*	lt. yellow	lt. pink-orange	Acetonitrile
red-orange	yellow	dk. yellow	Acetic Acid
red-pink	violet	violet	Ethanol
dk. blue*	lt. orange*	pink*	Chloroform
blue*	--	--	Xylene
blue-violet*	--	--	p-Dioxane
blue-violet*	lt. yellow	lt. pink	Methylene Chloride
pink	--	--	Amyl Alcohol
violet*	lt. yellow	lt. orange	Dimethylformamide
red-purple	yellow	lt. orange-pink	Dimethyl Sulfoxide
blue-green	--	--	Pyridine
dk. pink*	--	--	1-octanol

[a]An asterisk indicates solutions that require irradiation to show the visible color or that darken considerably under uv light.

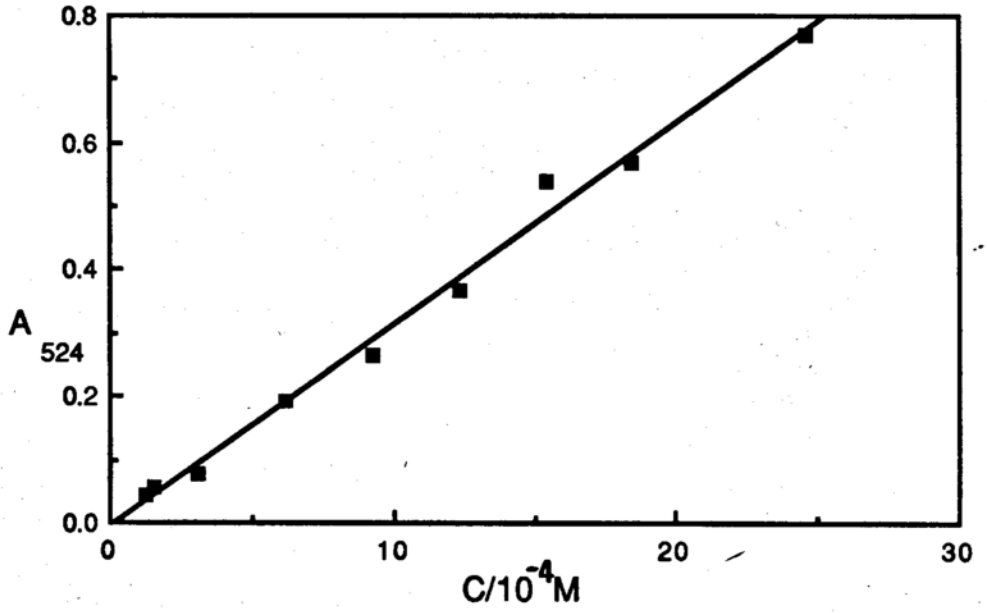

Figure 21. Apparent Beer's Law plot for 6-NO_2-BIPS in methanol (λ_{max} = 524 nm). Corr. = 0.9957, apparent absorptivity = 319 l/mole·cm.

for 6-NO_2-BIPS in methanol (λ_{max} = 524 nm). The correlation is good but the apparent absorptivity increases with time. After fifteen minutes of exposure to uv light, the absorbance of the lowest concentration data point increased from 0.042 to 0.192. The maximum wavelength remained invariant throughout the experiment. It is concluded that the magnitude of the absorbance is condition-dependent, but the λ_{max} is a characteristic property of the spiropyran/solvent system. Since qualitative observations proved that 6-NO_2-BIPS had the highest apparent absorptivities, λ_{max} values were recorded for this spiropyran in various solvents. Table XVI records the λ_{max} value, frequency of maximum absorption in cm^{-1}, and apparent absorptivities for 6-NO_2-BIPS in thirteen different solvents. Note the 16% decrease in $\varepsilon_{apparent}$ for 6-NO_2-BIPS in methanol obtained by recording the spectrum soon after preparation. No estimate of absorptivity was available for 6-NO_2-BIPS in H_2O; the extraction process used to record this spectrum was described earlier. Figure 22 shows the recorded spectrum of the orange aqueous solution; the spectrum was run twice and the curve was reproducible. The significant increase in polarity from methanol to H_2O produces a large shift (hypsochromic) in the λ_{max} value for 6-NO_2-BIPS. 6-H-BIPS and 6-OCH_3-BIPS spectra were not as easy to quantify versus solvent. They showed multiple peaks (similar to the 6-OCH_3-BIPS/cyclohexane spectrum in Figure 19), which changed in relative intensity with solvent, and often showed new peaks in alcoholic solvents.

Table XVI. 6-NO_2-BIPS Visible Peaks Versus Solvent.

Solvent	Absorptivity[a]	λ_{max}/nm	$\tilde{\nu}$/cm^{-1}[b]
Isopropanol	79	543.5	18,399
Acetone	49	564	17,730
Methylene Chloride	36	575	17,391
Acetonitrile	103	556	17,986
Ethanol	138	537	18,622
Chloroform	38	578	17,301
Amyl Alcohol	99	542	18,450
1-Octanol	60	547	18,282
DMF	166	559	17,889
DMSO	157	555.5	18,002
Methanol	271	523	19,120
Benzyl Alcohol	359	540	18,519
Water	-	492	20,325

[a] ε, in ℓ/mole·cm

[b] wavenumbers of maximum absorption

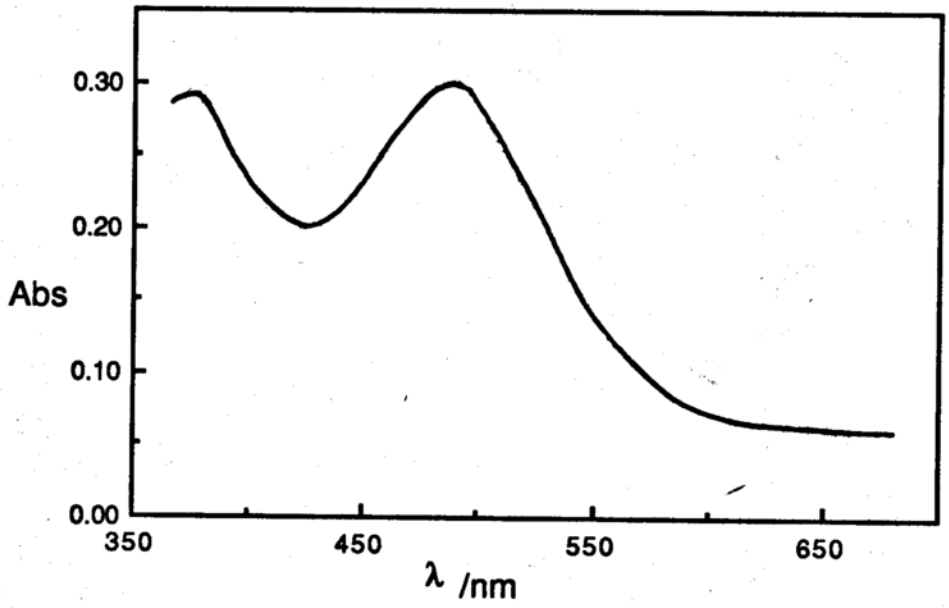

Figure 22. Visible spectrum of 6-NO_2-BIPS after extraction into water.

The spectrum of 6-NO_2-BIPS was determined as a function of water content in acetone/H_2O binary solvent mixtures, in an attempt to extend the polarity beyond that of methanol in spite of its low water solubility. Increasing amounts of water were included in acetone solutions of 6-NO_2-BIPS; the results are seen in Figure 23. λ_{max} is plotted as a function of the volume of water in the solution; the gradual color change is revealed by the reported colors. At more than 15 ml H_2O/25 ml solution, the solubility is too low to obtain a readable spectrum. The apparent absorptivities (ε, ℓ/mole·cm) are also shown versus the same abscissa. The tailing off of absorptivity is in part a real effect seen in merocyanine solutions (27, 28), and is in part an artifact due to solubility problems. The shift in λ_{max} versus solvent composition is monotonic and continuous; a single well-defined peak moves hypsochromically with an increase in solvent polarity. Table XVII gives the data in terms of mole fraction of water (X_{H_2O}) and frequency of absorption in cm^{-1} ($\overset{*}{\nu}$) for 6-NO_2-BIPS in acetone/H_2O mixtures. Mole fractions were determined from weights added and known densities; it is instructive to note that the X_{H_2O} = 0.747 solution results from adding sufficient H_2O to 60 ml acetone to result in 100 ml of solution. Figure 24 plots these data; they are roughly linear from X_{H_2O} = 0.25 to X_{H_2O} = 0.75, but deviate from linearity beyond these limits. Figure 25 is a color photograph of five of these solutions, illustrating the gradual color changes they exhibit. The first three solutions (from the left) contain 50 mg/100 ml, the fourth

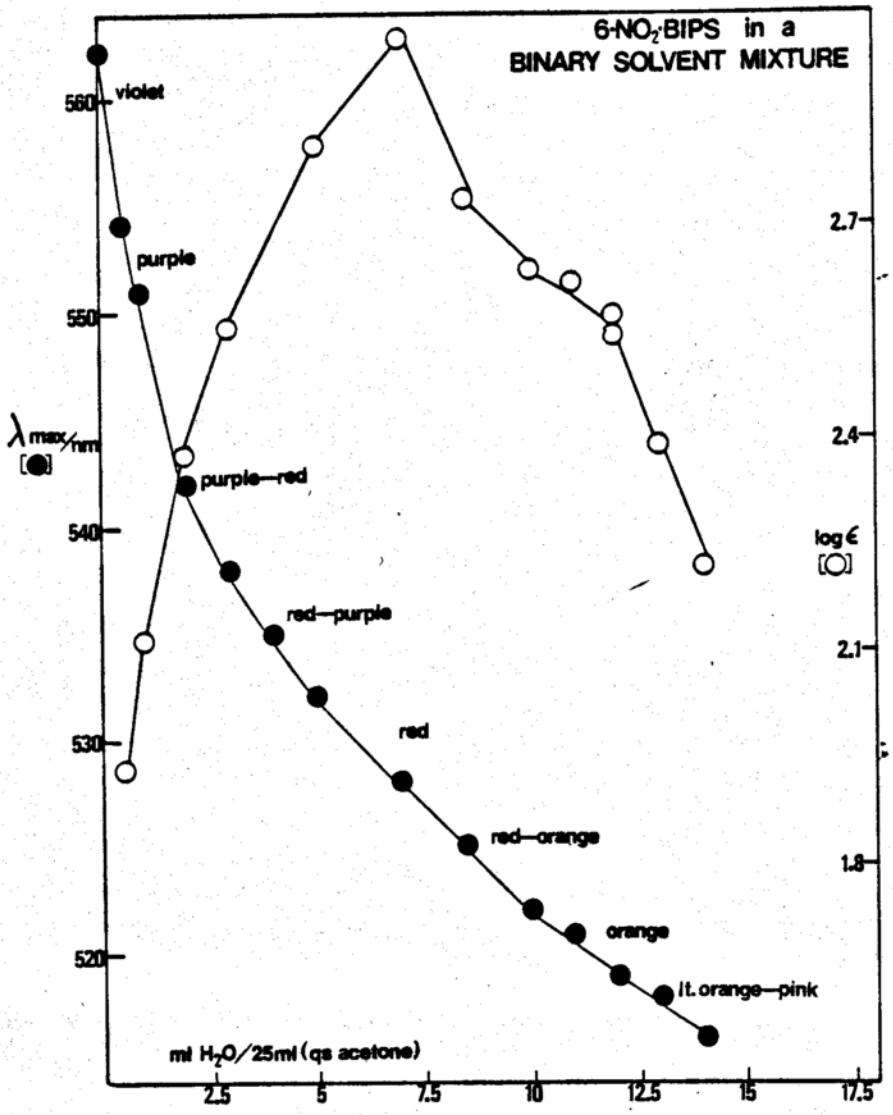

Figure 23. Spectral changes for 6-NO_2-BIPS in a binary solvent system.

Table XVII. Spectral Data for 6-NO_2-BIPS in Acetone/H_2O.

X_{H_2O}	λ_{max}/nm	$\tilde{\nu}$/cm^{-1}
0.000	562	17,794
0.062	555	18,018
0.213	545	18,349
0.282	542	18,450
0.359	539	18,553
0.461	534	18,727
0.539	531	18,832
0.606	527	18,975
0.661	524	19,084
0.707	520	19,231
0.747	516	19,380

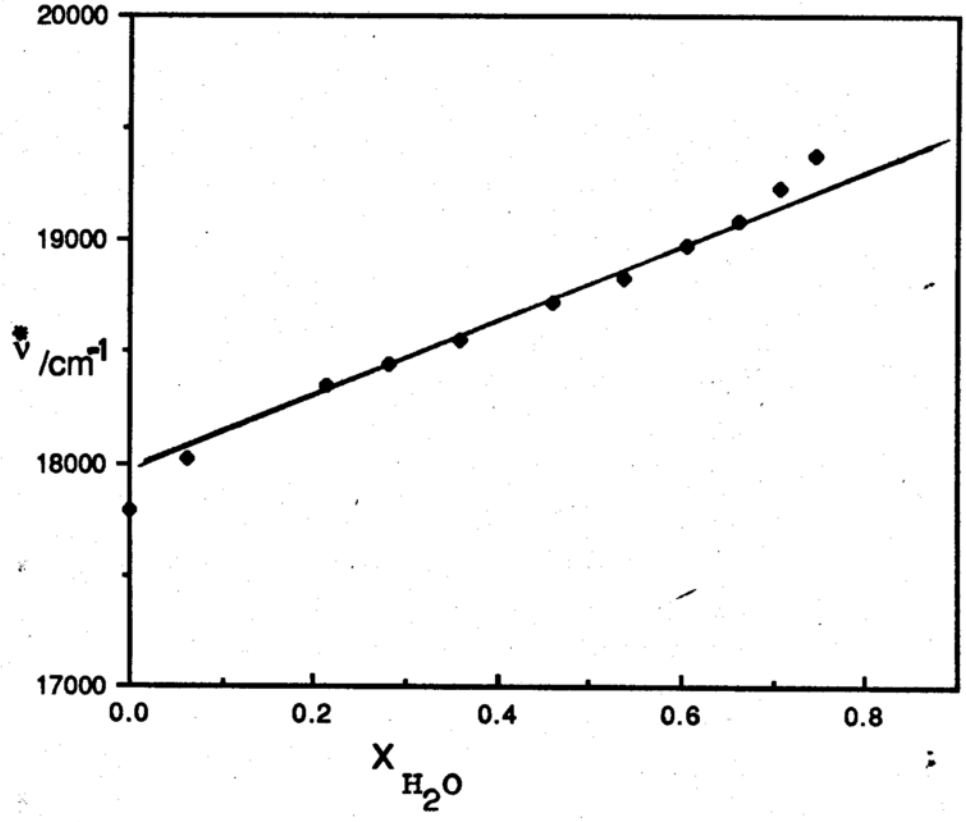

Figure 24. Spectral shifts for 6-NO_2-BIPS as a function of mole fraction water in acetone.

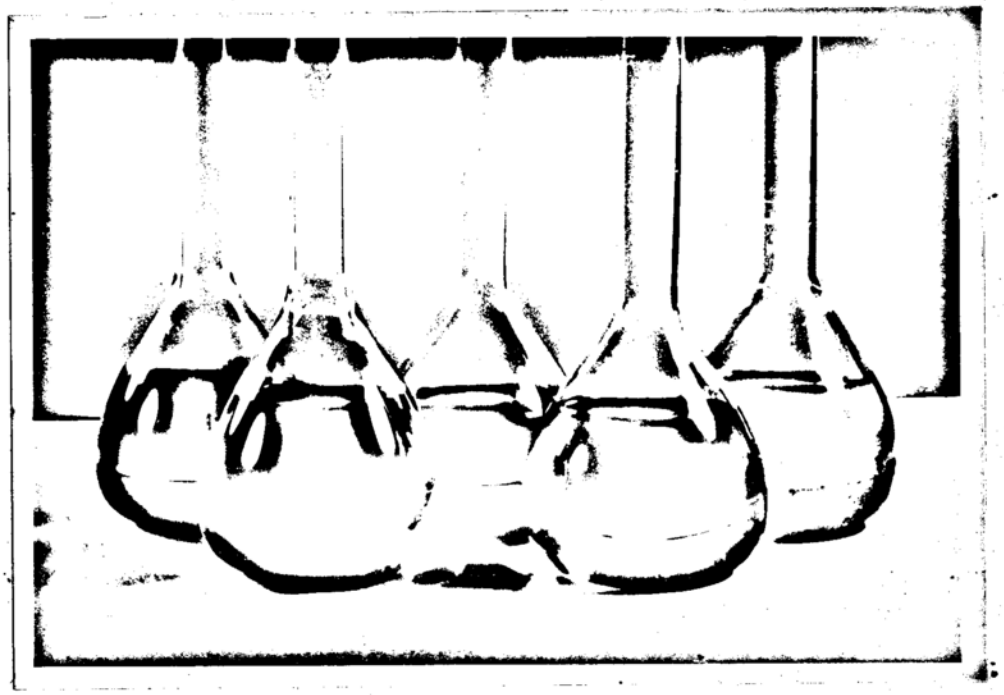

Figure 25. 6-NO_2-BIPS solutions in acetone/H_2O mixtures. Left to right: X_{H_2O} = 0.0, 0.213, 0.461, 0.661, and 0.747.

contains 25 mg, and the last contains only 10 mg as solubility problems set in.

The situation for INS dissolved in the same acetone/H_2O solutions is vastly different. There are two main absorption peaks in these solutions in the visible region. A solution of INS in pure acetone has a dominant peak at 543 nm and a secondary peak at approximately 510 nm. As water is added and the solution becomes more polar, the shorter-wavelength peak increases in intensity and shifts bathochromically. In the $X_{H_2O} = 0.747$ solution, the dominant peak is at 565 nm and the peak at 543 nm appears as a shoulder. Table XVIII lists the colors and peak positions of INS spectra in acetone/H_2O solutions. The peaks are often difficult to separate; parentheses are used to denote estimated λ_{max} values for obscured peaks. The general pattern is easier to fathom; there is a stationary peak at approximately 543 nm and a shifting peak that becomes more intense at higher wavelengths. The direction of that shift is bathochromic with polarity increases, exactly the opposite of the 6-NO_2-BIPS case. Because of the multiple peaks, it is much more difficult to follow this change than it was for 6-NO_2-BIPS. Figure 26 shows the spectra for INS and 6-NO_2-BIPS at two different solvent compositions; the greater simplicity and hypsochromic shifts for the 6-NO_2-BIPS solutions strongly contrast with the situation for INS solutions.

Table XVIII. Spectral Data for INS in Acetone/H_2O.

X_{H_2O}	Solution Color	Dominant Peak (nm)	Secondary Peak (nm)
0.000	orange	543	510
0.062	orange	543	(516)
0.213	orange-red	543	(516)
0.282	red-orange	543	(550)
0.359	red-pink	543	(558)
0.461	red-pink	(560)	543
0.539	pink-red	562	(543)
0.606	pink-red	564	(543)
0.661	pink	564	(543)
0.707	pink	564	(543)
0.747	pink-purple	565	(543)

Parentheses indicate estimates for obscured peaks.

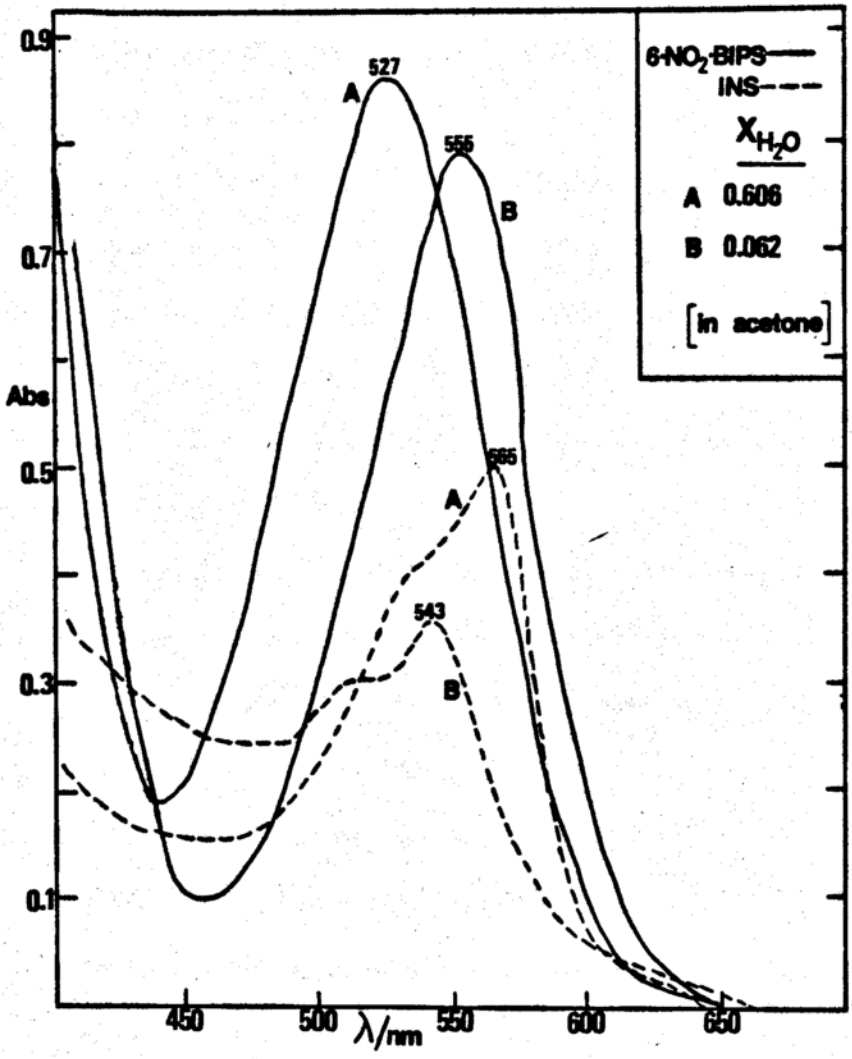

Figure 26. Spectral shifts for INS and 6-NO_2-BIPS in acetone/H_2O mixtures.

C. Adsorption Isotherms

A number of factors were found to influence the adsorptiochromic color of a spiropyran/adsorbent system in cyclohexane. The chemical properties of the adsorbent had a profound effect on the color produced by a given spiropyran adsorbed to the surface. One gram each of a number of different adsorbents was mixed into 100 ml lots of a 5×10^{-4} M 6-NO_2-BIPS solution (in cyclohexane), and the colors were observed after two hours. Table XIX lists the suspension colors and filtered solid colors for some of these systems. Almost the entire spectrum of colors is shown by this one spiropyran. Note the effect of the crystalline form of hydrated versus anhydrous aluminum chloride.

Adsorption to silica gel was also performed under uv light from blue (as opposed to colorless) cyclohexane/6-NO_2-BIPS solution. The same red-orange adsorbate/adsorbent powder resulted, at approximately the same rate of coloration.

Different spiropyrans produce different colors for a constant adsorbent. Table XX lists the suspension colors for four spiropyrans adsorbed onto nine adsorbents. It is evident that each spiropyran has certain characteristic shades: reds for 6-NO_2-BIPS, violets for INS, etc. The adsorbent surface determines the color in other cases regardless of spiropyran identity; e.g. pink for cellulose.

The amount of adsorbate on the adsorbent surface also

Table XIX. Adsorption Colors for 6-NO_2-BIPS.[a]

Adsorbent[b]	Suspension Color (2 hrs)	Dry Powder
acacia	lt. purple-pink	faint pink
alumina	orange	orange-pink
aminophylline	yellow	lt. yellow
bentonite	dk. orange-brown	dk. yellow
cellulose	off-white	pink
citric acid	lt. yellow	faint yellow-green
dextrose	pink-violet	lt. pink
fructose	purple-pink	pink
lactose	lt. purple-pink	lt. pink
magnesium sulfate	lt. orange	pale yellow
silica gel	red	red-orange
starch	off-white	off-white
sucrose	off-white	lt. pink
talc	yellow	lt. orange
tyrosine	lavender	faint pink
zinc oxide	yellow-brown	tan
$AlCl_3$, anhydrous	yellow-orange	bright yellow
$AlCl_3 \cdot 6H_2O$	green	yellow-green

[a] 5×10^{-4} M cyclohexane solutions + 1 gram adsorbent

[b] Dried one hour at 70°C (except $AlCl_3 \cdot 6H_2O$)

Table XX. Adsorption Colors of Spiropyrans.

Adsorbent	6-NO_2-BIPS	6-OCH_3-BIPS	6-H-BIPS	INS
silica gel	red-orange	dk. violet	orange-red	red-purple
alumina	yellow-orange	purple	pink-red	lt. purple
bentonite	burnt orange	dk. orange	yellow-brown	dull orange
talc	dk. yellow	pink-tan	lt. yellow-tan	pink-purple
silicic acid	red-orange	red-brown	dk. red	red-purple
Aerosil R-972	pink	--	--	lavender
cellulose	lt. pink	faint pink	faint pink	lavender pink
Cab-O-Sil	orange-red	dk. violet	orange	red-purple
Veegum[a]	bright yellow	bright orange	bright yellow	--

[a] colloidal Mg·Al·silicate

influences the observed color. A 6-NO_2-BIPS/alumina system is yellow, orange, or red in the order of increasing amount of surface coverage. A 6-NO_2-BIPS/silica gel system will reach the same dark red color as the alumina system at high coverage, but goes through a light pink, orange-pink, red-orange sequence at lower surface coverages. Figure 27 illustrates these changes for 6-NO_2-BIPS on alumina (top) and silica gel (bottom), with surface coverages expressed in nano·moles/m^2. The adsorbent particle size also plays a role in the effect, moderated through the scattering coefficient. Figure 28 shows that 6-OCH_3-BIPS/silica gel powders appear darker (at the same surface coverage) for the 300 m^2/g adsorbent (top) than for the 500 m^2/g adsorbent (bottom).

Cyclohexane was an ideal solvent for adsorption experiments; it is colorless, nonpolar, and relatively nontoxic. Silica and similar hydrophilic solids are insoluble in cyclohexane, and do not interact with cyclohexane as an adsorbate (119). ACS grade cyclohexane was not pure enough to give reliable uv assays of spiropyrans. ACS grade cyclohexane was passed through a silica-alumina column to pre-adsorb surface-active contaminants that might affect the measured capacity of an adsorbent. Discoloration of the column indicated the trapping of impurities; yet the capacity of a 6-NO_2-BIPS/alumina isotherm actually decreased 9% after passing the cyclohexane through the column. Even after passage through the column, ACS grade cyclohexane showed evidence of aromatic impurities when its spectrum was measured against deionized-distilled H_2O.

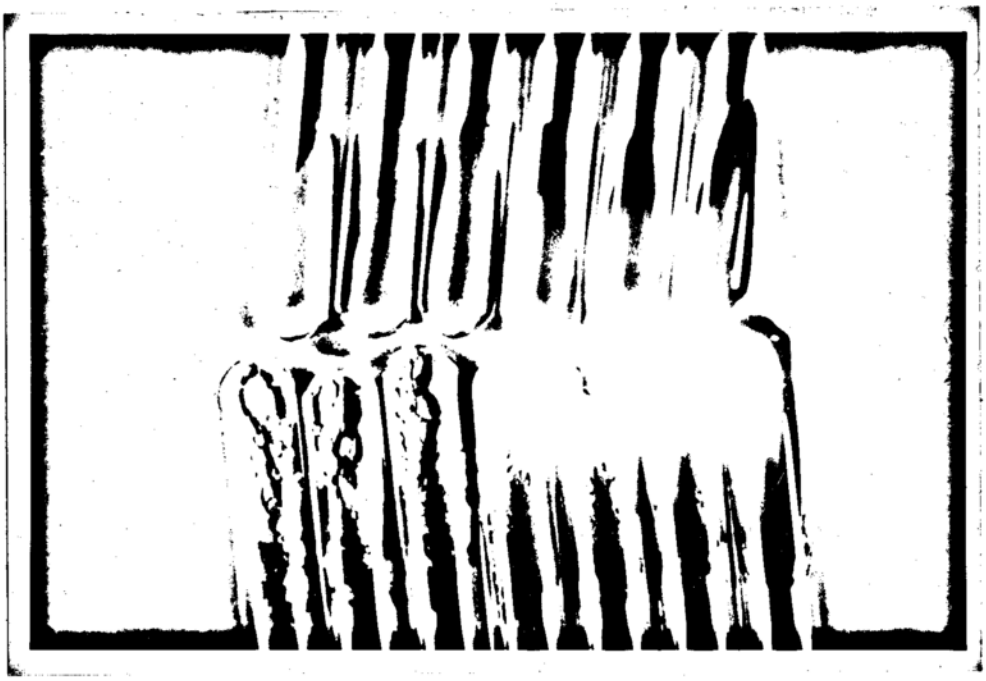

Figure 27. Concentration effect on adsorption color for 6-NO_2-BIPS on alumina (top) and silica gel (bottom). Surface coverages: top, g= 10.8,27,56,333,960,1493. bottom, g= 2.1, 8.4,16.1,38.5,87,123,944 nano·moles/m^2.

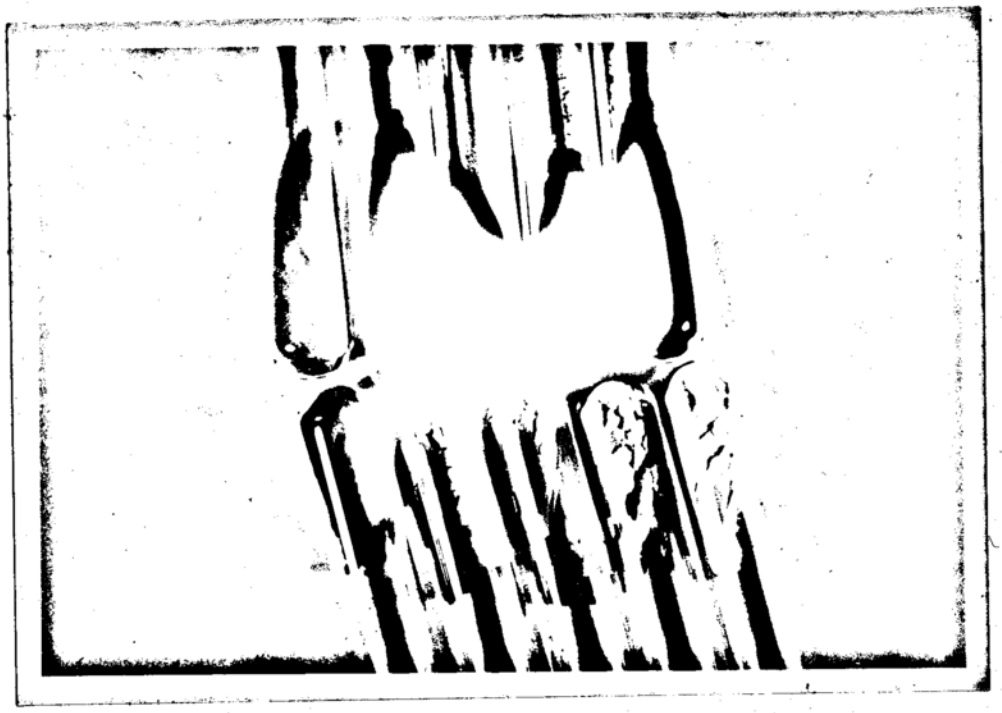

Figure 28. Effect of adsorbent particle size on apparent color. 6-OCH_3-BIPS on silica gel $300m^2/g$ (top) and $500m^2/g$ (bottom). Surface coverage (g)= 20.3,101,222,420, 1027 (top); and 389,167,83,25,4.3 (bottom) in nano moles/m^2.

Spectrophotometric grade cyclohexane showed no trace of impurities; the spectral comparison is shown in Figure 29. Consequently, spectrophotometric grade cyclohexane was used for determination of quantitative adsorption isotherms.

An experiment was undertaken to determine the effect of the filtration process on assayed concentration. Ten solutions of 6-NO_2-BIPS in cyclohexane ranging in concentration from 2×10^{-5}M to 1.2×10^{-4}M were read at 320 nm before and after filtration. The differences in absorbance were calculated and the average deviation was determined. The standard deviation (0.004) exceeded the average difference (-0.0025); hence the 95% confidence limits include zero.

Equilibration times were determined by experiment; they were a function of adsorbent and not of spiropyran. Cab-O-Sil and Aerosil R-972, the millimicron-sized fumed silicas, required equilibration times of less than 24 hours. Porous silica networks required up to one week for total equilibration; other solids fell between these two extremes. Table XXI shows equilibration data for 6-NO_2-BIPS/alumina, using an initial concentration of 6×10^{-3}M and approximately 300 mg of alumina. The loss of 6-NO_2-BIPS in the bulk solution is followed by the decrease in absorbance at 320 nm. Three days was chosen as the equilibration time for this system. Figure 30 shows the approach to equilibrium graphically for the 6-NO_2-BIPS/silicic acid system. Initial concentrations of 5×10^{-3}M and 5×10^{-4}M were used, along with 100 mg of silicic acid. At between 4 and 7 days the curves level off; one week was used to equilibrate

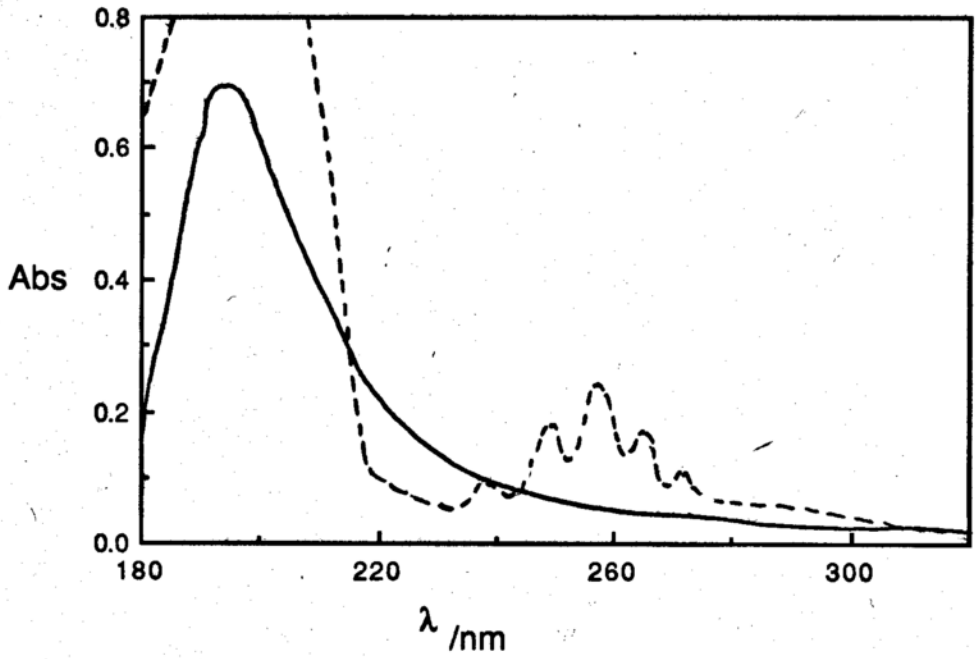

Figure 29. Comparison of ACS (----) versus spectrophotometric grade (——) cyclohexane; the reference cell contained distilled H_2O.

Table XXI. Equilibration Data for 6-NO_2-BIPS/alumina.

Time/hours	A_{320}[a]	mg adsorbed[b]
2.5	1.935	19.2
5	1.862	22.1
22	1.754	26.4
38	1.749	26.6
74	1.638	31.1
96	1.635	31.1
120	1.641	30.9

[a]Initial spiropyran concentration = 6×10^{-3}M

[b]300 mg alumina adsorbent

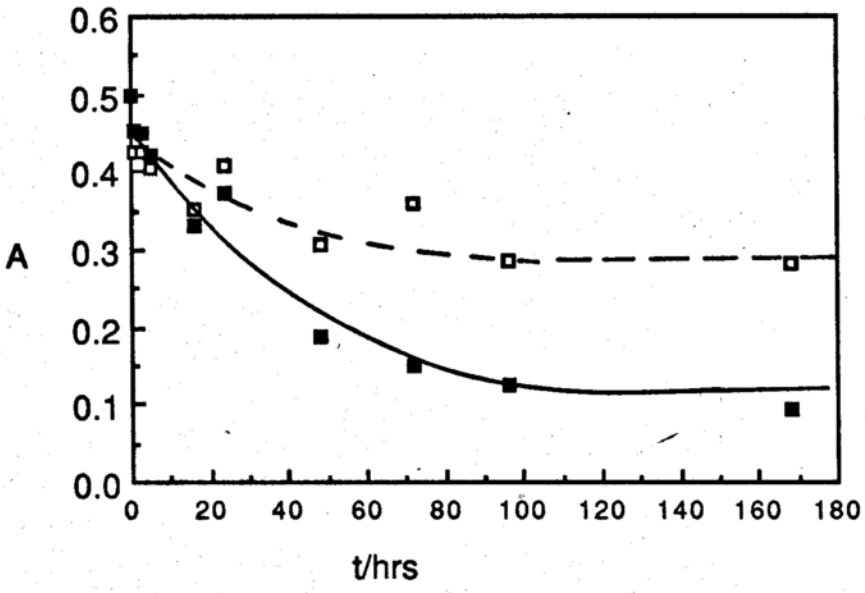

Figure 30. Decrease in A_{320} with time for the 6-NO_2-BIPS/silicic acid equilibration time determination.

□ initial concentration 5×10^{-3} M ($\frac{1}{10}$ dilution)

■ initial concentration 5×10^{-4} M.

these systems in isotherm measurements. Other porous adsorbents (talc, microcrystalline cellulose) were also given one week to equilibrate with spiropyran solutions.

These studies showed that adsorption took place for up to one week after system preparation. On the other hand, color formation was virtually complete within a few hours. Further adsorption neither darkened the adsorbent nor affected its visible absorption spectrum. Figures 31 and 32 illustrate the time dependence of color formation for silica gel in the presence of 6-NO_2-BIPS and INS, respectively. The adsorption process was qualitatively reversible; silica gel colored red by 6-NO_2-BIPS adsorption, shaken with fresh cyclohexane, rendered the solution photochromic. Complete desorption could not be achieved within 24 hours.

Adsorption isotherms were measured at 25.0°C for four different spiropyrans on both silica gel (300 m^2/g) and alumina. Isotherms on silica gel (500 m^2/g), silicic acid, talc, TiO_2, and Avicel microcrystalline cellulose were obtained for INS and 6-NO_2-BIPS. The fumed silicas (Cab-O-Sil and Aerosil R-972) were used for 6-NO_2-BIPS only. Figure 33 shows the low concentration portion of the 6-NO_2-BIPS/alumina isotherm; as expected from the Langmuir expression, low concentration data appear linear. Tables XXII-XLI list the data for the twenty isotherms measured. The equilibrium concentrations of unadsorbed spiropyran, amounts adsorbed in mg/g, and the ratio of the two (for construction of the Scott plot) are given. Table XLII summarizes the correlation coefficients and

Figure 31. Color formation with time, 1×10^{-4} M 6-NO_2-BIPS and silica gel. Left to right; 10 min., 2 min., and 15 sec. after preparation.

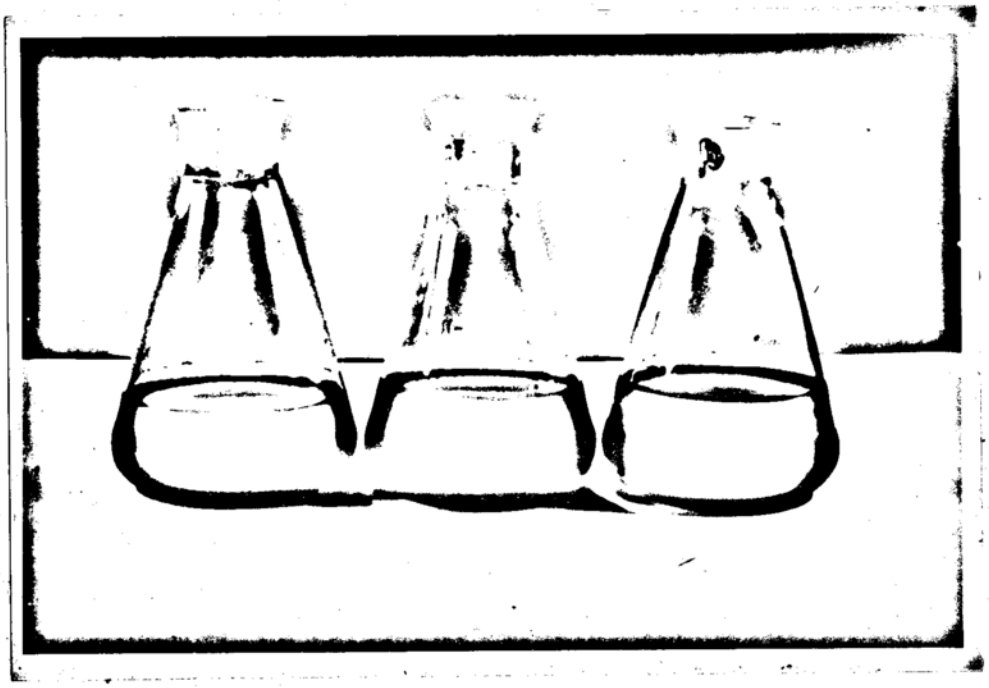

Figure 32. Color formation with time, 1×10^{-4} M INS and silica gel. Left to right; 10 min., 2 min., and 15 sec. after preparation.

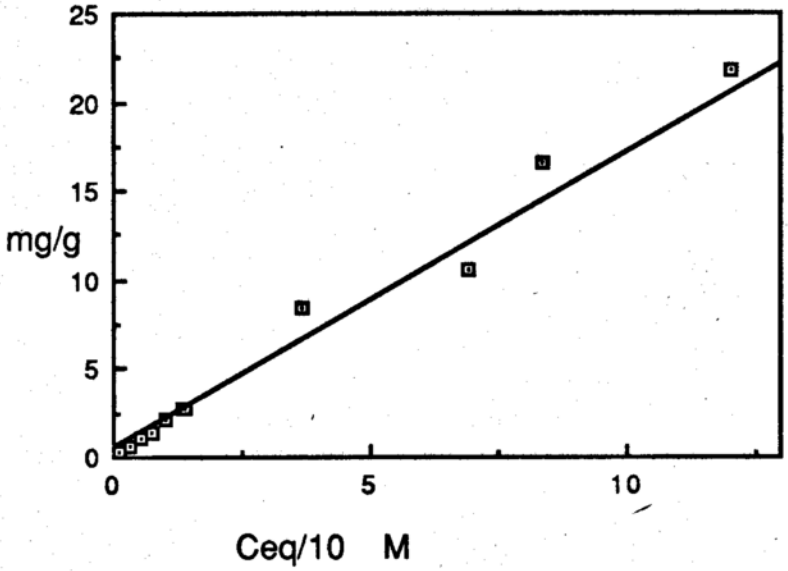

Figure 33. Low concentration linearity for 6-NO_2-BIPS/alumina isotherm.

parameter estimates obtained from the Scott plots. The number of data points is reduced because of the points rejected by means of Scatchard plot analysis. The rejected points are always those of the lowest equilibrium concentrations in the tabulated data set. Figures 34-53 show the graphed isotherms along with the fitted hyperbola obtained from the Duggleby program. The exception is the 6-NO_2-BIPS/Aerosil R-972 system, which does not exhibit strong enough binding to use the program. The binding for this system is so low and incomplete that it can be fit to a straight line, as can the initial data for the other isotherms. Table XLIII lists the parameters obtained for the rectangular hyperbola fitted to the other 19 data sets.

Preliminary results for the effect of temperature on the adsorption isotherms were obtained for 6-NO_2-BIPS and INS on silica gel (500 m^2/g). The capacities and binding constants are given in Table XLIV for studies at 18°C, 25°C, and 35°C. An isotherm for a permanent dye (malachite green) on silica gel (500 m^2/g) from water was also measured for comparative purposes. Table XLV gives the isotherm parameters from Scott plot and Duggleby nonlinear regression analysis for this system. Figure 54 shows these data graphically; they provide an excellent fit to the Langmuir model.

Table XXII. 25°C Isotherm Data, 6-NO_2-BIPS/Silica Gel (300 m^2/g).

$C_{eq}/10^{-4}M$	$(mg/g)_{ads}$	$10^6\ C_{eq}/(mg/g)$
43.7	107.3	40.74
38.3	107.9	35.46
29.3	104.6	28.05
20.1	101.5	19.82
13.0	91.6	14.18
11.2	98.0	11.43
8.25	80.8	10.21
5.55	82.5	6.73
2.48	64.5	3.84
2.35	59.9	3.92
1.30	63.6	2.04
1.01	34.1	2.96
0.79	52.1	1.52

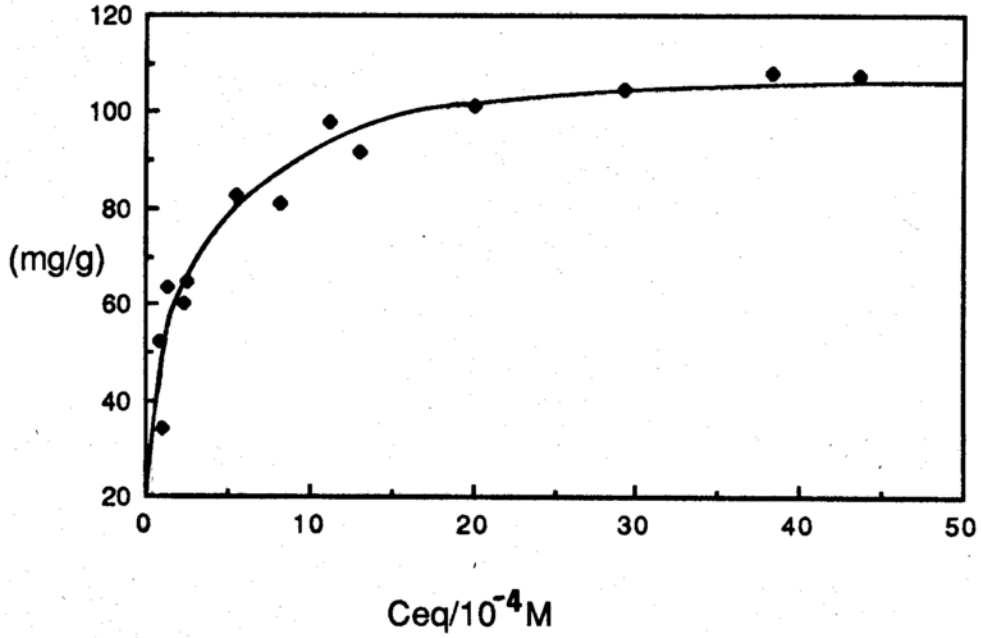

Figure 34. 6-NO_2-BIPS/silica gel (300m^2/g) isotherm, 25°C.

Table XXIII. 25°C Isotherm Data, 6-NO_2-BIPS/Alumina.

$C_{eq}/10^{-4}M$	$(mg/g)_{ads}$	$10^6\ C_{eq}/(mg/g)$
61.8	100.8	61.3
60.8	102.9	59.1
52.3	95.4	54.8
51.0	102.9	49.6
41.2	100.1	41.2
32.8	91.6	35.8
32.0	98.1	32.6
24.0	86.0	27.9
23.8	87.7	27.1
16.5	72.3	22.8
15.1	81.1	18.6
11.1	60.7	18.3
8.9	60.2	14.7
7.3	69.1	10.6
5.1	47.9	10.6
2.9	38.1	7.7
1.7	45.0	3.8
1.7	26.8	6.2
1.2	21.8	5.5
0.8	16.6	5.0

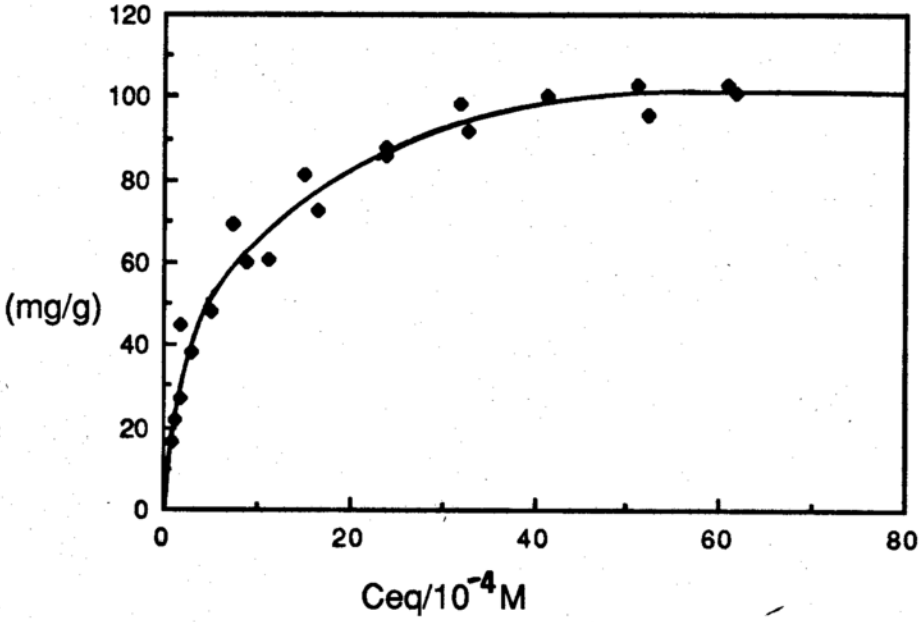

Figure 35. 6-NO_2-BIPS/alumina isotherm, 25°C.

Table XXIV. 25°C Isotherm Data, INS/Silica Gel (300 m^2/g).

$C_{eq}/10^{-4}M$	$(mg/g)_{ads}$	$10^6\ C_{eq}/(mg/g)$
213.9	127.3	168.1
165.5	121.7	136.0
119.2	107.9	110.5
94.0	109.3	86.0
71.0	102.7	69.1
48.1	95.4	50.4
29.2	73.0	40.0
22.8	83.2	27.4
14.3	58.8	24.4
9.81	52.5	18.7
9.23	55.9	16.5
3.38	42.0	8.05
2.78	30.9	9.00
2.69	34.5	7.78
2.16	19.4	11.17
1.83	28.4	6.44
0.59	15.6	3.80
0.59	8.65	6.86
0.47	15.80	2.97
0.15	4.82	0.31
0.12	6.54	1.80
0.06	1.94	2.87
0.04	3.35	1.15
0.04	0.93	4.38
0.01	0.49	2.18

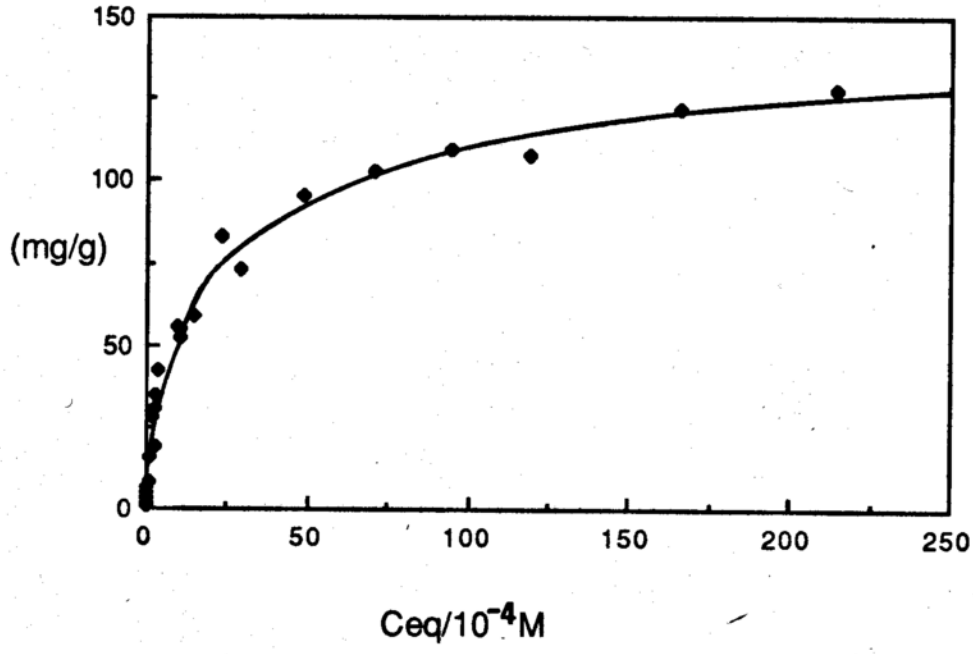

Figure 36. INS/silica gel ($300m^2/g$) isotherm, 25°C.

Table XXV. 25°C Isotherm Data, INS/Alumina.

$C_{eq}/10^{-3}M$	$(mg/g)_{ads}$	$10^5\ C_{eq}/(mg/g)$
17.56	54.7	32.1
17.05	48.0	35.5
12.87	50.9	25.3
11.78	49.8	23.6
9.72	51.3	18.9
8.14	41.7	19.5
7.37	42.7	17.3
6.01	44.2	13.6
5.31	43.9	12.1
4.24	39.5	10.8
2.31	38.2	6.05
1.98	32.8	6.04
1.39	29.4	4.74
0.717	27.6	2.60
0.285	21.5	1.32
0.182	18.3	0.99
0.050	12.2	0.41
0.019	8.5	0.22
0.012	6.3	0.19

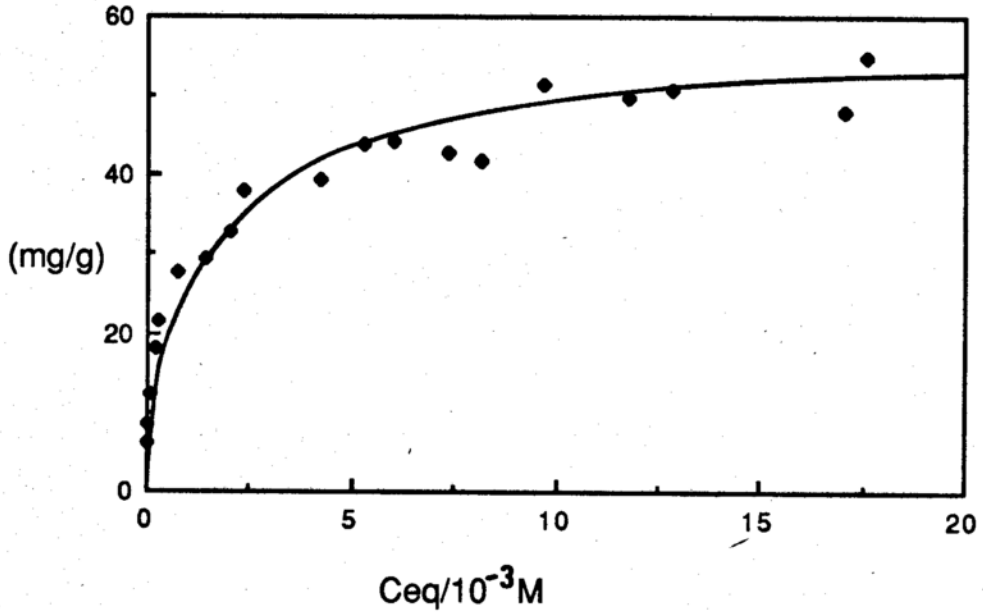

Figure 37. INS/alumina isotherm, 25°C.

Table XXVI. 25°C Isotherm Data, 6-H-BIPS/Silica Gel (300 m^2/g).

$C_{eq}/10^{-4}M$	$(mg/g)_{ads}$	$10^5\ C_{eq}/(mg/g)$
225.0	73.6	30.55
177.0	68.5	25.86
101.5	69.8	14.53
78.7	63.6	12.38
61.0	55.8	10.92
56.0	57.2	9.78
43.3	48.6	8.91
34.0	47.5	7.17
25.0	43.9	5.68
13.4	34.2	3.91
5.90	26.7	2.22
3.19	20.0	1.59
2.03	17.4	1.17
0.95	12.1	0.79
0.63	9.87	0.64
0.28	6.58	0.42
0.19	5.31	0.35
0.06	2.77	0.21

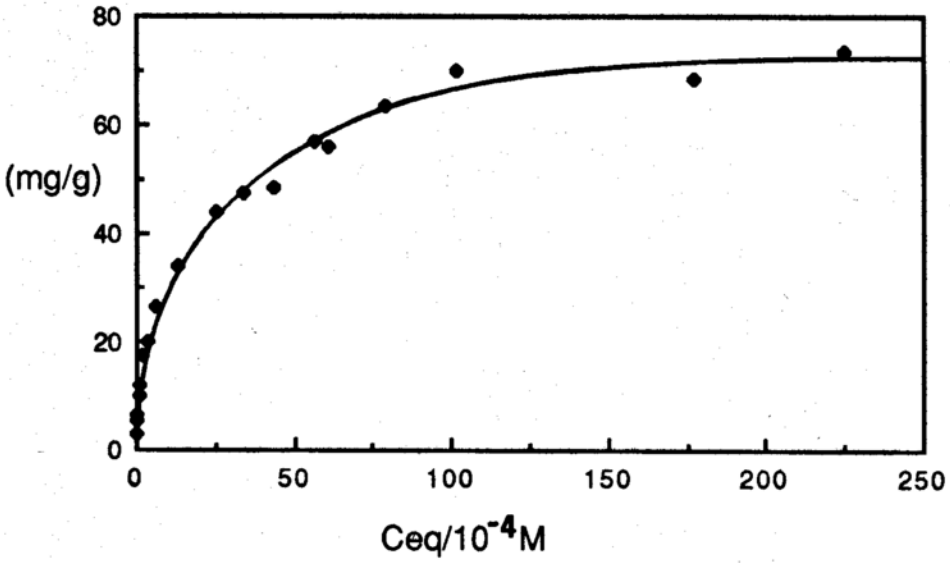

Figure 38. 6-H-BIPS/silica gel ($300m^2/g$) isotherm, 25°C.

Table XXVII. 25°C Isotherm Data, 6-H-BIPS/Alumina.

$C_{eq}/10^{-3}M$	$(mg/g)_{ads}$	$10^5\ C_{eq}/(mg/g)$
11.1	29.2	38.0
9.80	30.5	32.2
9.42	30.6	30.8
7.52	28.8	26.1
6.48	26.1	24.8
6.42	27.4	23.5
5.21	27.6	18.9
4.71	29.0	16.2
4.02	27.4	14.7
3.40	24.2	14.1
2.93	26.0	11.3
1.94	23.1	8.4
1.77	24.6	7.2
0.99	19.6	5.1
0.61	17.0	3.6
0.16	10.9	1.5
0.15	4.3	3.4

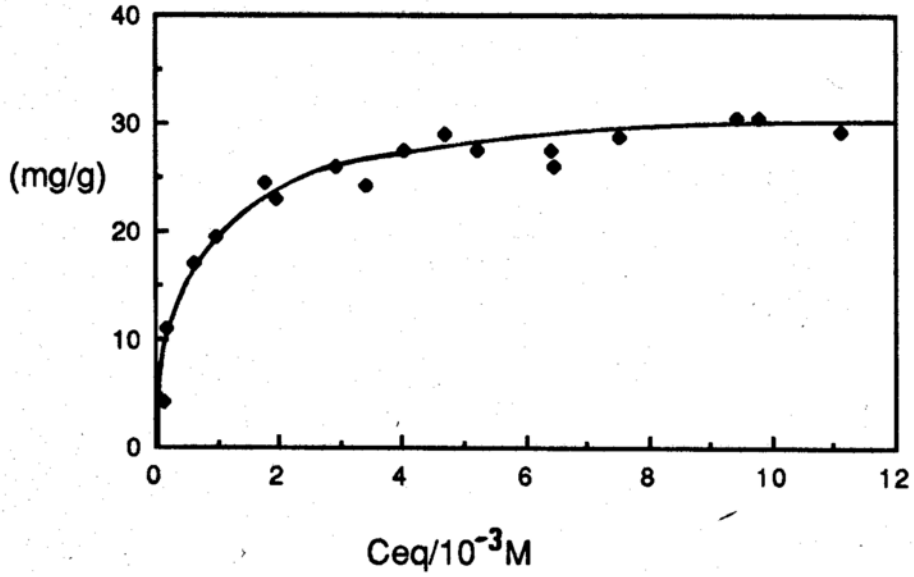

Figure 39. 6-H-BIPS/alumina isotherm, 25°C.

Table XXVIII. 25°C Isotherm Data, 6-OCH_3-BIPS/Silica Gel (300 m^2/g).

$C_{eq}/10^{-3}M$	$(mg/g)_{ads}$	$10^5\ C_{eq}/(mg/g)$
19.81	134.3	14.75
16.98	127.6	13.31
16.06	124.8	12.87
14.13	123.8	11.41
12.27	119.7	10.25
10.62	107.4	9.89
8.65	105.8	8.17
5.75	103.5	5.56
4.26	94.7	4.50
2.08	60.6	3.44
1.18	58.2	2.03
0.56	45.4	1.23
0.28	38.7	0.74
0.13	27.6	0.46
0.13	14.9	0.89
0.11	20.5	0.54
0.09	9.3	0.09
0.006	6.1	0.11
0.002	3.8	0.06
0.001	1.9	0.07

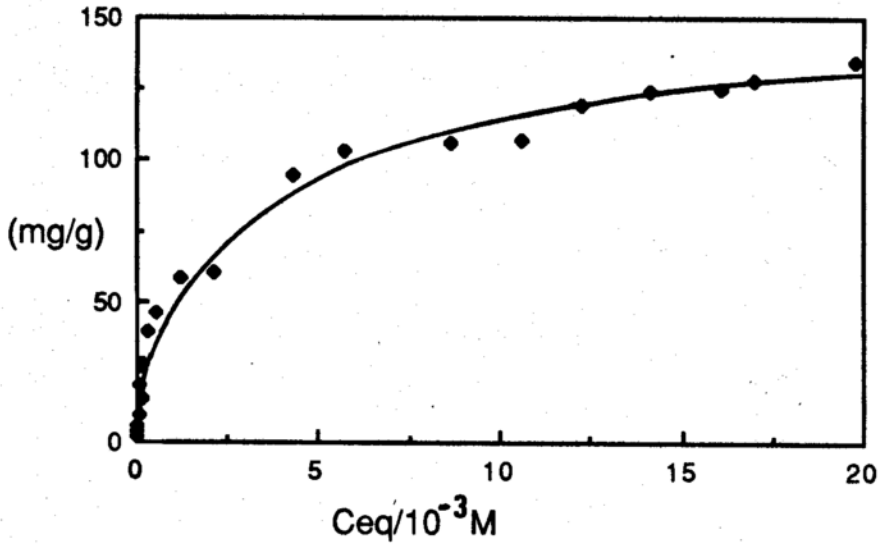

Figure 40. 6-OCH_3-BIPS/silica gel (300m^2/g) isotherm, 25°C.

Table XXIX. 25°C Isotherm Data, 6-OCH_3-BIPS/Alumina.

$C_{eq}/10^{-4}M$	$(mg/g)_{ads}$	$10^5\ C_{eq}/(mg/g)$
82.5	39.5	20.9
71.2	38.2	18.6
59.3	38.1	15.6
35.2	38.5	9.1
6.74	26.9	2.5
2.24	15.1	1.5
1.19	7.4	1.6
0.47	3.0	1.6

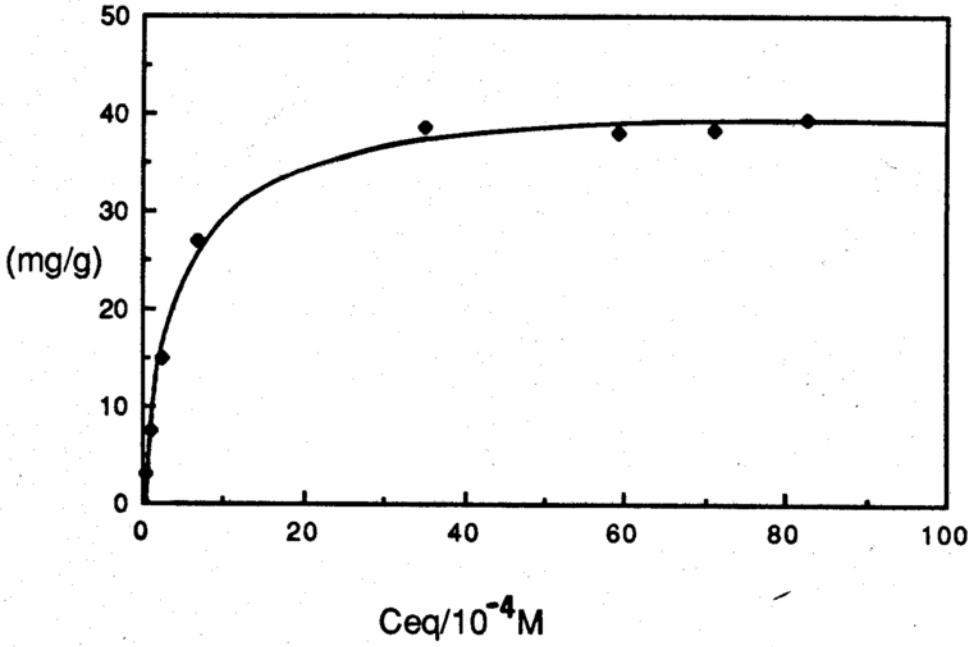

Figure 41. 6-OCH_3-BIPS/alumina isotherm, 25°C.

Table XXX. 25°C Isotherm Data, 6-NO_2-BIPS/Cab-O-Sil.

$C_{eq}/10^{-4}M$	$(mg/g)_{ads}$	$10^6\ C_{eq}/(mg/g)$
68.7	81.2	84.61
66.7	102.9	64.82
66.4	99.4	66.80
48.7	82.1	59.26
48.7	81.5	59.78
47.8	93.0	51.40
39.0	81.1	48.07
39.0	80.3	48.56
29.5	79.1	37.30
29.2	83.0	35.16
28.9	82.4	35.08
23.0	51.6	44.61
21.3	66.7	31.93
13.1	52.7	24.86
12.6	57.9	21.76
5.02	40.4	12.43
4.55	26.2	17.37
3.28	41.2	7.96
2.40	27.9	8.60
1.36	20.7	6.57
0.66	11.7	5.62

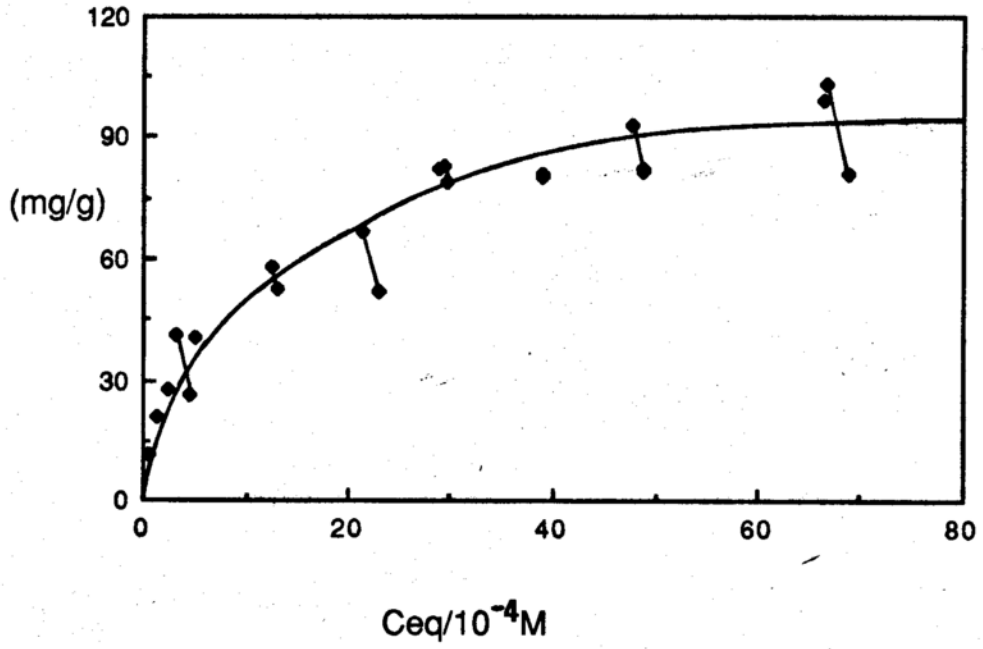

Figure 42. 6-NO_2-BIPS/Cab-O-Sil isotherm, 25°C.

Duplicate determinations are connected.

Table XXXI. 25°C Isotherm Data, 6-NO_2-BIPS/Aerosil R-972.

$C_{eq}/10^{-4}M$	$(mg/g)_{ads}$	$10^4\ C_{eq}/(mg/g)$
74.9	9.71	7.71
66.2	7.25	9.13
38.9	3.50	11.10
36.9	5.91	6.24
27.9	4.01	6.96
19.5	1.60	12.20
18.8	2.29	8.21
9.23	1.47	6.28
7.73	0.85	9.10
5.76	0.74	7.80
4.51	0.93	4.85
0.28	0.67	4.20
0.09	0.33	2.70

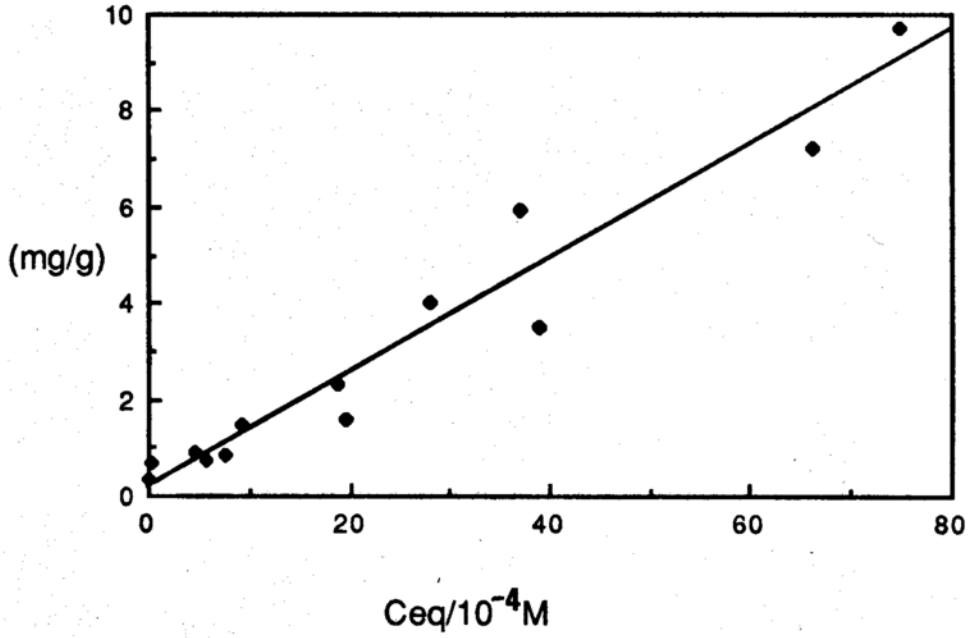

Figure 43. 6-NO_2-BIPS/Aerosil R-972 isotherm, 25°C. Follows (mg/g)= 1172 C_{eq}+ 0.219, with a correlation coefficient of 0.971.

Table XXXII. 25°C Isotherm Data, 6-NO_2-BIPS/Silicic Acid.

$C_{eq}/10^{-4}M$	$(mg/g)_{ads}$	$10^7\ C_{eq}/(mg/g)$
57.4	194.5	295
47.5	196.2	240
38.1	186.5	204
30.4	172.5	176
29.8	172.6	173
29.0	180.6	161
26.5	182.5	145
25.7	185.7	138
19.8	158.9	124
19.1	173.5	110
19.1	174.6	109
14.0	157.2	89
12.3	161.6	76
11.9	167.2	71
7.80	144.9	54
6.54	144.5	45
6.09	147.4	41
4.40	120.4	36.5
3.80	123.4	30.5

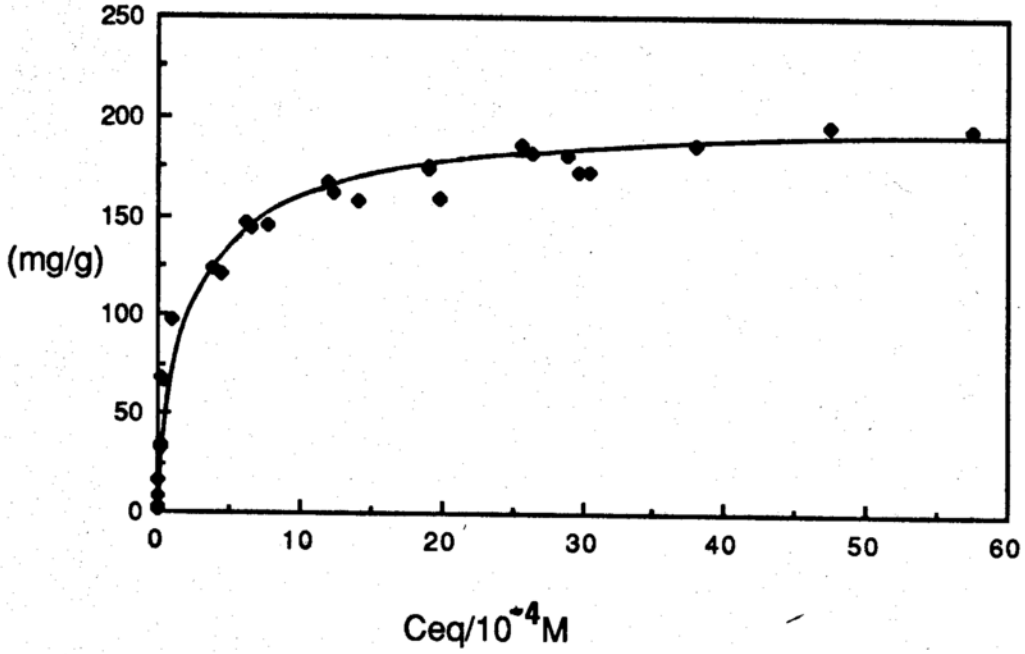

Figure 44. 6-NO_2-BIPS/silicic acid isotherm, 25°C.

Table XXXIII. 25°C Isotherm Data, INS/Silicic Acid.

$C_{eq}/10^{-4}M$	$(mg/g)_{ads}$	$10^6\ C_{eq}/(mg/g)$
75.8	153.9	49.25
64.8	149.2	43.43
53.3	145.7	36.58
43.4	139.9	31.02
30.2	145.4	20.77
21.1	148.0	14.26
12.1	139.1	8.70
5.4	119.6	4.52
1.0	94.3	1.09
0.6	55.9	0.11
0.1	27.9	0.04
0.1	11.0	0.08

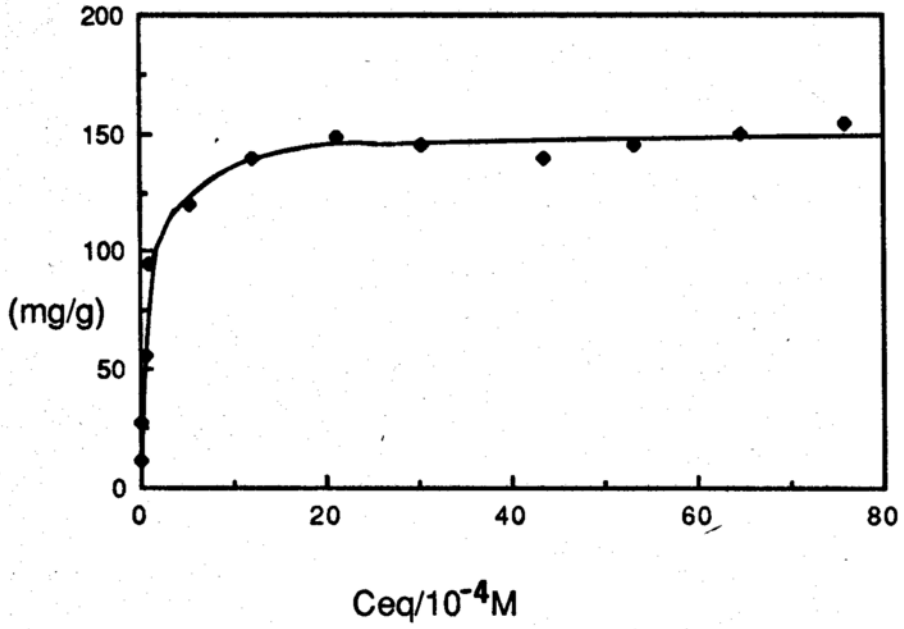

Figure 45. INS/silicic acid isotherm, 25°C.

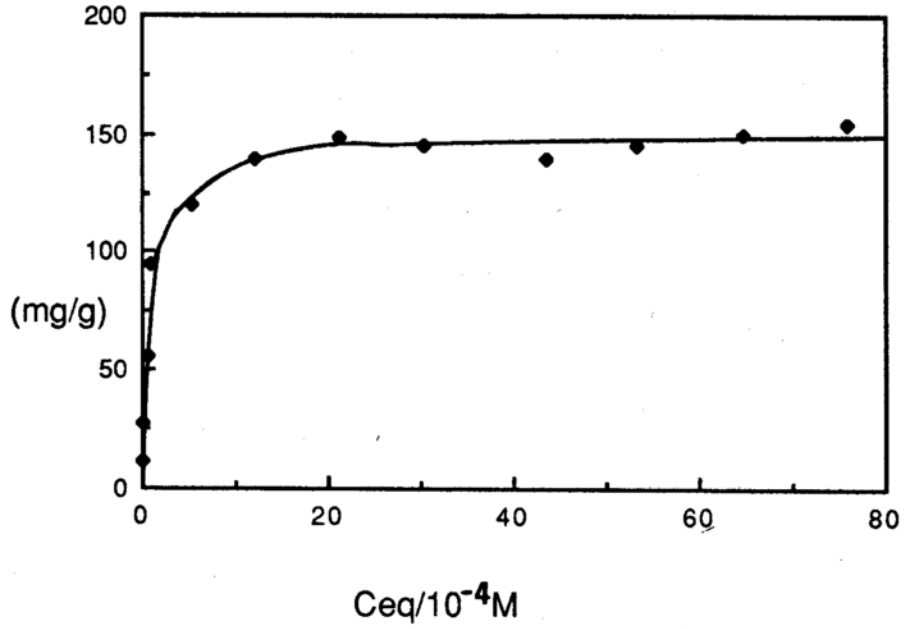

Figure 45. INS/silicic acid isotherm, 25°C.

Table XXXIV. 25°C Isotherm Data, 6-NO_2-BIPS/Talc.

$C_{eq}/10^{-4}M$	$(mg/g)_{ads}$	$10^5\ C_{eq}/(mg/g)$
62.6	2.28	275
46.8	1.96	239
38.8	1.95	199
38.6	2.36	164
30.7	2.18	141
22.8	2.00	114
22.7	2.04	115
15.0	2.01	73
14.8	1.95	76
10.9	1.75	63
7.2	1.58	45
6.9	1.81	38
4.0	1.59	25
3.1	1.40	22
2.4	1.27	19
0.095	1.07	8.9
0.026	0.88	2.9
0.001	0.50	0.2

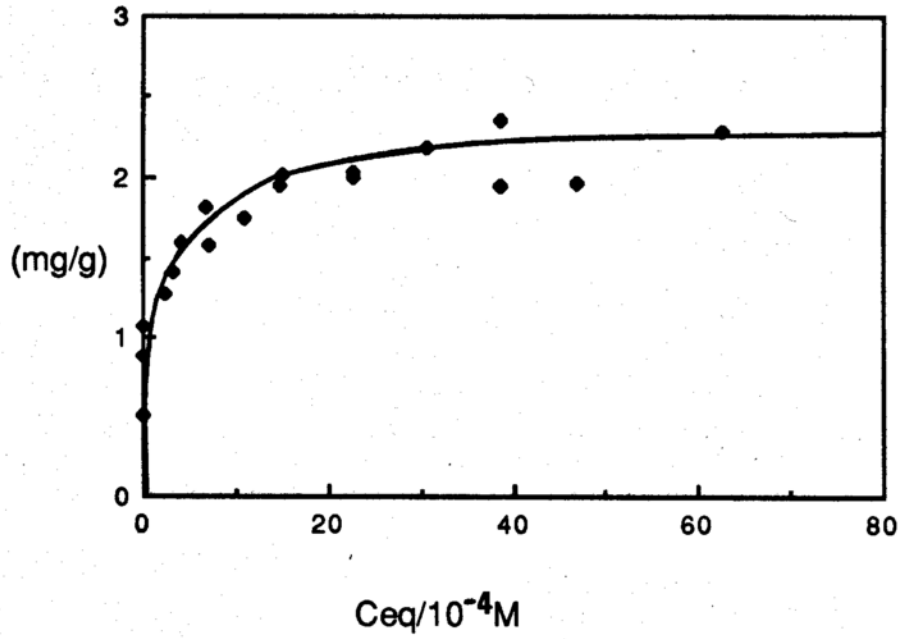

Figure 46. 6-NO_2-BIPS/talc isotherm, 25°C.

Table XXXV. 25°C Isotherm Data, INS/Talc.

$C_{eq}/10^{-4}M$	$(mg/g)_{ads}$	$10^5\ C_{eq}/(mg/g)$
118	1.643	718
93.4	2.134	438
70.3	1.396	504
45.8	1.805	254
22.0	1.643	134
10.6	1.151	92
5.7	1.233	46
2.3	1.068	22
1.21	0.976	12
0.24	0.788	3.1
0.01	0.582	1.9
0.00	0.197	—

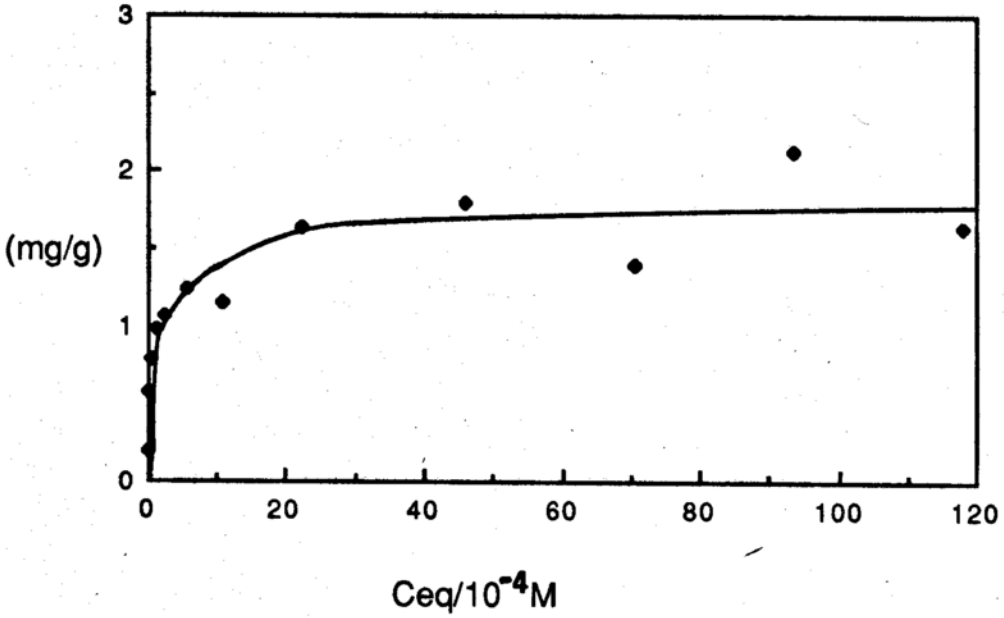

Figure 47. INS/talc isotherm, 25°C.

Table XXXVI. 25°C Isotherm Data, 6-NO_2-BIPS/Avicel.

$C_{eq}/10^{-4}M$	$(mg/g)_{ads}$	$10^3\ C_{eq}/(mg/g)$
78.3	0.465	16.8
62.8	0.329	19.1
31.0	0.273	11.4
24.8	0.218	11.4
18.6	0.164	11.4
12.3	0.137	9.0
6.18	0.061	10.1
3.06	0.038	8.1
1.50	0.026	5.7
1.20	0.021	5.8
0.90	0.016	5.7
0.60	0.011	5.4
0.30	0.005	6.1
0.15	0.002	1.0

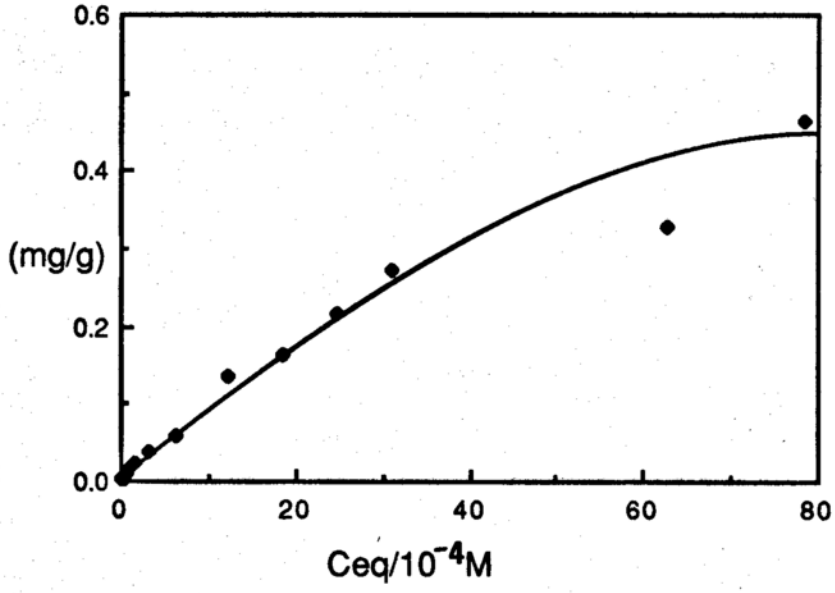

Figure 48. 6-NO_2-BIPS/Avicel microcrystalline cellulose isotherm, 25°C.

Table XXXVII. 25°C Isotherm Data, INS/Avicel.

$C_{eq}/10^{-4}M$	$(mg/g)_{ads}$	$10^4\ C_{eq}/(mg/g)$
92.7	0.919	100.9
68.5	0.984	69.6
44.5	0.975	45.6
22.7	0.362	62.7
13.4	0.270	49.8
9.20	0.113	81.6
4.38	0.116	37.8
2.23	0.047	47.9
1.35	0.026	51.4
0.90	0.018	49.2
0.44	0.011	39.3
0.21	0.008	26.1
0.08	0.010	8.1
0.03	0.005	6.4

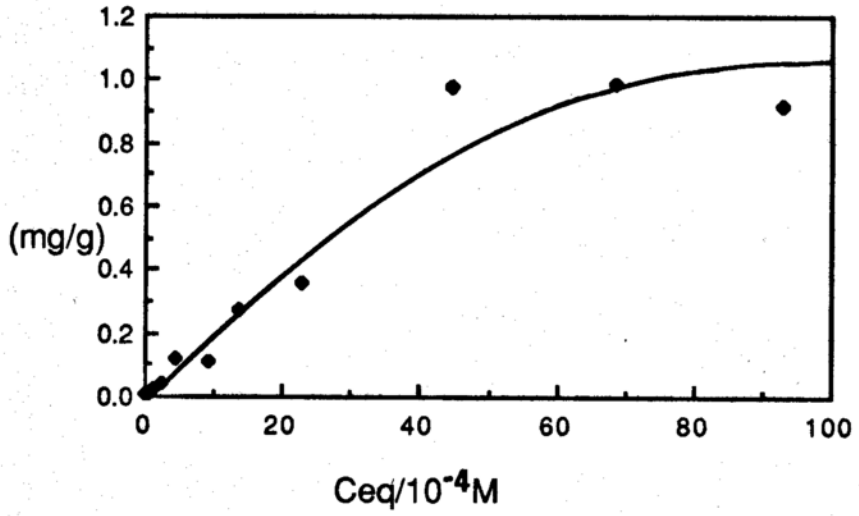

Figure 49. INS/Avicel microcrystalline cellulose isotherm, 25°C.

Table XXXVIII. 25°C Isotherm Data, 6-NO_2-BIPS/TiO_2.

$C_{eq}/10^{-4}M$	$(mg/g)_{ads}$	$10^5\ C_{eq}/(mg/g)$
77.5	4.03	192.3
61.4	4.20	146.2
37.5	4.03	93.1
21.7	3.72	58.3
13.8	3.56	38.8
6.33	2.70	23.4
3.28	2.45	13.4
0.69	1.47	4.7
0.27	0.86	3.1
0.02	0.61	0.4

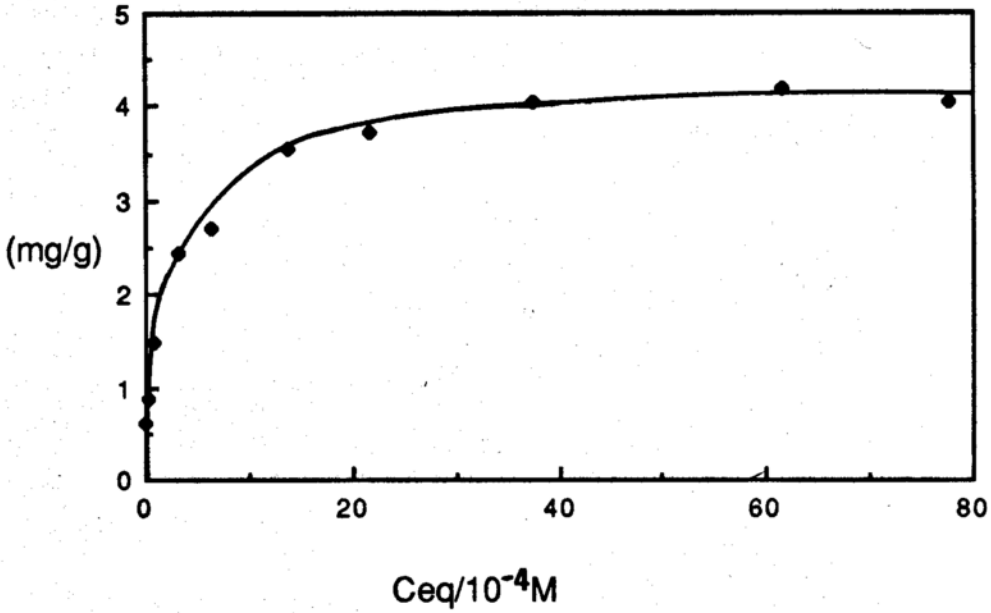

Figure 50. 6-NO_2-BIPS/TiO_2 isotherm, 25°C.

Table XXXIX. 25°C Isotherm Data, INS/TiO_2.

$C_{eq}/10^{-4}M$	$(mg/g)_{ads}$	$10^4\ C_{eq}/(mg/g)$
78.4	2.62	29.9
76.7	2.74	28.0
61.5	2.08	29.5
38.6	2.38	16.2
37.5	2.08	18.0
29.3	2.20	13.3
13.8	1.78	7.76
7.38	1.02	7.20
6.10	1.55	3.94
3.97	1.38	2.90
2.74	1.68	1.63
1.11	0.81	1.37
0.41	0.64	0.64
0.34	1.03	0.33

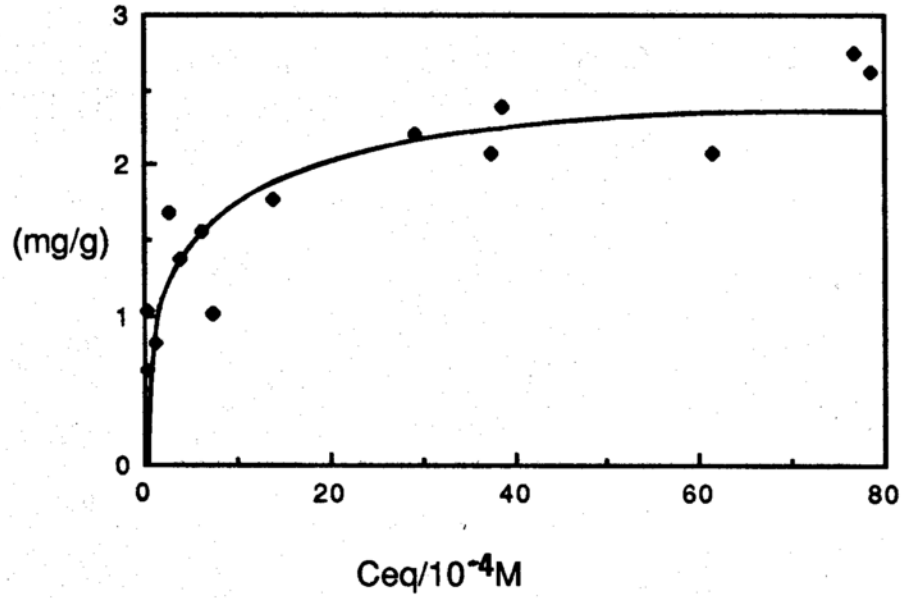

Figure 51. INS/TiO_2 isotherm, 25°C.

Table XL. 25°C Isotherm Data, 6-NO_2-BIPS/Silica Gel (500 m^2/g).

$C_{eq}/10^{-3}M$	$(mg/g)_{ads}$	$10^7\ C_{eq}/(mg/g)$
5.84	264.6	221
5.73	260.1	220
5.04	238.0	212
4.09	244.5	167
3.84	258.9	148
3.25	227.3	143
2.67	200.7	133
2.49	207.7	120
2.42	211.8	114
2.24	214.6	104
1.70	188.6	90.1
1.68	188.9	88.9
1.12	159.8	70.1
0.49	115.7	42.4
0.41	133.1	30.6
0.07	74.8	9.4
0.06	76.5	7.7
0.01	38.2	2.9
0.01	16.7	0.8

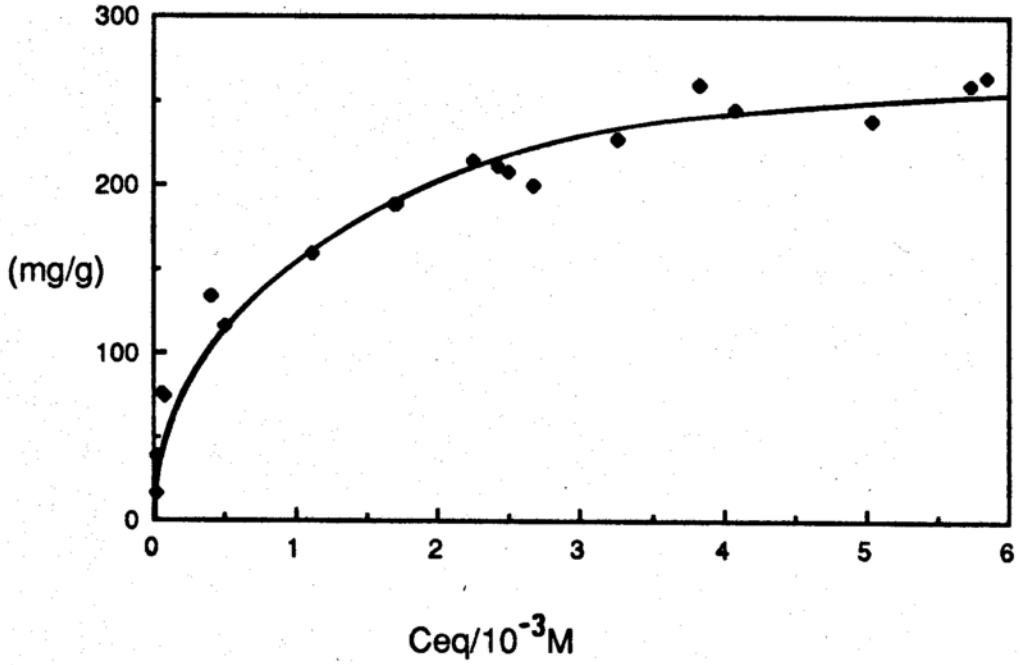

Figure 52. 6-NO_2-BIPS/silica gel (500m^2/g) isotherm, 25°C.

Table XLI. 25°C Isotherm Data, INS/Silica Gel (500 m^2/g).

$C_{eq}/10^{-4}M$	$(mg/g)_{ads}$	$10^6\ C_{eq}/(mg/g)$
44.8	186.0	24.06
30.8	165.4	18.64
17.2	146.3	11.74
8.7	106.3	8.21
3.2	57.0	5.56
2.1	47.2	4.40
1.6	35.0	4.57
0.54	25.4	2.12
0.20	12.9	1.56
0.06	5.2	1.33
0.04	2.6	1.50
0.02	1.3	1.51

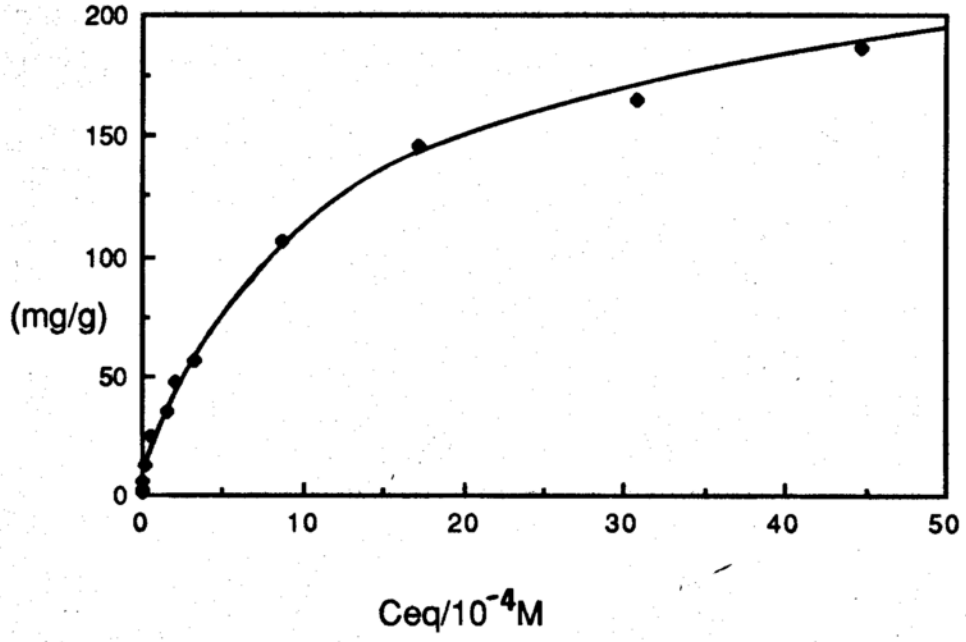

Figure 53. INS/silica gel (500m^2/g) isotherm,25°C.

Table XLII. 25°C Isotherm Scott Plot Parameters.

System	n	Correlation	Capacity (mg/g)	K/M^{-1}
6-NO_2-BIPS/silica gel (300 m^2/g)	12	0.99922	112.5	4.76×10^3
6-NO_2-BIPS/alumina	20	0.99153	110.4	1.57×10^3
INS/silica gel (300 m^2/g)	11	0.99706	134.4	5.32×10^2
INS/alumina	13	0.99177	55.6	6.59×10^2
6-H-BIPS/silica gel (300 m^2/g)	10	0.99771	79.6	4.60×10^2
6-H-BIPS/alumina	16	0.99662	31.1	1.69×10^3
6-OCH_3-BIPS/silica gel (300 m^2/g)	11	0.99536	146.7	3.75×10^2
6-OCH_3-BIPS/alumina	8	0.99939	41.4	2.19×10^3
6-NO_2-BIPS/Cab-O-Sil	18	0.97479	102.7	1.09×10^3
6-NO_2-BIPS/Aerosil R-972	13	0.44193	17.0	9.2×10^1
6-NO_2-BIPS/silicic acid	19	0.99719	203.0	3.09×10^3
INS/silicic acid	9	0.99886	152.6	7.02×10^3
6-NO_2-BIPS/talc	15	0.99296	2.25	4.35×10^3
INS/talc	9	0.97851	1.77	3.93×10^3
6-NO_2-BIPS/Avicel	13	0.93730	0.62	2.42×10^2
INS/Avicel	12	0.72136	2.07	1.08×10^2
6-NO_2-BIPS/TiO_2	9	0.99919	4.21	4.78×10^3
INS/TiO_2	13	0.98442	2.65	1.93×10^3
6-NO_2-BIPS/silica gel (500 m^2/g)	15	0.99255	293.5	1.16×10^3
INS/silica gel (500 m^2/g)	7	0.99874	217.9	1.17×10^3

Table XLIII. Isotherm Parameters from the Duggleby Program.

System	$(mg/g)_{max}$ (std. error)	Capacity in (mg/m^2)	$\mathring{A}^2$/ molecule	K/M^{-1} (std. error)
6-NO_2-BIPS / silica gel (300 m^2/g)	108.8 (3.6)	0.363	147.5	5.99×10^3 (0.97×10^3)
6-NO_2-BIPS / alumina	105.8 (4.3)	0.683	78.4	1.86×10^3 (0.32×10^3)
INS / silica gel (300 m^2/g)	128.4 (4.4)	0.428	127.1	6.51×10^2 (0.88×10^2)
INS / alumina	53.9 (1.8)	0.348	156.4	8.10×10^2 (1.47×10^2)
6-H-BIPS / silica gel (300 m^2/g)	79.0 (2.7)	0.263	175.0	4.74×10^2 (0.62×10^2)
6-H-BIPS / alumina	30.0 (0.7)	0.194	238.1	2.26×10^3 (0.35×10^3)
6-OCH_3-BIPS / silica gel (300 m^2/g)	142.0 (4.8)	0.473	107.9	4.38×10^2 (0.66×10^2)
6-OCH_3-BIPS / alumina	41.5 (0.8)	0.268	190.7	2.42×10^3 (0.24×10^3)
6-NO_2-BIPS / Cab-O-Sil	105.2 (6.8)	0.526	101.8	9.38×10^2 (2.30×10^2)
6-NO_2-BIPS / silicic acid	195.8 (3.4)	0.546	98.2	4.04×10^3 (0.44×10^3)
INS / silicic acid	147.9 (2.6)	0.412	132.0	1.50×10^4 (0.28×10^4)

Table XLIII. Duggleby Isotherm Parameters (continued)

System	$(mg/g)_{max}$ (std. error)	Capacity in (mg/m^2)	$\AA^2$/ molecule	K/M^{-1} (std. error)
6-NO_2-BIPS / talc	2.21 (0.06)	0.284	189.4	5.30×10^3 (0.89×10^3)
INS / talc	1.71 (0.13)	0.219	248.8	7.07×10^3 (3.39×10^3)
6-NO_2-BIPS / Avicel	0.775 (0.108)	0.646	82.8	1.56×10^2 (0.38×10^2)
INS / Avicel	1.75 (0.43)	1.458	37.3	1.63×10^2 (0.76×10^2)
6-NO_2-BIPS / TiO_2	4.09 (0.16)	0.470	115.7	5.36×10^3 (1.25×10^3)
INS / TiO_2	2.41 (0.17)	0.277	196.3	3.52×10^3 (1.27×10^3)
6-NO_2-BIPS / silica gel (500 m^2/g)	281.7 (11.0)	0.563	94.9	1.38×10^3 (0.23×10^3)
INS / silica gel (500 m^2/g)	217.7 (5.2)	0.435	124.9	1.15×10^3 (0.08×10^3)

Table XLIV. The Effect of Temperature on Isotherm Parameters.

A. 6-NO_2-BIPS/Silica Gel (500 m^2/g)

T/°C	K/M^{-1} (std. error)	capacity/(mg/g), (std. error)
18	8.60×10^2 (1.83×10^2)	207.0 (8.3)
25	1.15×10^3 (0.08×10^3)	217.7 (5.2)
35	1.49×10^3 (0.17×10^3)	132.3 (4.0)

B. INS/Silica Gel (500 m^2/g)

T/°C	K/M^{-1} (std. error)	capacity/(mg/g), (std. error)
18	6.17×10^3 (1.07×10^3)	223.1 (7.7)
25	1.38×10^3 (0.23×10^3)	281.7 (11.0)
35	4.16×10^3 (0.66×10^3)	181.1 (6.2)

Table XLV. Malachite Green/Silica Gel (500 m^2/g) 25°C Isotherm Data.

$C_{eq}/10^{-5}M$	$(mg/g)_{ads}$	$10^6\ C_{eq}/(mg/g)$
10.59	6.45	16.43
7.50	6.60	11.36
4.57	6.69	6.84
3.20	6.10	5.24
1.60	5.67	2.82
1.01	4.89	2.06
0.43	4.05	1.05
0.25	3.06	0.82
0.07	2.08	0.35
0.05	1.56	0.32

Scott plot	Duggleby program
n = 8	n = 8
correlation = 0.99934	capacity = 6.80 ± 0.12 mg/g
capacity = 6.72 mg/g	$K = 3.17 \times 10^5\ M^{-1}$ ($\pm 0.17 \times 10^5$)
$K = 3.65 \times 10^5 M^{-1}$	$Å^2$/molecule = 4457

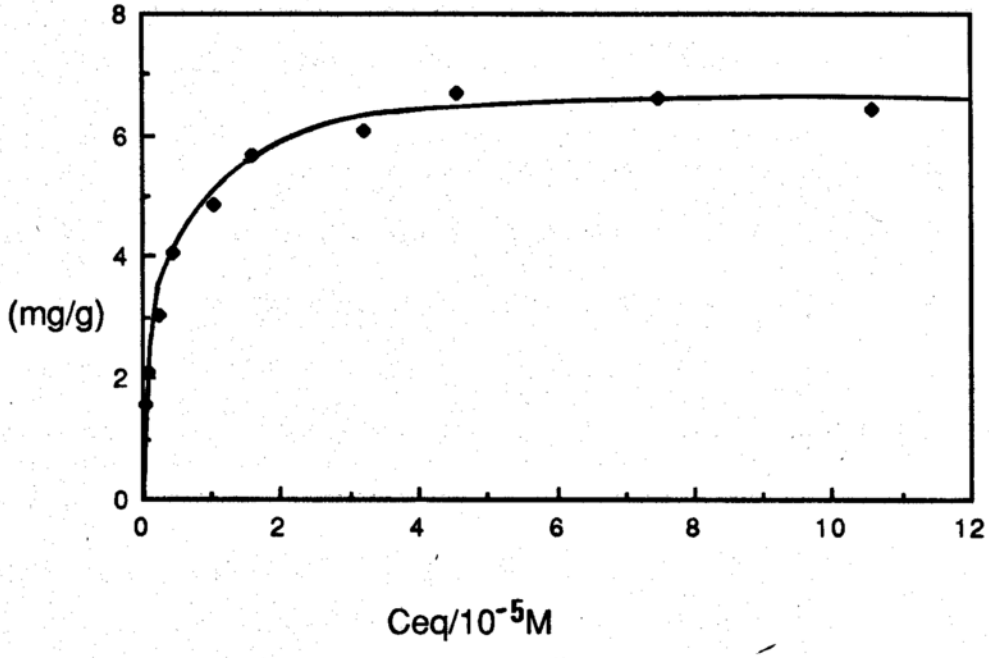

Figure 54. Malachite green/silica gel ($500 m^2/g$) isotherm, $25^0 C$.

D. Suspension Transmission Spectroscopy

Preliminary experiments showed that glycerin suspensions of colored powders gave spectra consistent with their colors. Red 6-NO_2-BIPS/silicic acid powders had a broad visible peak with λ_{max} = 510-516 nm. Adsorbents of the smallest particle sizes with high surface coverages of colored adsorbate gave the smoothest spectra. The spectra were not those of desorbed spiropyran dissolved in glycerin; the uv/visible absorption spectrum of a saturated solution of 6-NO_2-BIPS in glycerin showed no absorption at wavelengths longer than 400 nm. The ultraviolet portion of the spectrum is similar in appearance to that in cyclohexane or methanol ($\varepsilon = 9.6 \times 10^3$ and 9.4×10^3 at 320-340 nm peak, respectively). At 345 nm in glycerin, A = 0.117 indicates a solubility in glycerin of 4 mg/liter, incapable of producing the glycerin suspension transmission spectra obtained. Suspensions of 6-H-BIPS, 6-OCH_3-BIPS, and 6-NO_2-BIPS adsorbed into alumina and bentonite were also made in glycerin. The suspensions were appropriately colored (with regards to the initial powder color), but failed to yield visible spectra due to scattering by the adsorbents.

Silicic acid, silica gel, and Cab-O-Sil adsorbents had refractive indices allowing spectral measurements in the transmittance mode. 6-NO_2-BIPS was the adsorbate most frequently employed; it has a high absorptivity on silica and a simple one-peak visible spectrum resembling its solution spectra. The suspension

spectrum of an orange powder containing 6-NO_2-BIPS adsorbed on silicic acid is given in Figure 55. One hundred milligrams of the powder was dispersed in 20 ml glycerin, and the spectrum was taken versus glycerin. Six separate suspensions were made of a powder of lower surface coverage of spiropyran to study method reproducibility. The absorption at 508 nm was 0.261, with a standard deviation of 0.031. Spectra on Cab-O-Sil were very similar to those on silicic acid, with a slight shift in λ_{max} to 514 nm. These showed a characteristic minimum between 420 and 430 nm, which was present for all spiropyrans on all adsorbents used.

Points of known surface coverage taken from an adsorption isotherm study were subjected to the same treatment. Figure 56 shows the spectra obtained for a 214.6 mg/g 6-NO_2-BIPS/silica gel (500 m^2/g) powder at different suspension concentrations. The dark red powder was dispersed in glycerin (20 ml) in 5, 4, 3, 2, and 1 mg amounts to produce 0.025, 0.020, 0.015, 0.010, and 0.005 G% suspensions, respectively. The absorption values at λ_{max} plotted against suspension concentrations in G% produce straight lines. Figure 57 shows such a plot for 6-NO_2-BIPS/silica gel powders. The slopes increase with the surface coverage of colored adsorbate, eventually reaching an apparent saturation value. This corresponds to the same point at which the increased surface coverage is no longer apparent visually as a darker-colored powder.

The suspensions lose their color in 30-45 minutes if left exposed to room light. This decoloration did not take place for

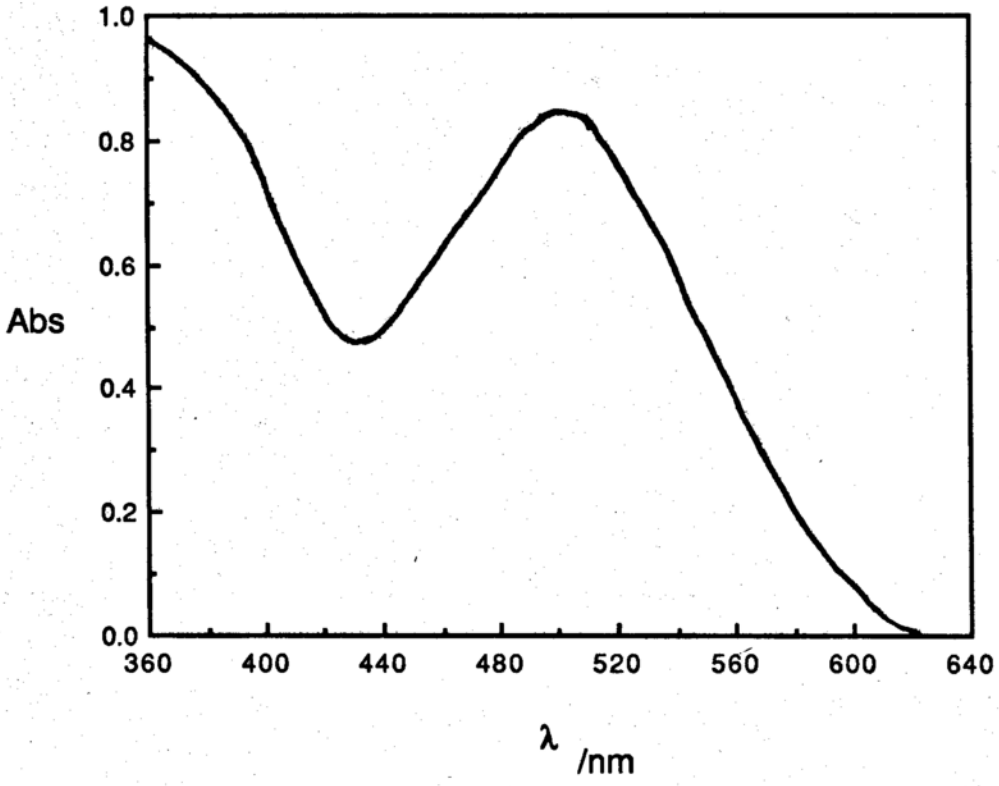

figure 55. Glycerin suspension spectrum of a 6-NO_2-BIPS/silicic acid powder.

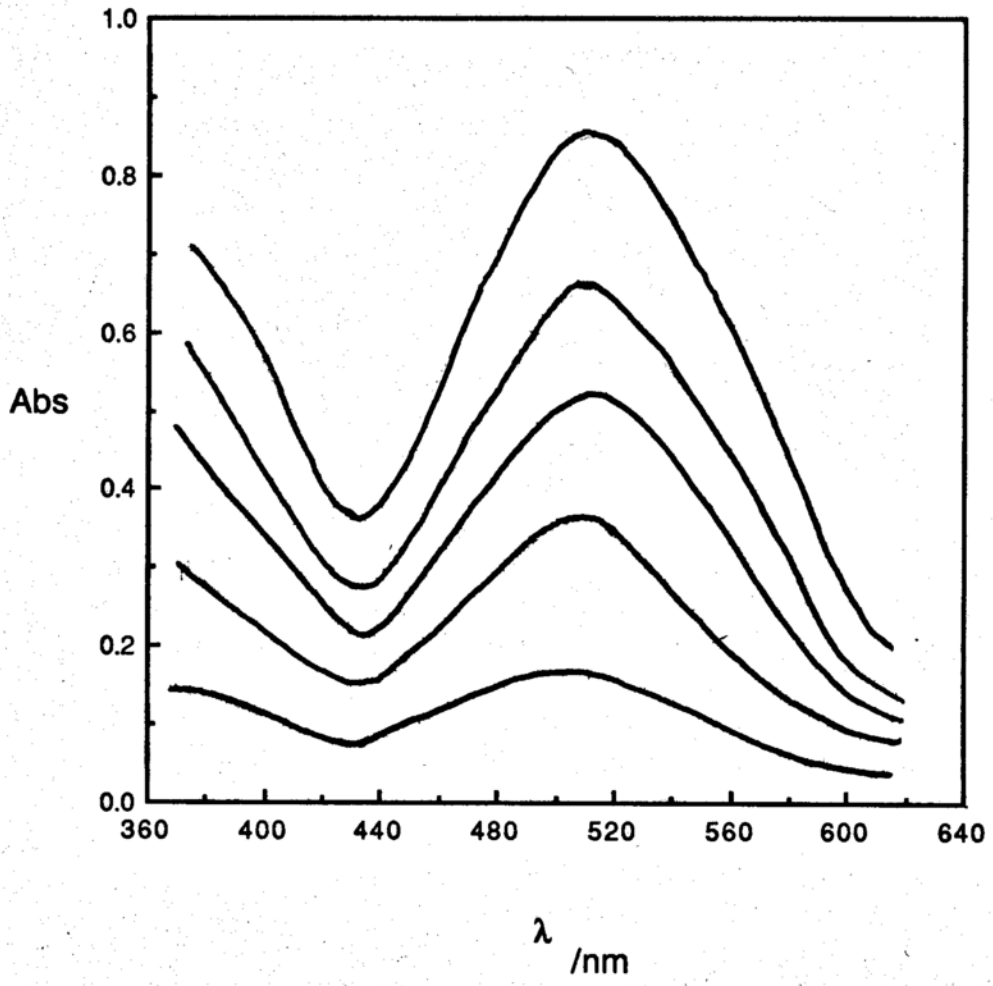

Figure 56. Glycerin suspension spectra of a powder containing 214.6 mg 6-NO_2-BIPS per gram of silica gel ($500m^2/g$).

20 ml glycerin was used to disperse. 1,2,3,4,and 5mg of the powder.

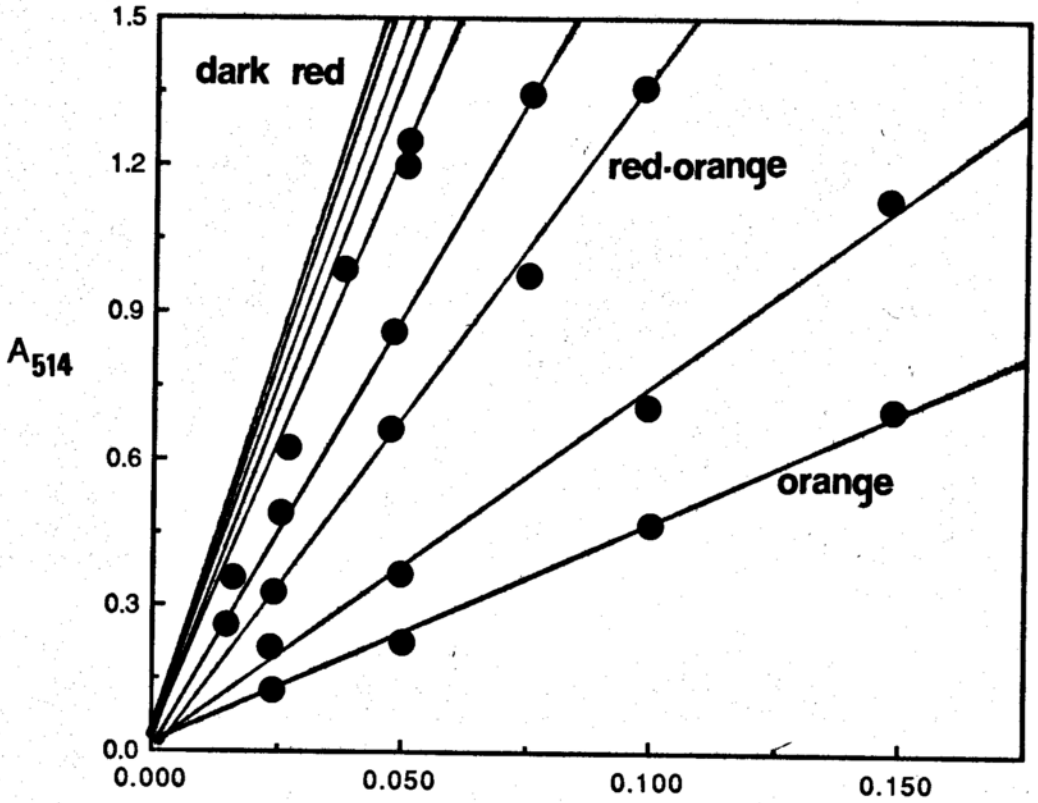

Figure 57. "Beer's Law" plots for 6-NO_2-BIPS/silica gel powders suspended in glycerin. Steeper slopes correspond to higher surface coverages. Slopes range from 4.8-36.7, with correlation coefficients 0.982-0.999.

suspensions protected from light, and was termed "photobleaching," a word originally describing spiropyrans reverting to their colorless forms in solution (53). The fading rate of a 6-NO_2-BIPS/silica gel powder at three different G% suspension concentrations was followed with time. The absorptions at 514 nm (λ_{max}) decreased to less than half the original value in 10 minutes. The color loss was pseudo-first-order after an initial period of slow fading; Figure 58 shows the semi-logarithmic plot for 0.03, 0.04, and 0.05 G% suspensions. Preparation of fresh suspensions prior to spectral measurements, and rapid handling, minimized this effect on the presented spectra.

The spectra of other spiropyrans adsorbed to silica gel and suspended in glycerin are given in Figure 59. Note that they all have the characteristic minimum at approximately 430 nm, but the spectra beyond 430 nm differ. Red-orange 6-NO_2-BIPS has only the peak at 514 nm, whereas purple-pink INS has a major peak at 470 nm and smaller peaks at 440 and 540 nm. The orange 6-H-BIPS suspension has a small peak at 640 nm, but in other respects resembles the violet-brown 6-OCH_3-BIPS spectrum with a major peak at 550 nm.

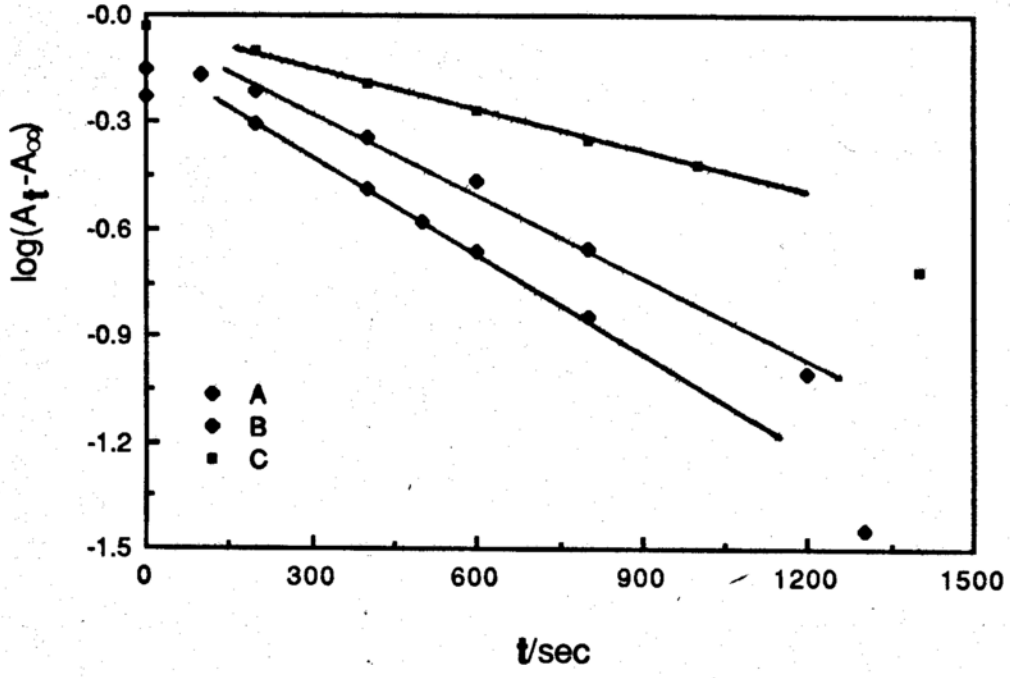

Figure 58. Color loss versus time at 514nm for glycerin suspensions of 6-NO_2-BIPS/ silica gel powders; A= 0.03, B=0.04, and C=0.05 gram percent.

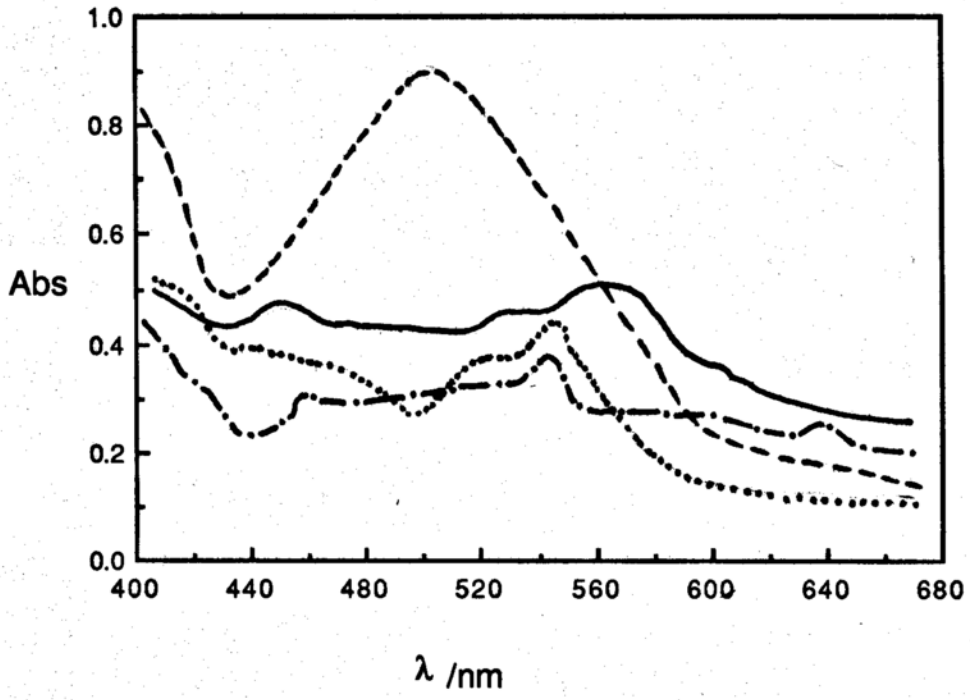

Figure 59. Glycerin suspension spectra of spiropyrans adsorbed to silica gel. 6-NO_2-BIPS(- - - - - -), INS(————), 6-OCH_3-BIPS(·····), and 6-H-BIPS (—·—·—·—).

E. Diffuse Reflectance Spectra

Diffuse reflectance spectra of methyl red and methyl violet adsorbed to silica gel were compared to solution spectra of these dyes to verify the method. Figure 60 shows these dye/silica reflectance spectra; arrows indicate the solution λ_{max} for each dye. The powder colors and qualitative spectra are similar to those in solution. The methyl red/silica gel spectrum was unchanged three weeks later, which shows both sample stability and good reproducibility for the method. Spiropyran/silica gel spectra were also highly reproducible. Figure 61 compares the spectra of a pink 6-NO_2-BIPS/Aerosil R-972 powder and a red 6-NO_2-BIPS/Cab-O-Sil powder; both were measured versus their respective pure diluent adsorbent references. Background correction with adsorbent eliminates any contribution to absorption by the adsorbent. The spectrum of adsorbed 6-NO_2-BIPS differs markedly from the spectrum of pure solid 6-NO_2-BIPS. Figure 62 shows the difference in spectra between the pure crystalline solid 6-NO_2-BIPS and 6-NO_2-BIPS adsorbed on silicic acid. The peak at the uv end of the visible range (380-410 nm) exists in both spectra, as does some absorption at 550 nm. The small peak at 440 nm in the pure solid is replaced (or perhaps, obscured) by a new dominant peak at 472 nm in the adsorbed case.

A number of variables have to be controlled in order to obtain consistent diffuse reflectance spectra. The amount of adsorbate

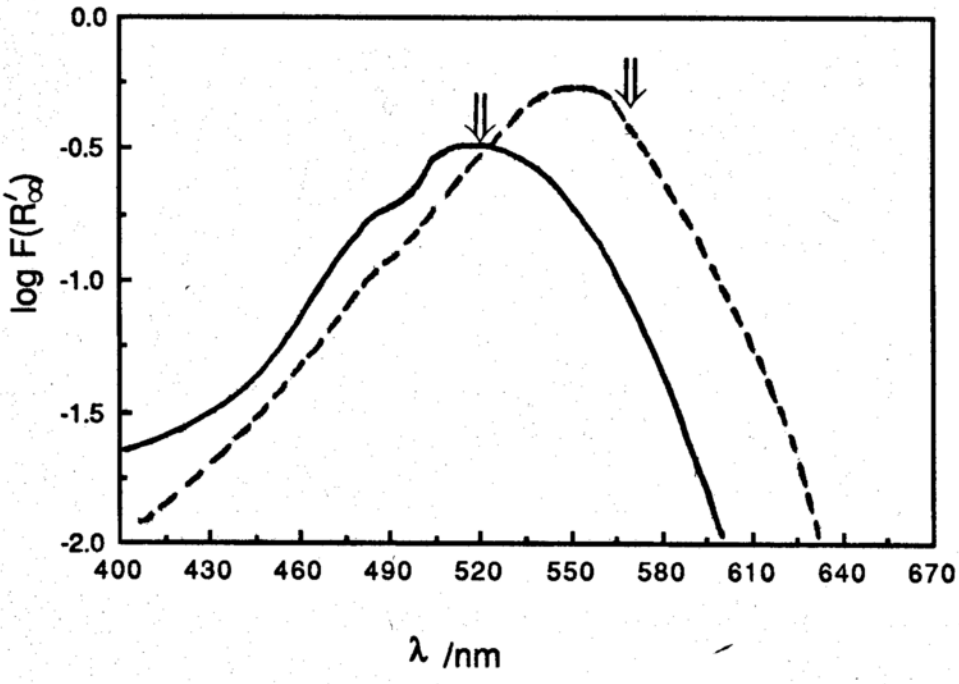

Figure 60. Reflectance spectra for methyl red (——) and methyl violet (----) adsorbed to silica gel. Arrows indicate the solution spectral λ_{max}.

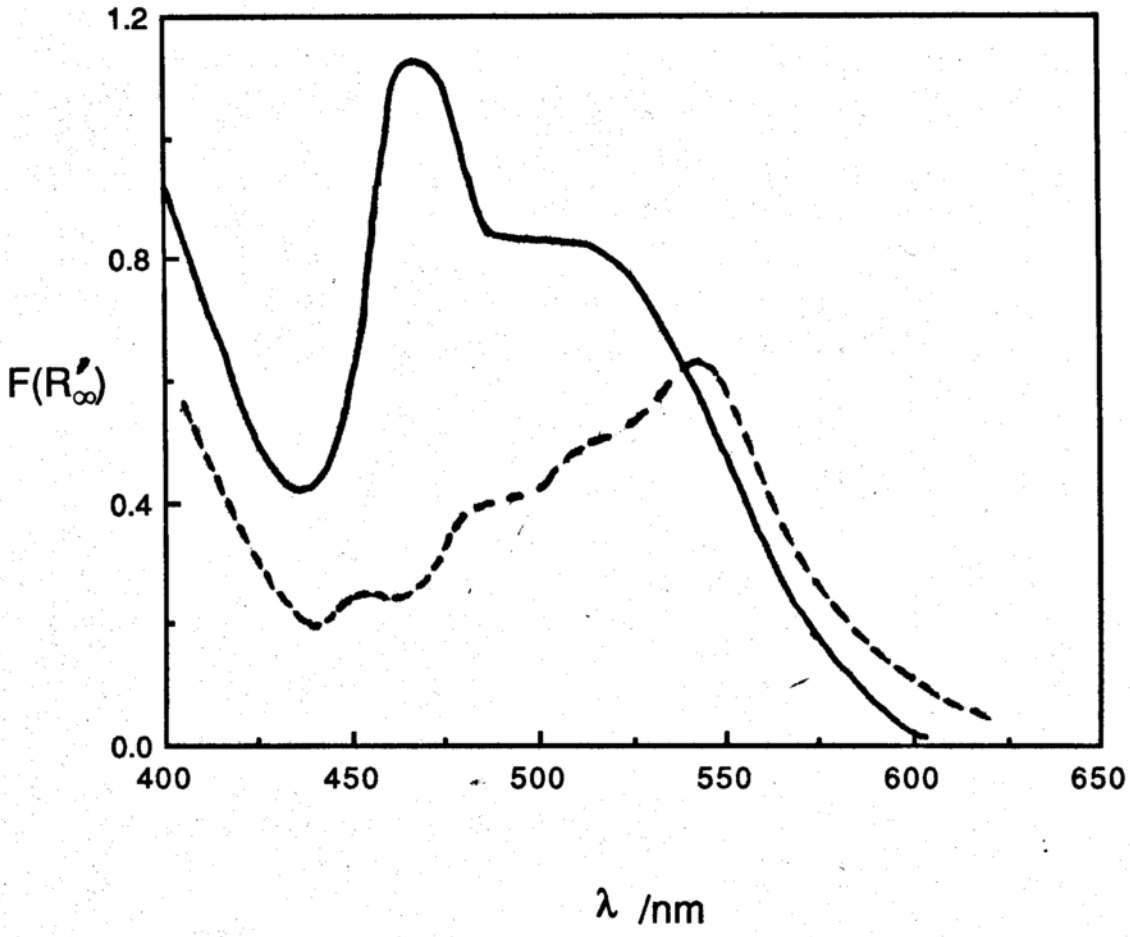

Figure 61. Reflectance spectra of 6-NO_2-BIPS/Cab-O-Sil (———) and 6-NO_2-BIPS/Aerosil R-972 (- - - - -) powders versus pure adsorbent.

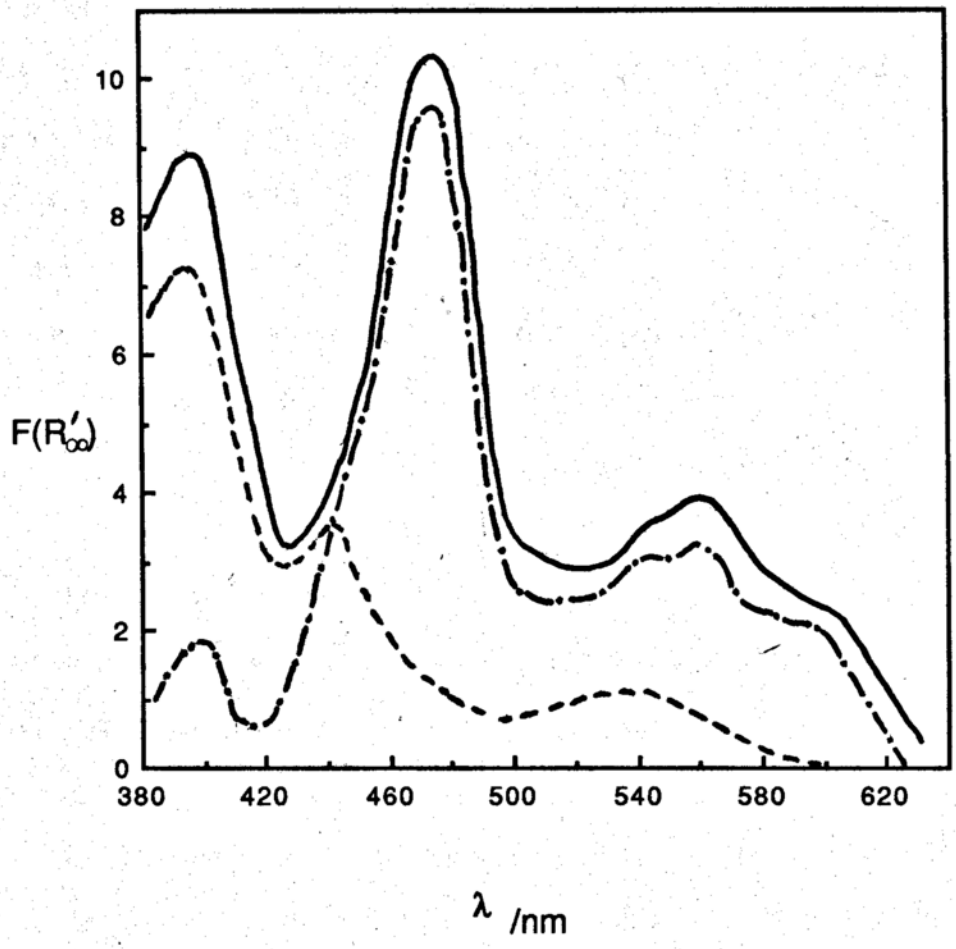

Figure 62. Reflectance spectra of pure solid 6-NO_2-BIPS (----), 6-NO_2-BIPS adsorbed to silicic acid (———), and the difference spectrum (—·—·).

present influences not only the intensity, but often also the shape of the spectrum, especially at high surface coverages. As was the case with the transmission spectra, a maximum absorption value for the reflectance spectra of spiropyrans adsorbed onto surfaces is seen. The same characteristic minimum at 430 nm is also present for spiropyran/adsorbent (but not dye/adsorbent) reflectance spectra. Diluting the spiropyran powder with extra adsorbent in the dry state is one method of reducing the absorption of a high coverage system without changing the peak shapes or positions. Figure 63 shows the effect on the resultant spectrum of diluting a 6-NO_2-BIPS/silica gel powder with additional silica gel.

Spiropyrans adsorbed onto solid surfaces are generally more stable than those in solution. Heat and light can still affect the spectrum, but usually to a greatly reduced degree. Powders stored in a dark, cool place gave unchanged spectra weeks after their initial preparation. Oven drying at temperatures greater than 50°C darkened red 6-NO_2-BIPS/silica gel powders to a dark red-maroon color. These changes show up in the diffuse reflectance spectra; INS/silica gel powders dried at 70°C for one hour darkened considerably to a deeper violet. $F(R'_\infty)$ was only 5.29 for a filter-dried INS/silica powder with g = 197, but increased to 7.10 for an oven-dried sample with g = 159. Residual cyclohexane from the adsorption process is easily volatilized at low temperatures in less than one hour or by prolonged drying under vacuum filtration. A dark orange powder formed by adding silicic acid to a 1×10^{-4} M

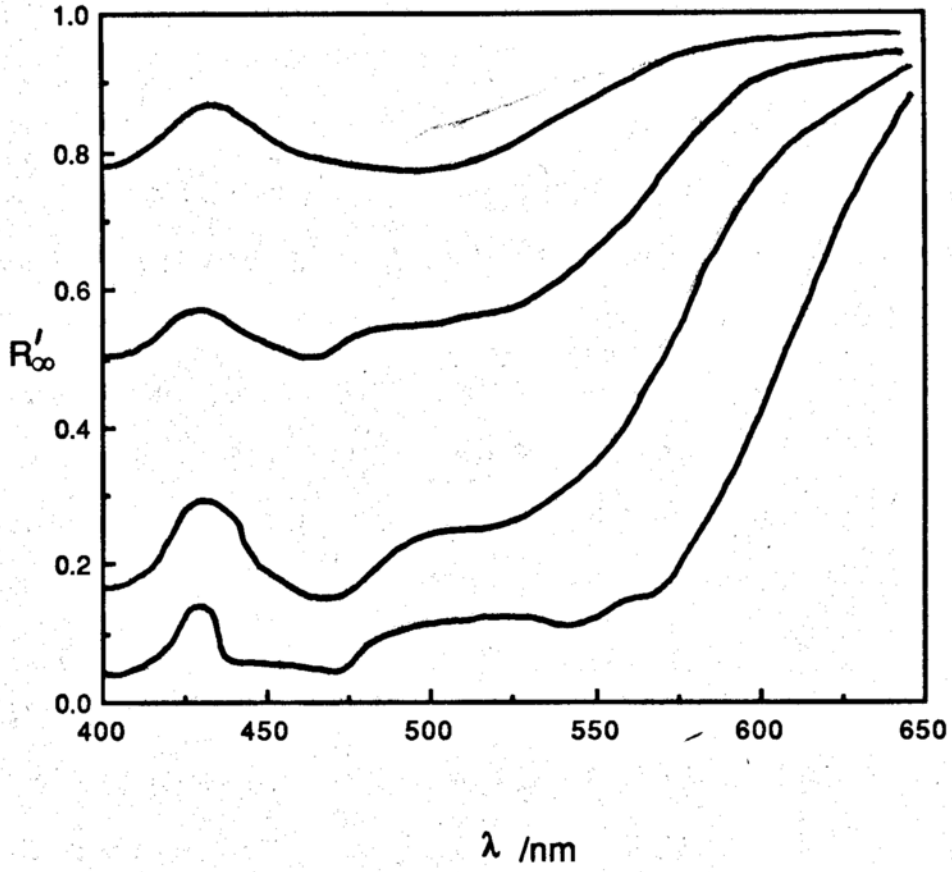

Figure 63. Dilution effect on reflectance spectra of 6-NO_2-BIPS/silica gel powders. Bottom to top: full strength, diluted with two parts adsorbent, diluted with ten parts adsorbent, and diluted with 100 parts adsorbent.

solution of 6-NO_2-BIPS in cyclohexane fades to light orange after 5 minutes directly under a fluorescent room light. The Kubelka-Munk parameter, $F(R'_\infty)$, decreased from 1.93 to 0.90 at λ_{max} (472 nm) in that same time span. When plotting $F(R'_\infty)$ versus g (surface coverage in nanomoles/m^2), the slope (f) is a quantification of the darkness of the colored powder. A decrease in this value is seen for 6-NO_2-BIPS/silicic acid powders left in the light prior to spectral measurement. 6-NO_2-BIPS/adsorbent systems photobleached to a greater extent than did INS/adsorbent systems. 6-H-BIPS powders also showed a significant loss of color under visible light. 6-OCH_3-BIPS/silica gel systems often darkened under visible light, changing from a light to a dark brown or from a brown to a purple-brown. All of these photo-induced changes could be effectively minimized by protecting the powders from light until spectral measurement.

The diffuse reflectance spectra were compared for different spiropyrans adsorbed to the same solid. Figure 64 compares the spectrum of 6-NO_2-BIPS to that of INS on silica gel 300 m^2/g. Figure 65 compares 6-H-BIPS to 6-OCH_3-BIPS on silica gel 500 m^2/g. All four spiropyrans are shown adsorbed to alumina, 6-H-BIPS and INS in Figure 66, and 6-NO_2-BIPS and 6-OCH_3-BIPS in Figure 67. It is instructive to show the changes that occur in the spectrum of a single adsorbate/adsorbent system with increasing surface coverage. Figure 14 is such a plot for INS/silicic acid, with the coverage expressed by g values. Figure 68 shows the same type of plot for

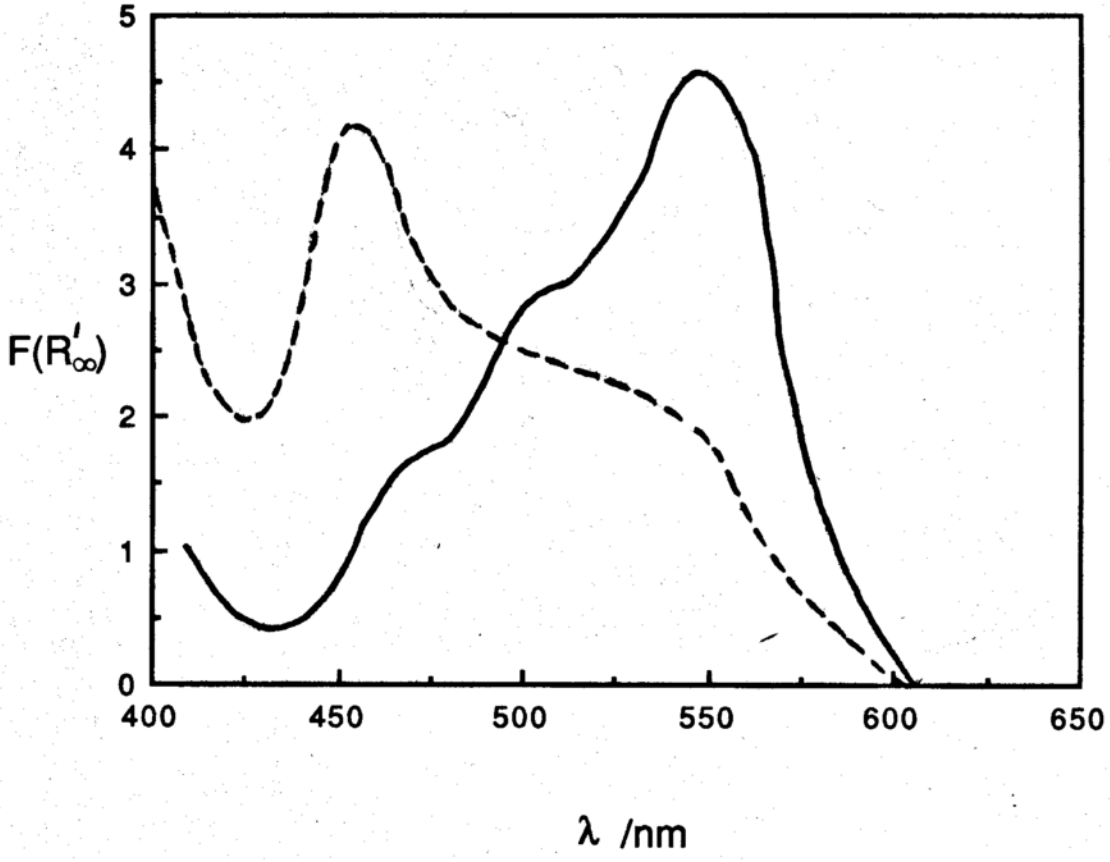

Figure 64. Comparison of reflectance spectra on silica gel, 300m^2/g. 6-NO_2-BIPS (----), g = 21.1 (orange). INS (——), g = 19.8 (lavender-pink).

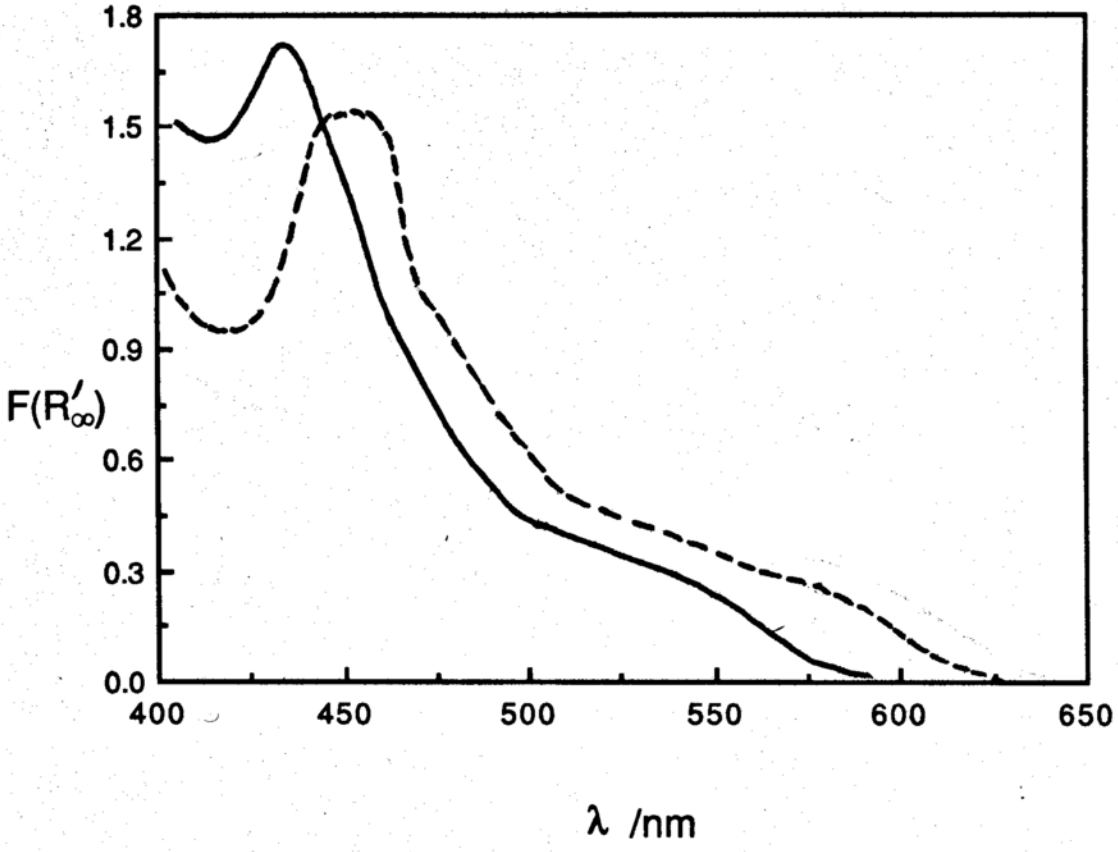

Figure 65. Comparison of reflectance spectra on silica gel 500m^2/g. 6-H-BIPS (——), g = 25.3 (yellow-orange). 6-OCH_3-BIPS (– – –), g = 25.3 (golden brown).

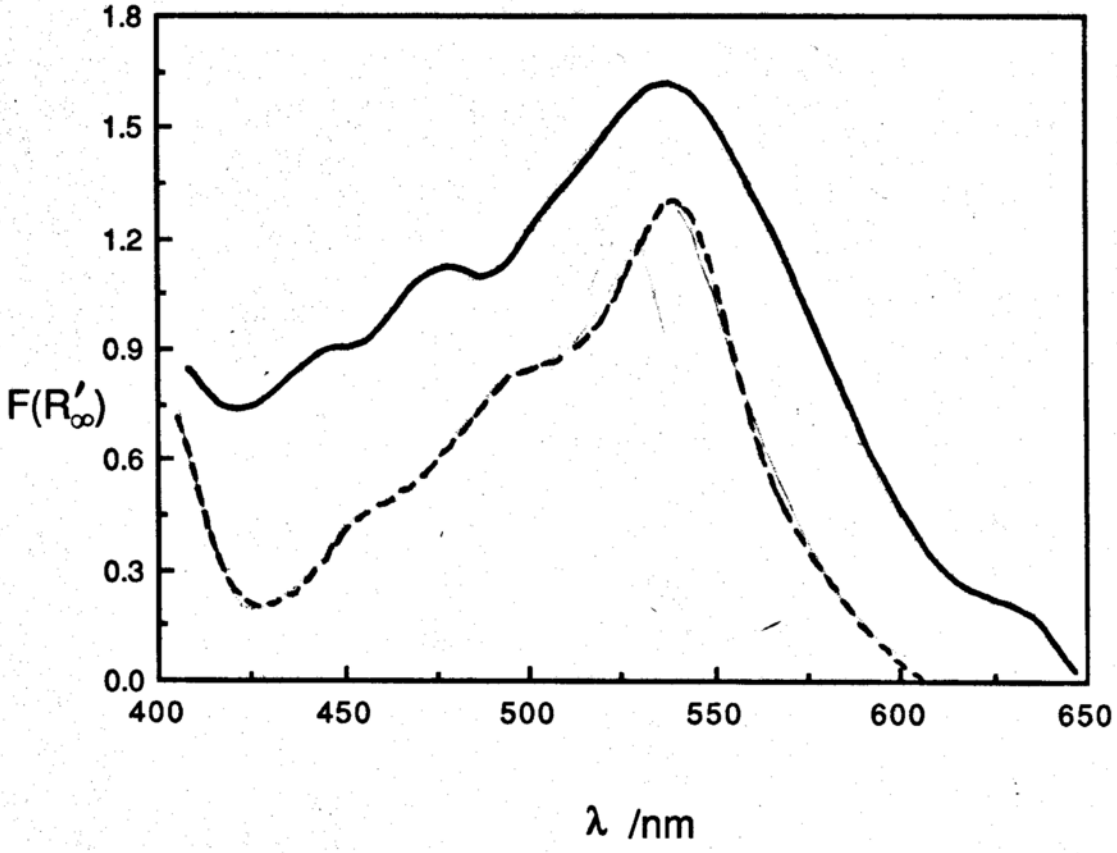

Figure 66. Comparison of reflectance spectra on alumina. INS (——), g = 104.5 (purple). 6-H-BIPS (- - - -), g = 64.5 (pink).

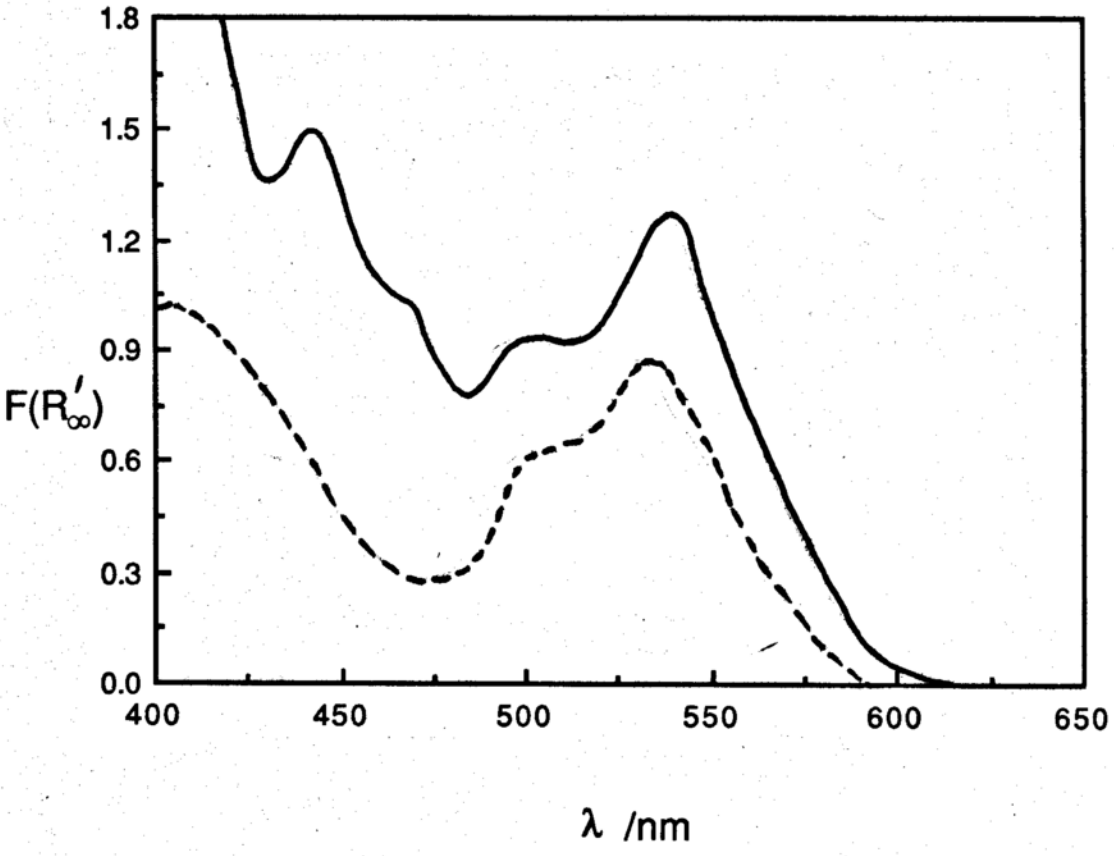

Figure 67. Comparison of reflectance spectra on alumina at low coverages. 6-NO_2-BIPS (——), g= 168.3 (orange). 6-OCH_3-BIPS (- - - -), g = 50.0 (pink-tan).

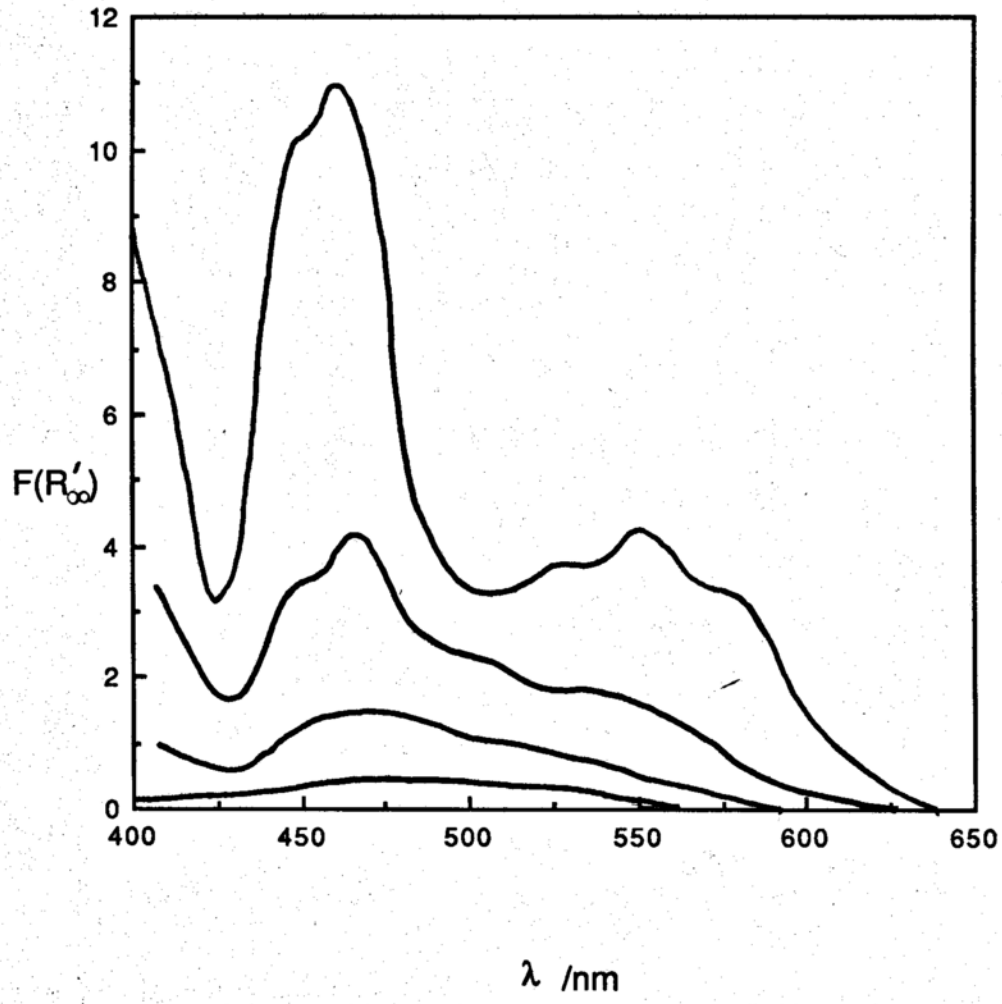

Figure 68. Reflectance spectra for 6-NO_2-BIPS on silicic acid with variable surface coverage. g = 1.27 (light orange), g = 5.86 (orange), g = 17.4 (orange-red), and g = 458.0 nano·moles/m^2 (dark red).

6-NO_2-BIPS/silicic acid. Figures 69-72 depict the four spiropyrans studied on silica gel (500 m^2/g); and Figures 73-76 do the same on alumina. Figures 77-82 show the spectra of adsorbed 6-NO_2-BIPS and INS on talc, TiO_2, and Avicel microcrystalline cellulose. The spectra of permanent dyes adsorbed on silica gel (500 m^2/g) are given in Figures 83-85. Figure 86 is a photograph of Janus Green B, Gentian Violet, Methyl Red, and Quinaldine Red adsorbed on silica gel, with their respective surface coverages. Note that the surface coverages required to produce the same degree of coloration are much less than those of the spiropyran/silica gel powders in Figure 27.

First derivative reflectance spectra ($D'-R'_\infty$) versus wavelength were useful for following the change in spectrum at early times after mixing the adsorbent with adsorbate solution. The positions of the peaks did not change much with time, but the magnitudes of the peaks did. Figure 87 shows the change in a $D'-R'_\infty$ spectrum of 6-NO_2-BIPS/alumina as the surface coverage increases.

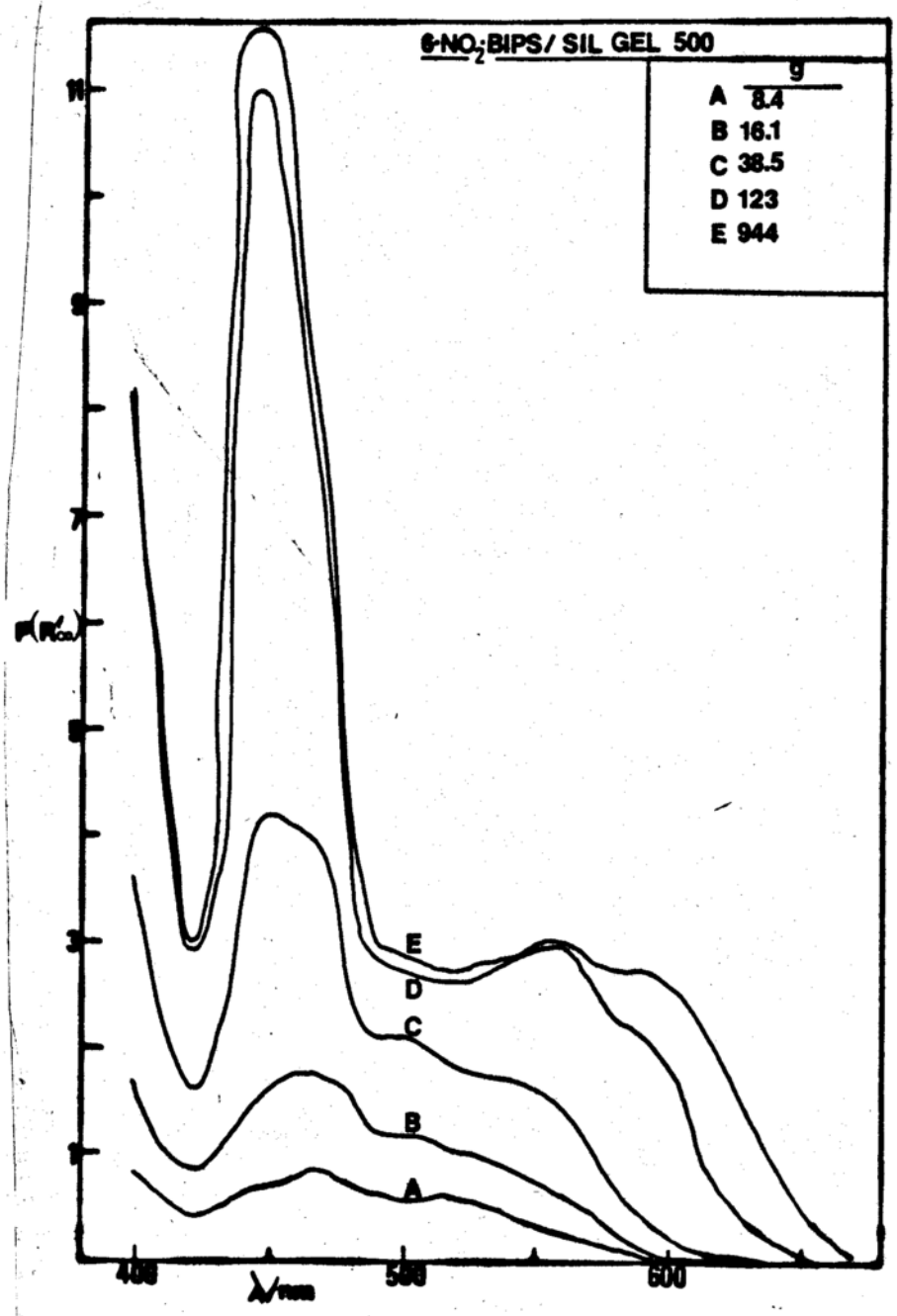

Figure 69. Reflectance spectra for 6-NO_2-BIPS on silica gel ($500m^2/g$), increasing coverages given in legend. Powders are pink, orange-pink, light orange, light orange, red-orange and red, respectively.

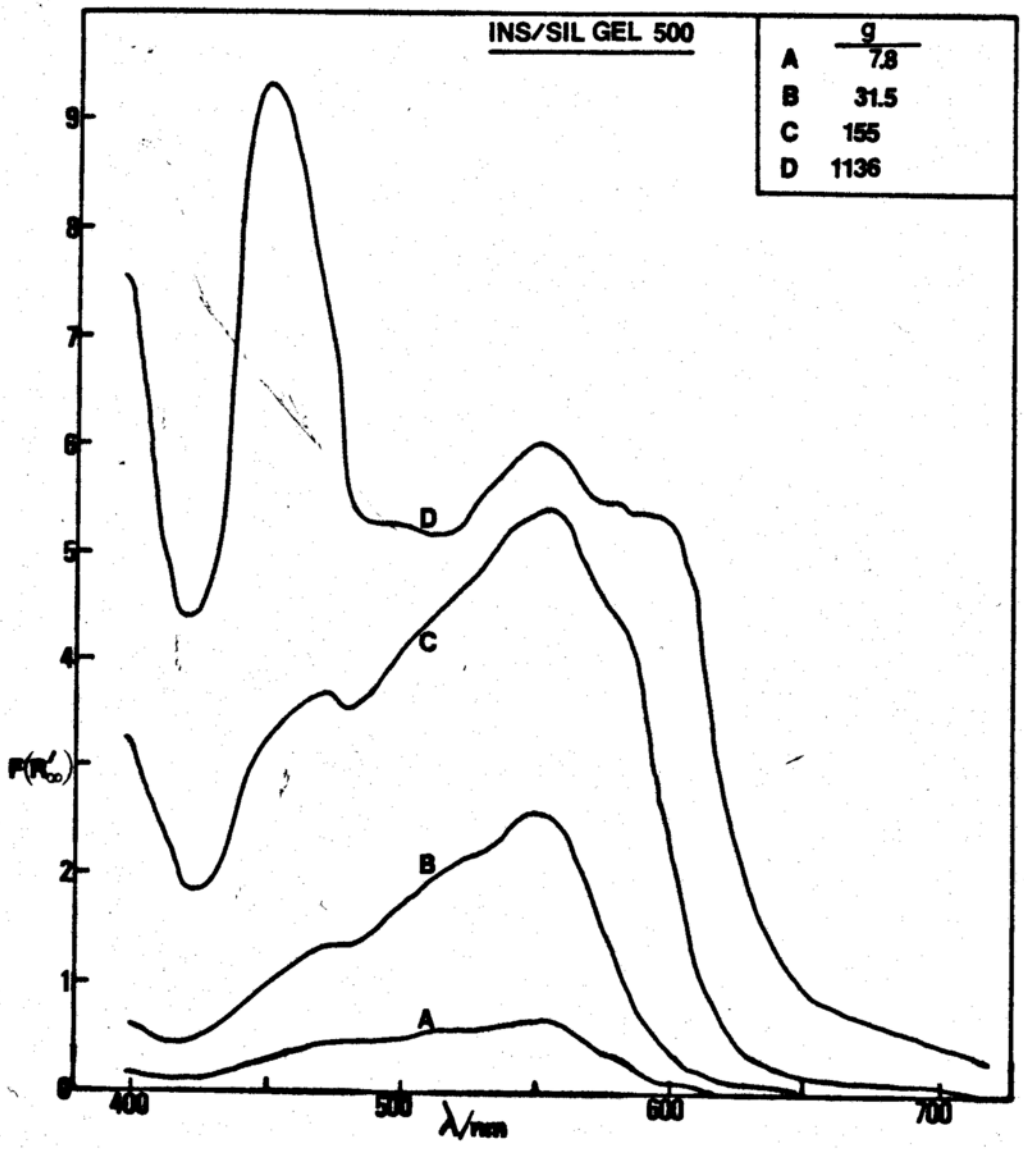

Figure 70. Reflectance spectra for INS on silica gel ($500 m^2/g$). Nanomoles/m^2 coverages are given in legend. Powders are faint pink, pink-purple, purple-pink, and dark red.

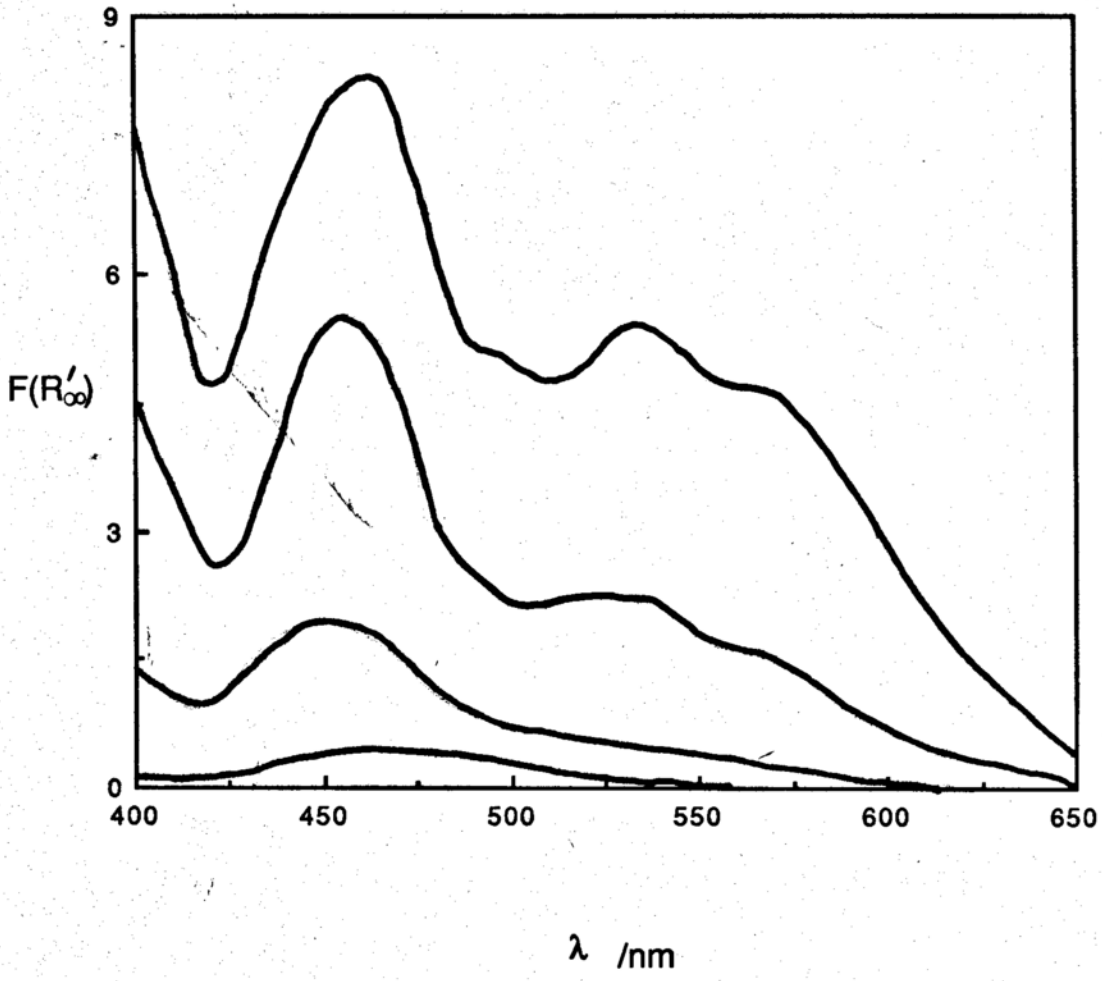

Figure 71. Reflectance spectra for 6-OCH_3-BIPS on silica gel ($500m^2/g$) with variable surface coverage. g = 4.3 (light yellow-tan), g = 25.3 (golden brown), g = 83.1 (light brown) and g = 245.5 (violet-brown).

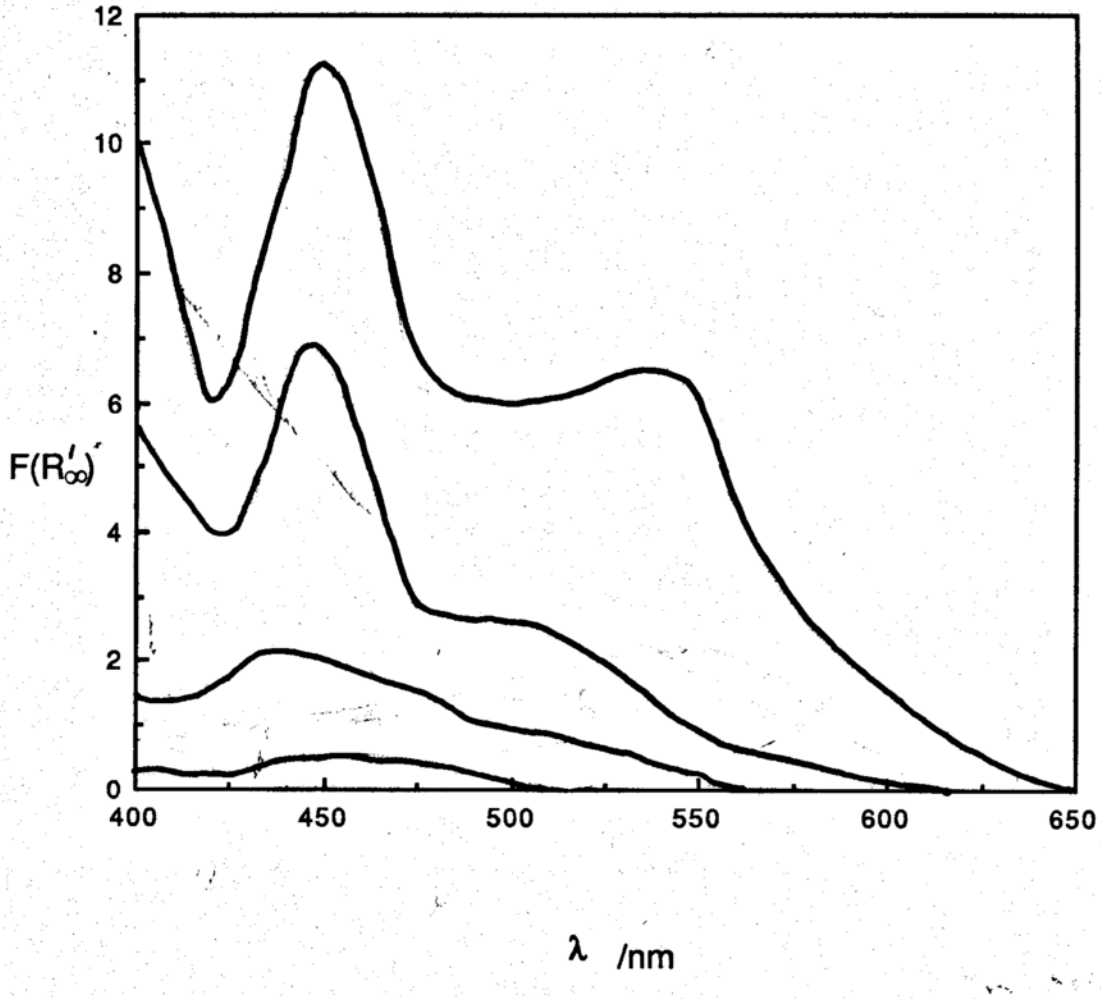

Figure 72. Reflectance spectra for 6-H-BIPS on silica gel ($500m^2/g$) with variable surface coverage. g = 4.3 (light yellow), g = 28.3 (yellow-orange), g = 82 (orange), and g = 329 (orange-red).

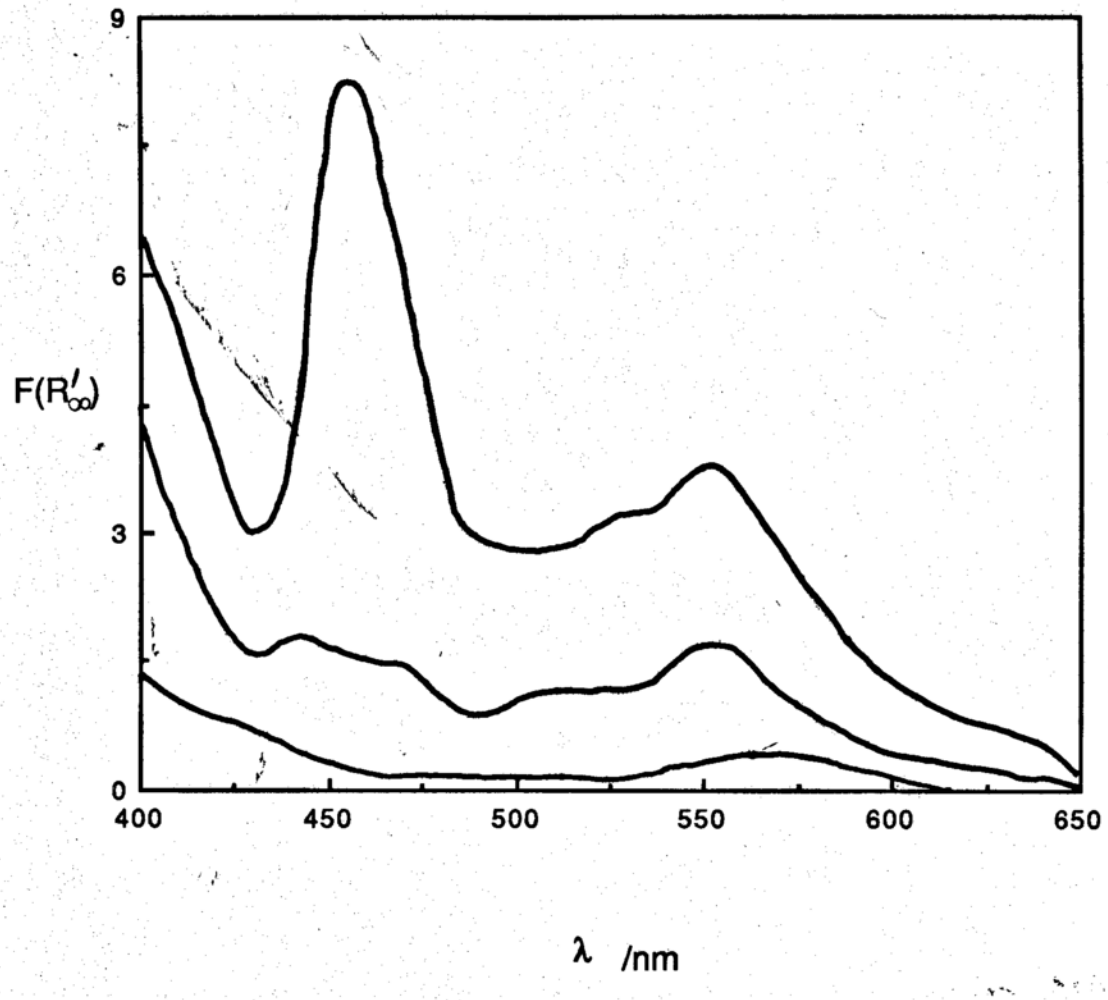

Figure 73. Reflectance spectra for 6-NO_2-BIPS on alumina with variable surface coverage. g= 27 (yellow), g= 168 (orange), and g= 960 (red).

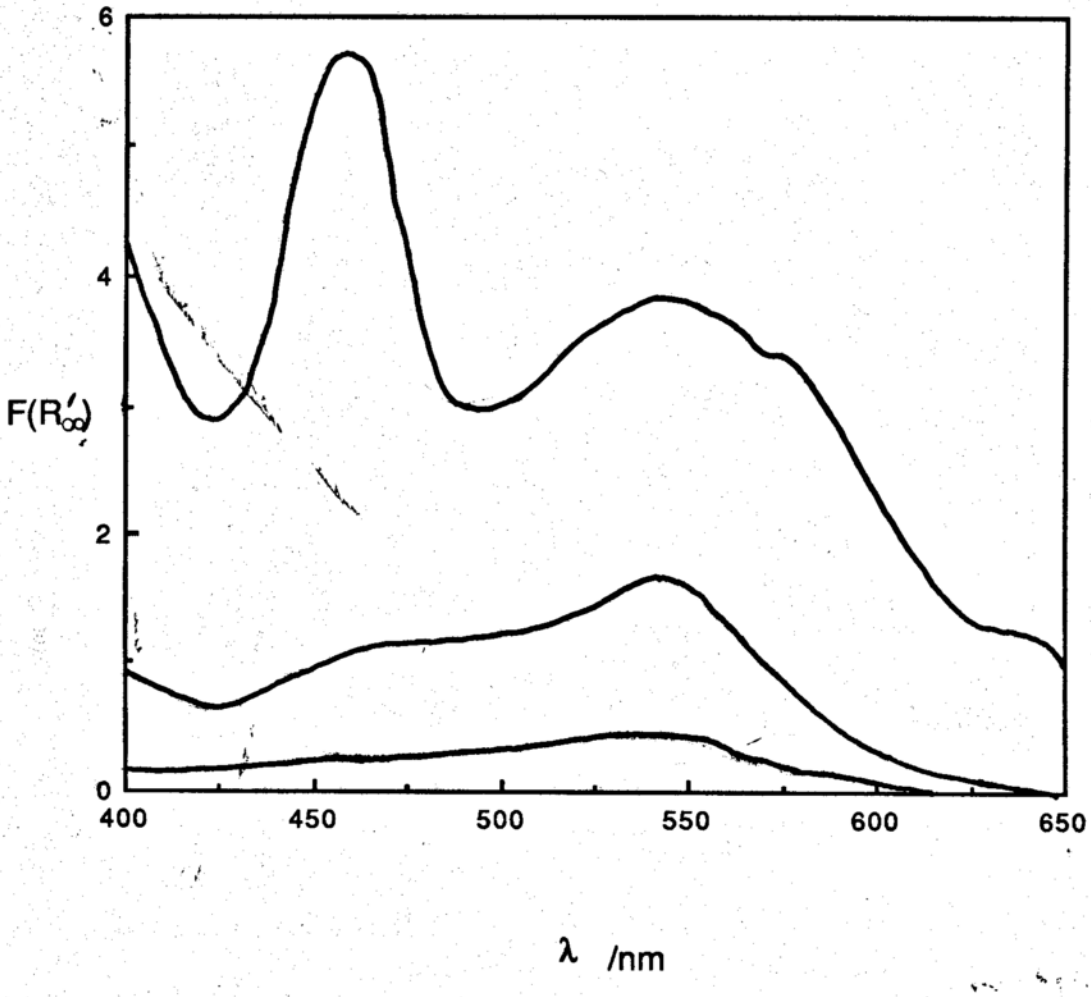

Figure 74. Reflectance spectra for INS on alumina with variable surface coverage. g = 23 (purple-pink), g = 104.5 (purple), and g = 982 (purple-red).

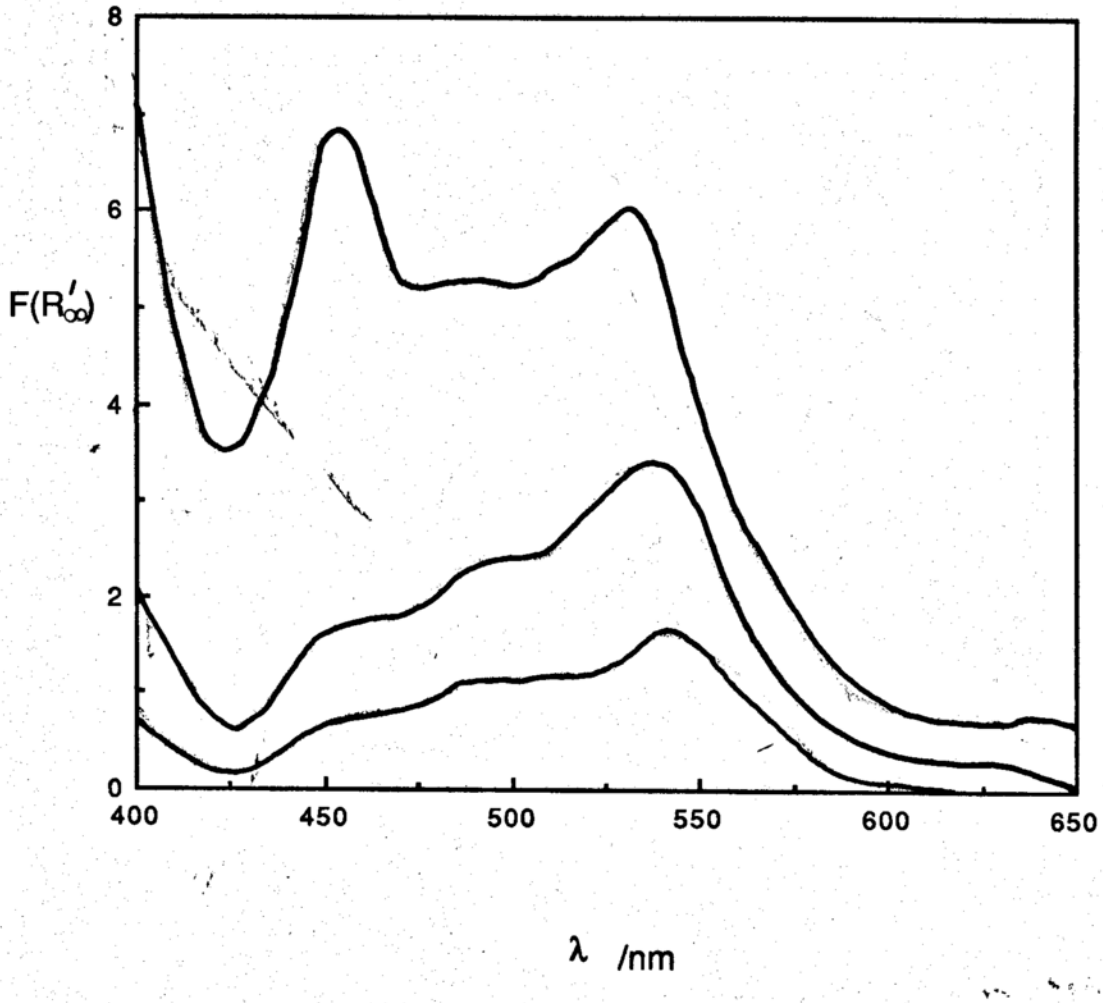

Figure 75. Reflectance spectra for 6-H-BIPS on alumina with variable surface coverage.
g= 64.5 (pink), g= 253 (red-pink), and
g= 679 (red).

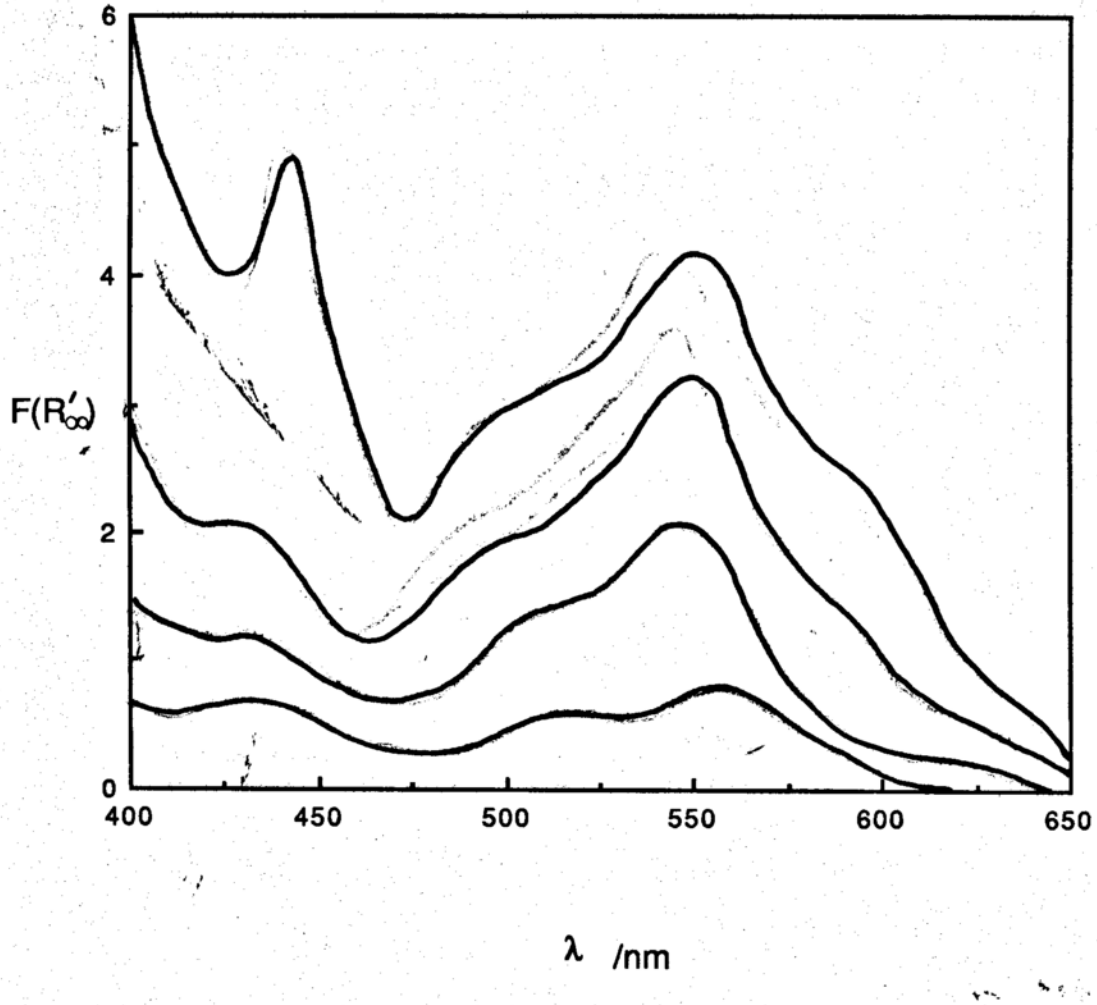

Figure 76. Reflectance spectra for 6-OCH_3-BIPS on alumina with variable surface coverage. g = 10.5 (light tan), g = 50 (pink-tan), g = 317 (brown-tan), and g = 808 (dark brown).

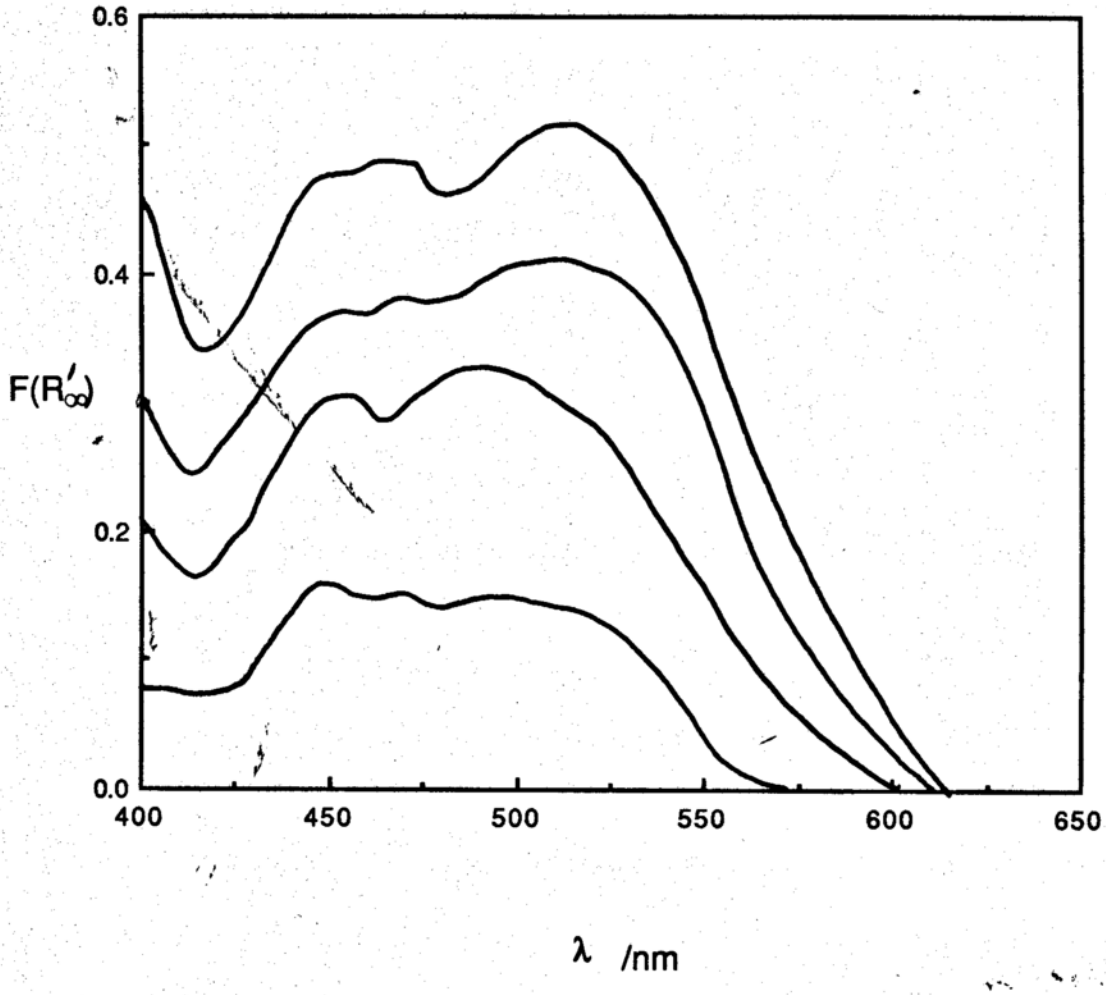

Figure 77. Reflectance spectra for 6-NO_2-BIPS on talc with variable surface coverage. g = 198 (faint peach), g = 502 (light orange-pink), g = 692 (pink), and g = 934 (dark pink).

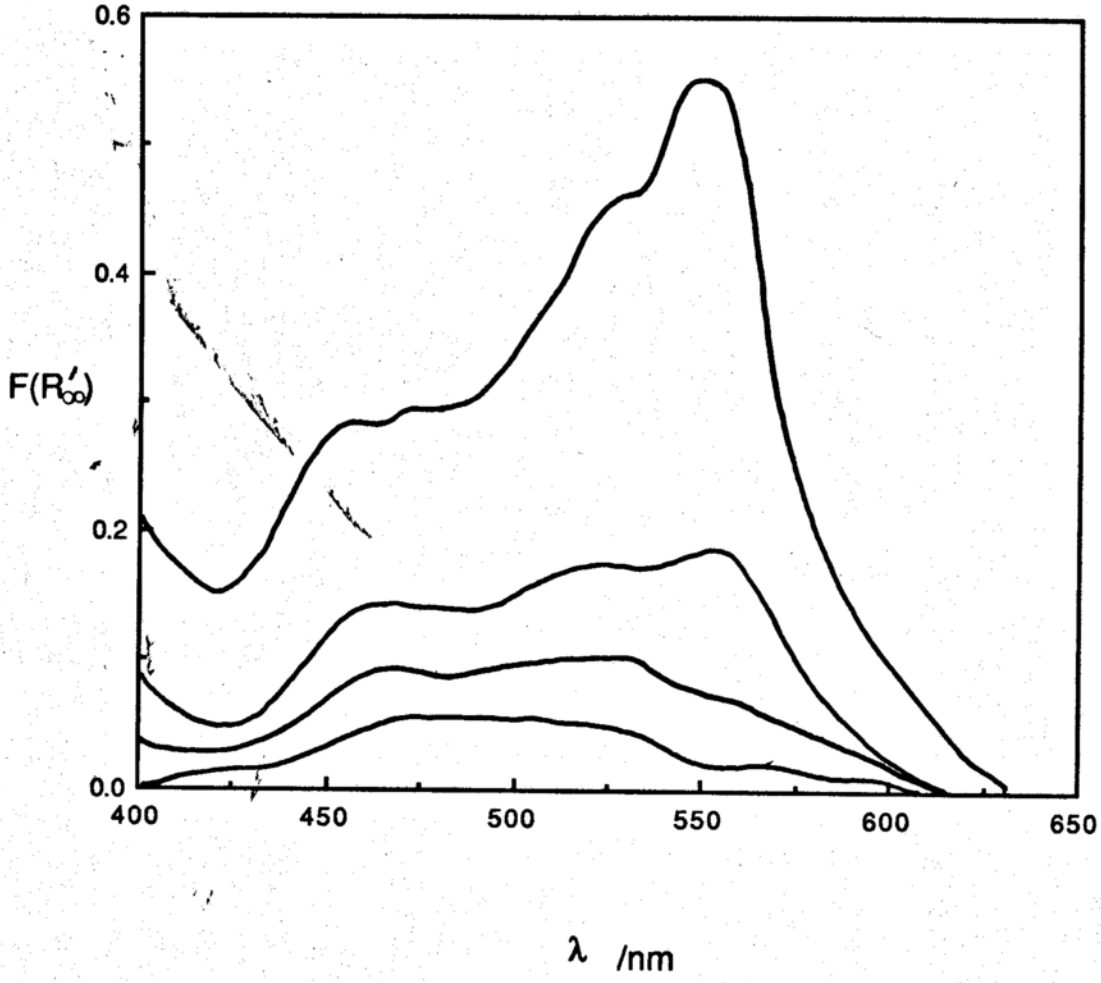

Figure 78. Reflectance spectra for INS on talc with variable surface coverage. g = 195 (light pink), g = 433 (pink), g = 644 (dark pink), and g = 1225 (purple-pink).

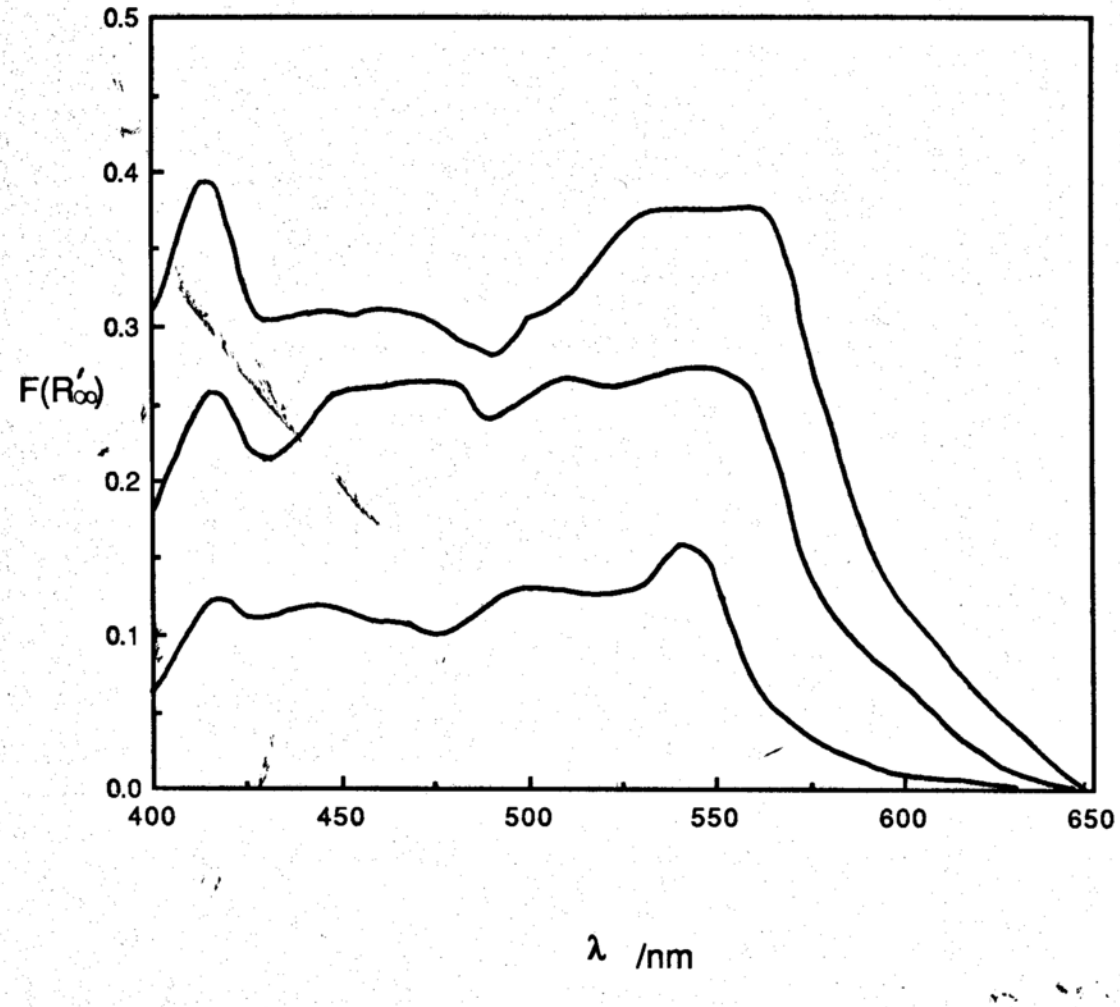

Figure 79. Reflectance spectra for 6-NO_2-BIPS on TiO_2 with variable surface coverage. g = 307 (light pink-tan), g = 963 (pink-tan), and g = 1498 (tan).

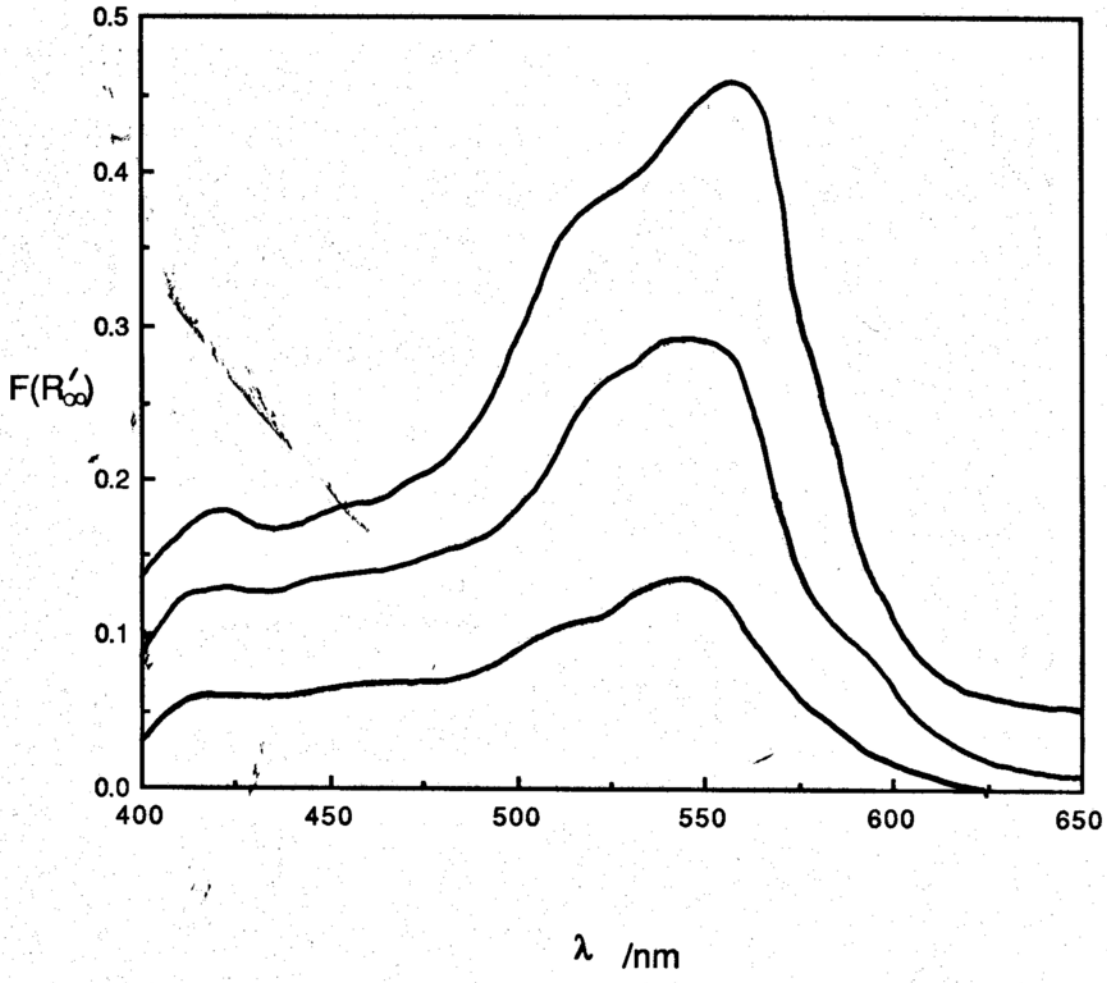

Figure 80. Reflectance spectra for INS on TiO_2 with variable surface coverage. g = 361 (pink), g = 544 (lavender), and g = 772 (purple).

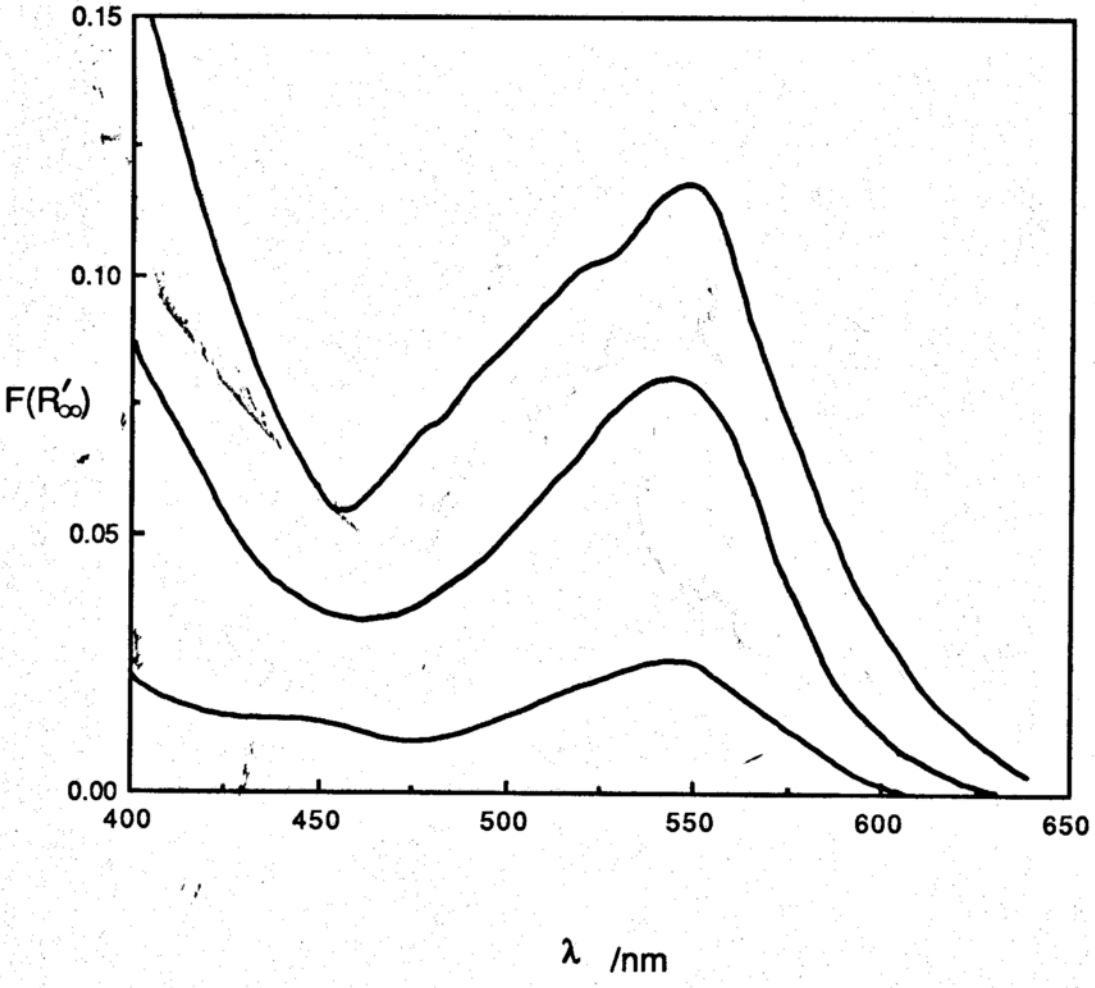

Figure 81. Reflectance spectra for 6-NO_2-BIPS on Avicel microcrystalline cellulose with variable surface coverage. g=98 (light pink), g=423 (pink), and g=1202 (dark pink).

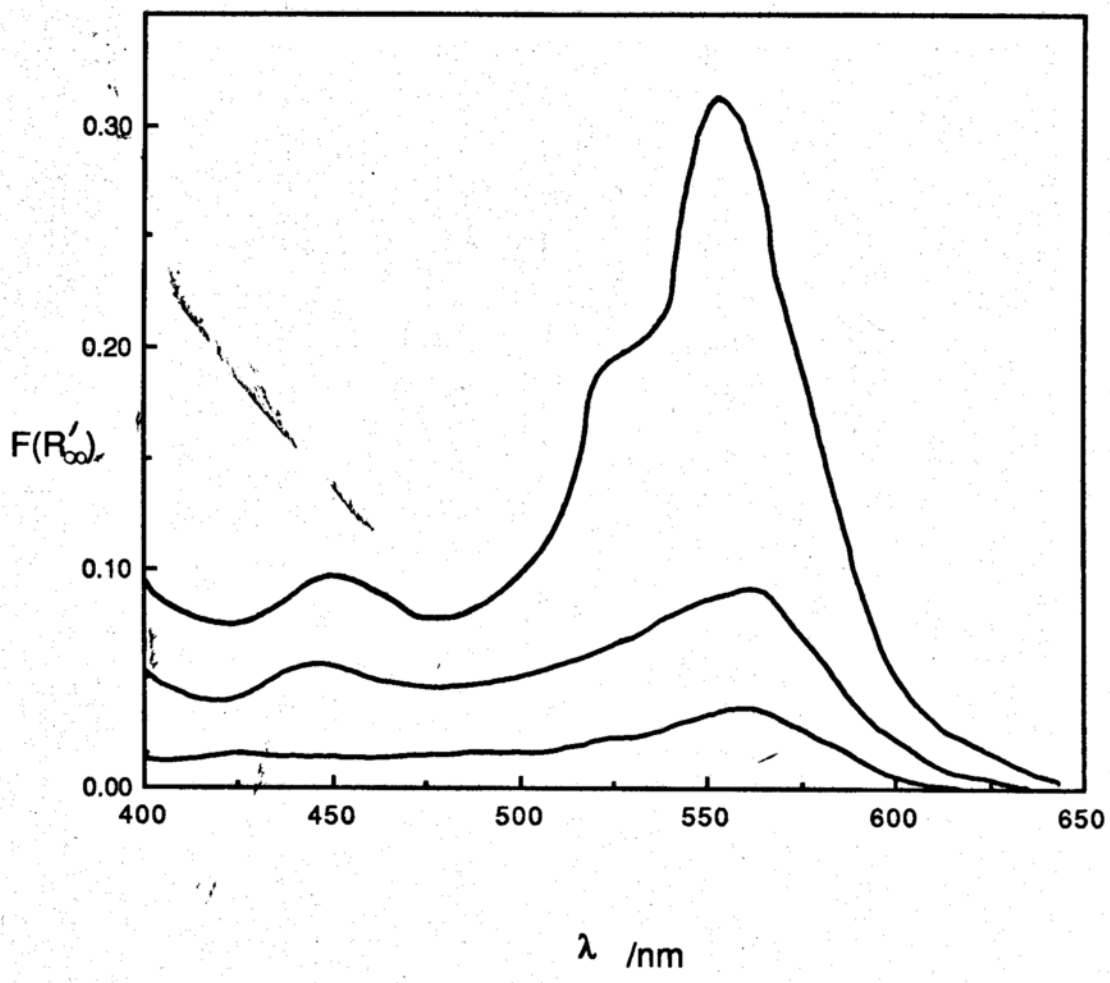

Figure 82. Reflectance spectra for INS on Avicel microcrystalline cellulose with variable surface coverage. g = 119 (light pink), g = 686 (pink), and g = 2505 (pink-purple).

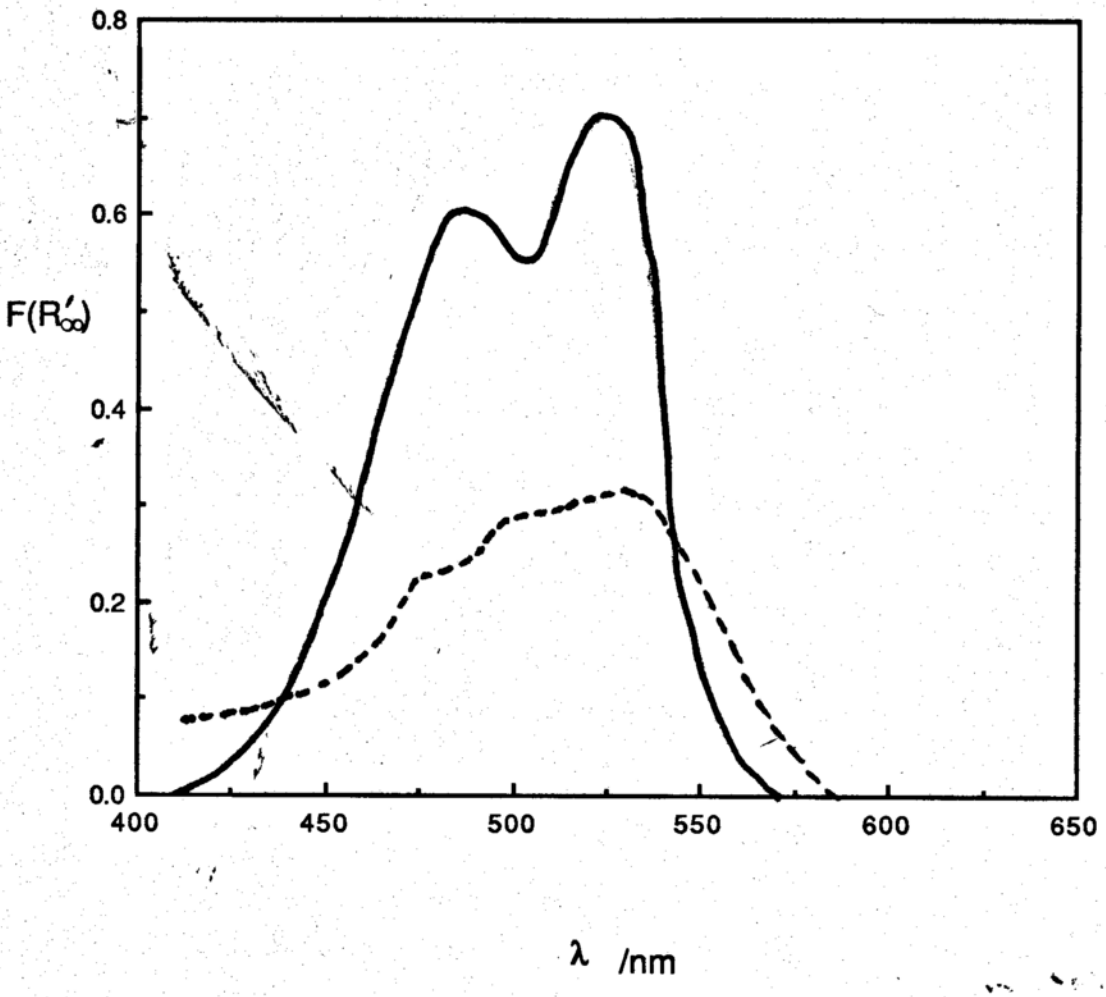

Figure 83. Reflectance spectra of cyanine dyes adsorbed to silica gel 500m^2/g.
Pseudocyanine (———), g = 18.02.
Merocyanine 540 (– – –), g = 19.28.

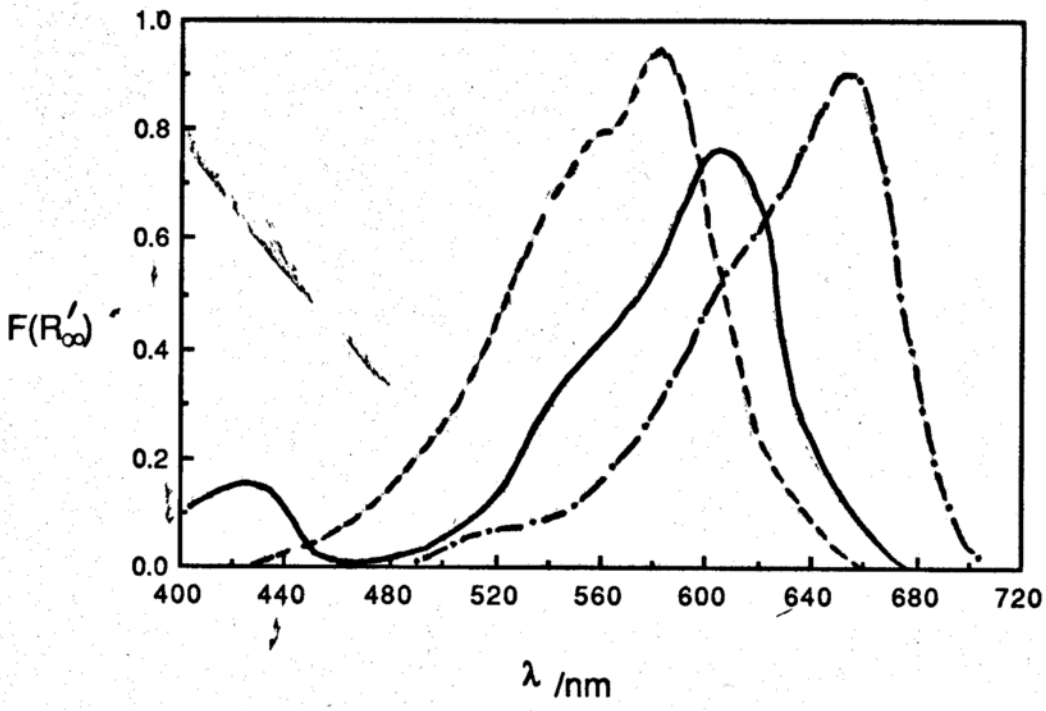

Figure 84. Reflectance spectra of cationic dyes adsorbed to silica gel 500m^2/g. Gentian violet (– – –), g=1.015. Malachite green (———), g=1.150. Methylene blue (—·—·), g=1.287.

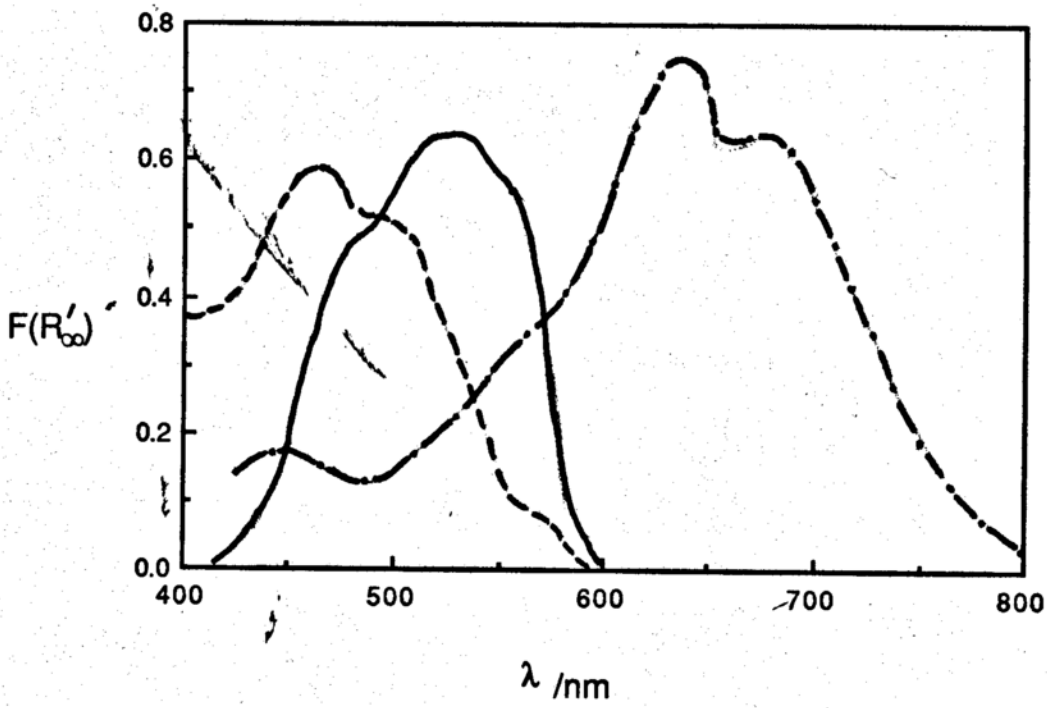

Figure 85. Reflectance spectra of cationic dyes adsorbed to silica gel 500m^2/g. Quinaldine red (----), g = 1.910. Methyl red (——), g = 1.738. Janus Green B (—·—·), g = 1.974.

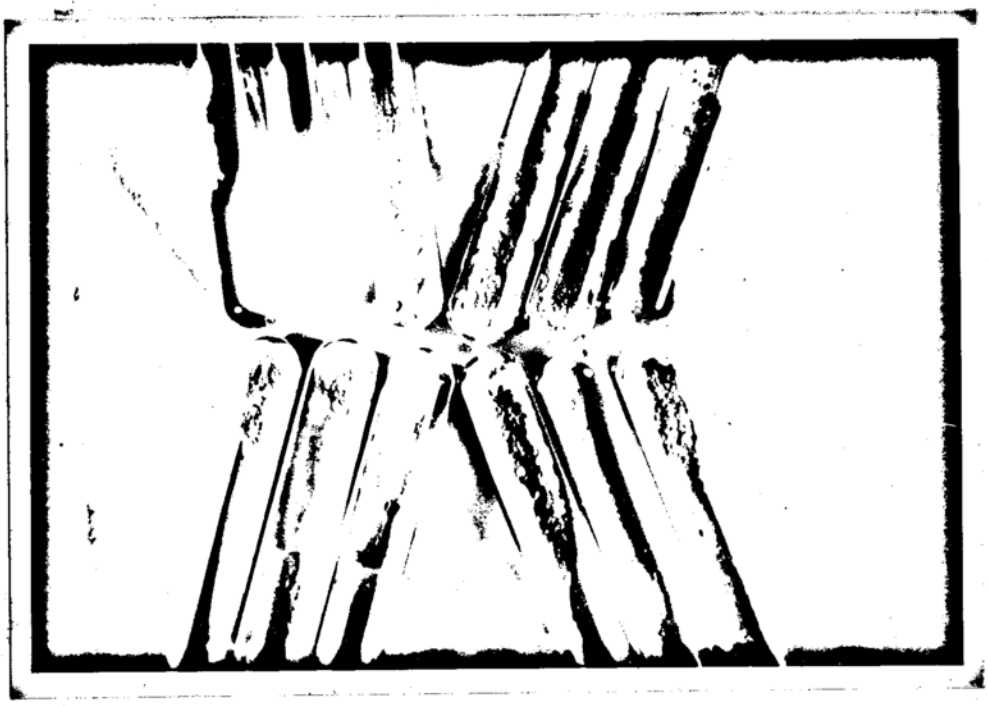

Figure 86. Dyes adsorbed to silica gel ($500 m^2/g$), Janus Green B (upper left, g = 10,5.5,0.8), Gentian Violet (upper right, g = 0.1,0.8, 2.5), Methyl Red (lower left, g = 0.5,1.7, 4.4), and Quinaldine Red (lower right, g = 0.2,1.9,9.6 nano·moles/m^2.

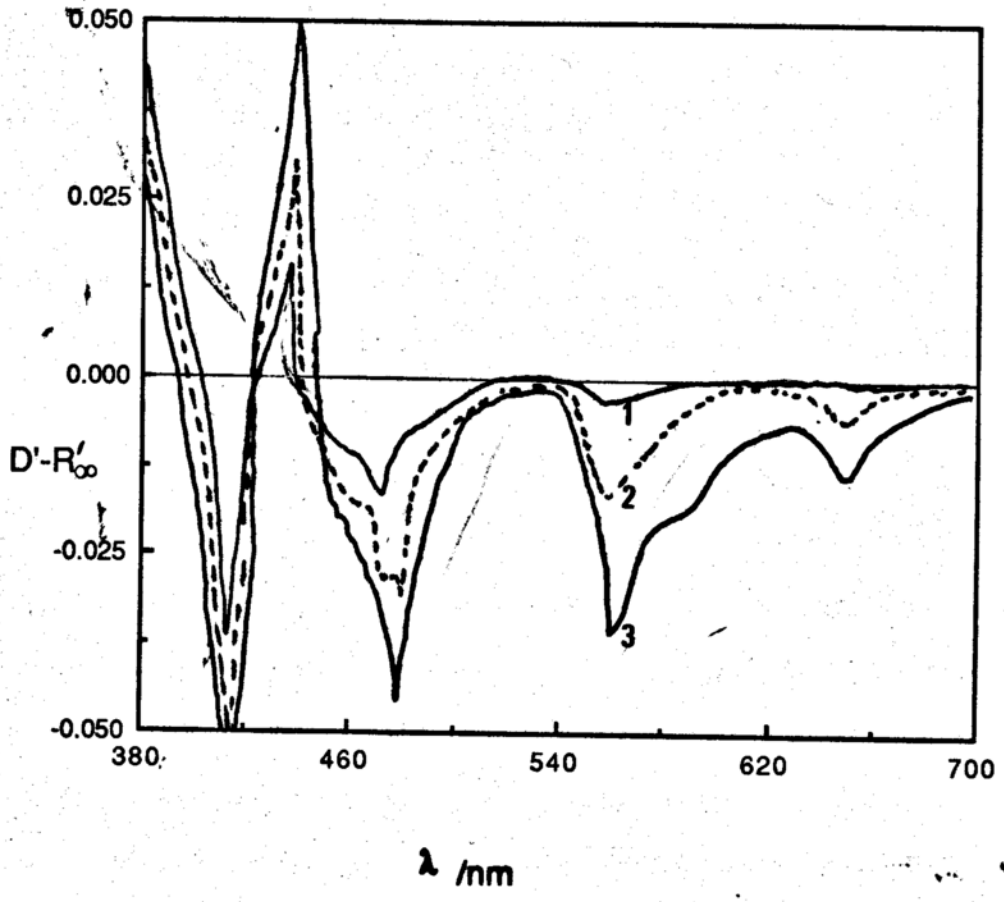

Figure 87. First derivative reflectance spectrum for 6-NO_2-BIPS adsorbing to alumina. The numbers represent increasing surface coverages of spiropyran with time.

V. DISCUSSION

A. Spiropyran Synthesis and Characterization of Materials

The crude yield of each spiropyran was in excess of 90%; the final yields given in Table X represent the amount recovered after loss from recrystallization. The melt colors and melting points correspond very well with those in the literature (1, 9, 10). Koelsch and Workman (10) obtained melting points of 179-180°C for 6-NO_2-BIPS and 92-94°C for 6-H-BIPS. Bertelson (1) gives the melting point of 6-OCH_3-BIPS as 68°C and that of INS as 183°C. The slight discrepancies that exist are most likely due to differences in the purity and recrystallization procedures. The λ_{max} values for 6-NO_2-BIPS in various solvents are very consistent throughout the literature in spite of slight differences in the melting point.

The BET surface areas were determined in order to calculate mg/m^2 coverages and the $Å^2$/molecule occupied on the surface. These values should be interpreted with caution, since the BET method measures the surface area of dry powders. The surface area of an adsorbent immersed in a solvent may change, either from swelling or contraction of the solid structure. Though MacDonald (119) has shown

that cyclohexane is not an adsorbate in the presence of silicas, their highly porous network allows some structural rearrangement. In hydrogen-bonding solvents, silica/solvent interactions can overcome some of the weaker silica/silica hydrogen bonds between particles or across narrow pores (90, 92).

B. Solvatochromic Studies

The solvatochromic data for 6-NO_2-BIPS in various solvents (Table XVI) show a hypsochromic shift of 86 nm when the polarity increases from that of $CHCl_3$ to that of H_2O. The energies of transition, calculated by equation (12), vary from 49.5 in $CHCl_3$

$$E_T = \frac{hc}{\lambda} = \frac{28600}{\lambda_{(nm)}} \text{ in kcal/mole} \qquad (12)$$

to 54.7 in MeOH to 58.1 in H_2O. This is an overall change in transition energy of 8.6 kcal/mole that is covered by these data.

A plot of the wavenumbers of maximum absorption versus solvent dielectric constants was only roughly linear. Notable exceptions to the correlation included DMF and DMSO, which have high dielectric constants that are not reflected by the λ_{max} of 6-NO_2-BIPS solutions. The use of empirical solvent polarity measures drastically improves the correlation. A plot using Brownstein's S values (43) as the abscissa is linear ($r = 0.986$) for nine of the ten solvents; H_2O produces a larger shift in λ_{max} than expected.

When Kosower's Z values (44) are used, the plot is linear for all ten solvents ($r = 0.992$); see Figure 88. The point for H_2O was produced by the extraction procedure previously described. It is interesting to note that after this extensive manipulation to determine λ_{max} in water, this point in fact improves the correlation coefficient with Z from 0.989 to 0.992. The measurement of the spectra of adsorbed spiropyrans (on silica-type solids) by the method of suspension transmission spectroscopy allows the placement of adsorbed 6-NO_2-BIPS on this plot. A Kosower's Z value of 86 (on silica gel) to 89 (on silicic acid) can be assigned to adsorbed 6-NO_2-BIPS from this correlation. Kosower found that a value of 86.4 corresponded to a solution of 70% ethanol in H_2O. Thus, it is concluded that the silica surface polarity, as measured by the 6-NO_2-BIPS probe, approximates that of a 70% ethanol in H_2O solution. Mayo et al. (72) used 5-Br-,6-NO_2-,8-OCH_3-BIPS in a similar manner to obtain an estimate of the polarity of a silica surface. Their results showed a surface that varied in polarity from that of a 40% methanol in water solution to that of a 30% methanol in water solution, depending on the surface silanol density. Their transmission spectra were determined on a dry benzene powder; yet the results are in good agreement.

The spectral data for 6-NO_2-BIPS in acetone/H_2O mixtures (Figure 24) produced a sigmoidal curve when wavenumbers are plotted against mole fraction water in acetone. This is not surprising in light of the fact that Kosower's Z values plotted against mole

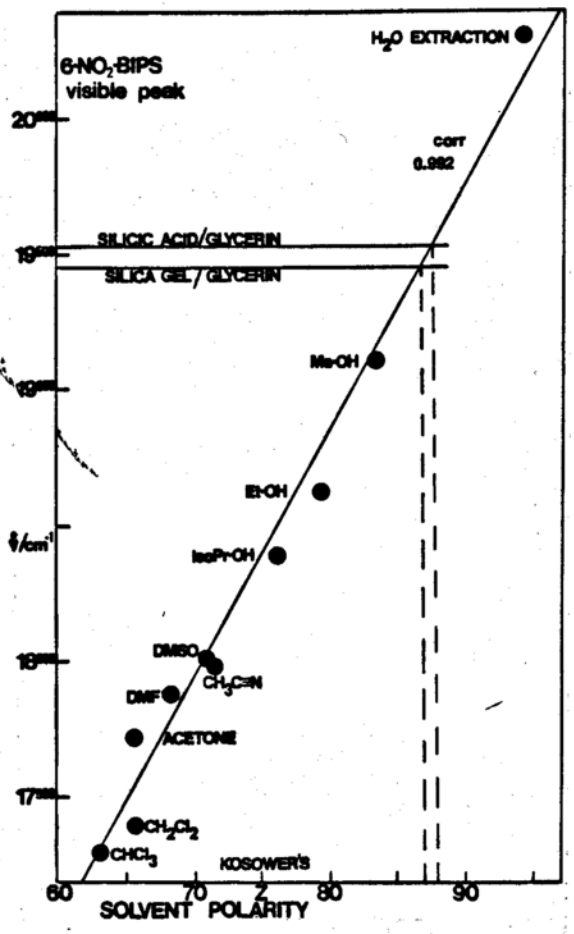

Figure 88. Plot of solvatochromic data for 6-NO_2-BIPS versus solvent polarity.

fraction water in acetone produce the same relationship. Kosower lists Z values for volume percent solutions of acetone in H_2O in his original work (44); preparation and weighing of these solutions can extract the mole fraction water for each case experimentally. Figure 89 shows the expected consequence, that wavenumbers plotted against Kosower's Z values or Brownstein's S values for 6-NO_2-BIPS in acetone/H_2O mixtures produce sigmoidal curves. When the binary solvent mixture becomes too rich in one component, the effect on λ_{max} is exaggerated; in the middle region of solvent polarity, wavenumbers of maximum absorption change less per unit change in the empirical polarity scale.

The marked difference in behavior shown by INS in acetone/H_2O mixtures is rather surprising, considering that it has only one extra aromatic ring and essentially the same structural skeleton as 6-NO_2-BIPS. The strong electron-withdrawing capabilities of the -NO_2 group may account for this difference, as may the increased conjugation path length possible for INS. INS has not only the bathochromic instead of hypsochromic shifts in its spectra with polarity, but also the polarity-independent peak at 543 nm.

3. Adsorption Isotherms

The majority of the isotherms determined produced a good fit to the Langmuir model. Figures 34-53 show a rapid rise in the amount adsorbed at low concentrations, a transition region, and a saturation plateau. Those adsorbents with the high surface areas

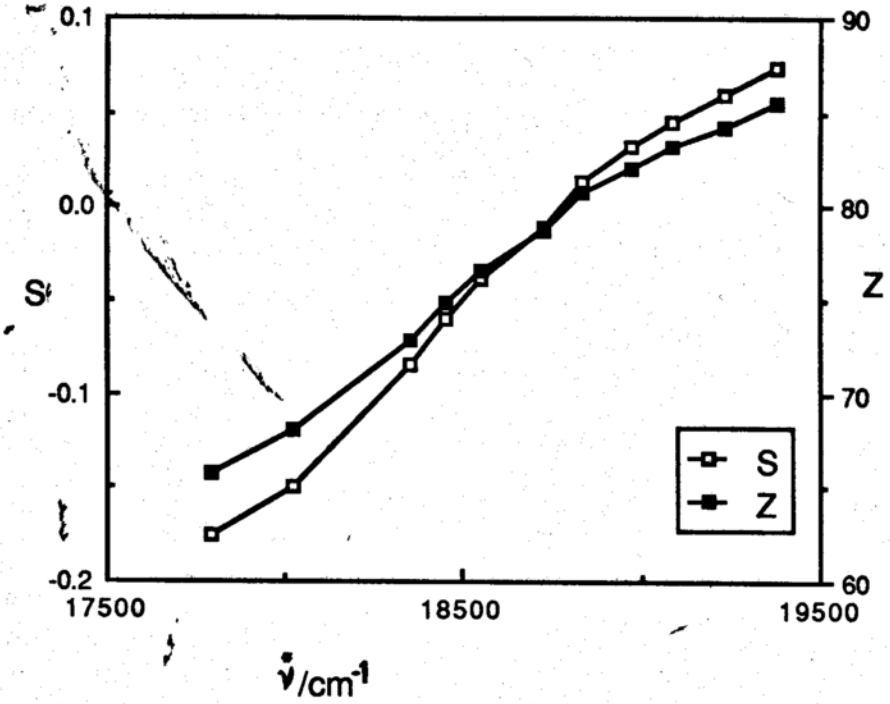

Figure 89. Brownstein's S and Kosower's Z values of empirical solvent polarity plotted versus wavenumber of maximum absorption for 6-NO_2-BIPS dissolved in acetone/water mixtures.

(by BET) usually produced the smoothest hyperbolas. Because of the long equilibration times that were often necessary (3-7 days), an effort was made to produce data points at multiple initial concentrations rather than to produce replicates. The scatter on plots with a large number of points (e.g., Fig. 35) gives a good indication of the reproducibility of the data. As previously discussed, most of the error is in the y axis and consequently is more apparent in the plateau region of the curve. Duplicates were obtained for the 6-NO_2-BIPS/Cab-O-Sil isotherm (Fig. 42); the y dependence of the error is evident. The poorest fit was obtained for Aerosil R-972, which had a binding constant about two orders of magnitude lower than most other adsorbents. Iler (90) found that methyl red only adsorbed to the few remaining free hydroxyl sites on esterils, and this may be the case for spiropyrans as well. The isolated nature of the binding (approximately 1000 $Å^2$/molecule) and the low binding constant combine to produce very limited binding for 6-NO_2-BIPS on this solid. As the legend for Figure 43 shows, a linear fit, usually limited to the low coverage range on other adsorbents, produced a reasonable fit for the entire isotherm. The isotherms on Avicel microcrystalline cellulose fall between these two cases; these isotherms are linear for half of the concentration range studied. Curvature then sets in, but saturation is never achieved in the concentration range studied (limited by the solubility). The rest of the isotherms give reasonable rectangular hyperbola fits, and have Scott plot correlation coefficients in

excess of 0.98.

The low concentration points, which are deviants on the Scatchard plots, produce higher apparent binding constants. These may be real, if they are interpreted as being caused by surface heterogeneity. Crystal defects, impurities, and irregularities are sites of higher energy, and would be expected to bind the first adsorbates, with higher apparent binding constants. This would make the use of the Langmuir isotherm improper, since its assumptions preclude the possibility of more than one type of binding site. The Langmuir isotherm was rigorously developed only for gas adsorption; its use in solute adsorption arises merely because it exhibits the proper curvature to fit the data for a saturable process. In this case the two parameters are still useful for comparative purposes, and give a good estimate of the average conditions over the concentration range employed. The experimental uncertainty explanation for the Scatchard plot deviants is also reasonable. Deviation in the direction seen can be explained not only by excess adsorption (because of higher energy sites), but also by a decrease in solution concentration. Either explanation produces the unexpectedly high value of $(mg/g)/C_{eq}$, the Scatchard plot ordinate. A decrease in C_{eq} may be attributed to a loss of adsorbate to the vessel walls. At high concentrations this is insignificant; consider the size of the flask (0.01 m^2 total surface area on the inside) compared with the area of the adsorbent (500 m^2/g for silica gel). At low concentration, where the amount adsorbed to the solid

is low, this may be a greater fraction. A greater percentage of the available adsorbate is lost from solution at low concentrations of spiropyran (see Figure 90); it is assumed to be adsorbed. The absolute change in adsorption is so low as to be undetectable on the binding isotherm plot, but the loss to vessel walls may account for Scatchard plot deviations at low concentration.

A comparison of the Scott plot parameters (Table XLII) with the Duggleby nonlinear regression parameters (Table XLIII) shows that these capacity estimates are usually within 5%, and are often almost identical. Provided sufficient data are available in the plateau region, this is the easiest parameter to estimate. The apparent binding constants appear to be more sensitive. From the Scott plot it is difficult to obtain a precise estimate of K; it is often part of a small intercept value. However, it still provides a decent estimate for the nonlinear regression program to determine K more precisely. It can be seen from the standard error values that K is not as precise a parameter as is $(mg/g)_{max}$.

The capacities are generally lowest for the low surface area adsorbents, as expected. When expressed in mg/m^2, the capacities are nearly all between 0.2 and 0.6, the INS/Avicel system being the lone exception. The area occupied per molecule is usually 100-200 $Å^2$. The binding constants vary from $4 \times 10^2\ M^{-1}$ to $60 \times 10^2\ M^{-1}$, except for the high value for INS/silicic acid of $150 \times 10^2\ M^{-1}$. The log of the binding constant was plotted versus the coverage at full capacity in mg/m^2 in an attempt to discover a pattern to the

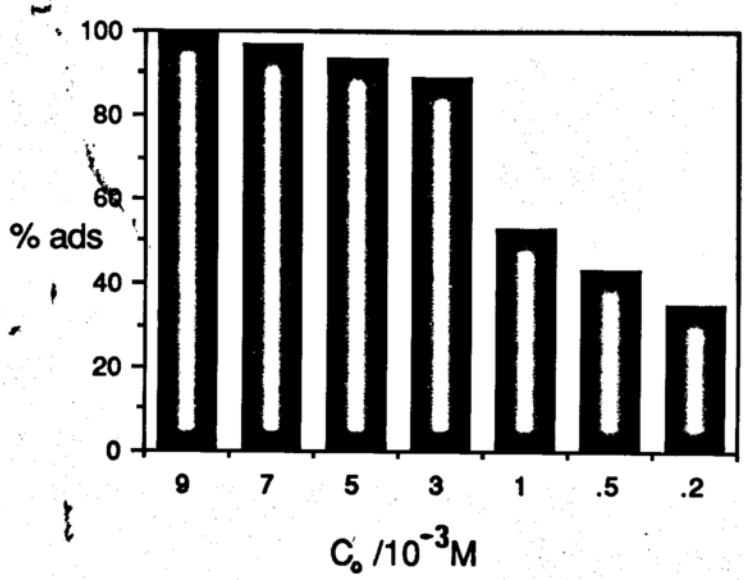

Figure 90. Percent of available adsorbate that is adsorbed from solution by 500m^2/g silica gel versus initial concentration of adsorbate. 50ml of 6-nitro-BIPS solution in cyclohexane was combined with 0.5 grams of adsorbent.

data; see Figure 91. The parameters are plotted for four spiropyrans on the four adsorbents of highest surface area. The parameters for malachite green adsorbed on silica gel 500 m^2/g are given for comparison. It shows much tighter yet more limited (4500 $Å^2$/molecule) binding when compared to the spiropyrans. The 6-H-BIPS systems show the lowest capacities; the 6-NO_2-BIPS systems show the highest capacities. INS and 6-OCH_3-BIPS systems fall in between these two. The binding constants are usually lowest for silica gel 300 m^2/g, except in the case of 6-NO_2-BIPS. The unexpectedly high binding constant for INS/silicic acid is evident in this plot. Generally, the data fall in one large grouping centered at log K = 3.25, capacity = 0.45 mg/m^2. The capacities are high, but the binding constants low, when compared to the dye malachite green. Secondary effects seem to group each spiropyran; 6-H-BIPS at the lower left, 6-NO_2-BIPS at the upper right, INS in the center. It is therefore evident that the isotherm parameters are a stronger function of the spiropyran than of the surface, and therefore cannot tell us much about the surface.

It was thought that the equilibrium in solution between open and closed forms, which differs for each spiropyran, might be affecting the apparent binding constant. A model was developed to determine, in theory, the manner in which the equilibria affect the Langmuir binding constant. The main features of this "equilibrium model" are given in Figure 92; see Appendix D for further details on the derivation. The model allows either colorless (L^o) or colored

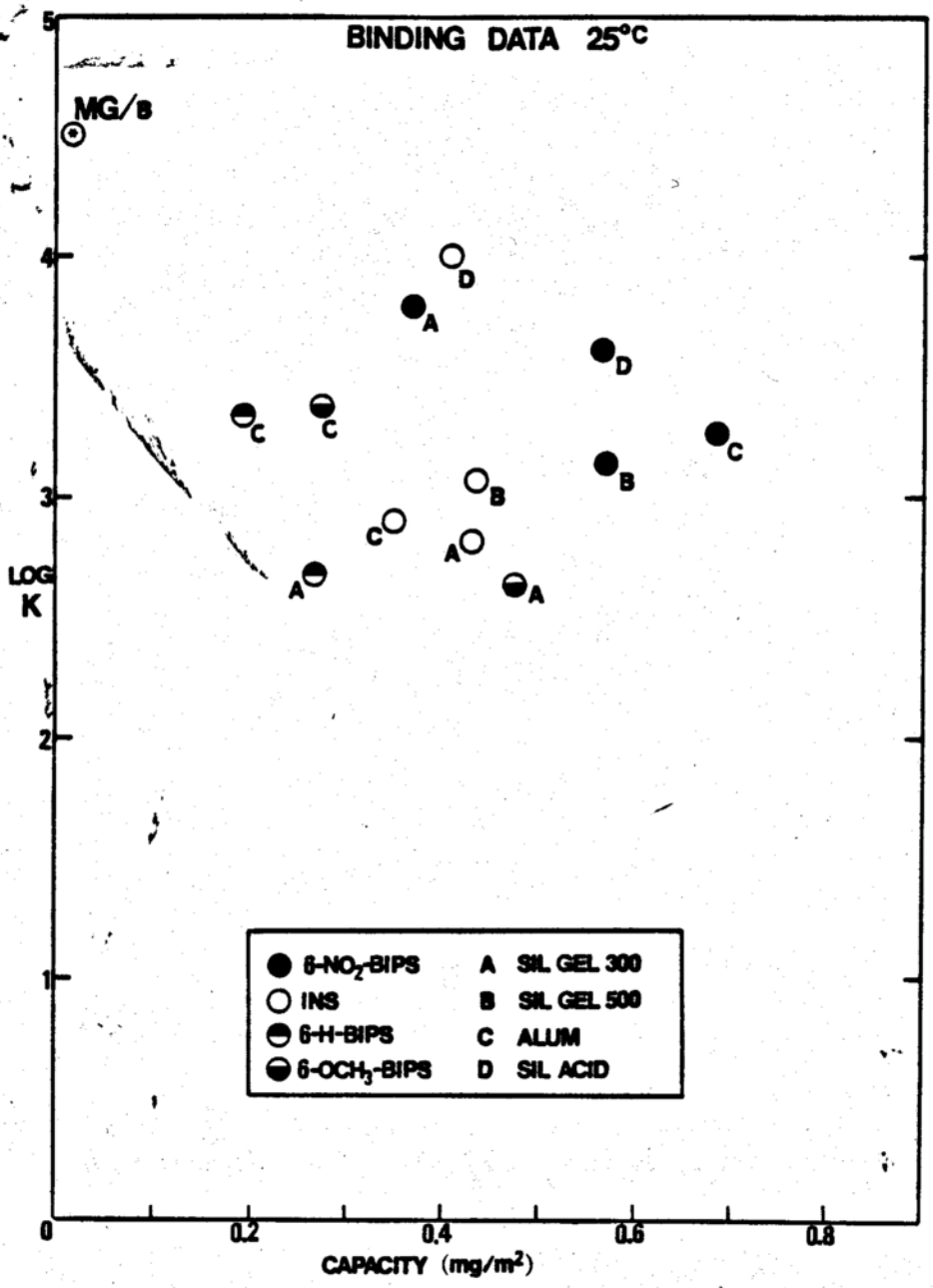

Figure 91. Adsorption isotherm parameters for spiropyrans via the Duggleby program.

EQUILIBRIUM MODEL

$$L^{\circ} \underset{}{\overset{K^{\pm}}{\rightleftharpoons}} L^{\pm}$$

$$\{+S\}\ K_{II} \Big\downarrow \qquad \Big\uparrow K_{I}\ \{+S\}$$

$$SL^{\circ} \underset{}{\overset{K'}{\rightleftharpoons}} SL^{\pm}$$

$$K'K_{II} = K_{I}K^{\pm}$$

BINDING STUDIES

$$K_{app} = \frac{K_{II} + K_{I}K^{\pm}}{[1 + K^{\pm}]}$$

$$= \frac{K^{\pm}K_{I}(1/K' + 1)}{[1 + K^{\pm}]}$$

$$= \frac{K_{II}(1 + K')}{[1 + K^{\pm}]}$$

If $K^{\pm} \ll 1$, $K_{app} = K_{II}(1 + K')$

Figure 92. Essential features of the equilibrium model for adsorption of spiropyrans. See Appendix D for derivation of these equations.

($L^{\pm}$) spiropyran to adsorb to the surface, and includes a possible post-adsorptive equilibrium between colored and colorless adsorbed spiropyran. Three of the four equilibrium constants completely define the cycle. In cyclohexane, most of the spiropyran exists as L^{o}; on the surface there is significant $SL^{\pm}$ (since the phenomenon of adsorptiochromism is seen). The relation between equilibrium constants given by equation (13) arises because there are two equivalent paths to go from L^{o} to $SL^{\pm}$.

$$K'K_{II} = K_I K^{\pm} \tag{13}$$

A mass balance is performed on the total available spiropyran and surface amounts, and the Langmuir equation is introduced. The general equation (14) is arrived at:

$$(mg/g)_{ads} = \frac{(mg/g)_{max}\,[K_{II} + K_I\,K^{\pm}]\;C_{eq}}{[1 + K^{\pm}][K_{II} + K_I K^{\pm}]\;C_{eq}} \tag{14}$$

after changing to the proper units and combining the adsorption expressions for colorless and colored spiropyran. Through comparison with equation (3), one can see that this is simply the Langmuir equation, where the apparent binding constant, K_{app}, is given by:

$$K_{app} = \frac{K_{II} + K_I\,K^{\pm}}{[1 + K^{\pm}]} \tag{15}$$

Because of the relationship between equilibrium constants, the alternative expressions from Figure 92 can be obtained. The first assumes that only colored form binds to the surface, the second allows only binding of the colorless form. We know that we go from essentially all L^{o} in cyclohexane, to a significant amount of $SL^{\pm}$ on hydrophilic surfaces. The question becomes, whether the spiro bond breaks (giving the colored form) prior to or after adsorption. The evidence up to now seems to favor the adsorption of the colorless form, with production of colored form on the surface. This was discussed on pages 29-33, and further evidence from the spectral work will be proposed later. If we conclude that most of the binding is of colorless form, the last formulation of the binding constant is the most appropriate:

$$K_{app} = \frac{K_{II}\,(1 + K')}{[1 + K^{\pm}]} \qquad (16)$$

In cyclohexane, where $K^{\pm} \ll 1$, this becomes:

$$K_{app} = K_{II}(1 + K') \qquad (17)$$

This tells us that both the pre- and post-adsorptive equilibria affect K_{app}, and that K_{app} may be smaller for spiropyrans than for malachite green because the former are not completely in the appropriate form.

The effect of the additional equilibria may control the

observed temperature dependence of K_{app}. Each equilibrium constant will have its own temperature coefficient, and the net effect may or may not reflect the exothermic nature of the binding process. Table XLIV shows that neither the INS/silica gel nor 6-NO_2-BIPS/silica gel system produces the expected relationship with temperature, namely, a decrease of K with T. For INS, the apparent binding constants actually increase with temperature, perhaps because the other equilibrium constants overshadow the decrease in the actual binding constant. It is reasonable to expect, considering the thermochromic effect, that the constants $K^{\pm}$ and K' would increase with temperature. Yet the binding constant (either K_I or K_{II}) is expected to decrease with temperature. The data for 6-NO_2-BIPS appear to be consistent, but the K_{app} rises at 35°C. The capacity should be invariant with temperature (ideally), and in both cases is reasonably so until 35°C. The sudden decrease in capacity at 35°C may indicate changes in the mode of binding which are reflected by this increase in K_{app} for 6-NO_2-BIPS on silica gel.

Figure 93 shows CPK models of the open form of INS (the largest spiropyran used) and 6-H-BIPS (the smallest spiropyran used). A 16 x 8 Å rectangle is shown to provide a scale. Figure 94 shows the same for 6-NO_2-BIPS and 6-OCH_3-BIPS. It is obvious that within the limits of experimental error, these four compounds are not different enough in size to yield much information from the capacity data. Any porous area accessible to one should be accessible to the others. Furthermore, the area occupied per molecule would not be

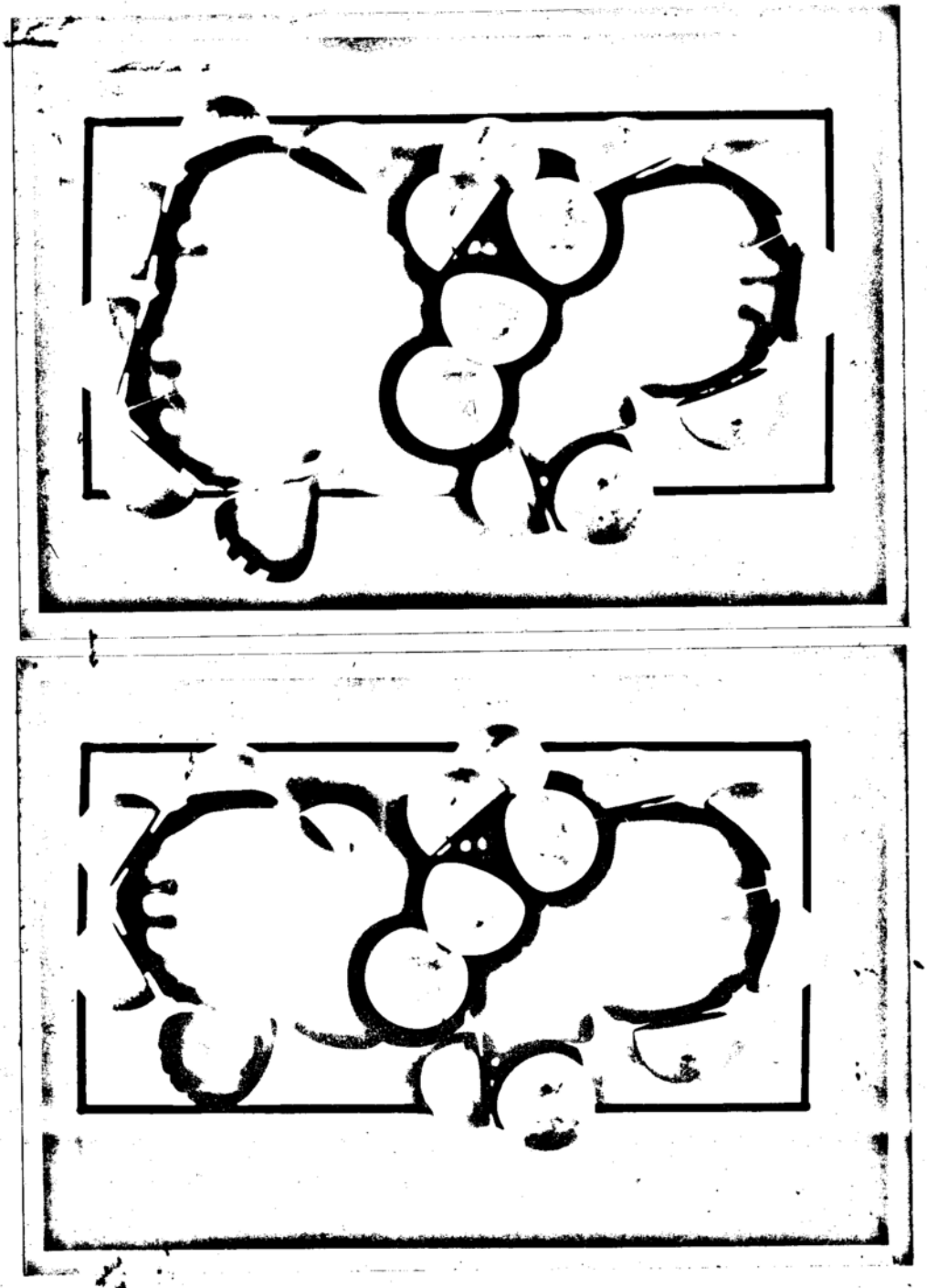

Figure 93. CPK models of open INS (top) and 6-H-BIPS (bottom).

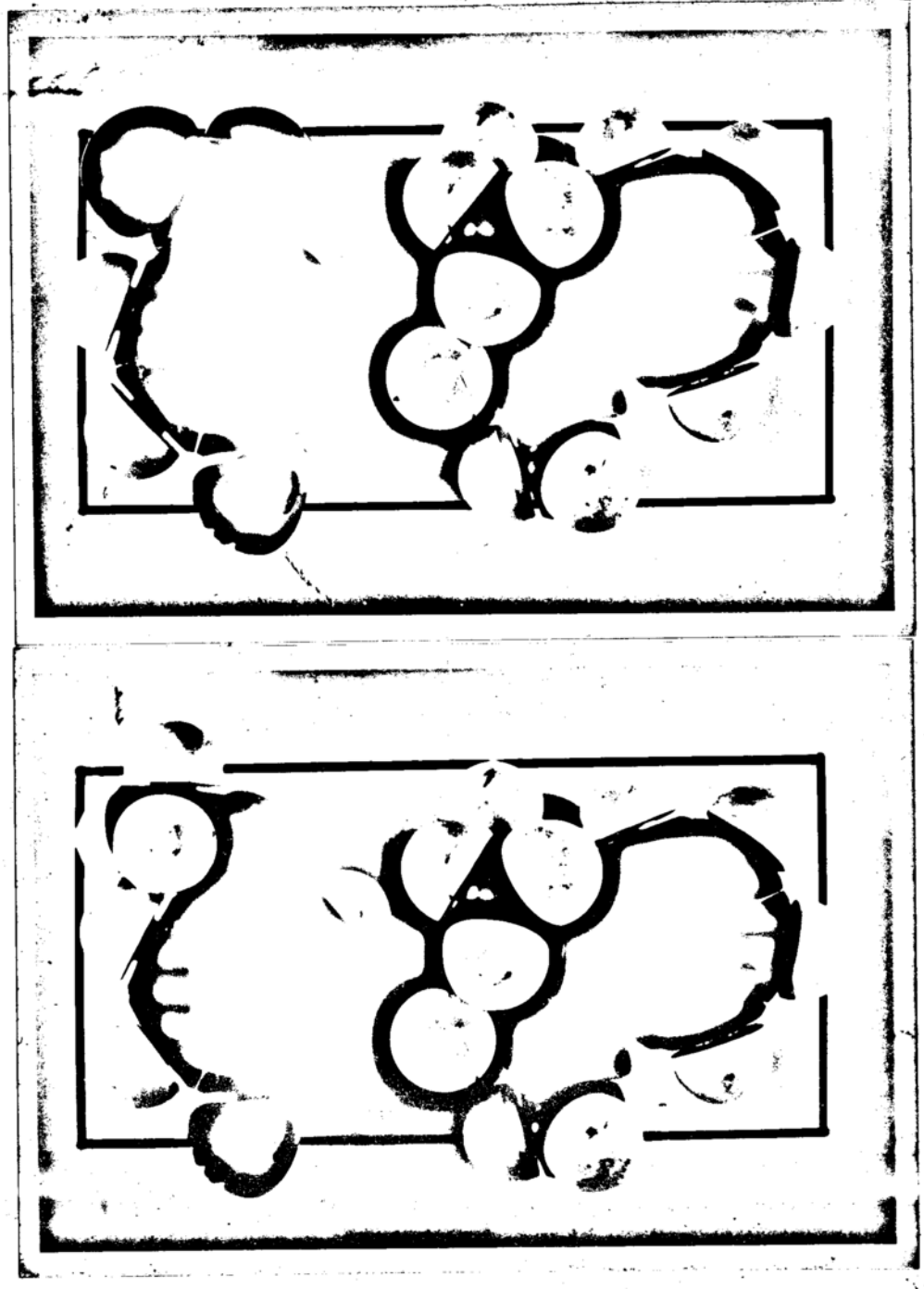

Figure 94. CPK models of open 6-NO_2-BIPS (top) and 6-OCH_3-BIPS (bottom).

greatly different for edge-on adsorption than for flat adsorption. That the area per molecule fluctuates in the narrow range of 100-200 $\AA^2$ is not surprising. Even molecules of N_2 can change their apparent cross-sectional area on different adsorbents through polar interactions with the surface (123). Experimental uncertainty in the capacity provides sufficient difference to account for the slight size differences of these four spiropyrans.

D. Suspension Transmission Spectroscopy

The spectra of spiropyran/silica powders suspended in glycerin (e.g., Figure 56) are remarkably smooth and free of scattering effects. The match in silica and glycerin refractive indices is as good as those of silica and cyclohexane; and the spectra that result are as smooth as those of Robin et al. (70) and Evans et al. (53). Glycerin has the added advantage of a high viscosity, leading to good suspension stability. This allows the spectral measurements of small amounts of colored silicas; the prior method (70) required enough powder to pack the cell full of a wet slurry of powder and cyclohexane.

"Beer's Law" plots such as Figure 57 validate the consistency of the method. Table XLVI lists additional parameters from this same data set. The adsorption isotherm for these 6-NO_2-BIPS/silica gel points is obtained by plotting $(mg/g)_{ads}$ versus C_{eq}/M. Note that the slopes of glycerin suspension spectra "Beer's Law" plots also increase steeply at low concentrations and "saturate" at higher

Table XLVI. Additional Parameters for 6-NO_2-BIPS/silica gel Powders.

Isotherm Data		Glycerin "Beer's Law" Plots	
$C_{eq}/10^{-4}M$	$(mg/g)_{ads}$	slope	correlation coefficient
58.4	264.6	32.2	0.9993
38.4	258.9	36.7	0.9967
40.9	244.5	30.3	0.9827
22.4	214.6	34.2	0.9981
24.9	207.7	36.1	0.9867
5.19	193.2	35.5	0.9972
1.20	230.3	27.4	0.9845
0.71	74.8	17.7	0.9996
0.59	76.5	23.6	0.9935
0.11	38.2	14.4	0.9965
0.02	38.3	7.8	0.9967
0.001	16.7	4.8	0.9991

concentrations. Figure 95 shows this relationship graphically; compare this to the isotherm in Figure 52, which contains these and other data points for this system. The rise in the ordinate value is much steeper with concentration for the glycerin spectral data, and this curve reaches a plateau level at a much lower concentration. In other words, the color of the suspended powder, and its apparent absorptivity, appear to saturate before the adsorption has been completed. This phenomenon will reappear in analysis of the diffuse reflectance spectra.

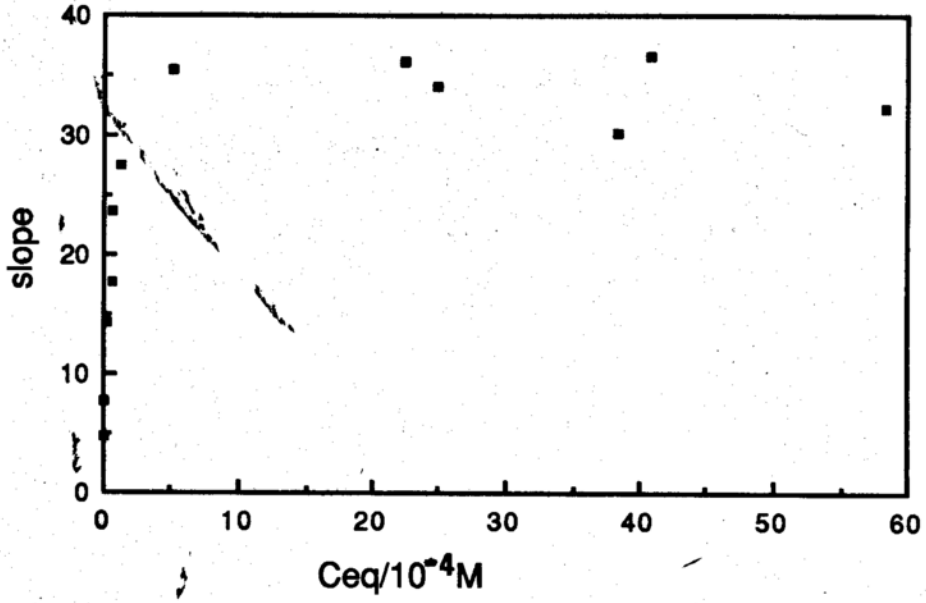

Figure 95. Plot of the "Beer's Law" slope of 6-NO_2-BIPS/ silica gel powders in glycerin versus the equilibrium adsorbate concentration.

E. Diffuse Reflectance Spectroscopy

The diffuse reflectance spectroscopic work provided the most insight into the adsorptiochromic phenomena of spiropyrans. These spectra were not as simple as those in solution, and did not show the expected "solvatochromic" shifts on different surfaces. Rather, the spectra invariably were composed of a peak between 436 and 472 nm and a peak at 550 nm. The spiropyran, the adsorbent, and most importantly, the surface coverage were factors that affected the relative absorption at these wavelengths. Certain spiropyrans or certain adsorbents seemed to favor one peak over the other. INS spectra emphasized the longer wavelength peak (see Figure 64), whereas 6-NO_2-BIPS spectra were dominated by the shorter wavelength peak. Alumina spectra (especially at low surface coverages) were dominated by the peak at 550 nm, as seen in Figures 66 and 67. The shorter wavelength peak ranged from 436 nm (6-H-BIPS) to 456 nm (6-OCH_3-BIPS) to 472 nm (6-NO_2-BIPS and INS) on silica gel. In Figures 68-82 there is often a change in the dominant peak with increased surface coverage. In 6-NO_2-BIPS/silicic acid spectra (Figure 68), the longer wavelength peak occurs only after the 472 nm peak has begun to show saturation. For INS on silica gel (Figure 70) the opposite is true, though ultimately the 472 nm peak reaches the higher "absorbance" value. The spectra on TiO_2 (Figures 79, 80) seem to be an exception; the low wavelength visible peak is between 406 nm (6-NO_2-BIPS) and 440 nm (INS). All spectra taken on TiO_2

showed a significant amount of absorption from 400-600 nm. This is why TiO_2 is useful as an opacifier in pigments; it is an efficient scatterer and absorber of visible light. One way to express the changes in spectra with surface coverage is to plot the ratio of the Kubelka-Munk parameter, $F(R'_\infty)$, at the shorter wavelength to the value of $F(R'_\infty)$ at 550 nm, against g, the nanomoles/m^2 surface coverage. Figure 96 shows this type of plot for four spiropyrans adsorbed on silica gel 500 m^2/g. The ratio decreases initially, and ultimately reaches a limiting value. For the three BIPS compounds, the rates of decrease to the ultimate value vary. For INS, the ratio rises to the final value, since the 550 nm peak becomes more dominant. Similar plots for INS on alumina or silica gel 300 m^2/g have ratios that began at less than 1.0 and increase with changing slopes to a plateau value. 6-NO_2-BIPS on silicic acid, alumina, or silica gel 300 m^2/g show initially high ratios ($\sim$10) that decrease smoothly to 2.0-3.0. The curve for 6-NO_2-BIPS/alumina takes a slight decrease before coming back up to the limiting level. The overall picture is similar to the solvatochromic studies; INS behaves qualitatively differently from the three BIPS spiropyrans.

Another productive method of depicting reflectance data was to plot $F(R'_\infty)$ versus g; the plot for 6-NO_2-BIPS adsorbed on silica gel 500 m^2/g is given in Figure 97. The overall appearance of the plot is hyperbolic, similar in shape to the adsorption isotherm. The initial portion of the curve, when it is looked at more closely, is found to be quite linear. The inset in Figure 97 shows the linear

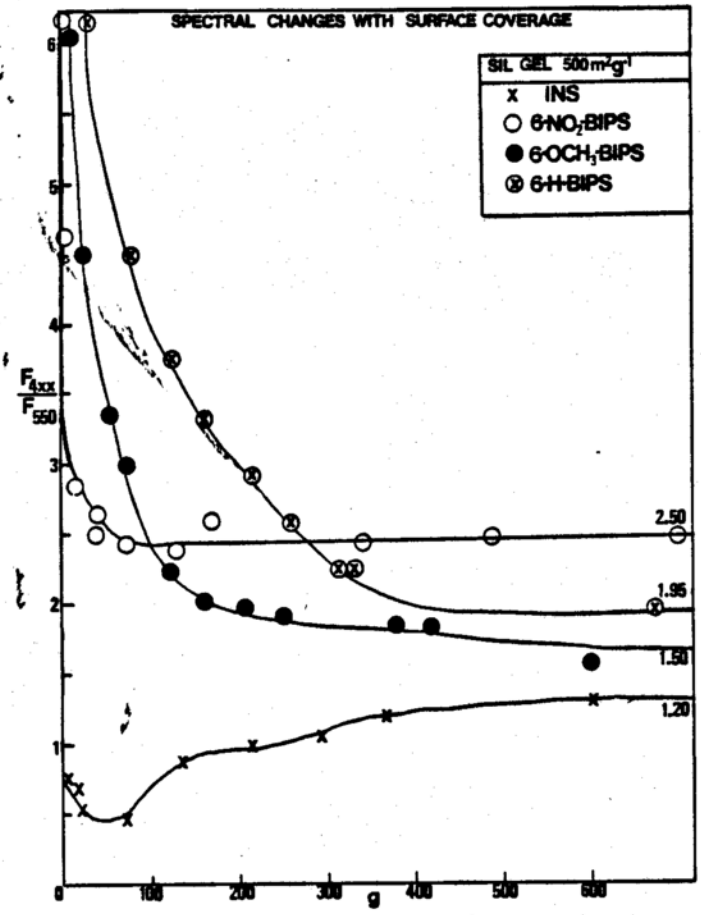

Figure 96. Coverage-dependent spectral changes for reflectance spectra of spiropyrans adsorbed on silica gel $500m^2/g$.

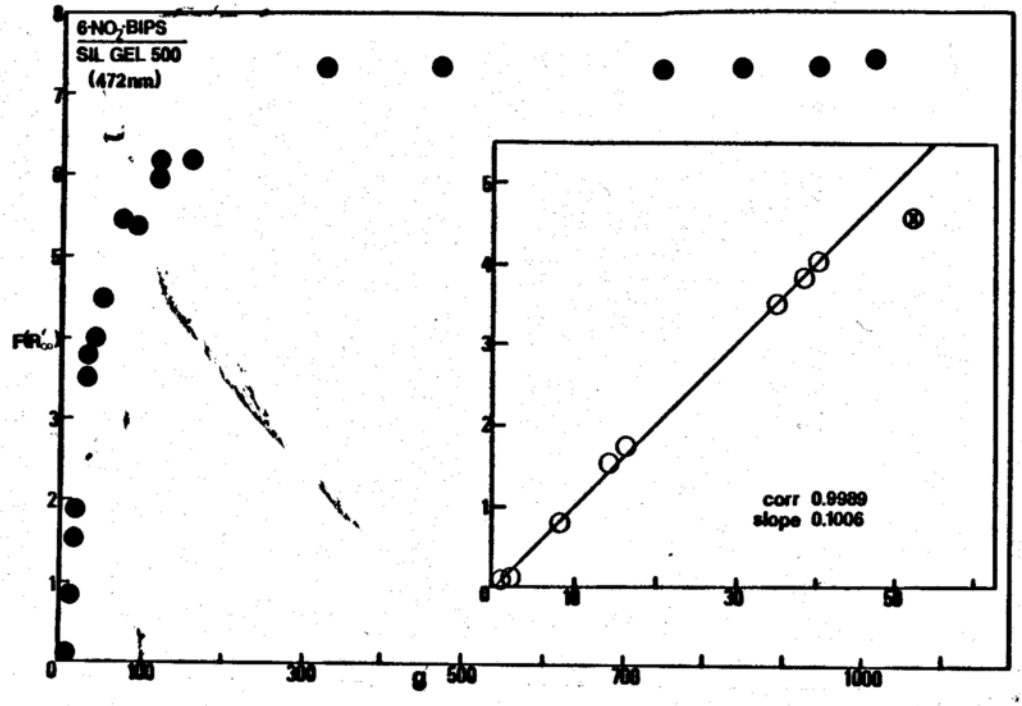

Figure 97. Kubelka-Munk reflectance parameter plotted against surface coverage in nanomoles/m^2 for 6-NO_2-BIPS adsorbed on silica gel 500m^2/g at 472nm.

portion of the plot. From equation (10), the slope is designated as "f", and is constant for a given wavelength at low g. The point at which the graph begins to level off, at g = 300, corresponds to 48 $(mg/g)_{ads}$. This means that the color formation with increasing coverage ceases when the adsorption is only one-fifth complete. This is consistent with the cessation of coloration ability seen with the glycerin suspension transmission spectra, and evidence that colorless adsorbed spiropyran (SL^{o}) exists. Visual observation reveals that some $SL^{\pm}$ exists, therefore the equilibrium constant K' exists on the surface, analogous to $K^{\pm}$ in solution. Alternatively, a single species may exist on the surface, but the observations would then require this species to have a decreasing absorptivity as the surface coverage increases.

The plot for 6-NO_2-BIPS on silica gel 300 m^2/g has the same shape, but reaches a plateau value of 12.2 instead of 7.36 (silica gel 500 m^2/g). The slope, f, is also larger; this is consistent with the qualitative observation that these powders are darker. Similar curves could be made for most of the systems studied, at both the 400-500 nm wavelengths and at the 550 nm wavelengths of maximum absorption. The curve for 550 nm in most cases showed saturation at lower g values and the plateau level $F(R'_{\infty})$ value was lower when compared to the curves at the shorter wavelength. $F(R'_{\infty})$ versus g curves were also generated for malachite green on silica gel (both 300 m^2/g and 500 m^2/g) and methylene blue on TiO_2 and silica gel (300 m^2/g). The curves for permanent dyes also showed

curvature beyond an initial linear segment. The point at which deviation from linearity begins is usually closer to the capacity in the case of dyes. The slope never approaches zero as it did with spiropyrans (at the plateau), though it decreases substantially from the initial linear portion. Nonidealities probably set in as the adsorbates are forced into close contact, but some contribution to the overall absorption is still seen for the last molecules to adsorb. Spiropyrans, on the contrary, cease being detectable by visible absorption soon after the linear region is surpassed with increasing coverage. Figure 98 shows the plot for malachite green on silica gel 300 m^2/g. Note that once the linearity fails, the points continue to rise. On silica gel 500 m^2/g, this rise continues until the capacity, g_{max}, is reached. All points near the capacity are bunched at a final value of $F(R'_\infty)$ indicative of complete coverage and coloration.

Fixed wavelength reflectance analysis gave linear plots for all spiropyrans on each adsorbent at low coverages. Table XLVII gives data for INS/silicic acid at the 550 nm peak. Figure 99 plots these data, which give a correlation coefficient of 0.998 and a slope (f) of 0.145. The slopes were reproducible within 1-5%, depending on the system. Reflectance analysis worked best at low coverages; hence it is well suited for the analysis of small amounts of colored adsorbates or impurities on a solid surface. Table XLVIII lists the results for spiropyran/adsorbent fixed wavelength reflectance analysis. For each system, the correlation coefficient, number of

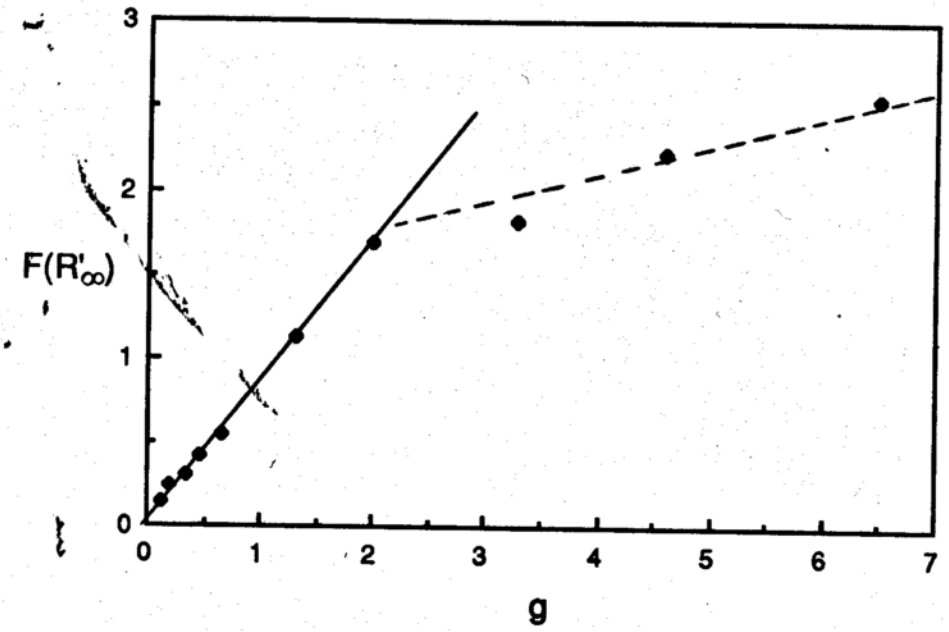

Figure 98. Reflectance data at 595 nm for malachite green on silica gel $300m^2/g$ versus surface coverage.

Table XLVII. Single-Wavelength Reflectance Analysis for INS/Silicic Acid.

g/(nanomoles/m^2)	R'_∞ (550 nm)	$F(R'_\infty)$
0.59	0.860	0.011
1.10	0.740	0.046
1.78	0.680	0.075
2.70	0.511	0.234
2.99	0.500	0.250
5.30	0.398	0.455
6.00	0.312	0.759
11.72	0.196	1.65
17.76	0.147	2.47
23.57	0.115	3.41
29.90	0.100	4.05

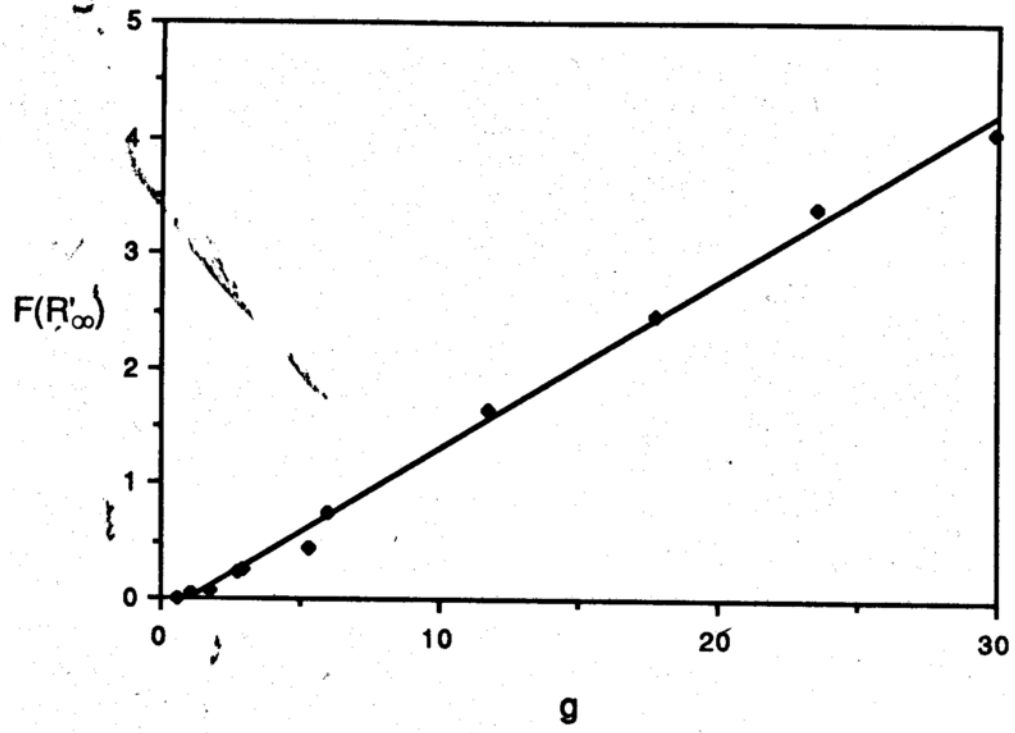

Figure 99. Linear portion of the diffuse reflectance data fixed wavelength analysis for INS on silicic acid at 550nm.

Table XLVIII. Results for Spiropyran/Adsorbent Low Concentration Reflectance Spectra Analysis.[a]

System	4xx nm peak[b]				550 nm peak			
	λ/nm	n	corr. coeff.	f_{4xx}	n	corr. coeff.	f_{550}	f_{4xx}/f_{550}
6-NO_2-BIPS / silica gel 300 m^2/g	472	5	0.996	0.193	5	0.998	0.094	2.053
6-NO_2-BIPS / alumina	436	5	0.999	0.016	7	0.997	0.005	3.200
INS / silica gel 300 m^2/g	472	5	0.997	0.077	3	0.980	0.177	0.435
INS / alumina	436	9	0.994	0.0074	9	0.988	0.015	0.493
6-H-BIPS / silica gel 300 m^2/g	436	6	0.993	0.114	7	0.995	0.042	2.714
6-H-BIPS / alumina	472	8	0.995	0.0083	7	0.985	0.0113	0.735

Table XLVIII. Results for Spiropyran/Adsorbent Low Concentration Reflectance Spectra Analysis (cont.)

System	4xx nm peak[b]				550 nm peak			
	λ/nm	n	corr. coeff.	f_{4xx}	n	corr. coeff.	f_{550}	f_{4xx}/f_{550}
6-OCH_3-BIPS / silica gel 300 m^2/g	456	6	0.992	0.109	7	0.997	0.053	2.057
6-OCH_3-BIPS / alumina	436	5	0.998	0.014	5	0.999	0.017	0.824
6-NO_2-BIPS / Aerosil R-972	472	5	0.996	0.0036	5	0.994	0.0064	0.563
6-NO_2-BIPS / silicic acid	472	7	0.999	0.197	7	0.998	0.071	2.775
INS / silicic acid	472	7	0.991	0.293	10	0.998	0.145	2.021
6-NO_2-BIPS / talc	472	7	0.988	4.93×10^{-4}	9	0.997	4.19×10^{-4}	1.177

Table XLVIII. Results for Spiropyran/Adsorbent Low Concentration Reflectance Spectra Analysis (cont.)

System	4xx nm peak[b]				550 nm peak			
	λ/nm	n	corr. coeff.	f_{4xx}	n	corr. coeff.	f_{550}	f_{4xx}/f_{550}
INS / talc	472	9	0.960	2.24×10^{-4}	5	0.977	1.49×10^{-4}	1.503
6-NO_2-BIPS / Avicel MCC	472	4	0.998	8.23×10^{-5}	7	0.993	1.63×10^{-4}	0.505
INS / Avicel MCC	436	6	0.924	2.94×10^{-5}	9	0.995	1.12×10^{-4}	0.263
6-NO_2-BIPS / TiO_2	406	8	0.998	2.31×10^{-4}	5	0.981	2.21×10^{-4}	1.045
INS / TiO_2	440	9	0.989	2.49×10^{-4}	8	0.993	6.87×10^{-4}	0.362
6-NO_2-BIPS / silica gel 500 m^2/g	472	8	0.999	0.101	7	0.998	0.042	2.405

Table XLVIII. Results for Spiropyran/Adsorbent Low Concentration Reflectance Spectra Analysis (cont.)

System	4xx nm peak[b]				550 nm peak			
	λ/nm	n	corr. coeff.	f_{4xx}	n	corr. coeff.	f_{550}	f_{4xx}/f_{550}
INS silica gel 500 m^2/g	472	3	0.992	0.038	3	0.990	0.079	0.435

[a]Linear portions of $F(R'_\infty)$ vs. g plots, f = slope.

[b]Absorption peak for the maximum between 400 and 500 nm.

points in the linear region, and slope are listed for both major absorption peaks. The position of the shorter wavelength peak is given in nanometers for each spiropyran/adsorbent combination. The ratio of slopes (f_{4xx}/f_{550}) is given in the last column; this is a relative measure of the absorption at the two major wavelengths at low coverage. Note once again that the INS systems usually have ratios less than 1.0, whereas BIPS compounds generally have ratios of 1.0 to 3.0. Other adsorbents which seem to favor absorption at 550 nm, such as alumina, also have ratios less than 1.0 for 6-OCH_3-BIPS and 6-H-BIPS. 6-NO_2-BIPS has a ratio of less than 1.0 only for the low binding Aerosil-R972 adsorbent.

Table XLIX gives similar data for dyes adsorbed to silica gel 500 m^2/g. The λ_{max}, correlation coefficients, and f values are listed for the linear low coverage region of an $F(R'_\infty)$ versus g plot. Two cyanine dyes are used, namely Pseudocyanine and Merocyanine 540. The other six dyes are cationic dyes that adsorb strongly to the acidic surface of silica gel. Bromcresol purple, nitrazine yellow, and orange II would not adsorb strongly enough to use them in the study; these dyes all were sulfonate salts and not quaternary ammonium cations. Figure 100 is a log-log plot of f against the aqueous absorptivity (ε) for the dyes and spiropyrans studied on silica gel 500 m^2/g. Spiropyrans are water insoluble and have absorptivities that are difficult to measure independently of the colorless/colored equilibrium. Literature estimates of the aqueous absorptivity are used in this case, with the range denoted

Table XLIX. Single-Wavelength Reflectance Analysis for Dyes Adsorbed to Silica Gel (500 m^2/g).

Dye	λ_{max}	correlation coefficient	f[a]	log f
Malachite Green	610	0.995	0.623	-0.206
Methylene Blue	648	0.987	0.766	-0.116
Methyl Red	520	0.995	0.385	-0.415
Janus Green B	640	0.995	0.394	-0.405
Quinaldine Red	470	0.999	0.344	-0.463
Gentian Violet	580	0.999	0.990	-0.004
Pseudocyanine	516	0.996	0.037	-1.432
Merocyanine 540	540	0.999	0.016	-1.796

[a]Slope of $F(R'_\infty)$ plotted against g at λ_{max}.

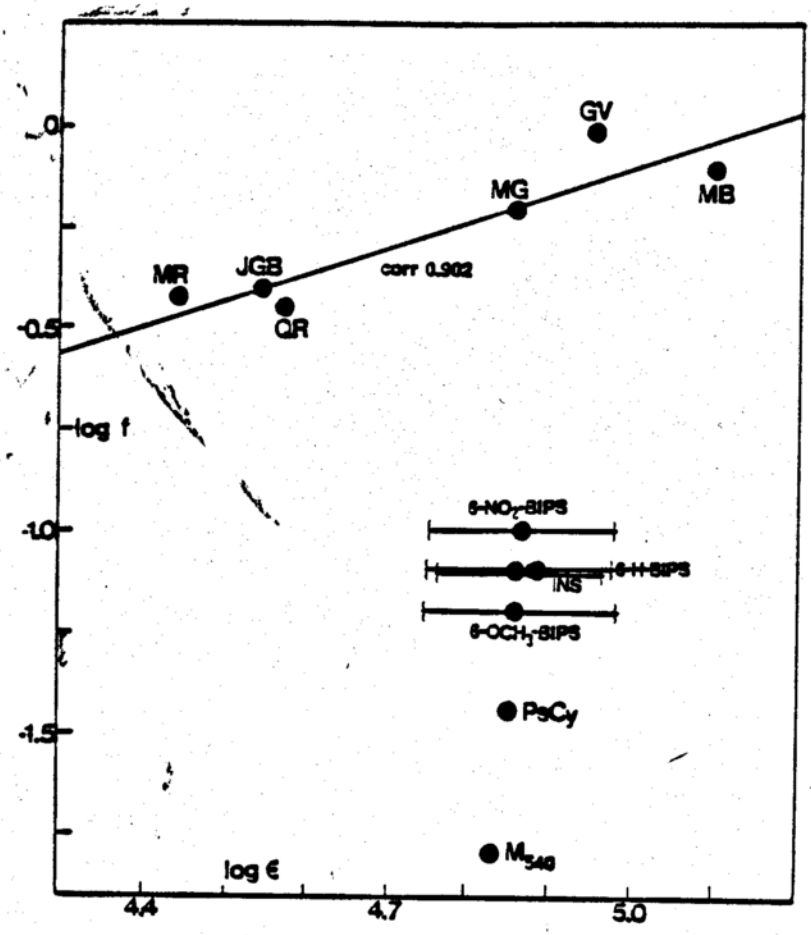

Figure 100. Spectral data for the absorption of dyes adsorbed to silica gel $500m^2/g$ plotted against the spectral data in aqueous solutions of the dye. Spiropyrans are water insoluble; their abscissa values are based upon literature absorptivity estimates.

by the brackets. Figure 101 depicts the same data set with f plotted directly versus $g_{0.5}$, the surface coverage required to produce a mid-range reflectance response of 0.5. The two axes are not independent; but are related by equation (18):

$$f = 0.25/g_{0.5} \qquad (18)$$

This relation is obtained by setting f equal to $\Delta y/\Delta x$ on a plot of $F(R'_\infty)$ versus g (this assumes an intercept of 0), and substituting 0.5 for R'_∞. The advantage of this plot is that ε need not be estimated for the spiropyrans. Any deviation the points show from the theoretical curve are due to nonzero intercepts in the $F(R'_\infty)$ versus g plots. Both Figure 100 and Figure 101 draw essentially the same conclusion: the six permanent cationic dyes form one family, whereas the two cyanine dyes plus the spiropyrans form a second family. This shows the merocyanine-like character of the open form of a spiropyran, which is predicted in the literature. Second, it shows that permanent cationic dyes follow a log-log linear relation between their surface absorptivity, represented by f, and their aqueous solution absorptivity (ε):

$$\log f = m \log \varepsilon + b \qquad (19)$$

The correlation coefficient for these "upper curve dyes" is 0.902; this means that these dyes have solution absorptivities that are predictive of their ability to color the silica surface. All of the dyes in this group contain one or more dialkylanilino groups

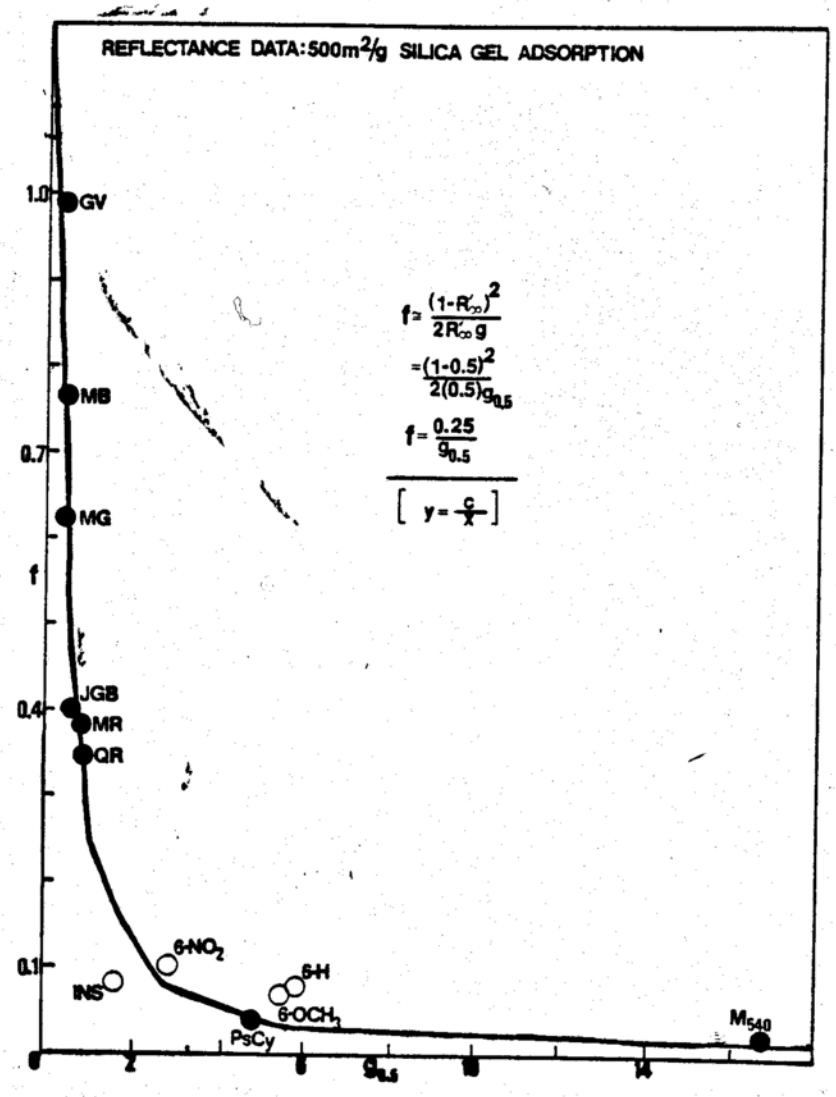

Figure 101. Reflectance analysis parameter (f) plotted versus surface coverage required to produce a 0.5 reflectance response for silica gel adsorption.

(Ar-NR_2), which are involved in electron delocalization in the colored forms of the dyes. The second group of compounds, comprised of cyanine dyes and spiropyrans, forms a distinct set whose f values are lower than might be predicted based upon their ε values. In other words, based on their ability to color a solution, one would expect them to produce more coloration on a silica surface. None of the compounds in the second group possesses a dialkylanilino group; the structures of all of the compounds in Figure 100 are given in Figures 7-9. The second group of compounds may form a separate, nearly vertical line, though it is difficult to tell since the abscissa values of the spiropyrans are only given by a possible range. Certainly, they do not fall in the same group as the cationic dyes; their ability to absorb light in the adsorbed state is markedly reduced. Both a one-state model and a two-state model can be advanced in an attempt to explain this difference.

The one-state model proposes that there is only one type of adsorbed compound for "lower curve dyes," and this adsorbed state has a reduced ability to absorb visible light. Cyanine dyes are known to aggregate extensively in the adsorbed state (see pages 33-36), and the resultant dye-dye interactions may result in aggregates that absorb light to a lesser extent than the same number of unaggregated dye molecules. Planar, open, colored spiropyrans may aggregate on the surface at higher coverages to a state that has a lessened ability to absorb visible light. This would make it difficult to explain the constant value region of $F(R'_\infty)$ vs g

graphs, unless the decreasing absorptivity exactly cancelled the increasing number of molecules as coverage increased in every case. Also, the slopes (f) used in Figure 100 are all obtained in the low coverage linear regions of the $F(R'_\infty)$ vs g plots, where aggregation is less likely.

The two-state model proposes an equilibrium between an adsorbed species of "normal" absorptivity and one of reduced or zero absorptivity. In the case of the spiropyrans, this means that some of the molecules are "hidden" in the colorless form, and the rest are in the open, colored form. This corresponds to the existence of the K' equilibrium constant in the equilibrium model derived in Appendix D. In this case, the deviation from the upper line represents the amount of spiropyran in the colorless form. The explanation for cyanine dyes may be similar; it is well-documented that merocyanine dyes can form closed spiropyran-like colorless forms in solution at low temperatures (30, 32). A third possibility is that cyanines deviate because of the one-state model interpretation and that spiropyrans deviate because of the two-state model interpretation. Besides the literature evidence for colored and colorless adsorbed spiropyrans (pages 32-33), the transmission and reflectance spectra both saturate at coverages much lower than the adsorption isotherms. The plot of log f vs log ϵ also suggests that not all of the adsorbed spiropyran is colored. One additional piece of evidence is the thermal and photochromic dependence of the reflectance spectra. The phenomenon of photobleaching indicates

that there is a variable fraction of colored spiropyran on the surface, as suggested in the equilibrium model. Apparently color-stable silica/spiropyran powders lighten gradually under visible light at low coverages (where the molecules are free to equilibrate) more readily than at high coverages (where nearest neighbors may prevent conformational changes). Furthermore, additional colored material seems to form in a drying oven. Neither of these changes is an all or none phenomenon; intermediate ratios seem to be possible. A gradual change in K' may account for some of the negative curvature in $F(R'_\infty)$ vs g plots, as the percent colored decreases with surface coverage. Analogous plots for permanent dyes suggest that this cannot account for all of the curvature; nonidealities at higher coverages are seen for compounds with no such equilibria.

If we assume that the two-state model is the correct interpretation, the log f vs log ε plot can be used to estimate the fraction of spiropyran in the colored form at low surface coverages. The upper curve dyes follow equation (20):

$$\log f = (0.646) \log \varepsilon - 3.33 \qquad (20)$$

Substituting literature estimates of ε gives us predicted values for f. The experimental f divided by the predicted f yields the equivalent fraction of colored spiropyran required to produce the experimental reflectance response based on the solution absorptivity coloration ability. Table L gives the λ_{max} of analysis for low

Table L. Estimates of Fraction Colored Spiropyran at Low Coverage.

Spiropyran[a]	λ/nm	% $L^{\pm}$	% L^{o}	K'
INS	550	12.0	88.0	0.14
6-NO_2-BIPS	472	16.8	83.2	0.20
6-H-BIPS	436	13.3	86.7	0.15
6-OCH_3-BIPS	456	10.6	89.4	0.12

[a]Adsorbed on silica gel 500 m^2/g.

coverages, the percent of spiropyran in the colorless (L^o) and colored ($L^{\pm}$) forms, and the resultant value of K' at low coverages for all four spiropyrans on silica gel 500 m^2/g. The colored species accounts for 10-20% of the adsorbed spiropyran by this treatment, an amount consistent with that expected for a polar environment. K' varies from 0.1 to 0.2, and now is interpreted as being a true constant only in the low coverage linear region. The fraction colored at higher coverage decreases, though the amount colored still increases. K' gradually decreases, as the higher coverage adsorption consists mainly of colorless spiropyran. The fraction colored, and hence K', is then a function of g, the surface coverage.

The fraction of colored spiropyran at the capacity, g_{max}, can be estimated by comparing the experimental $F(R'_\infty)$ at g_{max} with the extrapolated value of $F(R'_\infty)$ at g_{max} from the linear portion. Let A = the experimental $F(R'_\infty)$ at g_{max} and B = the extrapolated value of $F(R'_\infty)$ at g_{max} if the plot were linear up to g_{max}. For 6-NO_2-BIPS on silica gel 500 m^2/g, g_{max} = 1750, f = 0.101, and A = 7.36. This yields A/B = 7.36/176.75 = 0.0416. But this represents the decrease from the initial colored fraction, not from 100% colored fraction. Thus, the % $L^{\pm}$ at coverages exceeding the linear limit is given by equation (21):

$$\% L^{\pm} = (\% L^{\pm} \text{ at low coverage})\ (A/B) \qquad (21)$$

For 6-NO_2-BIPS on silica gel 500 m^2/g, this becomes:

$$\% L^{\pm} = 16.8\ (.0416) = 0.7\% \text{ at } g_{max} \qquad (22)$$

From Figure 97 or similar plots, the $\% L^{\pm}$ or K' can be calculated at any coverage by reading A off the plot and calculating B. For the 6-NO_2-BIPS/silica gel system, $\% L^{\pm}$ decreases to half of its original (low coverage) value by g = 125, where $F(R'_{\infty})$ = 6.2, A/B = 0.491, and $\% L^{\pm}$ = 8.3.

An examination of the f values of spiropyrans on various adsorbents (Table XLVIII) reveals that the data contain many internal consistencies. Plotting f for 6-NO_2-BIPS versus f for INS at either wavelength results in the straight lines in Figure 102. The f values fall along the lines in roughly the same order and spacing as a function of the adsorbent. The values for talc, TiO_2, and Avicel are all much lower, and would bunch near the origin on this plot. Essentially, these correlations are depicting the fact that both 6-NO_2-BIPS and INS give the same results for these solids. Those adsorbents which produce the higher f values (hence, greater percentage of $L^{\pm}$) for 6-NO_2-BIPS do so for INS. From the solvatochromic experiments, this implies that these solids are providing environments of different polarity for the spiropyran equilibria. That is, the spectral behavior is characteristic of the adsorbent. The more polar the interface, the more stable the open colored forms of the spiropyrans are in the adsorbed state.

The points for silicic acid do not fall on this correlation. INS yields higher than predicted f values based on those of

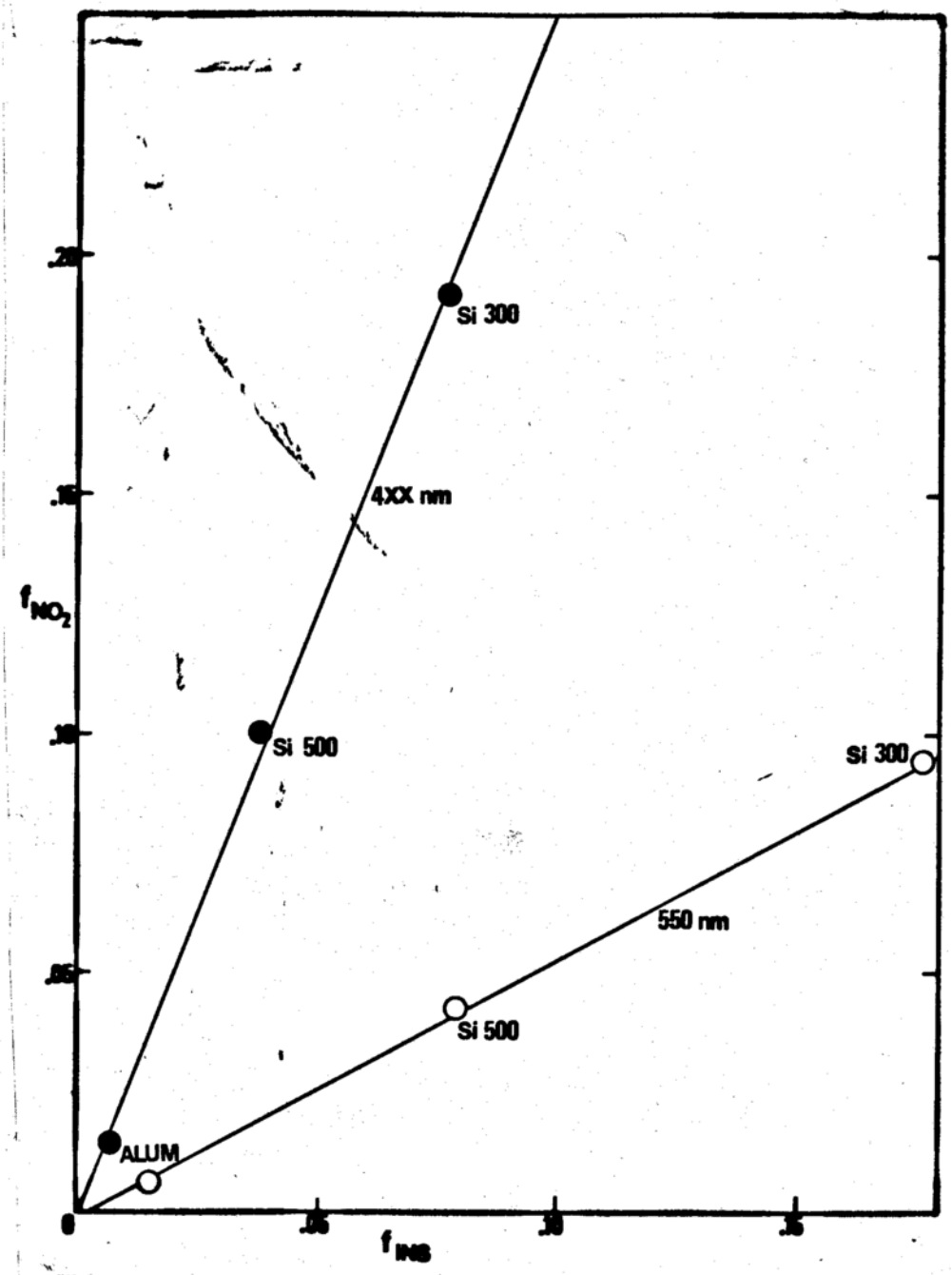

Figure 102. Reflectance parameters at low coverage for 6-NO_2-BIPS plotted versus INS.

6-NO_2-BIPS. The adsorption isotherm data also show an unexpectedly high value of K for the INS/silicic acid system. Furthermore, the $F(R'_\infty)$ vs g plot for this system saturates extremely early (g = 6-8) at 472 nm, but is otherwise normal at 550 nm. Table LI gives the ratios of f for 6-NO_2-BIPS to f for INS at both wavelengths on the four high surface area adsorbents. Note that at 550 nm the ratios are reasonably close, but at 472 nm the silicic acid ratio is very low. It appears that there may be a strong interaction between INS and silicic acid that produces a high binding constant and strong spectral components at 472 nm.

6-H-BIPS and 6-OCH_3-BIPS also gave f values that were consistent for the high surface area solids. Table LII expresses the f values for all four spiropyrans normalized to f = 1.00 for silica gel 500 m^2/g. The f ratios alumina:silica gel 500 m^2/g: silica gel 300 m^2/g show that the f values are in the same rank order and roughly the same proportion for all four spiropyrans on all three adsorbents. Some property of these solids produces f values for any spiropyran in this proportion. Since f values depend upon the fraction of $L^{\pm}$, known to be polarity-dependent, these ratios may reflect polarity differences in these adsorbent surfaces.

The data for the low surface area adsorbents (talc, TiO_2, and Avicel microcrystalline cellulose) show some similarities to the high surface area adsorbents; for instance, the ratios $f_{6\text{-}NO_2}/f_{INS}$ are 2-3 at the shorter wavelength and 0-2 at the 550 nm peak. However, the f values are so low (10^{-4}-10^{-5}) that they cannot be

Table LI. Comparison of 6-NO_2-BIPS and INS f Values.

Adsorbent	$f_{6\text{-}NO_2}/f_{INS}$, 472 nm	$f_{6\text{-}NO_2}/f_{INS}$, 550 nm
silica gel 500 m^2/g	2.66	0.53
silica gel 300 m^2/g	2.51	0.53
alumina	2.16	0.33
silicic acid	0.67	0.49

Table LII. Normalized f Values for Spiropyrans on Various Adsorbents.

	Alumina f:Silica Gel 500 m^2/g f:Silica Gel 300 m^2/g f	
Spiropyran	4xx nm peak	550 nm peak
6-H-BIPS	0.10 : 1.00 : 1.43	0.63 : 1.00 : 2.33
6-OCH_3-BIPS	0.22 : 1:00 : 1.70	0.77 : 1.00 : 2.41
6-NO_2-BIPS	0.16 : 1.00 : 1.91	0.12 : 1.00 : 2.23
INS	0.19 : 1.00 : 2.08	0.19 : 1.00 : 2.16

placed on the same plot (Figure 102) as the high surface area adsorbents. A plot of log f (INS) versus log f (6-NO_2) enables the points to be visualized on the same graph. Figure 102 goes through the origin; therefore it follows equation (21):

$$f\ (INS) = m\ f\ (6\text{-}NO_2) \qquad (21)$$

where m is the slope. A log-log plot should follow equation (22):

$$\log f\ (INS) = \log m + n \log f\ (6\text{-}NO_2) \qquad (22)$$

where log m is the y intercept (which arises from the slope of the linear plot) and n should equal 1.0 (the power of f(6-NO_2) in equation (21)). Figure 103 shows the log-log plot for the peak between 400 and 500 nm (the "4xx peak"). The correlation is good, and the slope is near 1.0. Silicic acid is not included in the correlation because of its unusually high f value at 472 nm. Inclusion of the silicic acid point weakens the correlation (r = 0.987) but leaves the slope near its expected value (n = 1.018). This plot shows that all of the points, including adsorbents of low surface area, belong to the same family. The same plot using f values at 550 nm reflects the same behavior, but shows more scatter. The silicic acid point fits well, since its f value at 550 nm was normal; and the slope is approximately 1.0.

In spite of the fact that g values are corrected for surface area, the data appear to be biased for surface area. This is because $F(R'_\infty)$ is a function of k/s, not just k, and the scattering

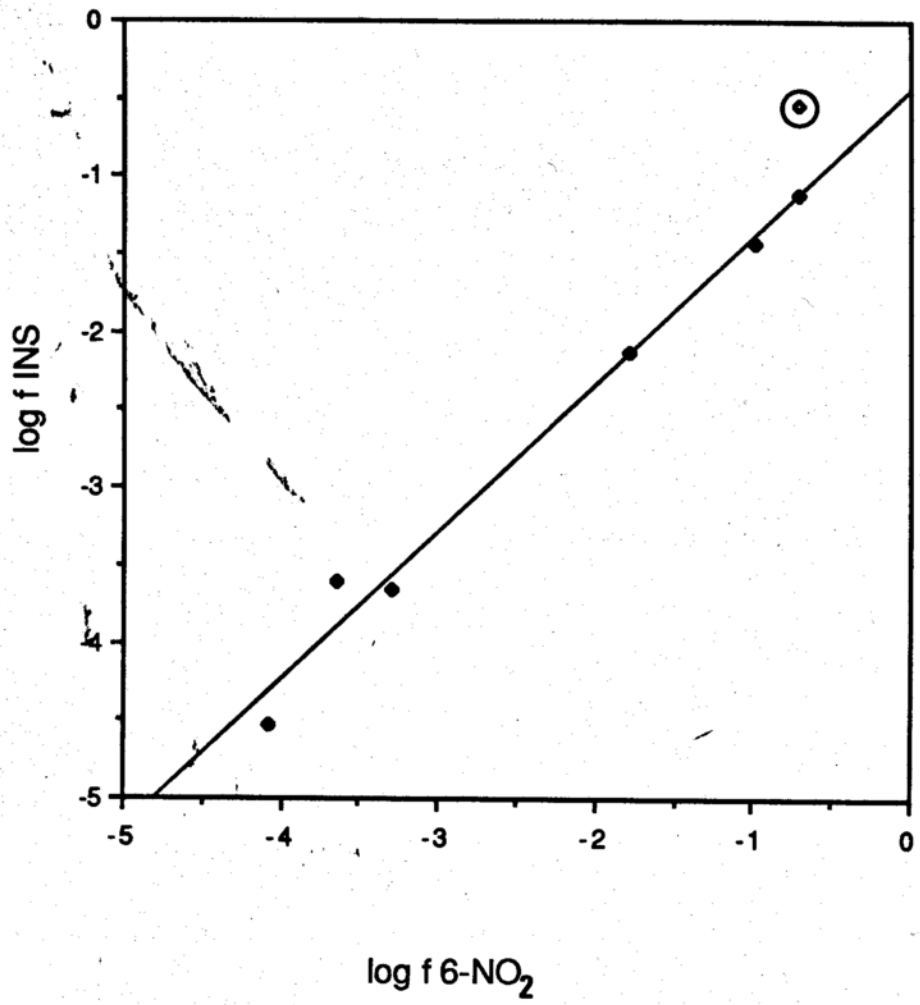

Figure 103. Reflectance parameter consistency at λmax nm peak for seven adsorbents. The circled point (silicic acid) is not included in the correlation. r = 0.993, slope = 0.952, y intercept = -0.4348.

coefficient s varies with particle size, geometry, and packing differences. Equation (2) shows that a plot of $F(R'_\infty)$ versus concentration yields a slope of ε/s. Coarser powders, other factors being equal, appear darker. This may explain why silica gel 300 m^2/g (50 micron particles) give larger f values than silica gel 500 m^2/g (10 micron particles). Avicel microcrystalline cellulose, however, also has an average particle diameter of 50 microns. The value of f is much lower, because k/s is much lower. The scattering coefficient may be roughly the same, since it depends on the number of scattering centers (adsorbent). The absorption coefficient (k) depends on the number of colored adsorbate molecules present, which increases with the surface area of adsorbent for a given powder volume.

The use of a reference substance that does not change its absorptivity with microenvironmental changes could place all of the adsorbents on an equal basis. Malachite green shows an increased f value on the larger particle size silica gel, as did the spiropyrans. It gave an f value at λ_{max} of 0.829, which is 1.31 times the value on the smaller particle size silica gel. Methylene blue produced an f ratio of 1.12, again with the higher value for the coarser adsorbent. Methylene blue f values were also determined on TiO_2 and talc. Table LIII shows the data for methylene blue/talc at λ_{max} (653 nm), and Figure 104 shows the plot of $F(R'_\infty)$ vs. g. The f value for methylene blue on silica gel 500 m^2/g is 232 times the value on talc. The f value on TiO_2 is only 1/360 times that

Table LIII. Single-Wavelength Reflectance Analysis Data for Methylene Blue/Talc.

g/(nanomoles/m^2)	R'_∞ (653 nm)	$F(R'_\infty)^a$
4.0	0.877	0.009
10.1	0.748	0.042
20.2	0.660	0.088
30.2	0.579	0.153
40.4	0.558	0.175
60.9	0.533	0.205
101.0	0.435	0.367
121.9	0.406	0.435
161.5	0.368	0.543

[a]At 653 nm = λ_{max}.

$F(R'_\infty)$ vs. g

correlation coefficient = 0.995

slope = f = 0.00331

y intercept = 0.0205

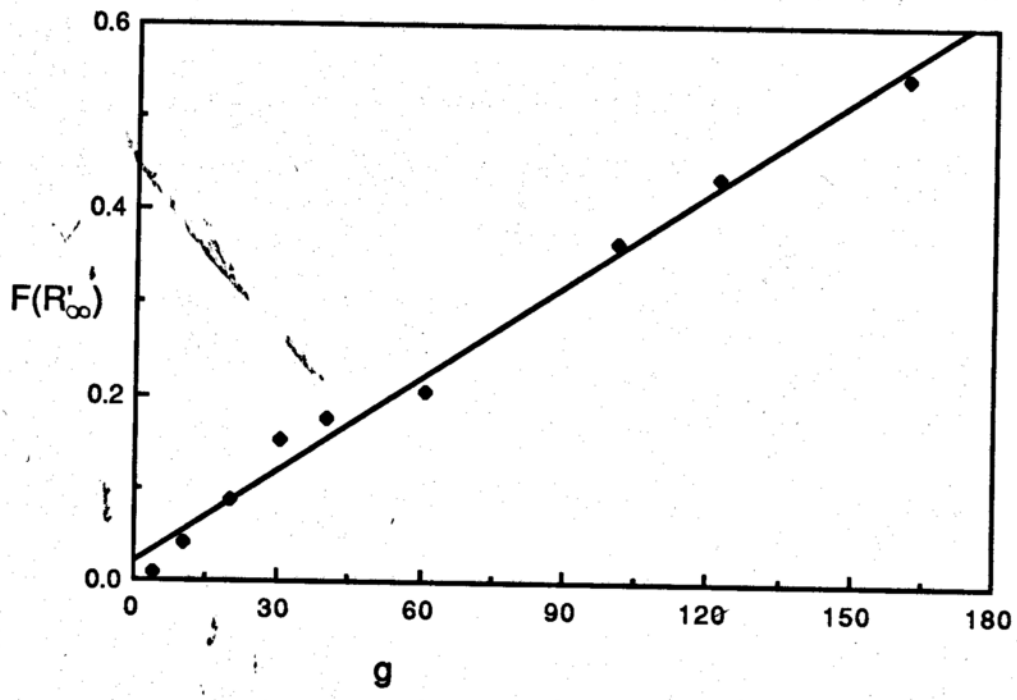

Figure 104. Fixed Wavelength Reflectance Analysis for Methylene Blue on Talc at 653 nm.

of silica gel 500 m^2/g. This means that methylene blue as a reference substance accounts for much of the difference in f values between high and low surface area adsorbents. In most cases, this does not account for the entire difference; part of the difference may still be due to a change in the absorption coefficient of spiropyrans as a function of the surface environment. Table LIV gives f ratios for 6-NO_2-BIPS and INS on talc and silica gel, and compares these to the ratios for permanent dyes. For both spiropyrans, the ratios for silica gel of different surface areas are quite consistent at either absorption peak. They exceed the ratios of either malachite green or methylene blue; hence, optical effects alone do not account for the increased coloration seen for spiropyrans on the coarser silica gel. The larger ratio for methylene blue between silica gel 500 m^2/g and talc indicates a greater optical difference between these two adsorbents. This is comparable to the ratios shown for spiropyrans at 472 nm, but at 550 nm the ratios are much higher. This means that the absorption at 550 nm is lessened on talc to a degree that cannot be explained by scattering effects alone.

If the optical effects (including scattering, geometry, particle size, and packing differences) can be corrected for, either through independent measurement or the use of a reference substance, the remaining portion of the f value can be related to k. This is the absorption coefficient as measured by reflectance, and is related to solution molar absorptivity (74). Since the

Table LIV. Reflectance f Value Ratios at λ_{max}.

A. Silica Gel 300 m^2/g / Silica Gel 500 m^2/g Ratios

Malachite Green = 1.31

Methylene Blue = 1.12

Spiropyran	472 nm	550 nm
INS	2.03	2.24
6-NO_2-BIPS	1.91	2.24

B. Silica Gel 500 m^2/g / Talc Ratios

Methylene Blue = 232

Spiropyran	472 nm	550 nm
INS	170	530
6-NO_2-BIPS	205	1002

absorptivities of spiropyrans are polarity-dependent, this should give a relative measure of solid surface polarities. Such measures are difficult to achieve (65), and a reliable method would be very useful. If solid surfaces can be shown to affect K', and hence the ability of spiropyrans to absorb visible light on a solid surface, this technique would provide such a method. Wet chemical techniques as a means of studying surface properties have been reviewed by Fowkes (65). Mishima et al. (68) and Nechiporenko et al. (69) have used adsorbed indicators to estimate solid surface acidity. Mukerjee et al. (47, 124, 125) have studied the use of nitroxides as indicators of microenvironment hydrophilicity. Ståhlberg et al. (67) used fluorescent pyrenes to estimate the polarity of modified silicas. Lindley et al. (66) modified the Kamlet-Taft solvent polarity method to analyze silica surfaces with nitroanisole and nitrobenzene absorption frequencies. Hamilton (126), Bagnall et al. (127), and Zografi et al. (128, 129) have used contact angle measurements to quantify surface energies. Numerous papers are available in which chromatographic techniques are used to estimate solid surface polarities (130, 131). The problem with a number of these methods is that they are not as general as solvent polarity measurements, often being restricted to compounds in a narrow range of polarity. Many are only qualitative, yielding a rank order of surface polarities. Additional techniques are needed which can analyze a wide range of solid surfaces. The lack of reference solids makes comparisons of the results between the various methods

not feasible at this time. There are hundreds of known spiropyrans, and suitable compounds might be found in this reservoir to analyze a number of properties of solid surfaces for a wide range of values.

F. Future Work

The results thus far suggest a number of paths that could be followed in continuing the work. The spectral studies show that the solid surface properties do affect the spectrum of an adsorbed spiropyran. Besides the solids described, several others had the necessary surface area and hydrophilicity to adsorb significant amounts of 6-NO_2-BIPS or INS, but they were not studied due to equipment and time limitations. These solids included zinc oxide, soluble starch, lactose, magnesium sulfate, Bentonite, and Veegum.

Other spiropyrans might be found that adsorb to less polar adsorbents; presently only hydrophilic adsorbents can be studied. Other properties of the surface may have significant effects on the reflectance spectra of adsorbed spiropyrans. Acidity is important in solution; it may be as important on the surface. Aluminas are commercially available in basic, neutral, and acidic forms. These could form a reference set from which the acidity of other surfaces might be assessed. It would be interesting to make a plot of log f vs log ϵ on alumina instead of silica gel for permanent and cyanine dyes.

The role of a number of variables in this work needs further research. The effect of relative humidity on the water content

and adsorption properties of the adsorbents was controlled primarily through drying to constant weight at 110°C. This does not necessarily mean that each "dried" adsorbent contained no remaining water or the same remaining H_2O content. This may account for some of the differences in binding constants and capacities. Photobleaching of the adsorbate/adsorbent powders was a variable factor. The rate and extent of photobleaching could be studied by diffuse reflectance spectroscopy as a function of light intensity, wavelength, temperature, and spiropyran. Since it was observed that only the lightest colored powders (those of low coverage) exhibited photobleaching, measurements of the maximum extent of photobleaching might indicate the surface coverage of isolated (unaggregated) spiropyrans.

The scattering coefficient is presently the least well-defined variable in the project. The use of the dilution method ensures that the scattering coefficients of the colored adsorbents are given by those of the white diluent adsorbent. These can be measured by scanning the reflectance of a thin layer of adsorbent against a black background, yielding R_o. Kortüm's book (74) gives an equation for calculating s as a function of R_∞ and R_o. When s is factored out of the Kubelka-Munk equation, the absorption coefficient (k) can be calculated. This would be a more direct measure of the amount of colored adsorbed spiropyran than is f. The polarity of the surface would then be the only factor governing the extent of transformation to the colored form.

G. Conclusions

1. 6-NO_2-BIPS shows hypsochromic solvatochromic shifts with an increase in solvent polarity; INS shows bathochromic shifts and also has a stationary visible peak.
2. The solvatochromic correlation with Kosower's Z values of empirical solvent polarity indicates that 6-NO_2-BIPS experiences an environment similar to that of 70% EtOH/H_2O when adsorbed to the silica surface.
3. Spiropyrans show Langmuirian adsorption from nonpolar solvents to hydrophilic adsorbents. The binding constants and capacities constitute one family when compared to the adsorption of malachite green, with weaker binding but higher capacities. Secondary effects group the data into subsets determined by the spiropyran adsorbate.
4. An equilibrium model demonstrates that the pre- and post-adsorptive equilibria between colorless and colored spiropyran affect the magnitude of the observed binding constant.
5. The adsorption colors of spiropyrans are a function of spiropyran identity, adsorbent identity, extent of surface coverage, and the relative absorptivities at a short wavelength visible peak (430-470 nm) and a longer wavelength visible peak (550 nm).
6. Spiropyrans and cyanine dyes have a reduced ability to color a

silica surface when compared to permanent cationic dyes, based on a comparison of their solution absorptivities. A two-state model assuming spiropyrans have a surface colored/colorless equilibrium adequately accounts for the observed effects.

7. Plots of $F(R'_\infty)$ vs surface coverage in nanomoles/m^2 (g) are linear at low coverage, then exhibit negative curvature and level off at a final plateau value. This may reflect a decrease in the fraction of colored spiropyran as well as nonidealities associated with the crowded surface at high coverages.

8. The initial slopes, f, of the $F(R'_\infty)$ vs g plots show consistencies between 6-NO_2-BIPS and INS, and are a function of the identity of the solid surface. Correction for scattering effects could yield estimates of the fraction of colored adsorbate, which is expected to be dependent on the polarity of the environment.

VI. REFERENCES

1. G. H. Brown, "Photochromism," Wiley-Interscience, Techniques of Chemistry, Volume III, New York, 1971.
2. A. Mustafa, Chem. Rev., 43, 509-523 (1948).
3. G. H. Brown, W. G. Shaw, Rev. Pure Appl. Chem., 11, 2-32 (1961).
4. C. A. Heller, D. A. Fine, R. A. Henry, J. Phys. Chem., 65, 1908-9 (1961).
5. J. H. Day, Chem. Rev., 63, 65-80 (1963).
6. R. Heiligman-Rim., Y. Hirshberg, E. Fischer, J. Chem. Soc., 1961, 156-63 (1961).
7. T. Bercovici, R. Heiligman-Rim, E. Fisher, Mol. Photochem., 1, 23-55 (1969).
8. J. B. Flannery, Jr., J. Am. Chem. Soc., 90, 5660-71 (1968).
9. C. Balny, P. Douzou, T. Bercovici, E. Fischer, Mol. Photochem., 1, 225-233 (1969).
10. C. F. Koelsch, W. R. Workman, J. Am. Chem. Soc., 74, 6288-9 (1952).
11. E. Berman, R. E. Fox, F. D. Thomson, J. Am. Chem. Soc., 81, 5605-8 (1959).
12. L. S. Atabekyan, A. K. Chibisov, J. Photochem., 31, 123-30 (1985).
13. R. N. Maćnair, Photochem. and Photobiol., 6, 779-797 (1967).
14. H. Bach, J. G. Calvert, J. Am. Chem. Soc., 92, 2608-2614 (1970).

15. J. Przystal, T. Rudolph, J. P. Phillips, Anal. Chim. Acta., 41, 391-4 (1968).

16. Y. Hirshberg, E. Fischer, J. Am. Chem. Soc., 1954, 3129-3137 (1954).

17. D. Lapienis-Grochowska, M. Kryszewski, B. Nadolski, J. Chem. Soc., Faraday Trans. II, 1979, 312-316 (1979).

18. J. Arnaud, J. Chim. Phys., 66, 159 (1969).

19. J. G. Calvert, J. N. Pitts, Jr., "Photochemistry," Wiley-Interscience, New York, 1966, p. 487.

20. R. C. Bertelson, J. Org. Chem., 30, 2875 (1965).

21. R. Guglielmetti, E. J. Vincent, J. Metzger, Bull. Soc. Chim. Fr., 4195 (1967).

22. K. Venkataram, "The Chemistry of Synthetic Dyes," Academic Press, New York, 1952, p. 1143-1186.

23. E. Abrahart, "Dyes and their Intermediates," Pergamon Press, New York, 1968.

24. M. C. Etter, B. N. Holmes, R. B. Kress, G. Filipovich, Isr. J. Chem., 25, 264-273 (1985).

25. W. T. Simpson, J. Chem. Phys., 16, 1124-36 (1948).

26. L. G. S. Brooker, G. H. Keyes, R. H. Sprague, R. H. Van Dyke, E. Van Lare, G. Van Zandt, F. L. White, J. Am. Chem. Soc., 73, 5326-32 (1951).

27. L. G. S. Brooker, G. H. Keyes, D. W. Heseltine, J. Am. Chem. Soc., 73, 5350-56 (1951).

28. L. G. S. Brooker, G. H. Keyes, R. H. Sprague, R. H. Van Dyke,

E. Van Lare, G. Van Zandt, F. L. White, H. W. J. Cressman, S. G. Dent, Jr., J. Am. Chem. Soc., 73, 5332-50 (1951).

29. L. G. S. Brooker, A. C. Craig, D. W. Heseltine, P. W. Jenkins, L. L. Lincoln, J. Am. Chem. Soc., 87, 2443-50 (1965).

30. Y. Hirshberg, E. Fischer, J. Chem. Phys., 22, 572-3 (1954).

31. I. Cabrera, F. Shvartsman, O. Veinberg, V. Kronganz, Science, 226, 341-3 (1984).

32. Y. Kalisky, T. E. Orlowski, D. J. Williams, J. Phys. Chem., 87, 5333-38 (1983).

33. G. R. Meredith, D. J. Williams, S. N. Fishman, E. S. Goldburt, V. A. Kronganz, J. Phys. Chem., 87, 1697 (1983).

34. E. E. Jelley, Nature, 139, 1009-10 (1936).

35. A. H. Herz, E. P. Danner, G. A. Janusonis, "Adsorption from Aqueous Solution," American Chemical Society, 1968, p. 173-197.

36. Y. Hirshberg, J. Am. Chem. Soc., 78, 2304-12 (1956).

37. E. Weitz, F. Schmidt, J. Singer, Z. Elektrochem., 46, 222-7 (1940).

38. L. D. Taylor, J. Nicholson, R. B. Davis, Tetra. Lett., 17, 1585-88 (1967).

39. J. P. Phillips, A. Mueller, F. Przystal, J. Am. Chem. Soc., 87, 4020 (1965).

40. J. Arnaud, C. Wippler, F. Beaure D'Augeres, J. Chim. Phys., 64, 1165 (1967).

41. J. C. Metras, M. Mosse', C. Wippler, J. Chim. Phys., 62, 659 (1965).

42. P. H. Vandewijer, G. Smets, J. Polym. Sci. Part C, 22, 231 (1968).

43. S. Brownstein, Can. J. Chem., 38, 1590-6 (1960).

44. E. M. Kosower, J. Am. Chem. Soc., 80, 3253-60 (1958).

45. R. Gautron, Bull. Soc. Chim. Fr., 3190-8 (1968).

46. P. Fruit, R. Gautron, C. Audic, Bull. Soc. Chim. Fr., 2237-43 (1968).

47. P. Mukerjee, J. Phys. Chem., 86, 3189-94 (1982).

48. P. Suppan, J. Chem. Soc. (A), 3125 (1968).

49. K. Namba, S. Suzuki, Bull. Chem. Soc. Jap., 48, 1323-4 (1975).

50. J. J. Van Voorhis, J. V. Cartmell, P. Y. Hsieh, J. Colloid Interface Sci., 33, 8 (1970).

51. A. Schönberg, A. Mustafa, W. Asker, J. Am. Chem. Soc., 74, 5640-3 (1952).

52. A. Schönberg, W. Asker, Science, 113, 56-57 (1951).

53. T. R. Evans, A. F. Toth, P. A. Leermakers, J. Am. Chem. Soc., 89, 5060-1 (1967).

54. A. Schönberg, A. Mustafa, W. Asker, J. Am. Chem. Soc., 73, 2876-9 (1951).

55. L. D. Weis, T. R. Evans, P. A. Leermakers, J. Am. Chem. Soc., 90, 6109-18 (1968).

56. C. Balny, P. Douzou, C. R. Acad. Sci., Paris, 264, 477 (1967).

57. G. Kortum, G. Bayer, Z. Physik. Chem., 33, 254-63 (1962).

58. E. Weitz, Z. Elektrochem., 46, 222 (1940).

59. J. A. Leermakers, B. H. Carroll, C. J. Staud, J. Chem. Phys.,

5, 878-88 (1937).

60. E. S. Emerson, M. A. Conlin, A. E. Rosenoff, K. S. Norland, H. Rodriguez, D. Chin, G. R. Bird, J. Phys. Chem., 71, 2396-2403 (1967).

61. E. P. Davey, Trans. Faraday Soc., 36, 323-9 (1940).

62. A. H. Herz, J. O. Helling, J. Colloid Interface Sci., 22, 391-403 (1966).

63. W. West, B. H. Carroll, D. H. Whitcomb, J. Am. Chem. Soc., 56, 1054-67 (1952).

64. G. Kortüm, W. Braun, G. Herzog, Angew. Chem. Int. Ed., 2, 333-404 (1963).

65. F. F. Fowkes, "Characterization of Solid Surfaces by Wet Chemical Techniques," ACS Symposium Series 199, Industrial Applications of Surface Analysis, L. A. Casper and C. J. Powell, editors, American Chemical Society, 1982, pages 69-88.

66. S. M. Lindley, G. C. Flowers, J. E. Leffler, J. Org. Chem., 50, 607-10 (1985).

67. J. Stahlberg, M. Almgren, Anal. Chem., 57, 817-21 (1985).

68. S. Mishima, T. Nakajima, J. Chem. Soc., Faraday Trans. I., 82, 1307-19 (1986).

69. A. P. Nechiporenko, T. A. Burenina, S. I. Kol'tsov, Zh. Ob. Khim., 55, 1907-12 (1985).

70. M. Robin, K. N. Trueblood, J. Am. Chem. Soc., 79, 5138-42 (1957).

71. P. A. Leermakers, H. T. Thomas, L. D. Weis, F. C. James,

J. Am. Chem. Soc., 88, 5075-83 (1966).

72. P. deMayo, A. Safarzadeh-Amiri, S. King Wong, Can. J. Chem., 62, 1001-2 (1984).

73. W. W. Wendlandt, "Modern Aspects of Reflectance Spectroscopy," Plenum Press, New York, 1968.

74. G. Kortüm, "Reflectance Spectroscopy," Springer-Verlag, New York, 1969.

75. J. Duclos, Instrumentation Research, 105-111, March (1985).

76. D. Patterson, "The Color of Pigment Crystals," in "Pigments. An Introduction to their Physical Chemistry," Elsevier Publishing Co., New York, 1967, p. 50-65.

77. H. G. Hecht, Anal. Chem., 48, 1775-9 (1976).

78. W. E. K. Middleton, C. L. Sanders, J. Opt. Soc. Am., 41, 419-24 (1951).

79. G. Kortüm, H. Schottler, Z. Elektrochem., 57, 353 (1953).

80. G. Kortüm, G. Schreyer, Angew. Chem., 67, 694 (1955).

81. G. Kortüm, D. Oelkrug, Z. Physik. Chem., 34, 58 (1967).

82. G. Kortüm, J. Vogel, W. Braun, Angew. Chem., 70, 651-5 (1958).

83. G. Kortüm, M. Kortum-Seiler, S. D. Bailey, J. Am. Chem. Soc., 66, 2439-42 (1962).

84. G. Kortüm, J. Vogel, Chem. Ber., 93, 706-19 (1960).

85. M. M. Frodyma, R. W. Frei, D. J. Williams, J. Chromatography, 13, 61-68 (1964).

86. B. Nagel, C. Bayer, U. Iske, F. Glombitza, Am. Biotech. Lab., 4, 12-17 (1986).

87. M. E. Everhard, F. W. Goodhart, J. Pharm. Sci., 52, 281-3 (1963).

88. A. Villari, A. Tommasini, P. Ficarra, R. Ficarra, G. Valenti, G. Mondio, Annali di Chimica, 75, 235-242 (1985).

89. M. E. Everhard, D. A. Dickcius, F. W. Goodhart, J. Pharm. Sci., 53, 173-8 (1964).

90. R. K. Iler, "Colloid Chemistry of Silica and Silicates," Cornell Univ. Press, Ithaca, NY, 1955.

91. "Aerosil, Manufacture, Properties and Application," Degussa Inc. Pigments Division, Technical Bulletin, Teterboro, New Jersey, 1977.

92. M. Verzele, C. Dewaele, D. Duquet, J. Chromatography, 329, 351-7 (1985).

93. H. R. Felton, "Moisture and Silica Gel," Technical Report 7905, Analtech, 1979.

94. G. D. Parfitt, K. S. W. Sing, "Characterization of Powder Surfaces," Chapter 8 (Silicas by D. Barby), Academic Press, New York, 1976.

95. "Cab-O-Sil Properties and Functions," Cabot Corporation, Technical Bulletin, Tuscola, Illinois, 1985.

96. I. Shapiro, I. M. Kolthoff, J. Am. Chem. Soc., 72, 776-82 (1950).

97. C. Misra, "Industrial Alumina Chemicals," American Chemical Society, Washington D.C., 1986.

98. J. B. Peri, R. B. Hannan, J. Am. Chem. Soc., 64, 1526-30

(1960).

99. R. L. Barwell, Jr., J. Catalysis, 86, 301-4 (1984).

100. H. Brockman, H. Schodder, Chem. Ber., 74, 73-81 (1941).

101. G. D. Parfitt, "The Surface of Titanium Dioxide," in "Progress in Surface and Membrane Science," Volume 11, 1976, p. 181-226.

102. Technical Bulletin. Pigments. Degussa, West Germany, 1984.

103. "Remington's Pharmaceutical Sciences," 15th edition, Mack

104. D. A. Battista, "Microcrystal Polymer Science," McGraw-Hill Book Company, St. Louis, 1975.

105. A. W. Adamson, "Physical Chemistry of Surfaces," 4th edition, Wiley-Interscience, New York, 1982, p. 521-533.

106. P. C. Hiemenz, "Principles of Colloid and Surface Chemistry," Marcel Dekker, Inc., New York, 1977, p. 287-298.

107. A. T. Florence, D. Attwood, "Physicochemical Principles of Pharmacy," Chapman and Hall, New York, 1981. Chapter 6.

108. K. A. Connors, "Binding Constants: The Measurement of Molecular Complex Stability," Wiley-Interscience, New York, 1987.

109. D. H. Everett, Pure and Appl. Chem., 58, 967-984 (1986).

110. L. Alzamora, J. Colloid Interface Sci., 106, 513-16 (1985).

111. M. J. Hey, A. C. Mackie, J. R. Mitchell, J. Colloid Interface Sci., 114, 286-9 (1986).

112. J. G. Gibb, P. D. Ritschie, J. Appl. Chem., 4, 483 (1954).

113. M. M. Allingham, J. M. Cullen, C. H. Giles, S. K. Jain, J. S. Woods, J. Appl. Chem., 8, 108 (1958).

114. N. Negishi, K. Ishihara, I. Shinohara, J. Polym. Sci., Polymer Lett. Ed., 19, 593-7 (1981).

115. Analtech, Inc. Catalog and Technical Bulletin. Newark, DE, 1985.

116. Aerosil Technical Bulletin. Degussa, Inc. Teterboro, NJ, 1977.

117. S. Brunauer, P. H. Emmett, E. Teller, J. Am. Chem. Soc., 60, 309 (1935).

118. G. Busca, H. Saussey, O. Saur, J. C. LaValley, V. Lorenzelli, Appl. Catalysis, 14, 245-260 (1985).

119. R. S. McDonald, J. Am. Chem. Soc., 79, 850-4 (1957).

120. "Handbook of Chemistry and Physics," CRC Press, 63rd edition, Boca Raton, Florida, 1982-83.

121. R. G. Duggleby, Anal. Biochem., 110, 9-18 (1981).

122. K. A. Connors, "A Textbook of Pharmaceutical Analysis," Third Edition, Wiley-Interscience, New York, 1982.

123. A. L. McClellan, H. F. Harnsberger, J. Coll. Interface Sci., 23, 577-79 (1967).

124. C. Ramachandran, R. A. Pyter, P. Mukerjee, J. Phys. Chem., 86, 3198-3205 (1982).

125. R. A. Pyter, C. Ramachandran, P. Mukerjee, J. Phys. Chem., 86, 3206-3210 (1982).

126. W. C. Hamilton, J. Coll. Interface Sci., 40, 219-222 (1972).

127. R. D. Bagnall, G. F. Green, J. Coll. Interface Sci., 68, 387-8 (1979).

128. G. Zografi, S. S. Tam, J. Pharm. Sci., 65, 1145-49 (1976).

129. B. A. Johnson, G. Zografi, J. Pharm. Sci., 75, 529-33 (1986).

130. D. S. Mathur, N. C. Saha, J. Chromatography, 138, 33-9 (1977).

131. S. P. Boudreau, W. T. Cooper, Anal. Chem., 59, 353-8 (1987).

APPENDIX A

Sample Calculations for the BET Method

Experimental data from surface area determinations consists of area-under-the-curve averages at three nitrogen contents, and an associated calibration at each nitrogen content. The data for Talc USP are tabulated below.

% N_2	AUC (avg.)	Calibration volume/ml	Calibration AUC (avg.)
10	426.3	1.25	419.0
20	492.7	1.50	512.5
30	545.7	1.625	532.7

The flow rates at each fraction N_2 are determined by the following equation:

$$\text{flow rate} = \frac{(\text{fraction } N_2)(\text{vapor pressure in mm Hg})}{(\text{ambient pressure})} \times (\text{total flow})$$

For 10% N_2, when the ambient pressure is measured at 742.5 mm Hg, and a total flow rate of 20 psi is desired, this becomes:

$$\text{flow rate}_{N_2} = \frac{0.1\ (771)}{(742.5)} \times 20 = 2.08 \text{ psi}$$

The flow rate for the inert gas, H_2, is simply the total flow rate minus the nitrogen flow rate, or 20 - 2.08 = 17.92 psi. Similar calculations are used at 20% and at 30% N_2. A constant (W) is then calculated from the tabulated data as follows:

$$W = \left(\frac{\text{AUC}}{\text{calib. AUC}}\right)\left(\frac{\text{calibration}}{\text{volume}}\right)\left(\frac{\text{ambient pressure}}{760}\right)\left(\frac{14.01}{RT}\right)$$

where 760 mm Hg is atmospheric pressure, 14.01 is the formula weight of N_2, T is expressed in ^{o}K, and R is the gas constant (82.1 ml·atm/^{o}K·mole). Another constant, y, is calculated to become the ordinate for the ensuing three point plot.

$$y = \frac{1}{W(P_o/P-1)}$$

W is taken from the calculation above, P_o = 1 atm, P = 0.1, 0.2, or 0.3 atm, respectively, and the resultant values for our sample data are:

N_2	W	y	$(P_o/P-1)$
0.1	7.1151×10^{-4}	156.16	9
0.2	8.0677×10^{-4}	309.88	4
0.3	9.3131×10^{-4}	460.19	2.33

Plotting y versus partial pressure of N_2 yields a straight line, with the following parameters:

slope = 1520.15

y intercept = 4.71333

correlation coefficient = 0.999979

The value x_m, the weight adsorbed at monolayer coverage, is calculated by:

$$x_m = \frac{1}{\text{slope} + \text{y intercept}} = 6.55796 \times 10^{-4}$$

The total surface area of the sample can then be obtained via:

$$S_t = \frac{x_m\ (N_{av})(16.2 \times 10^{-20})}{14.01} = m^2 \text{ of surface area.}$$

where N_{av} is Avogadro's number, the constant in the numerator is the area one nitrogen molecule occupies on the surface, and the denominator is the adsorbate molecular weight. The data sample becomes:

$$S_t = \frac{(6.5579 \times 10^{-4})(6.02 \times 10^{23})(16.2 \times 10^{-20})}{14.01}$$

$$= 4.565\ m^2$$

The sample tube is weighed, cleared of sample and dried, then reweighed. The specific surface area is then equal to the total surface area divided by the sample weight.

Specific Surface Area (Talc) = $4.565\ m^2/0.5833g = 7.8\ m^2g$

APPENDIX B

Calculations for the Binding Isotherm

The raw data obtained from binding isotherm measurements consist of an absorbance reading at λ_{max} for the spiropyran (or other) adsorbate. The exact weight of dried adsorbent (g adsorbent) and the volume of solution (50 ml) also come into the calculations. The sequence by which an absorbance reading is turned into a point on the adsorption isotherm follows:

1. $\frac{A_{\lambda_{max}}}{\varepsilon} = C_{eq}$ (molar)
2. C_o (initial concentration, molar) - $C_{eq} = C_{ads}$ (molar)
3. C_{ads} x 50 M = mg adsorbed, where M is the molecular weight of the adsorbate.
4. $\frac{\text{mg adsorbed}}{\text{g adsorbent}} = (mg/g)_{adsorbed}$

These values then are used to construct the isotherm:

5. Plot $(mg/g)_{ads}$ versus C_{eq} to give the binding isotherm.
6. Plot $C_{eq}/(mg/g)_{ads}$ vs. C_{eq} for the Scott plot.
7. Plot $(mg/g)_{ads}/C_{eq}$ vs. $(mg/g)_{ads}$ for the Scatchard plot.

The surface area occupied per adsorbed molecule ($\mathring{A}^2$/molecule) is calculated from the maximum capacity, $(mg/g)_{max}$, knowing the surface area of the adsorbent. The following scheme relates the calculation sequence:

8. $$\frac{(mg/g)_{ads}}{1000} = (g/g)_{ads}$$

9. $$\frac{(g/g)_{ads}}{M} = (moles/g)_{ads}$$

10. $(moles/g)_{ads}$ x Avogadro's number = $\left(\frac{\text{\# molecules adsorbed}}{\text{g adsorbent}} \right)$

If S_t = surface area of adsorbent in m^2/g, then

$S_t \times 10^{20}$ = surface area of adsorbent in $\mathring{A}^2/g$.

11. $$\frac{\text{Surface area, } \mathring{A}^2/g}{(\text{\# molecules adsorbed/g})} = \mathring{A}^2/\text{molecule}$$

APPENDIX C

Sample Printout of Duggleby Program

(Using the Data for INS on Alumina at 25°C)

```
■■■■
]RUN DUGGLEBY
FROM DUGGLEBY ANALYTICAL   BIOCHEMISTRY 110  9  1981
HOW MANY DATA POINTS
?13

WHAT TYPE OF WEIGHTING...
CONSTANT STD DEV     (C)
PROPORTIONAL STD DEV (P)
BETWEEN THE ABOVE    (B)
STD DEV SUPPLIED     (S)
?C

BISQUARE WEIGHTING TOO
?N

INPUT INDEPENDENT VARIABLE, DEPENDENT VARIABLE
?1.756E-2,54.74
?1.178E-2,49.84
?9.72E-3,51.28
?8.14E-3,41.66
?6.01E-3,44.24
?4.24E-3,39.45
?2.31E-3,38.18
?1.705E-2,47.96
?1.287E-2,50.92
?7.366E-3,42.68
?5.31E-3,43.93
?1.98E-3,32.78
?1.392E-3,29.37

ENTER ESTIMATES OF THE PARAMETERS
?55.6,1.518E-3

  B(1)          B(2)          SSQ
53.9292669       1.2297911E-03
106.41141
53.9289072       1.2346838E-03
94.7370895
53.930621        1.23493881E-03
94.7227092
53.9307086       1.23495162E-03
94.7226966
53.930713        1.23495226E-03
94.7226978
```

FINAL VALUES . . .

B(1)	=	53.930713
+/-		1.82791106
B(2)	=	1.23495226E-03
+/-		2.24200631E-04

WHAT YOU'LL GET NEXT IS A LISTING OF
X AND Y VALUES ON THE BEST-FIT LINE

X	Y	Y(HAT)	DIFF
.01756	54.74	50.389	964.3528904
.01178	49.84	48.819	911.02662091
9.72E-03	51.28	47.858	133.42889875
8.14E-03	41.44	46.824	88-5.16647881
6.01E-03	44.24	44.737	97-.49784643
4.24E-03	39.45	41.769	44-2.31588435
2.31E-03	38.17	35.143	253.02708754
.01705	47.96	50.288	22-2.32827216
.01287	50.92	49.208	551.71116449
7.366E-03	42.68	46.187	86-3.50716855
5.31E-03	43.93	43.954	85.175351471
1.98E-03	32.78	33.214	15-.43443150
1.392E-03	29.37	28.577	31.79256692

END OF PROGRAM

APPENDIX D

Derivation of the Equilibrium Model

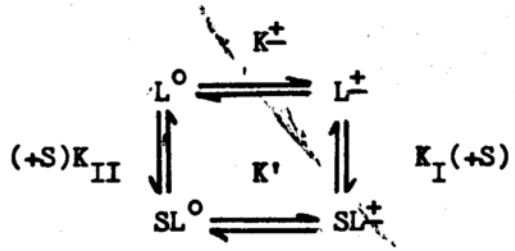

Symbols

L° = colorless spiropyran in solution (molar)

$L^{\pm}$ = colored spiropyran in solution (molar)

SL° = colorless adsorbed spiropyran (m^2/g)

$SL^{\pm}$ = colored adsorbed spiropyran (m^2/g)

S = solid surface (m^2/g)

$$K^{\pm} = \frac{(L^{\pm})}{(L^{\circ})} \text{, unitless.} \qquad \text{(solution equilibrium)} \qquad (1)$$

$$K' = \frac{(SL^{\pm})}{(SL^{\circ})} \text{, unitless.} \qquad \text{(solid surface equilibrium)} \qquad (2)$$

$$K_I = \frac{(SL^{\pm})}{(S)(L^{\pm})} \text{ in } M^{-1}, \quad \text{(colored form adsorbing)} \tag{3}$$

$$K_{II} = \frac{(SL^{o})}{(S)(L^{o})} \text{ in } M^{-1}, \quad \text{(colorless form adsorbing)} \tag{4}$$

$$S_t = (S) + (SL^{o}) + (SL^{\pm}), \text{ mass balance for total surface} \tag{5}$$

The general solution is obtained by allowing both forms of spiropyran to adsorb to the surface.

$$\theta = \text{fractional coverage} = \frac{(SL^{o}) + (SL^{\pm})}{(S) + (SL^{o}) + (SL^{\pm})} \tag{6}$$

$$\text{or} \qquad \theta = \frac{(SL^{o}) + (SL^{\pm})}{S_t} \tag{7}$$

Spiropyran mass balance:

$$\text{total L (moles)} = \underset{\text{(in solution)}}{(L^{o}) + (L^{\pm})} + \underset{\text{(on the surface)}}{(SL^{o}) + (SL^{\pm})} \tag{8}$$

Let V = total system volume, v_m = solution volume

v_s = surface volume

$$(L^{o}) = \frac{\text{moles } L^{o} \text{ in solution}}{v_m} \qquad (L^{\pm}) = \frac{\text{moles } L^{\pm} \text{ in solution}}{v_m} \tag{9}$$

$$\frac{\text{moles L adsorbed}}{\text{g solid}} = \left(\begin{array}{c}\text{m}^2/\text{g covered} \\ \text{by } L^{\pm}\end{array}\right)\left(\frac{\text{\# moles } L^{\pm}}{\text{m}^2 \text{ occupied space}}\right) + \left(\begin{array}{c}\text{m}^2/\text{g covered} \\ \text{by } L^{o}\end{array}\right)\left(\frac{\text{\# moles } L^{o}}{\text{m}^2 \text{ occupied space}}\right)$$

$$\text{\# moles L adsorbed/g} = (SL^{\pm})\ 10^9\ g_{max} + (SL^{o})\ 10^9\ g_{max} \qquad (10)$$

where g_{max} = spiropyran capacity expressed in nanomoles/m^2

Let a_s = amount of solid (in grams)

$$\text{\# moles L on solid} = 10^9\ g_{max}\ a_s\ [(SL^{o}) + (SL^{\pm})]$$

$$\text{total L(moles)} = v_m(L^{o}) + v_m(L^{\pm}) + 10^9\ g_{max}\ a_s\ [(SL^{o}) + (SL^{\pm})] \qquad (11)$$

From the binding constant and equilibrium constant definitions:

a. $(SL^{o}) = K_{II}(S)(L^{o})$

b. $(SL^{\pm}) = K_I(S)(L^{\pm})$

c. $(SL^{\pm}) = K'(SL^{o}) = K'\ K_{II}(S)(L^{o})$

Set b equal to c:

$$K_I(S)(L^{\pm}) = K'K_{II}(S)(L^{o})$$

$$\frac{(L^{\pm})}{(L^{o})} = \frac{K'K_{II}}{K_I} = K^{\pm}, \text{by definition} \qquad (12)$$

Note that there are two equivalent paths to colored adsorbate ($SL^{\pm}$) from colorless solute (L^{o}), hence:

$$K'K_{II} = K^{\pm}K_{I}$$

and three constants define the system, the fourth being determined through their relationship.

Combining, $S_t = (S) + K_{II}(S)(L^{o}) + K_{I}(S)(L^{\pm})$ (13)

$$S_t = (S)\left[\, 1 + K_{II}(L^{o}) + K_{I}(L^{\pm}) \,\right] \tag{14}$$

Eliminating $(L^{\pm})$, since $(L^{\pm}) = K^{\pm}(L^{o})$,

$$S_t = (S)\left[\, 1 + K_{II}(L^{o}) + K_{I}K^{\pm}(L^{o}) \,\right] \tag{15}$$

$$(S) = \frac{S_t}{\left[\, 1 + K_{II}(L^{o}) + K_{I}K^{\pm}(L^{o}) \,\right]} \tag{16}$$

$$\frac{(S)}{S_t} = (1-\theta) = \text{fraction of free surface} = \frac{1}{\left[\, 1 + K_{II}(L^{o}) + K_{I}K^{\pm}(L^{o}) \,\right]} \tag{17}$$

Combining (17) and (4),

$$\frac{(SL^{o})}{S_t K_{II}(L^{o})} = \frac{1}{\left[\, 1 + K_{II}(L^{o}) + K_{I}K^{\pm}(L^{o}) \,\right]} \tag{18}$$

and ~~(17)~~ and (3),

$$\frac{(SL^{\pm})}{S_t K_{II}(L^{\pm})} \qquad \frac{1}{\left[1 + K_{II}(L^{o}) + K_I K^{\pm}(L^{o})\right]} \tag{19}$$

Rearranging, (18) and (19) become:

$$\frac{(SL^{o})}{S_t} = \frac{K_{II}(L^{o})}{\left[1 + K_{II}(L^{o}) + K_I K^{\pm}(L^{o})\right]} \tag{20}$$

$$\frac{(SL^{\pm})}{S_t} = \frac{K_{II}(L^{\pm})}{\left[1 + K_{II}(L^{o}) + K_I K^{\pm}(L^{o})\right]} \tag{21}$$

Where (20) represents the fraction of surface covered with colorless spiropyran and (21) represents the fraction of surface covered with colored spiropyran.

Eliminating (L^{o}) from (21),

$$\frac{(SL^{\pm})}{S_t} = \frac{K_I K^{\pm}(L^{o})}{\left[1 + K_{II}(L^{o}) + K_I K^{\pm}(L^{o})\right]} \tag{22}$$

Total fraction of surface covered by spiropyran (θ) equals:

$$\theta = \frac{(SL^{o}) + (SL^{\pm})}{S_t} = \frac{K_{II}(L^{o}) + K_I K^{\pm}(L^{o})}{\left[1 + K_{II}(L^{o}) + K_I K^{\pm}(L^{o})\right]} \tag{23}$$

Rearranging:

$$(SL^{o}) + (SL^{\pm}) = \frac{S_t(L^{o})\left[K_{II} + K_I K^{\pm}\right]}{\left[1 + (L^{o})(K_{II} + K_I + K^{\pm})\right]} \tag{24}$$

To examine the units, let Y = moles L adsorbed/g solid

$$Y = 10^9 g_{max}\left[(SL^{\pm}) + (SL^{o})\right]$$

$$\left[(SL^{\pm}) + (SL^{o})\right] = \frac{Y}{10^9 g_{max}} \quad (\text{in } m^2/g) \tag{25}$$

$$C_{eq} = (L^{o}) + (L^{\pm}) = \text{free concentration of L at equilibrium} \tag{26}$$

$$C_{eq} = (L^{o})\left[1 + K^{\pm}\right] \tag{27}$$

$$(L^{o}) = C_{eq}/\left[1 + K^{\pm}\right] \tag{28}$$

Combining (28), (25), and (24),

$$\frac{Y}{10^9 g_{max}} = \frac{S_t C_{eq}\left[K_{II} + K_I K^{\pm}\right]}{\left\{1 + K^{\pm}\right\}\left\{1 + \left[\frac{C_{eq}(K_{II} + K_I K^{\pm})}{\left\{1 + K^{\pm}\right\}}\right]\right\}} \tag{29}$$

$$\frac{Y}{10^9 g_{max}} = \frac{S_t C_{eq}\left\{K_{II} + K_I K^{\pm}\right\}}{\left\{1 + K^{\pm}\right\} + C_{eq}(K_{II} + K_I K^{\pm})}$$

or

$$Y = \frac{10^9 g_{max} S_t C_{eq}\left\{K_{II} + K_I K^{\pm}\right\}}{\left\{1 + K^{\pm}\right\} + C_{eq}(K_{II} + K_I K^{\pm})} \tag{30}$$

Multiplying by 1000 Mol. Wt. yields:

$$(mg/g)_{adsorbed} = \frac{(mg/g)_{max} \{K_{II} + K_I K^{\pm}\} C_{eq}}{\{1 + K^{\pm}\} + \{K_{II} + K_I K^{\pm}\} C_{eq}} \quad (31)$$

Equation (31) is analogous to the Langmuir equation:

$$(mg/g)_{adsorbed} = \frac{(mg/g)_{max} K C_{eq}}{1 + K C_{eq}}$$

where $$K_{apparent} = \frac{K_{II} + K_I K^{\pm}}{\{1 + K^{\pm}\}} \quad (32)$$

which is equivalent to:

$$K_{app} = \frac{K_{II} (1 + K')}{\{1 + K^{\pm}\}} \quad (33)$$

If $K_{II} \ll 1$ (colored form only binds),

$$K_{app} = \frac{K_I K^{\pm}}{\{1 + K^{\pm}\}} \quad (34)$$

If $K^{\pm} \ll 1$ (for nonpolar solvents),

$$K_{app} = K_{II}(1 + K') \quad (35)$$

If most of the adsorbed form is colored, $K' \gg 1$,

$$K_{app} = K_{II} K'$$